Universiteit
Leiden
The Netherlands

hiPSC-derived 3D cardiac microtissue models with integrated immune cells and vasculature

Arslan-van Bergen, U.

Citation

Arslan-van Bergen, U. (2024, September 24). *hiPSC-derived 3D cardiac microtissue models with integrated immune cells and vasculature*. Retrieved from https://hdl.handle.net/1887/4092667

Version:	Publisher's Version
License:	Licence agreement concerning inclusion of doctoral thesis in the Institutional Repository of the University of Leiden
Downloaded from:	https://hdl.handle.net/1887/4092667

Note: To cite this publication please use the final published version (if applicable).

hiPSC-derived 3D cardiac microtissue models with integrated immune cells and vasculature

Ulgu Arslan-van Bergen
2024

Colophon

hiPSC-derived 3D cardiac microtissue models with integrated immune cells and vasculature

PhD thesis

This thesis was prepared at the department of Anatomy and Embryology of the Leiden University Medical Centre, Leiden, The Netherlands.

Copyright © Ulgu Arslan-van Bergen, Leiden, The Netherlands, 2024.

All rights reserved. No parts of this book may be reproduced or transmitted, in any forms and by any means, without permission in writing from the author. The copyright of the articles that have been published has been transferred to the respective journals.

The research described in this thesis as well as its publications was supported by the following grants: the European Union's Horizon 2020 research and innovation programme under grant
agreement No. 812954; The Novo Nordisk Foundation Center for Stem Cell Medicine is supported by Novo Nordisk Foundation grants (NNF21CC0073729).

ISBN: 978-94-6506-185-6
Printing: Ridderprint, www.ridderprint.nl

Cover: Cardiac microtissue with integrated immune cells (purple) and vasculature (red). Back cover is the human heart illustration. Front and back covers were made by Merlijn van Bijsterveld, who kindly gave the permission for the use of these images for this book.

Thesis layout was designed by Elies Thijs.

Financial support by the Dutch Heart Foundation for the publication of this thesis is gratefully acknowledged.

hiPSC-derived 3D cardiac microtissue models with integrated immune cells and vasculature

Proefschrift

ter verkrijging van
de graad van doctor aan de Universiteit Leiden,
op gezag van rector magnificus prof.dr.ir. H. Bijl,
volgens besluit van het college voor promoties
te verdedigen op dinsdag 24 september 2024
klokke 11.30 uur

door

Ulgu Arslan-van Bergen
geboren te Anamur, Turkije in 1994

Promotor
Prof. Dr. C.L. Mummery

Co-promoteren
Dr. V. Orlova

Promotiecommissie
Prof. Dr. P.S. Hiemstra
Prof. Dr. M.J.T.H Goumans
Prof. Dr. P. Loskill (University of Tubingen)
Prof. Dr. A.D. Van Der Meer (University of Twente)

With endless curiosity,
patient hearts and united minds...

Contents

Chapter 1
Introduction 10

Chapter 2
Perspectives for Future Use of Cardiac Microtissues from Human Pluripotent Stem Cells (Arslan et al., 2022) 28

Chapter 3
Microphysiological Stem Cell Models of The Human Heart (Arslan et al., 2022) 42

Chapter 4
Integration of hiPSC-derived macrophages into 3D cardiac microtissues (In preparation) 84

Chapter 5
Development of Vascularized hiPSC-derived 3D cardiac microtissue on chip (Arslan et al., 2023) 104

Chapter 6
Enhanced endothelial cell-cardiomyocyte crosstalk in hiPSC-derived vascularized 3D cardiac microtissue on chip through paracrine signalling (Arslan et al., 2023) 123

Chapter 7
Generation and characterization of hiPSC-derived vascularized-, perfusable cardiac microtissues-on-chip (Arslan et al., 2024) 136

Chapter 8
General Discussion 176

Appendix
Summary/ Samenvatting 190
List of Publications 194
Curriculum Vitae 195
Acknowledgment 196

1

Introduction

The heart and its microenvironment

The heart is one of the body's vital organs. Its rhythmic contraction continuously pumps blood through vessels around the whole body, transporting nutrient and oxygen to organs and tissues ensuring their health and function. The heart has four cavities (or chambers), two atria and two ventricles, one of each on left and right sides. These chambers control blood circulation: deoxygenated blood enters from the right atrium and is then transferred to the right ventricle from where it is pumped to the lungs for oxygenation. Oxygenated blood is next carried to the chambers on the left side via the pulmonary veins. Finally, oxygenated blood is circulated through the body via the aorta (HARVEY and LEAKE, 1929).

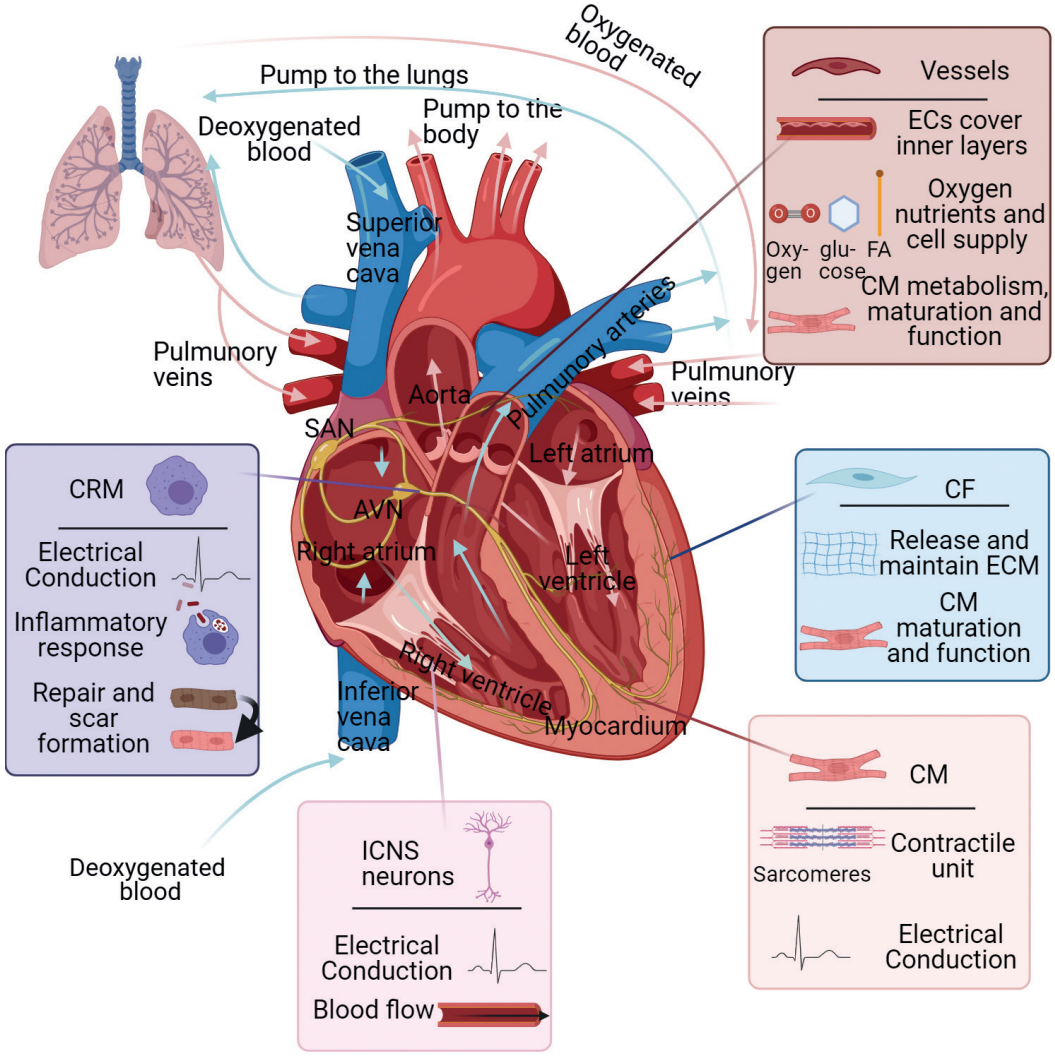

Figure 1: Schematic overview of the heart physiology and its cellular components. *SAN, Sinoatrial node; AVN, atrioventricular node; CRM, cardiac resident macrophages; ICNS, intrinsic cardiac nervous system; CM, cardiomyocytes; CF, cardiac fibroblasts; ECM, extracellular matrix; EC, endothelial cells.*

At the cellular level, the heart is a complex structure made up of multiple layers composed of multiple cell types (Figure 1).

The different cells in the heart can be distinguished in part by their expression of certain distinct proteins but also by their function, for example whether they contribute to contractility/electrical conduction, extracellular matrix (ECM) production, innervation and vascularization or whether they are part of the immune system. In order to function properly, well-regulated crosstalk between all of these cellular components as well as the heart cell microenvironment is essential (Reaume et al., 1995; Huang et al., 1998; Ming et al., 2009; Beny and Pacicca, 1994; Rook et al., 1992; Lo, 2000).

Cardiac contractility is critical as it circulates blood through the body via sequential contraction of each of the chambers (Moorman and Christoffels, 2003). Contractility is mainly regulated by cardiomyocytes (CMs) which contribute to the muscle wall of the myocardium. During embryonic development, the CM number and volume change significantly as they divide rapidly to form the complete heart at birth (de Boer et al., 2012). The fetal heart is composed of approximately 60% CMs. By contrast, in adult heart, CMs lose their proliferation capacity and contribute only 20-30% of the adult human heart by cell number, although form 80% of its total volume (Rubart and Field, 2006).
Specialized atrial and ventricular CMs are restricted to specific sites within each of the chambers. In addition to these CM types, there are also pacemaker cells and Purkinje fibers that are localized in the sinoatrial node (SAN). Together these form mechanical and electrical conduction system of the heart.

The ECM of the heart is involved in connecting cells and providing structural stability to the organ network and geometry (Novakovic et al., 2014; Rienks et al., 2014; Lockhart et al., 2011). It is mainly composed of interstitial matrix and basement membrane components: fibrillar and non-fibrillar collagens, fibronectin, hyaluronic acids, elastin and laminin (Rienks et al., 2014). ECM in the heart is mainly secreted and maintained by the cardiac fibroblasts (CFs) which form the largest population of non-myocyte cells. CFs also play an important role in regulating myocardium integrity in the case of cell death in the heart, for example after myocardial infarction (MI) (Dostal et al., 2015). After MI, CFs divide rapidly to replace the lost tissue and undergo a myofibroblast transition. This increases ECM secretion and the stiffness of the heart as a result of formation of the fibrotic scar tissue (Hall et al., 2021). Although these wound healing and repair functions of CFs are beneficial for proper heart function, excessive fibrosis can be detrimental, because the increased stiffness of the heart tissue makes contraction more work which can lead to heart failure and/or cardiac arrest (Lecomte et al., 1993).

The cardiac autonomic nervous system (ANS) contributes with a small population of cells to the heart. The ANS is a network of sympathetic and parasympathetic nervous systems that spreads from the brain to the heart and establishes the neuro-cardiac junction. At the organ level, there is also a rich intrinsic cardiac nervous system (ICNS) in the cardiac ganglia (Ardell and Armour, 2016). Sensory, motor and interconnecting neurons are integral parts

of the ICNS and they regulate the electrical and mechanical function of the heart (Zipes et al., 2017).

In this thesis, the main focus is on the vasculature and the immune components of the heart, how they contribute to its structure and function and how their interaction with the contractile cells of the heart can be modelled *in vitro*.

Vasculature

There are >90,000 km of blood vessels in the body, many in the heart. The heart is in fact among the most richly vascularized organs in the body. This is because the energy demand of CMs to beat 60 or more times a minute for many decades is enormous (Janssen et al., 2016). Vasculature in the heart forms a semi-permeable membrane through which it provides oxygen and selective nutrients to the surrounding cells in the organ. It is also involved in immune cell trafficking, for example in the case of inflammation. Vasculature is critical for supporting organ growth and function.

Constriction or complete closure of blood vessels of the heart caused by thrombosis (blood clots) or atherosclerosis leads to MI due to lack of oxygen which causes rapid death and permanent loss of CMs. It is therefore important to understand the interaction between different cell types involved in the structure and function of the vascular network of cardiac muscle.

On a cellular level, vasculature is formed by endothelial cells (ECs) and mural cells. ECs line the inner layer of the tubular (or lumenized) vessels where they control the vessel permeability, vasomotor tone, immune cell trafficking and angiogenesis (Aird, 2007). There are multiple EC compartments in the heart such as endocardium, capillaries and coronary vessels. ECs exhibit heterogeneity in their phenotype, function and genetic composition depending on the compartments in which they localize (Kumar et al., 1987; Turner et al., 1987). Mural cells like pericytes and smooth muscle cells are important part of the vasculature and are involved in the maintenance of vessel wall integrity, stability and function (Gaengel et al., 2009).

To understand vasculature-organ crosstalk in maintaining the oxygen and nutrient levels for cellular health, removing waste products and the response to tissue damage, it is useful to have tractable experimental models to study these processes. Mice are invaluable for investigating blood vessel development and function and vascular biology in general in health and disease. Their genetic composition can be easily manipulated allowing study of the direct impact on genetic changes or mutations on vessel behavior. In addition, physiological changes such as flow rate and vascular permeability associated with developmental defects or disease phenotypes can be addressed in mouse models (Korshunov and Berk, 2003). They are also cost-efficient, although in some jurisdictions they can be expensive, but this is the reason that mice (rather than rats or other larger mammals) are one of the most used animal

models for pre-clinical drug testing. However, physiological differences especially in their heart such as higher beat rate (±500 beats per minute versus ±60 in humans) and different hemodynamic properties, make translating results to humans challenging (Janssen et al., 2016). In this case, other animal models like pigs, dogs and non-human primates may be more useful in translation of some results to humans. However, larger animal models are more expensive, afre more challenging to genetically modify and ethical concerns around these models has driven the search by scientists for more suitable, easily accessible but realistic, human *in vitro* alternatives for some types of research question. This is in part the subject of this thesis.

Immune System

The immune system is composed of resident immune cells like cardiac-resident macrophages (CRMs) and infiltrating immune cells like blood-circulatory monocytes. CRMs regulate the electrical conduction in the myocardium through cellular crosstalk with CMs (Hulsmans et al., 2017; Harari et al., 2017; Tirziu et al., 2010). Besides electrical conduction, CRMs are involved in maintaining homeostasis, by removing mitochondrial waste of CMs, for example (José Nicolá s-A et al., 2020). They also take part in other physiological processes such as inflammation, tissue repair and regeneration upon injury, and angiogenesis. In particular, upon injury CRMs assist the complex cascade of events (Simões et al., 2020). For example, they first engulf and clear the dead cell debris, through the process called phagocytosis. They are involved in modulation of inflammation response to prevent prolonged inflammatory activity which can be detrimental. Furthermore, by releasing certain growth factors and other signaling molecules like cytokines that can help with proliferation and differentiation of cardiac cells, CRMs initiate the tissue repair and regeneration. They also support existing vessels (Moore et al., 2017) in the formation of new blood vessels (angiogenesis) which can supply oxygen and nutrients to the regenerating tissue. The final stage of the tissue regeneration is the formation of functional scar tissue which prevents the tissue collapse and heart rupture. On the other hand, blood circulatory monocytes are mostly involved in the inflammatory response itself (Bajpai et al., 2018).

Initial studies on macrophages claimed that their primary origin is bone marrow derived circulatory blood monocytes (van Furth and Cohn, 1968). However later studies showed more evidence that the macrophage ontogeny is more complex (Hoeffel and Ginhoux, 2015)(Figure 2). It is now clear that CRMs arise from the hemogenic endothelium of the yolk-sac during embryonic development (Yona et al., 2013; Ginhoux and Jung, 2014). CRMs mainly populate the atrioventricular node and in the neonatal heart, they can self-renew via local proliferation (Epelman et al., 2014; Hashimoto et al., 2013). It is thought that due to the high numbers of CRMs, neonatal heart is more regenerative. However, throughout adulthood, CRMs lose some of their self-renewal capacity and the population of CRMs is partially replaced by blood monocytes (Epelman et al., 2014; Dick et al., 2019). Due to this replacement of regenerative CRMs and the pro-inflammatory nature of blood monocytes, the adult heart becomes more pro-inflammatory than the neonatal heart. Although this

switch from regenerative- to pro-inflammatory phenotype is beneficial for tissue repair, excessive inflammatory response can be detrimental. It might lead to (1) apoptosis of cells, which results in further tissue damage and loss; (2) excessive scar tissue formation which makes the heart stiffer and results in cardiac arrest; (3) interference with the mechanical and electrical function of the heart, which can cause conditions like arrythmias. Therefore, maintaining the balance between the pro-inflammatory and anti-inflammatory responses is critical for proper tissue regeneration. Understanding CRM involvement in this balance is critical to harness their regenerative capacity and has potential for future therapeutic approaches to cardiac injury.

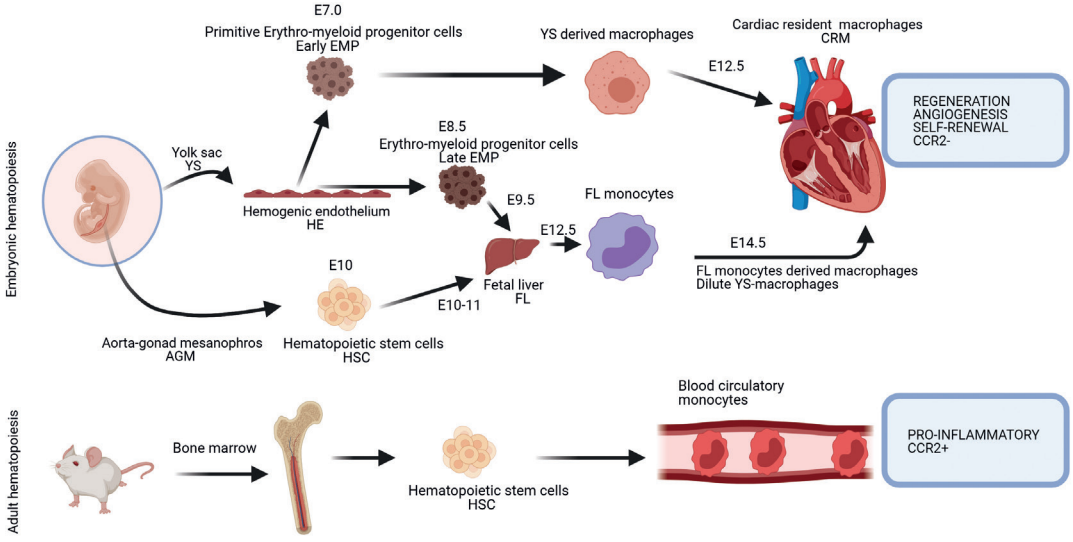

Figure 2: Schematic overview of the macrophage ontogeny in mice. *E, embryonic day.*

In vitro heart models to study the crosstalk in the heart

Crosstalk in the heart can be either between cells or between ECM and cells. Some ECM proteins are critical for cell adhesion, regulating ion channels and mechanical transduction especially in CMs by integrin interactions (Kim et al., 2000; Contard et al., 1991). Cellular crosstalk through direct cell contacts or secreted small molecules and proteins between EC-CM (Segers et al., 2018; Narmoneva et al., 2004; Brutsaert, 2003), CF-CM (Camelliti et al., 2004; Weber, 1989; Ieda et al., 2009; Giacomelli et al., 2020), CRM-CM (Hulsmans et al., 2017; Bajpai et al., 2018) and neural cardiac junctions (Li et al., 2023; Winbo et al., 2023) contributes to cardiac development and function in health and disease.

The discovery of human pluripotent stem cells (hPSCs) (Takahashi et al., 2007; Thomson, 1998) and their ability to differentiate into many different cell types has brought countless opportunities to study heart cells. The heart does not contain a stem cell population so it is not possible to derive and culture them from heart biopsies (Kretzschmar et al., 2018).

Human induced pluripotent stem cells (hiPSC) derived by reprogramming somatice cells from donors, are especially important because they carry the genome of individuals they are derived from; they present options for more precision medicine approaches for disease modelling and drug testing.

One of the first cardiac cell types that was differentiated from hPSCs were CMs (Mummery et al., 2003; Kehat et al., 2002). Patient-derived hPSC-CMs have proven useful over many years to model disorders like channelopathies as they express all ion channels of CMs (Davis et al., 2012; Braam et al., 2010; Denning et al., 2016; Liang et al., 2013; Moretti et al., 2010). However, hPSC-CMs often exhibit an immature phenotype in their genetic profile, structure and function, resembling fetal heart at around 16 weeks of gestation more than adult (Birket et al., 2015; Birket and Mummery, 2015; Ribeiro et al., 2015).

Several groups reported improved maturation in hPSC-CMs when they were cultured in 3D microenvironment (Beauchamp et al., 2015; Desroches et al., 2012; Soares et al., 2012). In addition, 2D hPSC-CMs lack cellular crosstalk with non-CMs, and thus fail to model more complex disorders. Co-culturing these cells with other cell components such as ECs and CFs in 3D tissue microenvironment improved their maturation even further (Beauchamp et al., 2020; Giacomelli et al., 2020; Mills et al., 2019; Richards et al., 2020). Multi-cellular 3D tissue cultures enabled integration of cellular, mechanical and electrical cues in a more controlled microenvironment mimicking the *in vivo* counterpart. These types of cultures can be scaffold-free or engulfed in a scaffold and formed by integrating either (1) hPSCs and differentiating them in 3D using growth factors (cardioids (Drakhlis et al., 2021; Hofbauer et al., 2021; Silva et al., 2020)) or (2) predifferentiated hPSC-derived cells (microtissues/spheroids (Giacomelli et al., 2017; Richards et al., 2020; Beauchamp et al., 2015; Mills et al., 2017)). Engineered heart tissues (EHT) can also integrate biomaterials and microenvironmental cues that can mimic structural properties of tissues like elasticity and organization (Eschenhagen et al., 1997; Zimmermann et al., 2002; Huebsch et al., 2016; Nunes et al., 2013; Dostanić et al., 2020; Mannhardt et al., 2017).

CM, EC and CFs are the most thoroughly studied cardiac cell types in 2D and 3D heart models. However, some studies suggest the important roles of CRMs (Simões et al., 2020; Farache Trajano and Smart, 2021; Dutta and Nahrendorf, 2015) in heart development and pathophysiology. Developing more complex models that can integrate more cell types like immune cells, complex disease such as MI and consequent fibrosis (Figure 3), where the crosstalk between vasculature and immune components is critical, can be better recapitulated.

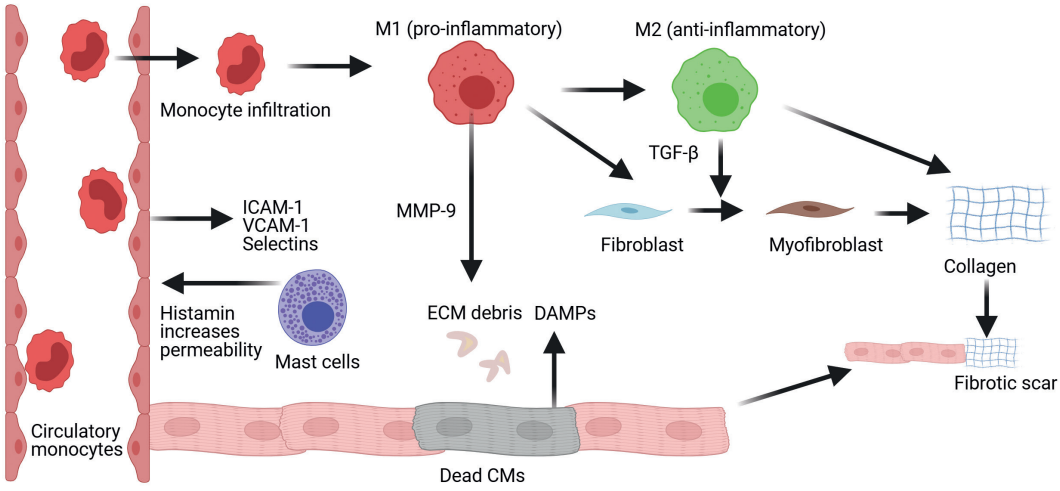

Figure 3: Schematic overview of MI and fibrosis showing the complex cascade of events taking place. *CM death releases damage associated molecular patterns (DAMPs). Mast cells activate the ECs by histamine release. With the increase in ICAM-1, VCAM-1 and Selectins as well as permeability, monocytes circulate to the injured area. First, monocytes are polarized towards the M1 macrophage phenotype which is pro-inflammatory. They clear the ECM debris by the secretion of matrix metallopeptidase (MMP-9). In the meantime, anti-inflammatory M2 macrophages activate myofibroblasts by TGF-β secretion which then deposits collagen to scar area. Macrophages also contribute to collagen deposition in this process (Simões et al., 2020). Consequently, the fibrotic scar is formed.*

Although some of these 3D models integrate ECs, which pre-vascularize these tissues by self-organization into a microvascular networks (Cakir et al., 2019; Homan et al., 2019; Vargas-Valderrama et al., 2020; Giacomelli et al., 2020), most of these models are maintained in static culture conditions. Therefore, they lack functional vasculature. Perfusion is one of the most important components for vessel stability and integrity as without it vessels regress over time (Ryan et al., 2021). Initial strategies to vascularize 3D tissue cultures involved transplanting them into living organisms where the host circulatory system invades the transplanted tissue and connects with its microvascular network (Mansour et al., 2018; Takebe et al., 2013; Ryan et al., 2021). Although this principle generated functional vasculature, translating the research into humans was challenging as inter-species differences lead to altered behavior and pattern of vascular structures (Brady et al., 2023).

Microfluidic Organ-on-Chip systems

Organ-on-chip (OoC) platforms offer alternatives to the static platforms described above, as they provide perfusable engineered microchannels. The first microscale platforms emerged in the early 2000s by microfabricating a hollow channel in the size of a small lung airway to detect changes in acoustic signals during liquid flow (Huh et al., 2007). Following a similar strategy, the design of the platform was later changed to include two parallel channels which allow compartmentalization of different cell types (Domansky et al., 2010; Huh et al., 2010). It also allowed the introduction of two variables in different channels, for example, perfusion

of liquid in EC channel and air in epithelial lung alveolar cell channel, recreating liquid-air interface (Huh et al., 2010). This simple two channel platform was later adapted by many groups to accommodate other tissue types including heart-on- chip models (Agarwal et al., 2013; Marsano et al., 2016; Mathur et al., 2015). These models introduced perfusion in the systems. However, they did not recapitulate the vascularized organ physiology as the flow was not through a vasculature. As a result, the tissues were exposed to the culture medium directly via passive diffusion through gel. More recent strategies like co-culturing of CM, ECs and CFs in an organ-on-chip platform (King et al., 2022) led to formation of perfusable vessels that are surrounded by CMs. However, the model requires high cell numbers, and it is challenging for some labs to upscale to these cell numbers. In addition, complete self-organization of the cells might result in less control in the cell distribution which might lead to heterogeneity in structure and function of the model in one channel. The enclosed chip environment further complicates the study of cellular crosstalk and its effect which is especially important when the immature hiPSC-derived CMs are seeded in the gel. On the other hand, following a similar strategy but integrating organoid/microtissue models in which these variables can be controlled better might offer an alternative.

Aim and the scope of this thesis

Based on the potentials and limitations of current *in vitro* 3D cardiac models that were discussed above, the development of a more complex culture system which can mimic more aspects of the heart *in vivo* would be of value.

This thesis consists of eight chapters and describes the importance of the heart microenvironment and ways to integrate more components of it in cardiac models. The overall aim is to develop cardiac models that incorporate (1) immune; and (2) vascular components, such as functional vasculature, in order to provide cellular crosstalk and study the impact on organ function and response to external stimuli.

In **chapter 2**, we shortly reviewed the current 3D cardiac models and the possible refinement strategies in their future use in the cardiac field.

In **chapter 3**, we reviewed the current cardiac microphysiological systems in a broader manner with their applications and readouts and discussed our future perspectives for their further implementation in academia and industry.

In **chapter 4**, we established optimal conditions to generate 3D cardiac microtissues that integrate hiPSC- derived macrophages (CMECFM0). We first showed that macrophages migrated outside of CMECFM0s in the standard V-bottom 96-well plates. Using ultra-low attachment plates eliminated this problem and macrophages remained in CMECFM0. We further described the effect of culture conditions and hiPSC-macrophages on different cell subsets in the microtissues. We showed that using macrophage colony-stimulating factor (M-CSF) increased the macrophage numbers in CMECFM0s in the early culture period.

However, it did not affect the number in later time period. Macrophages did not significantly alter vessel density and contraction parameters. Finally, we investigated the pro- and anti-inflammatory phenotypes of integrated macrophages, highlighting the importance of culture conditions on the macrophage identity.

In **chapter 5**, we generated a vascularized and perfusable hiPSC-derived 3D cardiac microtissues on a chip platform (VMToC) by combining prevascularized cardiac microtissues with additional vascular cells in fibrin hydrogel. We characterized the vessel parameters and showed that contraction of microtissues did not affect the vascularization process in chips. We further established flow conditions and showed that continuous perfusion improves the vessel density inside and outside the MTs. This work is a foundation of chapter 6 and 7.

In **chapter 6**, we established the utility of VMToCs in terms of the crosstalk between hiPSC-endothelial cells and cardiomyocytes. We first characterized the effect of vasculature on sarcomere organization and contraction parameters during spontaneous or paced beating. We showed that vascularization did not significantly alter sarcomere organization. However, vascularized tissues had significantly longer contraction duration and peak-to-peak times. We then challenged the crosstalk between hiPSC- endothelial cells and hiPSC-cardiomyocytes using (1) nitric oxide synthase inhibitor and (2) pro- inflammatory cytokine stimulation. Only vascularized tissues responded to these stimuli, highlighting the enhanced crosstalk in VMToC model and its effect on the functionality.

In **chapter 7**, we described a detailed protocol to generate VMToC. We then described protocols to characterize VMToCs (1) functionally by applying bead perfusion assay, showing the vessels were lumenized and perfusable, and by pacing; and (2) structurally by fixing and immunofluorescent staining.

In **chapter 8**, the findings of this thesis are summarized and a critical discussion provided of the limitations and advantages of the models described. Finally, we consider future perspectives for these types of vascularized 3D models in the field.

References

Agarwal, A., Goss, J. A., Cho, A., McCain, M. L., and Parker, K. K. 2013. *Microfluidic heart on a chip for higher throughput pharmacological studies.* Lab on a Chip 13:3599–3608.

Aird, W. C. 2007. *Phenotypic heterogeneity of the endothelium: I. Structure, function, and mechanisms.* Circulation Research 100(2):158-73.

Ardell, J. L., and Armour, J. A. 2016. *Neurocardiology: Structure-Based function.* Comprehensive Physiology 6(4):1635-1653.

Bajpai, G., Schneider, C., Wong, N., Bredemeyer, A., Hulsmans, M., Nahrendorf, M., Epelman, S., Kreisel, D., Liu, Y., Itoh, A., et al. 2018. *The human heart contains distinct macrophage subsets with divergent origins and functions.* Nature Medicine 24(8):1234-1245.

Beauchamp, P., Jackson, C. B., Ozhathil, L. C., Agarkova, I., Galindo, C. L., Sawyer, D. B., Suter, T. M., and Zuppinger, C. 2020. *3D Co-culture of hiPSC-Derived Cardiomyocytes With Cardiac Fibroblasts Improves Tissue-Like Features of Cardiac Spheroids.* Frontiers in Molecular Biosciences 7:14.

Beauchamp, P., Moritz, W., Kelm, J. M., Ullrich, N. D., Agarkova, I., Anson, B. D., Suter, T. M., and Zuppinger, C. 2015. *Development and Characterization of a Scaffold-Free 3D Spheroid Model of Induced Pluripotent Stem Cell-Derived Human Cardiomyocytes.* Tissue Engineering - Part C: Methods 21(8):852-61.

Beny, J. L., and Pacicca, C. 1994. *Bidirectional electrical communication between smooth muscle and endothelial cells in the pig coronary artery.* American Journal of Physiology - Heart and Circulatory Physiology 266(4 Pt 2):H1465-72.

Birket, M. J., and Mummery, C. L. 2015. *Pluripotent stem cell derived cardiovascular progenitors - A developmental perspective.* Developmental Biology 400(2):169-79.

Birket, M. J., Ribeiro, M. C., Kosmidis, G., Ward, D., Leitoguinho, A. R., van de Pol, V., Dambrot, C., Devalla, H. D., Davis, R. P., Mastroberardino, P. G., et al. 2015. *Contractile Defect Caused by Mutation in MYBPC3 Revealed under Conditions Optimized for Human PSC-Cardiomyocyte Function.* Cell Reports 13:733–745.

de Boer, B. A., van den Berg, G., de Boer, P. A. J., Moorman, A. F. M., and Ruijter, J. M. 2012. *Growth of the developing mouse heart: An interactive qualitative and quantitative 3D atlas.* Developmental Biology 368(2):203-13.

Braam, S. R., Tertoolen, L., van de Stolpe, A., Meyer, T., Passier, R., and Mummery, C. L. 2010. *Prediction of drug-induced cardiotoxicity using human embryonic stem cell-derived cardiomyocytes.* Stem Cell Research 4(2):107-16.

Brady, E. L., Prado, O., Johansson, F., Mitchell, S. N., Martinson, A. M., Karbassi, E., Reinecke, H., Murry, C. E., Davis, J., and Stevens, K. R. 2023. *Engineered tissue vascularization and engraftment depends on host model.* Scientific Reports 13(1):1973.

Brutsaert, D. L. 2003. *Cardiac endothelial-myocardial signaling: Its role in cardiac growth, contractile performance, and rhythmicity.* Physiological Reviews 83(1):59-115.

Cakir, B., Xiang, Y., Tanaka, Y., Kural, M. H., Parent, M., Kang, Y. J., Chapeton, K., Patterson, B., Yuan, Y., He, C. S., et al. 2019. *Engineering of human brain organoids with a functional vascular-like system.* Nature Methods 16(11):1169-1175.

Camelliti, P., Green, C. R., LeGrice, I., and Kohl, P. 2004. *Fibroblast Network in Rabbit Sinoatrial Node: Structural and Functional Identification of Homogeneous and Heterogeneous Cell Coupling.* Circulation Research 94(6):828-35.

Contard, F., Koteliansky, V., Marotte, F., Dubus, I., Rappaport, L., and Samuel, J. L. 1991. *Specific alterations in the distribution of extracellular matrix components within rat myocardium during the development of pressure overload.* Laboratory Investigation 64(1):65-75.

Davis, R. P., Casini, S., van den Berg, C. W., Hoekstra, M., Remme, C. A., Dambrot, C., Salvatori, D., Oostwaard, D. W., Wilde, A. A. M., Bezzina, C. R., et al. 2012. *Cardiomyocytes Derived From Pluripotent Stem Cells Recapitulate Electrophysiological Characteristics of an Overlap Syndrome of Cardiac Sodium Channel Disease.* Circulation 125:3079–3091.

Denning, C., Borgdorff, V., Crutchley, J., Firth, K. S. A., George, V., Kalra, S., Kondrashov, A., Hoang, M. D., Mosqueira, D., Patel, A., et al. 2016. *Cardiomyocytes from human pluripotent stem cells: From laboratory curiosity to industrial biomedical platform.* BBA - Molecular Cell Research 1863:1728–1748.

Desroches, B. R., Zhang, P., Choi, B. R., King, M. E., Maldonado, A. E., Li, W., Rago, A., Liu, G., Nath, N., Hartmann, K. M., et al. 2012. *Functional scaffold-free 3-D cardiac microtissues: A novel model for the investigation of heart cells.* American Journal of Physiology - Heart and Circulatory Physiology 302(10):H2031-42.

Dick, S. A., Macklin, J. A., Nejat, S., Momen, A., Clemente-Casares, X., Althagafi, M. G., Chen, J., Kantores, C., Hosseinzadeh, S., Aronoff, L., et al. 2019. *Self-renewing resident cardiac macrophages limit adverse remodeling following myocardial infarction.* Nature Immunology 20(1):29-39.

Domansky, K., Inman, W., Serdy, J., Dash, A., Lim, M. H. M., and Griffith, L. G. 2010. P*erfused multiwell plate for 3D liver tissue engineering.* Lab on a Chip 10(1):51-8.

Dostal, D., Glaser, S., and Baudino, T. A. 2015. Cardiac Fibroblast Physiology and Pathology. In Comprehensive Physiology pp. 887–909.

Dostanić, M., Windt, L. M., Stein, J. M., Van Meer, B. J., Bellin, M., Orlova, V., Mastrangeli, M., Mummery, C. L., and Sarro, P. M. 2020. *A Miniaturized EHT Platform for Accurate Measurements of Tissue Contractile Properties.* Journal of Microelectromechanical Systems 29(5):881-887.

Drakhlis, L., Biswanath, S., Farr, C. M., Lupanow, V., Teske, J., Ritzenhoff, K., Franke, A., Manstein, F., Bolesani, E., Kempf, H., et al. 2021. *Human heart-forming organoids recapitulate early heart and foregut development.* Nature Biotechnology 39(6):737-746.

Dutta, P., and Nahrendorf, M. 2015. *Monocytes in myocardial infarction. Arteriosclerosis, Thrombosis, and Vascular Biology* 35(5):1066-70.

Epelman, S., Lavine, K. J., Beaudin, A. E., Sojka, D. K., Carrero, J. A., Calderon, B., Brija, T., Gautier, E. L., Ivanov, S., Satpathy, A. T., et al. 2014. *Embryonic and adult-derived resident cardiac macrophages are maintained through distinct mechanisms at steady state and during inflammation.* Immunity 40(1):91-104.

Eschenhagen, T., Fink, C., Remmers, U., Scholz, H., Wattchow, J., Weil, J., Zimmermann, W., Dohmen, H. H., Schäfer, H., Bishopric, N., et al. 1997. *Three-dimensional reconstitution of embryonic cardiomyocytes in a collagen matrix: a new heart muscle model system.* The FASEB Journal 11:683–694.

Farache Trajano, L., and Smart, N. 2021. *Immunomodulation for optimal cardiac regeneration: insights from comparative analyses.* npj Regenerative Medicine 6:1–11.
van Furth, R., and Cohn, Z. A. 1968. *The origin and kinetics of mononuclear phagocytes.* The Journal of experimental medicine 128(3):415-35.

Gaengel, K., Genové, G., Armulik, A., and Betsholtz, C. 2009. *Endothelial-mural cell signaling in vascular development and angiogenesis.* Arteriosclerosis, Thrombosis, and Vascular Biology 29(5):630-8.

Giacomelli, E., Bellin, M., Sala, L., Meer, B. J. van, Tertoolen, L. G. J., Orlova, V. V, and Mummery, C. L. 2017. *Three-dimensional cardiac microtissues composed of cardiomyocytes and endothelial cells co-differentiated from human pluripotent stem cells.* Development 144:1008–1017.

Giacomelli, E., Meraviglia, V., Campostrini, G., Cochrane, A., Cao, X., van Helden, R. W. J., Krotenberg Garcia, A., Mircea, M., Kostidis, S., Davis, R. P., et al. 2020. *Human-iPSC-Derived Cardiac Stromal Cells Enhance Maturation in 3D Cardiac Microtissues and Reveal Non-cardiomyocyte Contributions to Heart Disease.* Cell Stem Cell 26:862-879.e11.

Ginhoux, F., and Jung, S. 2014. *Monocytes and macrophages: Developmental pathways and tissue homeostasis.* Nature Reviews Immunology 14(6):392-404.

Hall, C., Gehmlich, K., Denning, C., and Pavlovic, D. 2021. *Complex relationship between cardiac fibroblasts and cardiomyocytes in health and disease.* Journal of the American Heart Association 10(5):e019338.

Harari, E., Guo, L., Smith, S. L., Braumann, R. E., Virmani, R., and Finn, A. V. 2017. *Heart-resident macrophages: are they involved in the rhythm of every beat?* Journal of Thoracic Disease 9:2264–2267.

Harvey, w., And leake, c. D. 1929. *Exercitatio anatomica de motu cordis et sanguinis in animalibus.* The American Journal of the Medical Sciences 64(5):289.

Hashimoto, D., Chow, A., Noizat, C., Teo, P., Beasley, M. B., Leboeuf, M., Becker, C. D., See, P., Price, J., Lucas, D., et al. 2013. *Tissue-resident macrophages self-maintain locally throughout adult life with minimal contribution from circulating monocytes.* Immunity 38(4):792-804.

Hoeffel, G., and Ginhoux, F. 2015. *Ontogeny of tissue-resident macrophages.* Frontiers in Immunology 6:486.

Hofbauer, P., Jahnel, S. M., Papai, N., Giesshammer, M., Deyett, A., Schmidt, C., Penc, M., Tavernini, K., Grdseloff, N., Meledeth, C., et al. 2021. *Cardioids reveal self-organizing principles of human cardiogenesis.* Cell 184:3299-3317.e22.

Homan, K. A., Gupta, N., Kroll, K. T., Kolesky, D. B., Skylar-Scott, M., Miyoshi, T., Mau, D., Valerius, M. T., Ferrante, T., Bonventre, J. V., et al. 2019. *Flow-enhanced vascularization and maturation of kidney organoids in vitro.* Nature Methods 16(3):255-262.

Huang, G. Y., Cooper, E. S., Waldo, K., Kirby, M. L., Gilula, N. B., and Lo, C. W. 1998. *Gap junction- mediated cell-cell communication modulates mouse neural crest migration.* Journal of Cell Biology 143(6):1725-34.

Huebsch, N., Loskill, P., Deveshwar, N., Spencer, C. I., Judge, L. M., Mandegar, M. A., Fox, C. B., Mohamed, T. M. A., Ma, Z., Mathur, A., et al. 2016. *Miniaturized iPS-Cell-Derived Cardiac Muscles for Physiologically Relevant Drug Response Analyses.* Scientific Reports 6:1–12.

Huh, D., Fujioka, H., Tung, Y. C., Futai, N., Paine, R., Grotberg, J. B., and Takayama, S. 2007. *Acoustically detectable cellular-level lung injury induced by fluid mechanical stresses in microfluidic airway systems.* Proceedings of the National Academy of Sciences of the United States of America 104(48):18886-91.

Huh, D., Matthews, B. D., Mammoto, A., Montoya-Zavala, M., Yuan Hsin, H., and Ingber, D. E. 2010. *Reconstituting organ-level lung functions on a chip.* Science 328(5986):1662-8.

Hulsmans, M., Clauss, S., Xiao, L., Aguirre, A. D., King, K. R., Hanley, A., Hucker, W. J., Wülfers, E. M., Seemann, G., Courties, G., et al. 2017. *Macrophages Facilitate Electrical Conduction in the Heart.* Cell 169(3):510-522.e20.

Ieda, M., Tsuchihashi, T., Ivey, K. N., Ross, R. S., Hong, T. T., Shaw, R. M., and Srivastava, D. 2009. *Cardiac Fibroblasts Regulate Myocardial Proliferation through β1 Integrin Signaling.* Developmental Cell 16(2):233-44.

Janssen, P. M. L., Biesiadecki, B. J., Ziolo, M. T., and Davis, J. P. 2016. *The need for speed: Mice, men, and myocardial kinetic reserve.* Circulation Research 119(3):418-21.

José Nicolá s-A, A. A., Lechuga-Vieco, A. V, Esteban-Martínez, L., Bernal, J. A., Enríquez, J. A., Hidalgo, A., Nicolá s-A, J. A., Sá nchez-Díaz, M., Díaz-García, E., Santiago, D. J., et al. 2020. *A Network of Macrophages Supports Mitochondrial Homeostasis in the Heart.* Cell 183:94–109.

Kehat, I., Kenyagin-Karsenti, D., Snir, M., Segev, H., Amit, M., Gepstein, A., Livne, E., Binah, O., Itskovitz-Eldor, J., and Gepstein, L. 2002. *Human embryonic stem cells can differentiate into myocytes with structural and functional properties of cardiomyocytes.* Journal of Clinical Investigation 108:407–414.

Kim, H. E., Dalal, S. S., Young, E., Legato, M. J., Weisfeldt, M. L., and D'Armiento, J. 2000. *Disruption of the myocardial extracellular matrix leads to cardiac dysfunction.* Journal of Clinical Investigation 106(7):857-66.

King, O., Cruz-Moreira, D., Sayed, A., Stevens, M. M., Rasponi, M., and Terracciano, C. M. 2022. *Functional microvascularization of human myocardium in vitro.* Cell Reports Methods 2(9):100280

Korshunov, V. A., and Berk, B. C. 2003. *Flow-Induced Vascular Remodeling in the Mouse: A Model for Carotid Intima-Media Thickening. Arteriosclerosis, Thrombosis, and Vascular Biology* 23(12):2185-91.

Kretzschmar, K., Post, Y., Bannier-Hélaouët, M., Mattiotti, A., Drost, J., Basak, O., Li, V. S. W., van den Born, M., Gunst, Q. D., Versteeg, D., et al. 2018. *Profiling proliferative cells and their progeny in damaged murine hearts.* Proceedings of the National Academy of S ciences of the United States of America 115 (52) E12245-E12254.

Kumar, S., West, D. C., and Ager, A. 1987. *Heterogeneity in endothelial cells from large vessels and microvessels.* Differentiation 36(1):57-70.

Lecomte, D., Fornes, P., Fouret, P., and Nicolas, G. 1993. *Isolated Myocardial Fibrosis as a Cause of Sudden Cardiac Death and Its Possible Relation to Myocarditis.* Journal of Forensic Sciences 38(3):617-21.

Li, N., Edel, M., Liu, K., Denning, C., Betts, J., Neely, O. C., Li, D., Paterson, D. J., Li, D., and Paterson, D. J. 2023. *Human induced pluripotent stem cell- derived cardiac myocytes and sympathetic neurons in disease modelling.* Philos Trans R Soc Lond B Biol Sci 378(1879):20220173.

Liang, P., Lan, F., Lee, A. S., Gong, T., Sanchez-Freire, V., Wang, Y., Diecke, S., Sallam, K., Knowles, J. W., Wang, P. J., et al. 2013. *Drug screening using a library of human induced pluripotent stem cell-derived cardiomyocytes reveals disease-specific patterns of cardiotoxicity.* Circulation 127(16):1677-91.

Lo, C. W. 2000. *Role of gap junctions in cardiac conduction and development: Insights from the connexin knockout mice.* Circulation Research 87(5):346-8.

Lockhart, M., Wirrig, E., Phelps, A., and Wessels, A. 2011. *Extracellular matrix and heart development.* Birth Defects Research Part A - Clinical and Molecular Teratology 91:535–550.

Mannhardt, I., Saleem, U., Benzin, A., Schulze, T., Klampe, B., Eschenhagen, T., and Hansen, A. 2017. *Automated contraction analysis of human engineered heart tissue for cardiac drug safety screening.* Journal of Visualized Experiments 2017:1–10.

Mansour, A. A., Gonçalves, J. T., Bloyd, C. W., Li, H., Fernandes, S., Quang, D., Johnston, S., Parylak, S. L., Jin, X., and Gage, F. H. 2018. *An in vivo model of functional and vascularized human brain organoids.* Nature Biotechnology 36(5):432-441.

Marsano, A., Conficconi, C., Lemme, M., Occhetta, P., Gaudiello, E., Votta, E., Cerino, G., Redaelli, A., and Rasponi, M. 2016. *Beating heart on a chip: A novel microfluidic platform to generate functional 3D cardiac microtissues.* Lab on a Chip 16:599–610.

Mathur, A., Loskill, P., Shao, K., Huebsch, N., Hong, S. G., Marcus, S. G., Marks, N., Mandegar, M., Conklin, B. R., Lee, L. P., et al. 2015. *Human iPSC-based cardiac microphysiological system for drug screening applications.* Scientific Reports 5:1–7.

Mills, R. J., Parker, B. L., Quaife-Ryan, G. A., Voges, H. K., Needham, E. J., Bornot, A., Ding, M., Andersson, H., Polla, M., Elliott, D. A., et al. 2019. *Drug Screening in Human PSC-Cardiac Organoids Identifies Pro-proliferative Compounds Acting via the Mevalonate Pathway.* Cell Stem Cell 24:895-907.e6.

Mills, R. J., Titmarsh, D. M., Koenig, X., Parker, B. L., Ryall, J. G., Quaife-Ryan, G. A., Voges, H. K., Hodson, M. P., Ferguson, C., Drowley, L., et al. 2017. *Functional screening in human cardiac organoids reveals a metabolic mechanism for cardiomyocyte cell cycle arrest.* Proceedings of the National Academy of Sciences 114:E8372–E8381.

Ming, J., Li, T., Zhang, Y., Xu, J., Yang, G., and Liu, L. 2009. *Regulatory effects of myoendothelial gap junction on vascular reactivity after hemorrhagic shock in rats.* Shock 31(1):80-6.

Moore, E. M., Ying, G., and West, J. L. 2017. *Macrophages Influence Vessel Formation in 3D Bioactive Hydrogels.* Advanced Biosystems 1:1600021.

Moorman, A. F. M., and Christoffels, V. M. 2003. *Cardiac chamber formation: Development, genes, and evolution.* Physiological Reviews 83:1223–1267.

Moretti, A., Bellin, M., Welling, A., Jung, C. B., Lam, J. T., Bott-Flügel, L., Dorn, T., Goedel, A., Höhnke, C., Hofmann, F., et al. 2010. *Patient-specific induced pluripotent stem-cell models for long-QT syndrome.* New England Journal of Medicine 363:1397–1409.

Mummery, C., Oostwaard, D. W., Doevendans, P., Spijker, R., Brink, S. van den, Hassink, R., Heyden, M. van der, Opthof, T., Pera, M., Riviere, A. B. de la, et al. 2003. *Differentiation of human embryonic stem cells to cardiomyocytes: role of coculture with visceral endoderm-like cells.* Circulation 107:2733–2740.

Narmoneva, D. A., Vukmirovic, R., Davis, M. E., Kamm, R. D., and Lee, R. T. 2004. E*ndothelial cells promote cardiac myocyte survival and spatial reorganization: Implications for cardiac regeneration.* Circulation 110(8):962-8.

Novakovic, G. V., Eschenhagen, T., and Mummery, C. 2014. *Myocardial Tissue Engineering : In Vitro Models.* 1–16.

Nunes, S. S., Miklas, J. W., Liu, J., Aschar-Sobbi, R., Xiao, Y., Zhang, B., Jiang, J., Massé, S., Gagliardi, M., Hsieh, A., et al. 2013. *Biowire: A platform for maturation of human pluripotent stem cell- derived cardiomyocytes.* Nature Methods 10:781–787.

Reaume, A. G., De Sousa, P. A., Kulkarni, S., Langille, B. L., Zhu, D., Davies, T. C., Juneja, S. C., Kidder, G. M., and Rossant, J. 1995. *Cardiac malformation in neonatal mice lacking connexin43.* Science 267(5205):1831-4.

Ribeiro, M. C., Tertoolen, L. G., Guadix, J. A., Bellin, M., Kosmidis, G., D'Aniello, C., Monshouwer- Kloots, J., Goumans, M. J., Wang, Y. li, Feinberg, A. W., et al. 2015. F*unctional maturation of human pluripotent stem cell derived cardiomyocytes invitro - Correlation between contraction force andelectrophysiology.* Biomaterials 51:138-150.

Richards, D. J., Li, Y., Kerr, C. M., Yao, J., Beeson, G. C., Coyle, R. C., Chen, X., Jia, J., Damon, B., Wilson, R., et al. 2020. *Human cardiac organoids for the modelling of myocardial infarction and drug cardiotoxicity.* Nature biomedical engineering 4:446–462.

Rienks, M., Papageorgiou, A.-P., Frangogiannis, N. G., and Heymans, S. 2014. *Myocardial Extracellular Matrix.* Circulation Research 114:872–888.

Rook, M. B., Van Ginneken, A. C. G., De Jonge, B., El Aoumari, A., Gros, D., and Jongsma, H. J. 1992. *Differences in gap junction channels between cardiac myocytes, fibroblasts, and heterologous pairs.* American Journal of Physiology - Cell Physiology 263(5 Pt 1):C959-77.

Rubart, M., and Field, L. J. 2006. *CARDIAC REGENERATION: Repopulating the Heart.* Annual Review of Physiology 68:29–49.

Ryan, A. R., England, A. R., Chaney, C. P., Cowdin, M. A., Hiltabidle, M., Daniel, E., Gupta, A. K., Oxburgh, L., Carroll, T. J., and Cleaver, O. 2021. *Vascular deficiencies in renal organoids and ex vivo kidney organogenesis.* Developmental Biology 477:98-116.

Segers, V. F. M., Brutsaert, D. L., and De Keulenaer, G. W. 2018. *Cardiac remodeling: Endothelial cells have more to say than just NO.* Frontiers in Physiology 9:382.

Silva, A. C., Matthys, O. B., Joy, D. A., Kauss, M. A., Natarajan, V., Lai, M. H., Turaga, D., Alexanian, M., Bruneau, B. G., and McDevitt, T. C. 2020. *Developmental co-emergence of cardiac and gut tissues modeled by human iPSC-derived organoids.* bioRxiv.

Simões, F. C., Cahill, T. J., Kenyon, A., Gavriouchkina, D., Vieira, J. M., Sun, X., Pezzolla, D., Ravaud, C., Masmanian, E., Weinberger, M., et al. 2020. *Macrophages directly contribute collagen to scar formation during zebrafish heart regeneration and mouse heart repair.* Nature Communications 11(1):600.

Soares, C. P., Midlej, V., de Oliveira, M. E. W., Benchimol, M., Costa, M. L., and Mermelstein, C. 2012. *2D and 3D-organized cardiac cells shows differences in cellular morphology, adhesion junctions, presence of myofibrils and protein expression.* PLoS ONE 7:e38147.

Takahashi, K., Tanabe, K., Ohnuki, M., Narita, M., Ichisaka, T., Tomoda, K., and Yamanaka, S. 2007. *Induction of Pluripotent Stem Cells from Adult Human Fibroblasts by Defined Factors.* Cell 131(5):861-72.

Takebe, T., Sekine, K., Enomura, M., Koike, H., Kimura, M., Ogaeri, T., Zhang, R. R., Ueno, Y., Zheng, Y. W., Koike, N., et al. 2013. *Vascularized and functional human liver from an iPSC-derived organ bud transplant.* Nature 499(7459):481-4.

Thomson, J. A. 1998. *Embryonic stem cell lines derived from human blastocysts.* Science 282(5391):1145-7.

Tirziu, D., Giordano, F. J., and Simons, M. 2010. *Cell communications in the heart.* Circulation 122(9):928-37.

Turner, R. R., Beckstead, J. H., Warnke, R. A., and Wood, G. S. 1987. *Endothelial cell phenotypic diversity. In situ demonstration of immunologic and enzymatic heterogeneity that correlates with specific morphologic subtypes.* American Journal of Clinical Pathology 87(5):569-75.

Vargas-Valderrama, A., Messina, A., Mitjavila-Garcia, M. T., and Guenou, H. 2020. *The endothelium, a key actor in organ development and hPSC-derived organoid vascularization.* Journal of Biomedical Science 27:67.

Weber, K. T. 1989. *Cardiac interstitium in health and disease: The fibrillar collagen network.* Journal of the American College of Cardiology 13(7):1637-52.

Winbo, X. A., Ramanan, S., Eugster, E., Jovinge, S., Skinner, J. R., and Montgomery, J. M. 2023. *Functional coculture of sympathetic neurons and cardiomyocytes derived from human-induced pluripotent stem cells.* Am J Physiol Heart Circ Physiol 319(5):H927-H937.

Yona, S., Kim, K. W., Wolf, Y., Mildner, A., Varol, D., Breker, M., Strauss-Ayali, D., Viukov, S., Guilliams, M., Misharin, A., et al. 2013. *Fate Mapping Reveals Origins and Dynamics of Monocytes and Tissue Macrophages under Homeostasis.* Immunity 38(1):79-91.

Zimmermann, W. H., Schneiderbanger, K., Schubert, P., Didié, M., Münzel, F., Heubach, J. F., Kostin, S., Neuhuber, W. L., and Eschenhagen, T. 2002. *Tissue Engineering of a Differentiated Cardiac Muscle Construct.* Circulation Research 90:223–230.

Zipes, D. P., Jalife, J., and Stevenson, W. G. 2017. *Cardiac Electrophysiology: From Cell to Bedside.* Elsevier Health Science: Seventh Edition.

Perspectives for Future Use of Cardiac Microtissues from Human Pluripotent Stem Cells

Authors and Affiliations

Ulgu Arslan, Valeria V. Orlova, Christine L. Mummery*

Department of Anatomy and Embryology, Leiden University Medical Centre, Einthovenweg 20, 2333ZC Leiden, The Netherlands

* Corresponding author: C.L.Mummery@lumc.nl

Published in ACS Biomaterials Science and Engineering, 2022 Nov 14, 8(11):4605-4609.
DOI: 10.1021/acsbiomaterials.1c01296.

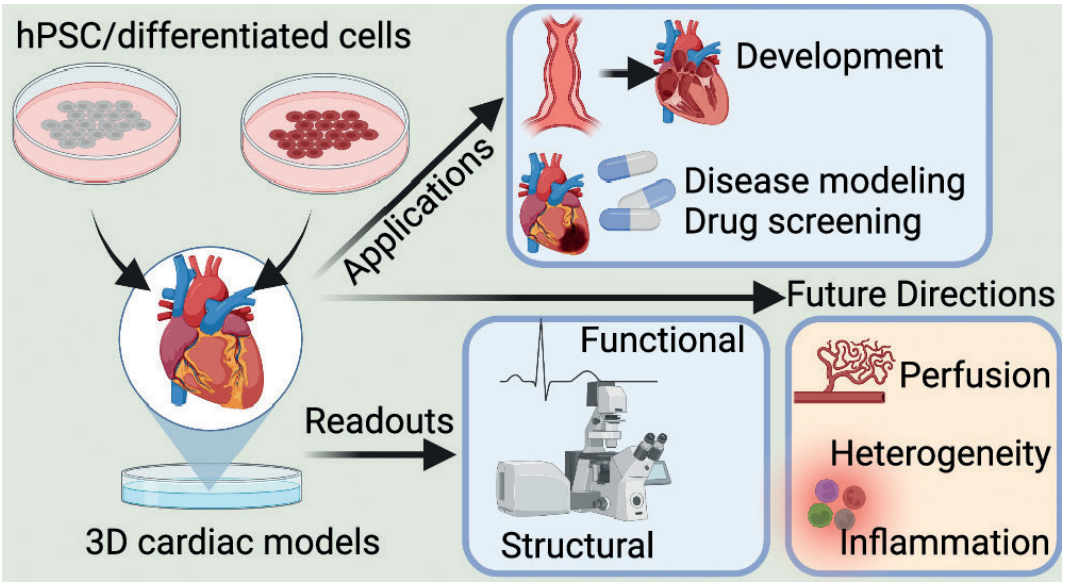

Graphical abstract

Abstract

Cardiovascular disorders remain a critical health issue worldwide. While animals have been used extensively as experimental models to investigate heart disease mechanisms and develop drugs, their inherent drawbacks have shifted focus to more human-relevant alternatives. Human embryonic and induced pluripotent stem cells (hESCs and hiPSCs, collectively called hPSCs) have been identified as a source of different cardiac cells, but to date, they have rarely offered functional and structural maturity of the adult human heart. However, the combination of patient derived hPSCs with microphysiological tissue engineering approaches has presented new opportunities to study heart development and disease and identify drug targets. These models often closely mimic specific aspects of the native heart tissue including intercellular crosstalk and microenvironmental cues such that maturation occurs and relevant disease phenotypes are revealed. Most recently, organ-on-chip technology based on microfluidic devices has been combined with stem cell derived organoids and microtissues to create vascularized structures that can be subjected to fluidic flow and to which immune cells can be added to mimic inflammation of tissue postinjury. Similarly, the integration of nerve cells in these models can provide insight into how the cardiac nervous system affects heart pathology, for example, after myocardial infarction. Here, we consider these models and approaches in the context of cardiovascular disease together with their applications and readouts. We reflect on perspectives for their future implementation in understanding disease mechanisms and the drug discovery pipeline.

Keywords:

pluripotent stem cells, human induced pluripotent stem cells, engineered heart tissue, cardiac microtissues

Introduction

Cell sources for human cardiac models

Animals like mice are tractable experimental models, widely used in biomedical research, to study the effects of disease and drugs. However, their distinct physiology for example in the contraction kinetics and ion channel regulation in the heart, limits translation of outcomes to humans (reviewed in[1]). For this reason, there is increasing interest in developing more relevant models that recapitulate human (patho)physiology. Among these options are human pluripotent stem cells (hPSCS). hPSCs can divide indefinitely in culture and differentiate into all cells of the body including those of the heart. Since the first generation of human embryonic stem cells in 1998[2], research accelerated particularly over the last decade with the advent of somatic cell reprogramming that allows hPSCs to be derived from any healthy individual or patient as human induced pluripotent stem cells (hiPSC)[3]. In many cases, defined media have been designed and become commercially available for robust culture and directed differentiation. To study development and disease

in the human heart, it is now feasible to generate not only beating cardiomyocytes but also the specialized somatic cells of the heart like cardiac fibroblasts and cardiac endothelial cells[4,5]. The heart additionally consists of smooth muscle cells, pericytes, immune cells and (sympathetic/parasympathetic)neurons with different lineage origins (cardiac mesoderm, the proepicardium and cardiac neural crest[6]) some of which can also be generated from hiPSC. When combined in 2D- or 3D formats, intercellular dialogue that is either paracrine or mediated by gap junction formation is initiated between these different cell types[4]. This can result in maturation of the cardiomyocytes which, like most hPSC-derivatives, are immature and fetal-like. As a result, exciting new opportunities are arising to capture features of healthy and diseased human tissues in cell culture, based on stem cells. The challenge now is to transform these modalities into reproducible formats with tailored readouts and sensors to monitor cell physiology, preferably in situ.

2D and 3D cardiac models and their use

The simplest human stem cell cardiac models are 2D monolayer cultures of beating cardiomyocytes. These cells essentially have the full complement of ion channel genes and are widely used for screening potential cardiotoxicity of certain compounds on the heart[7,8]. Certain drugs can cause sudden cardiac death by affecting ion channels (like the HERG channel) and individuals with mutations in ion channel genes can undergo fatal arryhthmia[9]. Other compounds (such as some chemotherapeutics like doxorubicin) can cause heart failure[10].

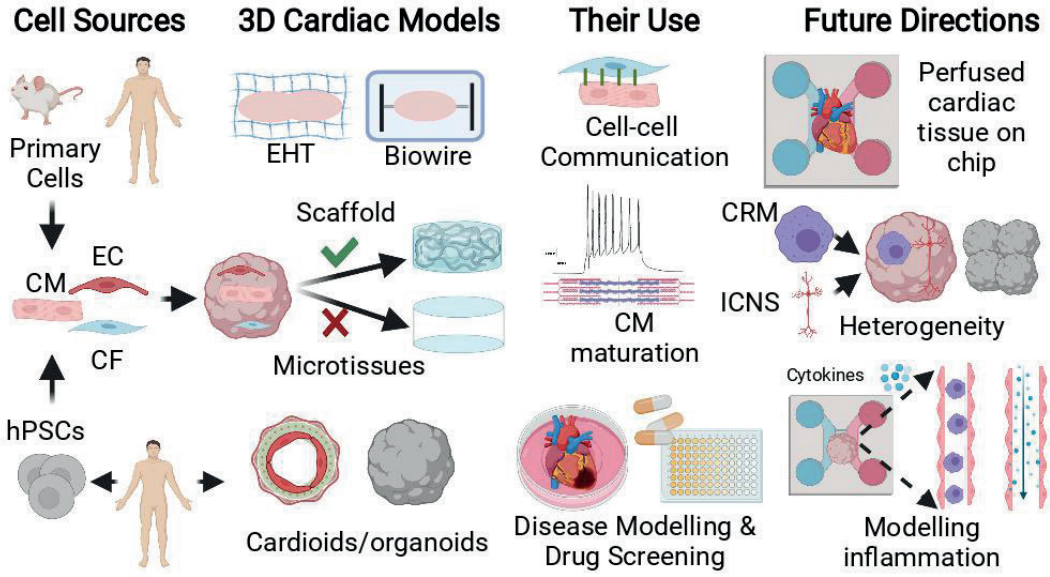

Figure 1: 3D cardiac models, their use and future directions. *hPSC, human pluripotent stem cell; CM, cardiomyocyte; EC, endothelial cell; CF, cardiac fibroblast; EHT, engineered heart tissue; CRM, cardiac resident macrophage; ICNS, intrinsic cardiac nervous system. This figure is created with BioRender.com.*

The immaturity of hPSC-derived cardiomyocytes in 2D monolayer cultures is their drawback for modelling diseases or drug responses that affect the adult heart. In addition, where non-cardiomyocyte cell types contribute to the disease phenotype, then these simple monotypic 2D models might fall short. Here, more complex 3D models that incorporate stromal cells or mechanical and microenvironmental cues may be of value (Figure 1).

These include for example self-organized 3D cardiac microtissues, engineered heart tissues (EHTs) and "biowires" which are assembled from pre-differentiated hPSCs[11,12], or, more recently, "cardioids", derived by directed differentiation of hPSCs as cell aggregates[13] and multi-cell type cardiac organoids[14]. These models recapitulate several features of native heart tissue, such as 3D structure, contractile function, maturation state and development. There are many variants of these basic models (recently reviewed in[15]) but they are essentially the groundwork for future implementation both in academia and in the drug development pipeline. Including perfusable vasculature in these models might increase their functionality even further (as discussed below) and combining (patient) hiPSC-derived cardiac models with Organ-on-Chip devices may enhance wider utility. Current Organ- on-Chip devices generally culture cells or tissues on permeable membranes or in 3D scaffold materials; they are beginning to be used to investigate cardiovascular disease or assess drug responses (reviewed in [16,17]).

Readouts

Several studies have described assays of electrical activity (such as field potential duration measured by microelectrode array[18]), calcium transients (measured semi-automatically using intracellular calcium-sensitive dyes[19]) or contraction (measured using software like MUSCLEMOTION to quantify movement on video images of contracting cardiomyocytes[20]). Simultaneous measurement of action potential, calcium transients and contraction using dyes with appropriate sensitivities ("triple transient measurements"[21]) can predict drug responses in humans particularly accurately in both 2D and 3D models.
Aside from functional analysis of simple and complex human cardiac tissues, assessment of structure can provide useful information on (changes in) cell behaviour, distribution of specific cell types within the culture (for example, extent of self-organisation), cellular crosstalk (for example, through gap junction formation) or cellular (ultra)structure (for example, sarcomere alignment and length). Widefield and confocal microscopy are widely used for this purpose but give low axial resolution and high photo-damage so that imaging live cultures is particularly challenging. Light sheet microscopy (among multiple advanced imaging systems) is an emerging solution to this problem since it allows high speed and precise acquisition of images of (intra-)cellular and tissue structures ranging from microns to millimetres in size[22].

Multicell type disease models

As mentioned above, hPSC can be derived from any individual so that when generated by reprogramming from a patient with an inherited cardiac condition (as hiPSC), it is possible

to create multicell type cardiac microtissues of pre-differentiated cardiomyocytes, cardiac fibroblasts and cardiac endothelial cells from the mutant hiPSC and/or their genetically corrected controls. Isogenic series of microtissues (or EHTs) can thus be generated in which just one of the (three) cells types carry the mutation. In this way, we have shown for example, that for a genetic condition called Arrhythmic CardioMyopathy (ACM) caused by a mutation in the desmosomal PKP2 gene, simply introducing mutant hiPSC-cardiac fibroblasts with healthy control cardiomyocytes and cardiac endothelial cells in a microtissue is sufficient to result in arrhythmias upon electrical pacing at rates >2Hz4. This is despite the cardiomyocytes being normal and indicates the cardiac fibroblasts can be the cellular "co-culprit" in this disease.

Future Directions

From the above we clearly see a wealth of *in vitro* models are now available to study the human heart that may well have benefits over mouse models because the cardiac cellular (patho)physiology is closer to that of patients. As a simple example, the human heart beats at ±60 times per minute, the mouse heart at 5001.

How might we consider making these models of even broader applicability?

Integration of perfusable microvascular networks

Endothelium is essential in the heart as it provides a barrier for selective nutrient, oxygen and drug delivery to heart cells and is involved in immune cell trafficking[23]. Current 3D cardiac organoid and microtissue models often show evidence of organized microvasculature incorporation but usually depend solely on passive diffusion for external molecular and cellular access due to the lack of living or engineered microfluidic channel access. Transplantation of microtissues into live animals has been used as one way to promote vascular network invasion *in vivo* to form functional vasculature[24,25]. Recently however, advanced biofabrication techniques and microfluidic systems like organs-on-chip have been able to offer new opportunities to recapitulate this process *in vitro*. Vasculature can be engineered into tissue models using advanced bioassembly technologies which include micropatterning by 3D bioprinting using synthetic or natural protein scaffolds or scaffold-free printing. Of note, scaffolds may limit cell-to-cell crosstalk within the tissue. Bioprinting usually defines the structural arrangement of cells such that there is coordinated organization of tissue components and these tissue models become perfusable (reviewed in[26]). An alternative to bioprinting, which may be a closer mimic of transplantation *in vivo*, is to pre-vascularize microtissues. This can be done for example by co-culturing (hiPSC-derived) vascular endothelial- and smooth muscle cells with the microtissue components then adding an external vascular network which then self-organizes around- and invades the microtissue. In a microfluidic organ-on-chip device, this would facilitate interconnection with pre- existing microvessels[27]. This is called anastomoses: a biological process where branches of endothelium connect and form a continuous perfusable vascular network in

the body. Intrinsic or extrinsic pro-angiogenic factors can direct endothelial cell growth for anastomoses in these *in vitro* models. When connected to microfluidic flow reservoirs, these systems could support perfusion of small molecules, growth factors, drugs and/or immune cells from the external vascular network, for example to allow better metabolic maturation of the tissue, modelling of inflammation and drug screening.

Integration of other cell types to achieve heterogeneity in 3D models

Even when cell types that enhance complexity and maturation are present in the microtissues, addition of other cell types in different ways may further increase clinical relevance. Cardiac resident macrophages (CRM), for example, regulate the electrical activity of cardiomyocytes by increasing their excitability and decreasing their refractory period through direct connection with cardiomyocytes via gap junctions which contain connexin 43 [28,29]. These maintain cardiac homeostasis by removing, among other things, dysfunctional mitochondria "ejected" by cardiomyocytes[30]. There is compelling evidence for involvement of CRMs in collagen deposition to scar areas after damage and consequent fibrosis[31] and cardiac regeneration[32,33] but their precise role still needs further investigation. In addition, the cardiac autonomic nervous system is a network of neurons that spreads from the brain to the heart and regulates the electrical and mechanical function of the heart34. At the organ level, there is also a rich intrinsic cardiac nervous system (ICNS) which is mainly located in the cardiac ganglia[34]. The ICNS is composed of sensory, motor and interconnecting neurons that contribute to the heart rate, contractility, conduction and blood flow [35]. ICNS involvement in cardiac pathophysiology has been recognized previously[36] and, in some cases, a therapeutic option has been to sever these nerves but the effects of nerve cells in 3D cardiac models *in vitro* are largely unexplored[37,38]. This may help in understanding the dialogue between the nervous system in the heart and the cardiomyocytes.

Finally, tissue or spheroid/microtissue fusion or "stacking" of cardiomyocyte sheets can be used to create mechanical and cellular heterogeneity, by altering cell density and other features such as size, shape and conductivity[39]. This may support elucidation of the role of tissue heterogeneity on structure and function in healthy and diseased states[40] and offer new tools for regenerative medicine[41].

Modelling inflammation in the heart following damage or (infectious) disease

As a response to tissue injury, a complex cascade of events takes place at the injury site which includes trafficking of immune cells, activation of fibroblasts and synthesis of extracellular matrix components. These events suffice for tissue healing in cases of minor and non-repetitive injury. However, where there is severe or repetitive injury, deregulation of the inflammatory response could lead to chronic inflammation and consequently endothelial dysfunction. This is a major contributor to heart failure. Besides genetic factors, cellular heterogeneity and plasticity, cytokine release and dynamic cell-cell crosstalk, for example between CRMs and T cells in infectious diseases or CRMs, cardiac fibroblasts and endothelial

cells in fibrosis, play important roles in mediating the inflammatory response[42,43]. Due to the complex multicellular nature of pathophysiological and specifically human mechanisms underlying inflammation and resulting disease, current *in vivo* models in mice may not be fit-for-purpose. There is therefore still an unmet need for *in vitro* models that can bridge the gap between *in vivo* studies and clinical trials. Taking advantage of microfluidic technologies, incorporation of vasculature, relevant stromal- and immune cells together with microenvironmental cues and perfusion, may provide unique solutions to understand inflammation. Valuable information can thus be accrued on cell-cell interaction and cytokine mediation of the inflammatory response and potential therapeutic targets.

Conclusions

We summarized here various 3D microphysiological systems that have been used to model human heart tissue, including cell sources, applications and readouts. These models are already providing valuable insights into (patho)physiological mechanisms in cardiac development and disease. We also provide a perspective on how these models could be further improved to provide even better mimics of native human heart tissue: incorporating (vascular and immune cell) perfusion, creating greater cellular and mechanical heterogeneity by including non-cardiomyocyte cells types or using tissue fusion techniques. We expect these refinements to the models will enhance their utility for disease modelling and drug screening even further and perhaps support the discovery of treatments for presently incurable conditions of the heart such as chronic heart failure.

Funding Sources

The authors' work is supported by the European Union's Horizon 2020 research and innovation programme under grant agreement No. 812954 and the Netherlands Organ-on-Chip Initiative, an NWO Gravitation project funded by the Ministry of Education, Culture and Science of the government of the Netherlands (024.003.001).

References

1. Janssen, P. M. L.; Biesiadecki, B. J.; Ziolo, M. T.; Davis, J. P. *The Need for Speed: Mice, Men, and Myocardial Kinetic Reserve.* Circ. Res. 2016, 119 (3). https://doi.org/10.1161/CIRCRESAHA.116.309126.
2. Thomson, J. A. *Embryonic Stem Cell Lines Derived from Human Blastocysts.* Science (80-.). 1998. https://doi.org/10.1126/science.282.5391.1145.
3. Takahashi, K.; Tanabe, K.; Ohnuki, M.; Narita, M.; Ichisaka, T.; Tomoda, K.; Yamanaka, S. *Induction of Pluripotent Stem Cells from Adult Human Fibroblasts by Defined Factors.* Cell 2007. https://doi.org/10.1016/j.cell.2007.11.019.
4. Giacomelli, E.; Meraviglia, V.; Campostrini, G.; Cochrane, A.; Cao, X.; van Helden, R. W. J.; Krotenberg Garcia, A.; Mircea, M.; Kostidis, S.; Davis, R. P.; van Meer, B. J.; Jost, C. R.; Koster, A. J.; Mei, H.; Míguez, D. G.; Mulder, A. A.; Ledesma-Terrón, M.; Pompilio, G.; Sala, L.; Salvatori, D. C. F.; Slieker, R. C.; Sommariva, E.; de Vries, A. A. F.; Giera, M.; Semrau, S.; Tertoolen, L. G. J.; Orlova, V. V.; Bellin, M.; Mummery, C. L. *Human-IPSC-Derived Cardiac Stromal Cells Enhance Maturation in 3D Cardiac Microtissues and Reveal Non-Cardiomyocyte Contributions to Heart Disease.* Cell Stem Cell 2020. https://doi.org/10.1016/j.stem.2020.05.004.
5. Giacomelli, E.; Bellin, M.; Sala, L.; Meer, B. J. van; Tertoolen, L. G. J.; Orlova, V. V; Mummery, C. L. *Three-Dimensional Cardiac Microtissues Composed of Cardiomyocytes and Endothelial Cells Co-Differentiated from Human Pluripotent Stem Cells.* Development 2017, 144 (6), 1008–1017. https://doi.org/10.1242/dev.143438.
6. Brade, T.; Pane, L. S.; Moretti, A.; Chien, K. R.; Laugwitz, K. L. *Embryonic Heart Progenitors and Cardiogenesis.* Cold Spring Harbor Perspectives in Medicine. 2013. https://doi.org/10.1101/cshperspect.a013847.
7. Brandao, K. O.; Tabel, V. A.; Atsma, D. E.; Mummery, C. L.; Davis, R. P. *Human Pluripotent Stem Cell Models of Cardiac Disease: From Mechanisms to Therapies*. DMM Disease Models and Mechanisms. 2017. https://doi.org/10.1242/dmm.030320.
8. Giacomelli, E.; Mummery, C. L.; Bellin, M. *Human Heart Disease: Lessons from Human Pluripotent Stem Cell-Derived Cardiomyocytes.* Cell. Mol. Life Sci. 2017, 74 (20), 3711–3739. https://doi.org/10.1007/s00018-017-2546-5.
9. Recanatini, M.; Poluzzi, E.; Masetti, M.; Cavalli, A.; De Ponti, F. *QT Prolongation through HERG K+ Channel Blockade: Current Knowledge and Strategies for the Early Prediction during Drug Development.* Medicinal Research Reviews. 2005. https://doi.org/10.1002/med.20019.
10. Octavia, Y.; Tocchetti, C. G.; Gabrielson, K. L.; Janssens, S.; Crijns, H. J.; Moens, A. L. *Doxorubicin-Induced Cardiomyopathy: From Molecular Mechanisms to Therapeutic Strategies.* Journal of Molecular and Cellular Cardiology. 2012. https://doi.org/10.1016/j.yjmcc.2012.03.006.
11. Nunes, S. S.; Miklas, J. W.; Liu, J.; Aschar-Sobbi, R.; Xiao, Y.; Zhang, B.; Jiang, J.; Massé, S.; Gagliardi, M.; Hsieh, A.; Thavandiran, N.; Laflamme, M. A.; Nanthakumar, K.; Gross, G. J.; Backx, P. H.; Keller, G.; Radisic, M. *Biowire: A Platform for Maturation of Human Pluripotent Stem Cell-Derived Cardiomyocytes.* Nat. Methods 2013, 10 (8), 781–787. https://doi.org/10.1038/nmeth.2524.

12. Feric, N. T.; Pallotta, I.; Singh, R.; Bogdanowicz, D. R.; Gustilo, M. M.; Chaudhary, K. W.; Willette, R. N.; Chendrimada, T. P.; Xu, X.; Graziano, M. P.; Aschar-Sobbi, R. *Engineered Cardiac Tissues Generated in the Biowire II: A Platform for Human-Based Drug Discovery.* Toxicol. Sci. 2019, 172 (1), 89–97. https://doi.org/10.1093/toxsci/kfz168.
13. Hofbauer, P.; Jahnel, S. M.; Papai, N.; Giesshammer, M.; Deyett, A.; Schmidt, C.; Penc, M.; Tavernini, K.; Grdseloff, N.; Meledeth, C.; Ginistrelli, L. C.; Ctortecka, C.; Šalic, Š.; Novatchkova, M.; Mendjan, S. *Cardioids Reveal Self-Organizing Principles of Human Cardiogenesis.* Cell 2021, 184 (12). https://doi.org/10.1016/j.cell.2021.04.034.
14. Lewis-Israeli, Y. R.; Wasserman, A. H.; Gabalski, M. A.; Volmert, B. D.; Ming, Y.; Ball, K. A.; Yang, W.; Zou, J.; Ni, G.; Pajares, N.; Chatzistavrou, X.; Li, W.; Zhou, C.; Aguirre, A. *Self-Assembling Human Heart Organoids for the Modeling of Cardiac Development and Congenital Heart Disease.* Nat. Commun. 2021, 12 (1). https://doi.org/10.1038/s41467-021-25329-5.
15. Stein, J. M.; Mummery, C. L.; Bellin, M. *Engineered Models of the Human Heart: Directions and Challenges.* Stem Cell Reports. 2021. https://doi.org/10.1016/j.stemcr.2020.11.013.
16. Paloschi, V.; Sabater-Lleal, M.; Middelkamp, H.; Vivas, A.; Johansson, S.; van der Meer, A.; Tenje, M.; Maegdefessel, L. *Organ-on-a-Chip Technology: A Novel Approach to Investigate Cardiovascular Diseases.* Cardiovasc. Res. 2021, 117 (14). https://doi.org/10.1093/cvr/cvab088.
17. Ribas, J.; Sadeghi, H.; Manbachi, A.; Leijten, J.; Brinegar, K.; Zhang, Y. S.; Ferreira, L.; Khademhosseini, A. *Cardiovascular Organ-on-a-Chip Platforms for Drug Discovery and Development.* Appl. Vitr. Toxicol. 2016, 2 (2). https://doi.org/10.1089/aivt.2016.0002.
18. Tertoolen, L. G. J.; Braam, S. R.; van Meer, B. J.; Passier, R.; Mummery, C. L. *Interpretation of Field Potentials Measured on a Multi Electrode Array in Pharmacological Toxicity Screening on Primary and Human Pluripotent Stem Cell-Derived Cardiomyocytes.* Biochem. Biophys. Res. Commun. 2018, 497 (4), 1135–1141. https://doi.org/10.1016/J.BBRC.2017.01.151.
19. Halaidych, O. V.; Cochrane, A.; van den Hil, F. E.; Mummery, C. L.; Orlova, V. V. *Quantitative Analysis of Intracellular Ca 2+ Release and Contraction in HiPSC-Derived Vascular Smooth Muscle Cells.* Stem Cell Reports 2019, 12 (4). https://doi.org/10.1016/j.stemcr.2019.02.003.
20. van Meer, B. J.; Sala, L.; Tertoolen, L. G. J.; Smith, G. L.; Burton, F. L.; Mummery, C. L. *Quantification of Muscle Contraction In Vitro and In Vivo Using MUSCLEMOTION Software: From Stem Cell-Derived Cardiomyocytes to Zebrafish and Human Hearts.* Curr. Protoc. Hum. Genet. 2018, 99 (1), e67. https://doi.org/10.1002/cphg.67.
21. van Meer, B. J.; Krotenberg, A.; Sala, L.; Davis, R. P.; Eschenhagen, T.; Denning, C.; Tertoolen, L. G. J.; Mummery, C. L. *Simultaneous Measurement of Excitation-Contraction Coupling Parameters Identifies Mechanisms Underlying Contractile Responses of HiPSC-Derived Cardiomyocytes.* Nat. Commun. 2019, 10 (1), 1–9. https://doi.org/10.1038/s41467-019-12354-8.
22. Fei, P.; Lee, J.; Packard, R. R. S.; Sereti, K.; Xu, H.; Ma, J.; Ding, Y.; Kang, H.; Chen, H.; Sung, K.; Kulkarni, R.; Ardehali, R.; Kuo, C. J.; Xu, X.; Ho, C.; Hsiai, T. K. *Cardiac Light-Sheet Fluorescent Microscopy for Multi-Scale and Rapid Imaging of Architecture and Function.* Sci. Rep. 2016, 6 (1), 0–12. https://doi.org/10.1038/srep22489.

23. Aird, W. C. Phenotypic Heterogeneity of the Endothelium: I. *Structure, Function, and Mechanisms. Circulation Research.* 2007. https://doi.org/10.1161/01.RES.0000255691.76142.4a.
24. Mansour, A. A.; Gonçalves, J. T.; Bloyd, C. W.; Li, H.; Fernandes, S.; Quang, D.; Johnston, S.; Parylak, S. L.; Jin, X.; Gage, F. H. *An in Vivo Model of Functional and Vascularized Human Brain Organoids.* Nat. Biotechnol. 2018, 36 (5). https://doi.org/10.1038/nbt.4127.
25. Takebe, T.; Sekine, K.; Enomura, M.; Koike, H.; Kimura, M.; Ogaeri, T.; Zhang, R. R.; Ueno, Y.; Zheng, Y. W.; Koike, N.; Aoyama, S.; Adachi, Y.; Taniguchi, H. *Vascularized and Functional Human Liver from an IPSC-Derived Organ Bud Transplant.* Nature 2013, 499 (7459). https://doi.org/10.1038/nature12271.
26. Harley, W. S.; Li, C. C.; Toombs, J.; O'Connell, C. D.; Taylor, H. K.; Heath, D. E.; Collins, D. J. *Advances in Biofabrication Techniques towards Functional Bioprinted Heterogeneous Engineered Tissues: A Comprehensive Review.* Bioprinting. 2021. https://doi.org/10.1016/j.bprint.2021.e00147.
27. Zhang, S.; Wan, Z.; Kamm, R. D. *Lab on a Chip CRITICAL REVIEW Vascularized Organoids on a Chip: Strategies for Engineering Organoids with Functional Vasculature.* 2021, 21, 473. https://doi.org/10.1039/d0lc01186j.
28. Hulsmans, M.; Clauss, S.; Xiao, L.; Aguirre, A. D.; King, K. R.; Hanley, A.; Hucker, W. J.; Wülfers, E. M.; Seemann, G.; Courties, G.; Iwamoto, Y.; Sun, Y.; Savol, A. J.; Sager, H. B.; Lavine, K. J.; Fishbein, G. A.; Capen, D. E.; Da Silva, N.; Miquerol, L.; Wakimoto, H.; Seidman, C. E.; Seidman, J. G.; Sadreyev, R. I.; Naxerova, K.; Mitchell, R. N.; Brown, D.; Libby, P.; Weissleder, R.; Swirski, F. K.; Kohl, P.; Vinegoni, C.; Milan, D. J.; Ellinor, P. T.; Nahrendorf, M. *Macrophages Facilitate Electrical Conduction in the Heart.* Cell 2017. https://doi.org/10.1016/j.cell.2017.03.050.
29. Harari, E.; Guo, L.; Smith, S. L.; Braumann, R. E.; Virmani, R.; Finn, A. V. *Heart-Resident Macrophages: Are They Involved in the Rhythm of Every Beat?* J. Thorac. Dis. 2017, 9 (8), 2264–2267. https://doi.org/10.21037/jtd.2017.07.43.
30. José Nicolá s-A, A. A.; Lechuga-Vieco, A. V; Esteban-Martínez, L.; Bernal, J. A.; Enríquez, J. A.; Hidalgo, A.; Nicolá s-A, J. A.; Sá nchez-Díaz, M.; Díaz-García, E.; Santiago, D. J.; Rubio-Ponce, A.; LiangYao Li, J.; Balachander, A.; Quintana, J. A.; Martínez-de-Mena, R.; Castejó n-Vega, B.; Pun-García, A.; Travé, P. G.; Bonzó n-Kulichenko, E.; García-Marqué, F.; Cussó, L.; A-Gonzá lez, N.; Gonzá lez-Guerra, A.; Roche-Molina, M.; Martin-Salamanca, S. *A Network of Macrophages Supports Mitochondrial Homeostasis in the Heart.* Cell 2020, 183, 94–109. https://doi.org/10.1016/j.cell.2020.08.031.
31. Simões, F. C.; Cahill, T. J.; Kenyon, A.; Gavriouchkina, D.; Vieira, J. M.; Sun, X.; Pezzolla, D.; Ravaud, C.; Masmanian, E.; Weinberger, M.; Mayes, S.; Lemieux, M. E.; Barnette, D. N.; Gunadasa-Rohling, M.; Williams, R. M.; Greaves, D. R.; Trinh, L. A.; Fraser, S. E.; Dallas, S. L.; Choudhury, R. P.; Sauka-Spengler, T.; Riley, P. R. *Macrophages Directly Contribute Collagen to Scar Formation during Zebrafish Heart Regeneration and Mouse Heart Repair.* Nat. Commun. 2020, 11 (1). https://doi.org/10.1038/s41467-019-14263-2.
32. Farache Trajano, L.; Smart, N. *Immunomodulation for Optimal Cardiac Regeneration: Insights from Comparative Analyses.* npj Regen. Med. 2021, 6 (1), 1–11. https://doi.org/10.1038/s41536-021-00118-2.

33. Nahrendorf, M.; Swirski, F. K.; Aikawa, E.; Stangenberg, L.; Wurdinger, T.; Figueiredo, J. L.; Libby, P.; Weissleder, R.; Pittet, M. J. *The Healing Myocardium Sequentially Mobilizes Two Monocyte Subsets with Divergent and Complementary Functions.* J. Exp. Med. 2007. https://doi.org/10.1084/jem.20070885.
34. Ardell, J. L.; Armour, J. A. *Neurocardiology: Structure-Based Function.* In Comprehensive Physiology; John Wiley & Sons, Inc.: Hoboken, NJ, USA, 2016; Vol. 6, pp 1635–1653. https://doi.org/10.1002/cphy.c150046.
35. Zipes, D. P.; Jalife, J.; Stevenson, W. G. *Cardiac Electrophysiology: From Cell to Bedside:* Seventh Edition; 2017. https://doi.org/10.1161/01.cir.0000146800.76451.65.
36. Wake, E.; Brack, K. *Characterization of the Intrinsic Cardiac Nervous System.* Auton. Neurosci. 2016, 199, 3–16. https://doi.org/10.1016/j.autneu.2016.08.006.
37. Das, S.; Gordián-Vélez, W. J.; Ledebur, H. C.; Mourkioti, F.; Rompolas, P.; Chen, H. I.; Serruya, M. D.; Cullen, D. K. *Innervation: The Missing Link for Biofabricated Tissues and Organs.* npj Regenerative Medicine. Nature Research December 1, 2020. https://doi.org/10.1038/s41536- 020-0096-1.
38. Soucy, J. R.; Bindas, A. J.; Brady, R.; Torregrosa, T.; Denoncourt, C. M.; Hosic, S.; Dai, G.; Koppes, A. N.; Koppes, R. A. *Reconfigurable Microphysiological Systems for Modeling Innervation and Multitissue Interactions.* Adv. Biosyst. 2020, 4 (9). https://doi.org/10.1002/adbi.202000133.
39. Kim, T. Y.; Kofron, C. M.; King, M. E.; Markes, A. R.; Okundaye, A. O.; Qu, Z.; Mende, U.; Choi, B. R. *Directed Fusion of Cardiac Spheroids into Larger Heterocellular Microtissues Enables Investigation of Cardiac Action Potential Propagation via Cardiac Fibroblasts.* PLoS One 2018, 13 (5), e0196714. https://doi.org/10.1371/journal.pone.0196714.
40. Daly, A. C.; Davidson, M. D.; Burdick, J. A. *3D Bioprinting of High Cell-Density Heterogeneous Tissue Models through Spheroid Fusion within Self-Healing Hydrogels.* Nat. Commun. 2021, 12 (1). https://doi.org/10.1038/s41467-021-21029-2.
41. Shimizu, T.; Sekine, H.; Yamato, M.; Okano, T. *Cell Sheet-Based Myocardial Tissue Engineering: New Hope for Damaged Heart Rescue.* Curr. Pharm. Des. 2009, 15 (24). https://doi.org/10.2174/138161209788923822.
42. Shah, S. J.; Borlaug, B. A.; Kitzman, D. W.; McCulloch, A. D.; Blaxall, B. C.; Agarwal, R.; Chirinos, J. A.; Collins, S.; Deo, R. C.; Gladwin, M. T.; Granzier, H.; Hummel, S. L.; Kass, D. A.; Redfield, M. M.; Sam, F.; Wang, T. J.; Desvigne-Nickens, P.; Adhikari, B. B. Research *Priorities for Heart Failure with Preserved Ejection Fraction: National Heart, Lung, and Blood Institute Working Group Summary. Circulation.* 2020. https://doi.org/10.1161/CIRCULATIONAHA.119.041886.
43. Henderson, N. C.; Rieder, F.; Wynn, T. A. *Fibrosis: From Mechanisms to Medicines.* Nature. 2020. https://doi.org/10.1038/s41586-020-2938-9.

Microphysiological Stem Cell Models of The Human Heart

Authors and Affiliations

Ulgu Arslan[1*], Alessia Moruzzi[2,3*], Joanna Nowacka[4*], Christine Mummery[1], Dominik Eckardt[4#], Peter Loskill[2,3,5#], Valeria Orlova[1#]

[1] Department of Anatomy and Embryology, Leiden University Medical Centre, Leiden, The Netherlands

[2] NMI Natural and Medical Sciences Institute at the University of Tübingen, Reutlingen, Germany

[3] Institute for Biomedical Engineering, Eberhard Karls University Tübingen, Tübingen, Germany

[4] Miltenyi Biotec B.V. & Co. KG, Bergisch Gladbach, Germany

[5] 3R-Center for *In vitro* Models and Alternatives to Animal Testing, Tübingen, Germany

* and # Contributed equally

Correspondence to dominike@miltenyi.com, peter.loskill@uni-tuebingen.de or v.orlova@lumc.nl

Published in Materials Today Bio, 2022 Apr 14, 14:100259.
DOI: 10.1016/j.mtbio.2022.100259

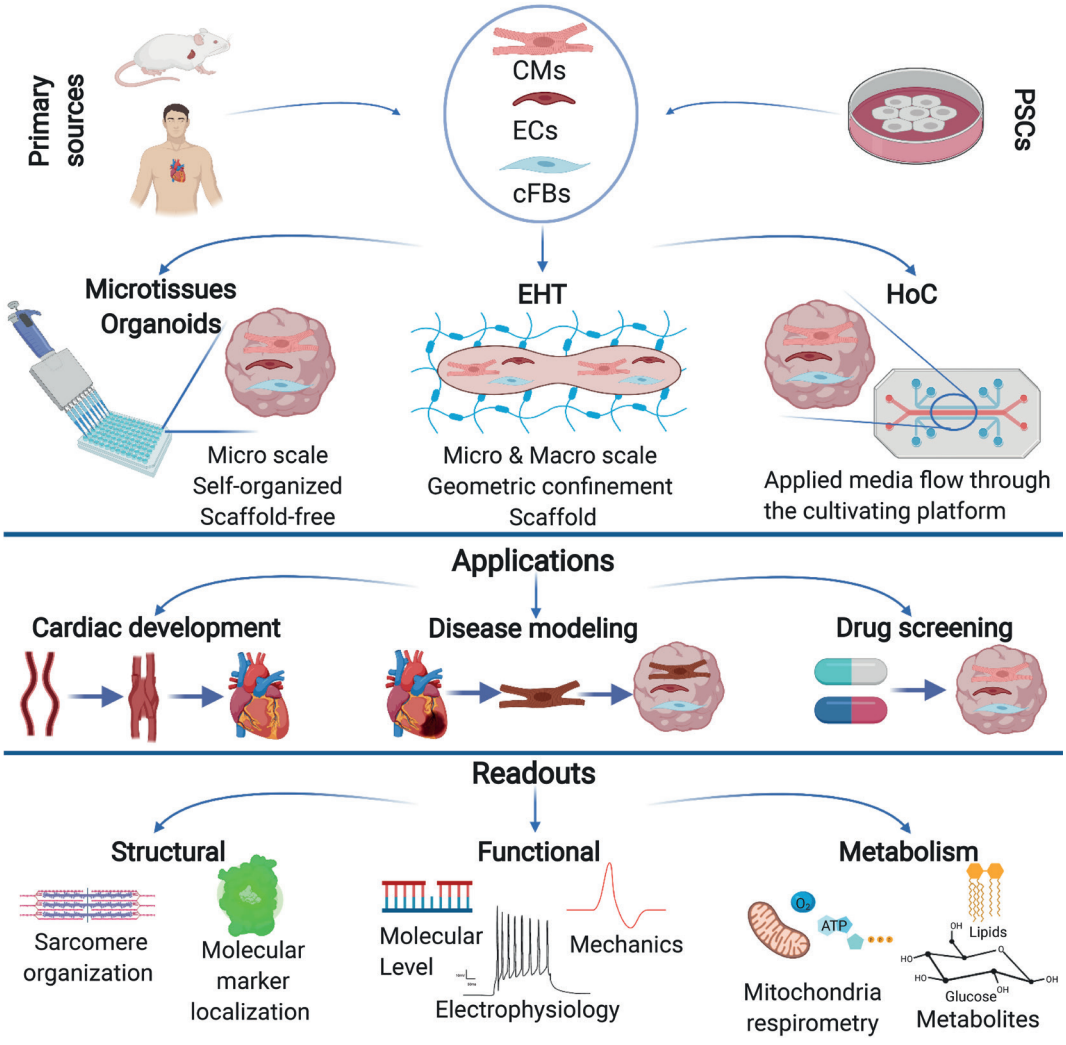

Graphical abstract

Abstract

Models of heart disease and drug responses are increasingly based on pluripotent stem cells (hPSCs) since their ability to capture human heart (dys-)function is often better than animal models. Simple monolayer cultures of hPSC-derived cardiomyocytes, however, have shortcomings. Some of these can be overcome using more complex, multi cell-type models in 3D. Here we review modalities that address this, describe efforts to tailor readouts and sensors for monitoring tissue- and cell physiology (exogenously and in situ) and discuss perspectives for implementation in industry and academia.

Keywords:

human induced pluripotent stem cells; cardiac microtissue; engineered heart tissue; heart-on-chip; cardiomyocyte maturation; multicellular cell diseases and drug efficacy platform; structural readout; functional readout.

1. Introduction

Animal models have been very useful in understanding how the heart develops and the molecular mechanisms underlying congenital heart defects. They have been less successful in identifying the genetic and other causes of cardiac dysfunction or predicting the effects of drugs, largely because of differences in animal and human physiology. The advent of human pluripotent stem cells (hPSCs) [1,2] has however opened new avenues to study the human heart and its pathologies. We review here state-of-the-art models now being used to investigate the human heart, how they are being used to monitor human heart (patho-) physiology, their shortcomings and the expectations for the future.

Cardiomyocytes (CM) were among the first cell types to be differentiated from hPSCs [3,4], specifically from human embryonic stem cells (hESC). Differentiation protocols initially entailed culture of undifferentiated cells as aggregates in suspension, called "embryoid bodies", in the presence of growth factors. Since these first reports, many groups have developed methods to differentiate CMs in 2D (reviewed in [5]) and to form three dimensional (3D) cardiac tissues (table 1). Whilst strikingly evident because of their cyclic contraction, at most 5% of the differentiated cells were initially CMs. This meant that most analysis was based on methods suitable for single cells such as patch clamp electrophysiology and immunostaining of sarcomeric proteins. hPSC-derived CMs (hPSC-CMs) were also immature compared to primary adult CMs with respect to their morphology, contractility, electrophysiology, metabolism and gene expression [6–8]. Nevertheless, various studies have shown that hPSC-CMs can be valuable for disease modelling and drug screening even if the CMs are immature, especially if they are derived as hiPSC from patients [9–13]. Notably, all cardiac ion channels are expressed in hPSC-CMs so that modelling channelopathies caused by mutations in ion channel genes has been particularly successful. hiPSC carry the genetic background of the individuals from whom they are derived and thus allow diseased

genomes or disease predisposition to be captured in the derivative cardiac cell types; they thus support more personalized approaches to disease modelling and drug screening.
hPSC-CM immaturity has, however, been a challenge to modelling disease other than channelopathies and improving maturation state has been studied extensively over the last several years. Several reports have shown that culturing hPSC-CMs in 3D, mimicking the environment of cardiac tissue *in vivo*, improves the physiological and functional properties of CMs compared to 2D monolayers [14–16]. Moreover, if these 3D models also capture the complexity of native heart tissue, such as the communication between CMs and cardiac stromal- and vascular cells, then maturation is improved even further [17–20]. Initially, primary endothelial cells (EC) such as those from human umbilical vein (HUVECs), or dermal fibroblasts (FB) were used in these 3D models but more recently it has been possible to generate ECs (specifically cardiac ECs) and cardiac FBs (cFB) from hPSC [18,21,22]. These have been combined in different ratios with CMs in microphysiological heart tissues (MHTs) (table 1). The results broadly showed benefits for hPSC-CM maturation using cFB rather than dermal FBs and that this was mediated by junctional coupling with CMs [18]. 3D MHTs not only offer the advantage of being able to integrate multiple cell types but also microenvironmental cues, such as forced electrical or mechanical "pacing" or those mediated by the tissue scaffold, to closely mimic native heart. In this review, we first describe current MHT models, then summarize their applications with an overview of structural and functional readouts that can be used to report (patho-)physiology and drug/compound responses. Finally, we discuss how the field might move forward in refining and implementing these in the near future.

2. Current Microphysiological Tissue Models

MHTs can be broadly divided into three types: those based on self-organized aggregates of cells (also referred to as spheroids, microtissues or organoids), those relying on biomaterials and bioengineering (engineered heart tissues (EHT)) and finally those in which perfusion can be integrated (Heart-on-chip). Human MHT models together with their cell sources, applications and readouts are summarized in tables 1-3. These tables are based on the selection from many studies in the field with a focus on more recent studies.

Microtissues (or spheroids) and organoids commonly refer to 3D tissue models although these terms are not always used as originally described. Lancaster and Knoblich defined organoids as "self- organized tissues that develop from PSCs or progenitor cells by recapitulation of embryonic development" [23]. The term "spheroid" has traditionally been used to describe aggregates of terminally differentiated cells. Subsequently though, many groups used the word "organoid" to describe any collection of PSCs or adult SCs that were differentiated into region specific cells of the organ with the help of growth factors (reviewed in [24]). For the heart, all three terms have been used as well as "cardioids" to describe beating aggregates of differentiated hPSCs whether they have formed spontaneously or have been created by mixing multiple pre-differentiated heart cell types. These beating aggregates can be formed entirely scaffold-free, e. g. on a non-adhesive surface (see reviews

[25–27] where cFBs produce their own extracellular matrix (ECM), or by integration of natural ECM or substitute scaffolds (e.g. hydrogels). These models generally have different applications and some are useful for studying early heart development [28–30] but it is of note that unlike for many organs, organoids cannot be formed from stem cells in the adult heart since despite earlier claims, it does not seem that such a population is present to any extent after birth [31]. This may in part explain why the adult mammalian heart repairs poorly after damage.

Integration of biomaterials and tissue engineering principles provides environmental cues that further benefit tissue organization, cell-cell communication and results in elasticity properties close to the human heart [32–35]. One of the first EHTs was generated by seeding a mixture of cells and extracellular matrix around Velcro-coated glass posts which allowed contraction of tissues against resistance. These structures resembled *in vivo* cardiac muscle fibers and allowed direct measurement of contraction force from deflection of the posts [36]. Several groups adopted and improved this simple yet effective system to quantify the change in contractile force of tissues, for example upon external metabolic or electromechanical stimulus (reviewed in [37]).

Two main strategies were employed to generate the EHTs - geometric confinement and mechanical load. Providing appropriate geometric confinement to the tissue is important for tissue morphology and functionality. For example, a rectangular frame induced CMs to exhibit a more rod-shape morphology, uniaxial calcium flow and improved sarcomeric organization compared to square frames or monolayer cultures in multi-well plates [6,38]. In addition, physiological mechanical stretching is important for tissue development and maturation [39–41].

Microtissues and EHTs can recapitulate several physiological features of heart muscle tissue (multiple cell types, typical contraction rates, 3D structure). However, they lack perfusable vessel-like structures, which *in vivo* transport oxygen, nutrients and cells. Organ-on-chip (OoC) technologies offer opportunities to integrate perfusion through microfluidics and study neovasculogenesis of the tissue constructs; vessel structures and transport processes are thus created much like those *in vivo* (reviewed in [42–44]).

Heart-on-chip systems (HoCs) are typically devices made of polymer modules featuring microscale networks of channels and chambers. The chambers commonly house the microtissues, while the channels act as ducts that supply the tissues with nutrients, growth factors, gases, soluble compounds and (blood or immune) cells. The tissue chambers can be separated by a semi- permeable barrier (e.g. micro-channels or porous membranes) from the direct flow of fluid to protect the tissues from sheer stress, yet allow perfusion of nutrients [45–48]. Some HoCs allow detection of contractile forces by introducing cantilevers that moved with CM contraction [49]. They integrate cyclic mechanic stimulation mimicking contraction of the heart which in turn induces the pulsating flow [45] or electrical pacing [50]. Depending on the targeted research question and experimental requirements, chip designs might differ from one another to suit the specific purpose but ultimately tailored

or in-house designs create challenges for standardization. There are a number of systems now commercially available that address this to some extent by ensuring that at least the manufacturing process is standardized.

Collectively, MHT models are poised to advance the cardiovascular field as their potential to study CM maturation and disease models and carry out drug screening begins to be exploited.

3. Applications

Aside from supporting CM maturation, MHTs are already being implemented in several areas including some mentioned above: studying cardiogenesis, investigating disease mechanisms, identifying which cardiac cell types are responsible for pathophysiology, assessing cardiotoxicity and identifying potential drug therapies. For all applications, models from any of the three MHT categories might be most suitable depending on the specific research questions. The model of choice should be as simple as possible but as complex as necessary.

3.1 Mediating cardiomyocyte maturation

One application of MHT models is to study intercellular communication in the heart which is important for heart development and maturation. Integration of CMs with ECs into microtissues improved structure and functionality of hPSC-CM [51]. Inclusion of cFBs enhanced CM maturation in their contraction force and frequency, gene expression, Ca2+ handling, sarcomere assembly and β-adrenergic receptor signaling proteins [17,18]. In addition, 3D tissue formats prevented cFBs forming stress fibers compared to monolayer cultures and eliminated profibrotic growth factors for cFB activation and trans-differentiation into myofibroblasts [17]. Furthermore, combining all three cell types (CMs, ECs and cFBs) in these tissues increased intracellular cAMP levels in CMs through CM-
31

cFB crosstalk; this was further enhanced by Endothelin-mediated signaling from ECs to CMs [18]. Together, this resulted in better assembly of Connexin43 (Cx43) gap junctions and further promoted maturation of CMs. This was in line with *in vivo* studies [52]. Crosstalk between CMs and FBs and resulting maturation was not seen when dermal FBs replaced cFBs [18]. Dermal FBs express low or negligible levels of Cx43, depending on the particular batch which might explain why they are less effective in mediating maturation compared to cFBs. However, other tissue sources of FBs may express Cx43 and promote maturation. In addition, any paracrine effects of FBs may be independent of Cx43.
In addition to co-culture, other approaches to tissue maturation have used EHTs, in which systematic optimization of ECM components and regulation of exogenous mechanical- and metabolic factors (including energy substrates) have resulted in significant benefit [41,53–55].

These studies demonstrated that multiple cues must be carefully orchestrated to govern distinct aspects of the adult CM phenotype. Therefore, although much progress has been made and there are multiple ways to induce a postnatal CM phenotype, none is yet definitive and obtaining fully mature/adult CMs in MHTs (or any other model) remains a challenge.

3.2 Disease Modelling

2D hPSC-CMs are easy to generate and use and are adequate for modeling ion channelopathies and cardiomyopathies caused by specific mutations, as mentioned earlier [51]. However, for more complex disorders, MHTs provide better structural, functional and metabolic maturation as well as allowing integration of multiple cell types and simulation of environmental conditions. These 3D models have also been used for studying inflammation subsequent to myocardial infarction or other injury [20,56]; or fibrosis [57,58].

Bacterial or viral infection can affect the heart. Severe acute respiratory syndrome coronavirus (SARS- CoV-2) infection causes coronavirus disease (COVID-19). Many groups worldwide are investigating viral infection and disease mechanisms using human stem cell models. Although the predominant pathology is observed in the respiratory system, several studies have shown that the cardiovascular system is also affected by this virus [59,60]. 20-30% of all COVID-19 patients suffer from severe cardiac symptoms and increased levels of cardiac protein troponin I in their blood which indicates heart damage and is linked to increased risk of morbidity [61,62]. 3D culture systems discussed here are also increasingly used to investigate how inflammation causes heart damage and the effects of therapy on the heart [63–65].

Taking advantage of the ability to integrate differentiated cardiac cells from healthy- (genetically corrected) and patient derived hiPSCs, multiple cardiac pathologies such as hypertrophy [66–68], arrhythmogenic cardiomyopathy [18], long QT syndrome type 3 (LQT3) [33] and Barth syndrome [69] have been modelled using different MHTs. Aside from providing insights into disease mechanisms, they have also been used to identify potential therapeutics [69,70].

These models are potentially useful for providing insights into disease mechanism but to date they have lacked immune/inflammatory cells, involved in triggering or sustaining these pathological processes [71], or nerve cells that can invade heart excessively and cause arrhythmias after myocardial infarction [72].

3.3 Cardiotoxicity assessment

Cardiotoxicity is still a major reason that drugs in development fail to reach the clinic or are labelled as high risk after market entry. Rodents do not always accurately predict drug effects on humans because the physiological parameters like contraction kinetics such as the beat rate of the human heart differ significantly from those in widely used laboratory animals (reviewed in [73]). In addition, direct translation of drug efficacy and toxicology from rodents to humans is limited due to differences in pharmacokinetic properties. Large

animals such as non-human primates or dogs are more predictive but have financial and ethical burdens. Alternative models to animals are thus of growing interest.

One of the first major milestones towards using hiPSC-CMs among these alternatives is the Comprehensive *in vitro* Proarrhythmia Assay (CiPA) initiative, a collaboration between academia, pharmaceutical industries, regulatory authorities and stem cell companies [74]. This showed a good correlation between the assay outcome in hiPSC-CMs and known toxicity in humans. In a Iater study, simultaneous measurement of contraction kinetics, action potentials and Ca2+ transients using voltage and calcium- sensitive dyes, was shown to be even more predictive of cardiac toxicity [75,76]. It is an ongoing effort to assess the drug-induced proarrhythmic risk using hiPSC-CMs and emerging *in vitro/in silico* assays. Collectively, these studies provided evidence that assays based on hiPSC-CMs could eventually replace traditional toxicology studies with the combination of 3D *in vitro* models and *in silico* tools.

MHT platforms are also being used to test functional toxicity of a number of drugs [21,77,78]. In these studies, tissues exhibited alterations in cardiac contraction in response to inotropic or non- inotropic drugs with an ability to predict *in vivo* outcome with high sensitivity and specificity [21]. Moreover, these models were able to distinguish between negative and positive inotropic compounds as opposed to previous studies on hiPSC-CM monolayer cultures [79]. This confirmed improved accuracy of risk assessment for a spectrum of compounds. Structural cardiotoxicity of FDA approved compounds was also assessed [80]. Morphological assessment of drug-exposed MHTs showed changes in structural integrity and cellular viability. Together, these studies revealed the potential value of MHTs in drug screening even though, because of their size and formats, they are not yet suitable for large scale compound screens. Pharmaceutical companies are increasingly adopting MHTs and more specifically OoC platforms for drug effectivity assessment and disease modelling [81] with current efforts on more standardized protocols.

Addressing drug metabolization and multi-organ effects, especially in OoC platforms integrating multiple organ systems with perfusion, are providing new opportunities to evaluate possible side effects of drug treatment and off-target tissues. For example, a heart-liver-lung multi-organ on chip platform showed that bleomycin, an anti-cancer drug that causes lung inflammation, also induced cardiotoxicity [82]. Another example was described by Lee at al. (2021), who connected HoC to a breast-cancer-on-chip to examine chemotherapy induced cardiotoxicity [83]. Combining cancer patient-derived hiPSC-CMs in this model could in the future aid prediction of individual cardiotoxic risk.

3.4 Development of cardiac therapeutics

Complementary studies also used hiPSC-CMs to predict drug-induced electrophysiological- and contractile changes (reviewed in [84]). 2D hiPSC-CMs and 3D EHTs [85,86] were compared for their (blinded) response to a list of known drugs. This resulted in highest

predictivity and sensitivity from 3D-EHTs based on measuring force of contraction although combined measurement of contraction, action potential and calcium transients in 2D hiPSC-CM monolayer culture also gave high predictivity as mentioned above [76,84]. Several EHT and HoC drug screening platforms are scalable and have shown drug responses comparable to *in vivo* clinical observations [19,87–89].

Scalability (and corresponding cost) is important for pharma in large compound screens for therapeutics. EHTs and HoCs have additional advantages for some drug screens in providing an endothelial (or vascular wall) barrier (in Transwell® inserts). Drugs can be added on the basal side of the endothelial barrier whilst the cardiac tissue is on the apical side[89]. These models allow assessment of drug availability through the vasculature. Together, these platforms are increasingly used to develop de novo cardiac therapeutics.

4. Readouts

How cell responses can best be measured in situ preferably in real-time, is a crucial question for their utility. Readouts constitute an integral part of any model and are necessary to validate MHTs prior to implementation. Two important features of these heart models are relevant to translation: cardiac structure and function. In this section, we summarize the commonly used assays, both in situ in real time and terminal; these are summarized in tables 1-3.

4.1. Microscopy-based analysis of MHT assembly and composition

CMs in the heart are tightly coupled to create the structure necessary for highly synchronized, repetitive contraction and electrical conduction. This is evidenced as aligned sarcomeres that form characteristic “bands” in the heart. Thus, proper physiology requires defined 3D structure in the tissue. MHTs may thus include architectural guidelines to shape the *in vitro* model e.g. scaffolds, spatial constraints or anchoring points. However, the structure of cardiac microtissues can vary from spheroid-like to extended fibers. Analysis of the tissue structure is thus highly relevant to demonstrate enhanced maturation or quantify pathological changes in disease. Here, we summarize microscopic methods and their readouts used for this purpose.

When designing MHTs, the material properties, such as transparency, refractive index and organic solvent compatibility, must be considered. In addition, the thickness of the material should be taken into account for imaging with short or long-distance objectives. If the platform does not have the same footprint as microscope slides or plates, tailored holders are needed that fit on the microscope stage. Moreover, when live imaging is preferred, an on-stage incubator for climate control is required.

The main ways to visualize MHT structure and its cellular components are label free imaging, immunofluorescence and use of fluorescent reporter cell lines. Label-free [89] and reporter

cells [90] do not require additional steps such as antibody staining before imaging. On the other hand, immunofluorescent labelling may have higher specificity for protein detection and allow multiple proteins to be imaged simultaneously. Another post-fixation labelling technique is standard histology where various cellular and intracellular structures are visible and can be characterized [50]. In addition to labelling, tissue clearing techniques are increasingly used to improve image quality. 3D tissue imaging might be limited due to the scattered light by the lipids, intracellular or extracellular fluids present in the tissue. Tissue clearance eliminates these components and allows penetrate of light into the tissue by keeping refractive indices equal [91,92]. As a result, thicker tissue samples can be visualized by different microscopic techniques while preserving the 3D integrity of the sample.

Optical microscopy is the gold standard to image tissue structures. It includes a wide range of techniques from widefield to high-resolution microscopy. Transmitted light microscopy, such as bright-field or phase contrast, provides information on microtissue compaction, shape and motion (see table 1,2 and 3) without requiring additional labeling or fixation, and is suitable for live imaging. However, transmitted light microscopy is usually unable to distinguish specific cell types and their intracellular structures. Confocal microscopy and super-resolution microscopy overcome this. They also provide high spatial resolution with the possibility of optical sectioning, imaging in the Z- direction and 3D-reconstruction although this adds additional labor and time in the post-imaging process [93]. However, photo damage remains a limitation of these techniques. In addition, higher magnification objectives and corresponding short working distances (<1mm) may require removing the microtissue from the platform [94] which may be challenging and affect structural integrity of the microtissue. Two-photon microscopy can also provide 3D information. In comparison to confocal microscopy, it has better penetration depth due to greater wavelengths of photons used for imaging allowing visualization of deeper regions. It does not require optical clearance of the tissue and reduces photobleaching. Additionally, second harmonic generation allows label-free imaging of specific cell structures, like collagen deposition [67,95]. Light sheet microscopy based on illuminating an entire plane of tissue by laser in the form of a light sheet, has proven particularly useful for imaging 3D objects in particular because photo-bleaching is lower than conventional confocal imaging. Although not yet broadly applied to MHTs, first reports indicate advantages for tissue imaging on microfluidic chips [96].

Electron microscopy uses electron beams instead of light to generate a projection image. Compared to optical microscopy, electron microscopy provides much higher resolution. However, it requires fixed samples and often tissue slices, which make it a terminal assay. It also presents tissue collection challenges for HoC platforms [38,97].

4.2. Functional Readouts

Functional analysis of cardiac tissue models can broadly be divided into four approaches: molecular (e.g. protein or gene expression), electrophysiological, mechanical and metabolic readouts.

4.2.1. Molecular Analysis

Molecular analysis is not generally regarded as a direct functional readout but it does reveal expression profiles and pathways relevant for functionality. Commonly used assays for both *in vivo* and *in vitro* studies is high-throughput next generation sequencing (NGS) for transcriptome, genome and epigenome analysis. Besides well-known techniques like RT-PCR, RNA sequencing (RNAseq) is used increasingly either on bulk cell populations, where it reports average signal expression in cell populations, or on single cells. Bulk measurements on thousands to millions of cells is straightforward but does not distinguish different cell populations thereby potentially missing rare events that could be highly relevant to a disease mechanism [98–100]. By contrast, single cell analysis allows tracking of individual cell populations and detection of rare events (reviewed in [101– 105]). RNAseq has been used for microtissues, organoids and EHTs but not so far for HoCs, probably due to difficulties in extracting the tissues from chips. Whilst highly informative, RNAseq lacks the corresponding protein expression profiles and require disruption of tissues and cells. Disruption itself can upregulate stress genes [106] and thereby introduce artefacts and spatial information is lost. Batch-to-batch and line-to-line variability may in the future be addressed by automation of procedures. Alternative high content imaging methods e.g Co-detection by indexing (CODEX) [107], imaging mass cytometry [108], MACSima imaging cycling staining (MICS) [109] or RNAscope [110] complement the toolbox for protein and RNA expression profiling. Spatial transcriptomics, although not yet commonly applied to MHTs offer next generation methodology for in situ tissue profiling [111]. Other approaches include collecting tissue-conditioned media for biomarker detection or recent impedimetric immunosensors with antibody coated electrodes which transmit electrical signals when biomarkers or pathogens bind to them [112]. These methods are currently used for quality control of embryos derived from *in vitro* fertilization where invasive cell sampling carries high risk [113–116]. Clinical cardiac biomarkers [117,118] can also be used on conditioned media and all of these non-invasive methods allow long-term monitoring of live tissues.

4.2.2. Electrophysiology

Electrophysiological properties such as the action potential (AP) profile of the heart reflect functionality of CMs. Rapid ion transfer in and out of membrane channels alters the membrane voltage which results in AP changes. The AP starts with depolarization of the membrane by sodium ion influx and continues with initial repolarization by potassium (K+) ion efflux and a plateau phase in which calcium ions (Ca+2) move inwards. Further repolarization by K+ currents bring the membrane potential back to the resting level of -85 mV. Intracellular recordings of electrophysiological parameters are obtained using sharp electrodes or single cell patch clamp; these remain the benchmark for quantification of functionality in microtissues and EHTs. Voltage sensitive dyes [119] and integration of (non-invasive) electrodes are alternatives for extracellular recordings of field potential. Voltage sensitive dyes can be used in any platform and is suitable for whole tissue analysis [120]. However, they can be cytotoxic and are sensitive to photobleaching. Multielectrode arrays

(MEAs) are culture plates with embedded electrodes [121] which are widely used for real-time estimation of QT-prolongation (an important safety parameter) [122] and conduction velocity [123]. They are mostly used for 2D cell cultures as it is a challenge to record the whole tissue electrophysiology considering their limited surface interface between the electrodes and the tissue. Adopting a similar strategy, self-rolling biosensor arrays which wraps around the 3D microtissue/organoid [124], or microelectrodes integrated in EHT and HoC platforms allow continuous and multiplexed recording of electrophysiological signals [88,121,125].

4.2.3. Mechanics

Excitation-contraction coupling is one of the key indications of a functional cardiac tissue and Cc2+ is one of the key ions of this process. Sarcoplasmic reticulum releases Ca2+ ions in response to electrical excitation during the AP plateau phase which increases the level of intracellular Ca2+. Coupling and uncoupling of intracellular Ca2+ with troponin C in myofilaments activates and deactivates contraction, respectively. In order to reflect the physiological properties of the 3D models with respect to their Ca2+ level changes, fluorescent dyes with a variety of excitation ranges and Ca2+ affinities are used. Although this technique is real-time, fast and efficient, it is not suitable for long- term analysis and sensitivity of recordings depends highly on the type of the dye. Genetically modified hPSC lines that encode a calcium indicator (GECI) circumvents limitations of Ca2+ dyes and offer user-independent possibilities to measure and analyze Ca2+ flux and contractility [126].

Optical tracking of cells, tissues, beads [127], pillars or cantilevers around which tissues have compacted [88,128] is another way to retrieve contraction parameters as relative pixel displacement or absolute contraction force. Traction force microscopy, fractional shortening of sarcomere length and micropost displacement are examples of such techniques mainly used for single cells [54,129]. Software such as MuscleMotion [130] and OpenHeartWare [47] are user-friendly and open access tools for optical tracking of live contracting tissue from video recordings or image stacks. This type of automated contraction analysis enables quantification of contraction changes in diseased and healthy states or in response to drugs and can also be used for MHTs discussed earlier (tables 1-3; [47,131]). However, precise and consistent tracking becomes a challenge with increased heterogeneity in contrast and texture of 2D or 3D models; this may create measurement artefacts. In addition, preload dependent mechanics cannot be well analyzed with optical tracking. Therefore, classical isometric force measurements remain the gold standard in biomechanical characterizations of the heart muscle. Integrated sensors in MHTs allow continuous electronic examination of contractile stress and beat rate [89]. Such analysis does not require invasive methodology and is user-friendly.

4.2.4 Metabolic Readouts

The adult heart has a low energy reserve. To meet the high energy demand, CMs produce ATP from several metabolic substrates (e.g. glucose, pyruvate, triglycerides, glycogen, lactate, ketone bodies, fatty acids (FAs) and some amino acids) based on environmental conditions [132,133]. During early heart development, glucose and lactate are the major energy sources and glycolysis the major metabolic pathway to produce ATP. Postnatally though, the mitochondrial oxidative capacity increases and FA beta oxidation becomes the major energy source [134,135]. Recapitulating this "metabolic switch" from glycolysis to mitochondrial oxidative phosphorylation is an important reflection of maturity in MHTs [53].

Oxygen consumption and glycolysis measurements

Several commercially available kits and instruments (e.g. BioProfile Analyzers and Biochemistry Analyzers) allow quantification of extracellular glucose and lactate levels by colorimetric and fluorometric detection in cell culture media and are thus non-invasive. The Seahorse (extracellular flux) XF Analyzer is a fast and comprehensive approach that allows simultaneous recording of the oxygen consumption rate (OCR) and extracellular acidification rate (ECAR) of live cells and tissues. Three main metabolic assays can be performed with this technology: (I) mitochondrial stress; (II) glycolytic stress and (III) palmitate oxidation [136].

Quantification of metabolites and cell secretome

Conventional biochemical assays (RNAseq, LC-MS, ELISA) are widely used to detect metabolic changes in static cultures such as EHTs and microtissues/organoids and in a time-resolved manner for perfused systems. Secretome analysis can provide insight into disease mechanisms [137] and microenvironmental changes in the ECM, for example during hPSC differentiation into CMs [138]. However, proteome and secretome data acquisition and interpretation are challenging, even when applied to simple systems (e.g. monocultures). Low concentration of analytes, serum components in the media, protein splice variants can all result in false negatives and positives; this might be the reason why this technique has not been widely adopted in more complex cardiac systems (e.g. co- culture of different cell types).

Nuclear magnetic resonance spectroscopy (NMR) detects extra-/intra-cellular metabolites in MHTs in tissue supernatants and lysates. The technique can be used non-invasively and the data gives valuable input in the metabolic state of the tissues[18]. Alternatively, RAMAN spectroscopy provides non-invasive measurement of intracellular metabolites, and it is already in use to monitor hPSC-CM maturity [139,140] as well as ECM components in tissues [141,142].

Microtissues/Organoids				
Study	Cell Types	Application	Readouts	
			Structural	Functional
Archer et al., 2018	hiPSC-CM Primary human cardiac ECs Primary human cFBs	Drug Screening	Histology Confocal Imaging – immuno-fluorescence	Gene expression (qRT-PCR) Cell viability assay (cellular ATP content)
Beauchamp et al., 2015; 2020	hiPSC-CM human embryonic-cFBs	Cardiac development Disease modelling - cardiac fibrosis	Confocal imaging-immunofluorescence Electron microscopy Histology	Cell viability assay (live-dead staining) Ca2+ imaging Pharmacological analysis Gene expression (qRT-PCR) Western Blot Motion analysis Patch clamp
Drakhlis et al., 2021	hECS-CM	Cardiac development	Histology Multiphoton microscopy – immunofluorescence Live Optical fluorescence imaging - reporter cells; DiI-Ac- LDL Cell composition analysis – Flow cytometry Electron microscopy	Ca2+ imaging Patch clamp Gene expression (microarray, RNAseq)
Giacomelli et al., 2017	hiPSC or hECS-CM hiPSC or hESC-cardiac EC	Cardiac development Cardiac Maturation	Optical Microscopy Confocal Imaging-immunofluorescence	Gene expression (qRT-PCR) FACS Motion analysis Patch clamp MEA analysis

Microtissues/Organoids				
Study	Cell Types	Application	Readouts	
			Structural	Functional
Giacomelli et al., 2020	hiPSC-CM hiPSC-cardiac EC hiPSC-cFBs	Cardiac development Cardiac maturation Disease modelling - arrtyhmogenic cardiomyopathy	Confocal Imaging-immunofluorescence Electron microscopy	Gene expression (qRT-PCR, RNA seq) Western Blot Motion analysis Patch clamp Sharp electrode electrophysiology Ca+2 imaging Mitocondrial stress test- seahorse ELISA-cAMP level Nuclear magnetic resonance spectroscopy
Pointon et al., 2015; 2017	hiPSC-CM Primary human cardiac microvascular EC Primary human cFBs	Drug Screening	Confocal imaging-immunofluorescence	Gene expression (qRT-PCR) Motion analysis Cell viability assay (cellular ATP content)
Ravenscroft et al., 2016	hESC-CM Primary human EC Primary human cFBs or FBs	Drug Screening Toxicity Testing	Confocal imaging-immunofluorescence	Gene expression (qRT-PCR) Motion analysis Ca+2 Imaging

Microtissues/Organoids				
Study	**Cell Types**	**Application**	**Readouts**	
			Structural	**Functional**
Richards et al., 2020	hiPSC-CM HUVECs Primary human cFBs	Disease modelling - myocardial infraction	Confocal imaging- immunofluorescence	Gene expression (qRT-PCR) Motion analysis Ca+2 imaging Mitochondrial stress test - seahorse
Silva et al., 2020	hiPSC-CM	Cardiac development Cardiac maturation	Optical and light sheet microscopy – immunofluorescence Histology	Ca^{+2} imaging Patch clamp Gene expression (RNAseq)
Lee et al., 2019	hESC-CM hESC-mesenchymal stem cells	Disease modelling Cardiac Fibrosis	Optical Microscopy Confocal imaging- immunofluorescence	Gene expression (qRT-PCR, microarray) FACS Motion analysis MEA analysis
Hofbauer et al., 2021	hiPSC-CM hESC-CM Human cardiac microvascular EC Chicken embryo	Cardiac development	Optical Microscopy Confocal imaging- immunofluorescence Histology Electron microscopy	Ca^{+2} and voltage imaging Motion analysis Gene expression (RNAseq) Reporter cell lines Proteomics analysis

Table 1: Literature summary of microtissues/organoids.

Ehts				
Study	Cell Types	Application	Readouts	
			Structural	Functional
Dostanić et al., 2020	hiPSC-CM hiPSC-cFBs	Miniaturized cardiac tissues - Collagen/ Matrigel hydrogel		Motion analysis Force measurement
Nunes et al., 2013; Feric et al., 2019; Zhao et al., 2019; Wang et al., 2019	hiPSC-CM Human ventricular cFBs	Cardiac maturation Disease modelling Drug screening - Collagen/Matrigel/Fibrin hydrogel	Histology Confocal imaging-immunofluorescence Electron microscopy Second harmonic generation	Force measurement Motion analysis Ca2+ imaging Pharmacological analysis Gene expression (qRT-PCR; RNAseq) Electrophysiological measurements Western Blot Viability assay Pharmacological analysis
Huebsch et al., 2015; 2016	hiPSC-CM Stromal cells	Miniaturized cardiac tissues - geometric confinment	Confocal imaging-immunofluorescence	Force measurement Motion analysis MEA analysis Ca2+ Imaging Patch-clamp Pharmacological analysis
Leonard et al., 2018	hiPSC-CM	Cardiac Maturation - Fibrin hydrogel	Optical and confocal imaging-immunofluorescence Electron microscopy	Force measurement Motion analysis Gene expression (qRT-PCR) Ca2+ Imaging Western Blot

Ehts				
Study	Cell Types	Application	Readouts	
			Structural	Functional
Lind et al., 2017	hiPS-CM HUVEC Neonatal Rat Ventricular CM	Drug screening	Confocal imaging-immunofluorescence	Motion analysis + sensors
Lu et al., 2017	hiPSC-CM	Drug screening - Fibrin hydrogel	Confocal imaging-immunofluorescence Electron microscopy	Cell viability assay (MTS) Gene expression (qRT-PCR) Motion analysis Pharmacological analysis
Ma et al., 2014; 2015	hESC-CM hiPSC-CM	Geometric confinement Disease modeling	Confocal imaging-immunofluorescence	Motion analysis MEA analysis Gene expression (qRT-PCR) Cell proliferation assay (EdU) Cell migration imaging Pharmacological analysis
Macqueen et al., 2018	Neonatal rat ventricular CM hiPSC-CM	Disease modelling - Polycaprolactone (PCL)/ gelatin nanofibres scaffold	Confocal imaging-immunofluorescence	Ca2+ Imaging Pressure-volume measurements Echocardiology

Ehts				
Study	Cell Types	Application	Readouts	
			Structural	Functional
Mannhardt et al., 2016; 2020	hiPSC-CM	Drug screening - Fibrin hydrogel	Confocal imaging-immunofluorescence Histology Electron microscopy	Motion analysis Pharmacological analysis Gene expression (RNAseq)
Prondzynski et al., 2019	Human primary CM hiPSC-CM	Disease modelling - Fibrin/Matrigel hydrogel	Confocal imaging-immunofluorescence	Gene expression (RNAseq, nanoString nCounter) Western Blot Motion analysis Action potential measurement (electrodes and patch clamp)
Ronaldson-Bouchard et al., 2018	hiPSC-CM human FBs	Cardiac maturation - Fibrin/hydrogel	Confocal imaging-immunofluorescence Electron microscopy	Force measurement Path-clamp Motion analysis Ca2+ imaging Gene expression (qRT-PCR) Pharmacological analysis Mitochondrial respirometry - Seahorse
Takeda et al., 2018	hiPSC-CM	Drug cytotoxicity	Confocal imaging-immunofluorescence Histology	Gene expression (qRT-PCR) MEA analysis Cell viability assay (cellular ATP content) LDH assay Ca2+ imaging Motion analysis

Ehts				
Study	Cell Types	Application	Readouts	
			Structural	Functional
Tiburcy et al., 2017	hPSC-CM human FBs	Cardiac maturation Disease modelling - Collagen hydrogel	Cell composition analysis – Flow cytometry; Confocal imaging-immunofluorescence	Force measurement Motion analysis Gene espression (qRT-PCR, RNAseq) Action potential measurement – electrodes
Mills et al., 2017, 2019	hESC-CM Neonatal Rat Ventricular CM	Cardiac Maturation Drug screening - Collagen/Matrigel Hydrogel	Optical and Confocal imaging - Immunofluorescence Cell composition analysis – Flow cytometry Electron microscopy	Motion analysis Ca2+ imaging Patch-clamp Gene expression (qRT-PCR, RNAseq) Mass Spectrometry - proteomic analysis; Central carbon metabolite analysis Mitochondrial respirometry - Seahorse
Bailey et al., 2021	hiPSC-CM hiPSC-fibroblasts Primary macrophages	Disease modelling - SARS-CoV-2	Confocal imaging-immunofluorescence Histology Electron microscopy	Gene expression (qRT-PCR; RNAseq; RNAscope) Motion analysis Cell viability assay (TUNEL)

Table 2: Literature summary of EHTs.

HoCs				
Study	Cell Types	Applications	Readouts	
			Structural	Functional
Lee at al., 2021	HER-2-overexpressing human breast cancer cell line hiPSC – CM	Disease modeling	Optical microscopy – brightfield Confocal microscopy – immunofluorescence	Biosensors on micro-electrodes
Maoz et al., 2017	hiPSC – CM	Drug screening	Electron microscopy Confocal microscopy – immunofluorescence	MEA analysis
Marsano et al., 2016	neonatal rat ventricular CM hiPSC – CM	Disease modelling	Optical microscopy – brightfield Confocal microscopy – immunofluorescence	Motion analysis
Mastikhina et al., 2020	human cFBs hiPSC – CM	Disease modelling	Optical microscopy – brightfield Confocal microscopy – immunofluorescence	Atomic force microscopy Gene expression (RNAseq) Pharmacological analysis
Mathur et al., 2015	hiPSC – CM	Drug cytotoxicity	Optical microscopy – brightfield Confocal microscopy – immunofluorescence	Motion analysis Ca2+ imaging Pharmacological analysis
Schneider et al., 2019	hiPSC – CM		Optical microscopy – brightfield Confocal microscopy – immunofluorescence	Motion analysis

HoCs				
Study	Cell Types	Applications	Readouts	
			Structural	Functional
Schneider et al., 2022	hiPSC – CM human primary dermal fibroblasts		Optical microscopy – brightfield Confocal microscopy – immunofluorescence	Motion analysis Ca2+ imaging O2 sensors
Wang et al., 2014	hiPSC -CM	Disease modelling	Confocal microscopy – immunofluorescence	Motion analysis
Skardal et al., 2017	human hepatic stellate cells hiPSC – CM human lung microvasculature ECs human airway stromal mesenchymal cells human bronchial epithelial cells	Drug screening	Optical microscopy - brightfield Confocal microscopy - immunofluorescence	LC-MS metabolic profiling electromechanical biosensors
Tanumihardja et al., 2021	hiPSC – CM		Electron microscopy	pH and O2 sensors
Xiao et al., 2014	primary neonatal rat CM hESC-CM	Drug screening	Optical microscopy - brightfield Confocal microscopy - Immunofluorescence Electron microscopy	Motion analysis

HoCs				
Study	Cell Types	Applications	Readouts	
			Structural	Functional
Zhang et al., 2017; 2021	human primary hepatocytes hiPSC – CM	Drug screening	Brightfield microscopy - cellular morphology Fluorescence microscopy – cardiac markers	Electromechanical biomarkers sensors Motion analysis
Shen et al., 2017	Murine ESC-CM hESC-CM	Cardiac maturation	Confocal microscopy – immunofluorescence	Ca2+ imaging RAMAN spectroscopy

Table 3: Literature summary of HoCs.

5. Perspectives

MHTs have become much more robust and reproducible over the last several years but individually, each system still has issues to overcome before widespread application in the cardiovascular field. MHTs based on hPSCs can mimic aspects of embryonic development and integrate multiple (pre- differentiated) cell types. Cell types that have not yet been integrated into these models include (i) cardiac resident macrophages (CRM) that link with CMs and can regulate electrical activity and cardiac homeostasis [143–145] and (ii) the cardiac autonomic nervous system that mediates the electrical and mechanical signals from the brain to the heart [146]. Additionally, the intrinsic cardiac nervous system (ICNS) with its sensory, motor and interconnecting neurons regulates electrical conduction in the heart [147]. Several studies have indicated important roles of CRMs [145,148,149] and ICNS (reviewed in [150] in cardiac pathophysiology *in vivo*. Moreover, many differentiation protocols, cell lines and platform designs mean little standardization between the systems, precluding the direct comparison of outcomes. One example of the challenge this presents is that identical EHTs made from different hiPSC lines exhibited different baseline contractile force, kinetics, and beating rate [86]. It is unclear whether this derives from different genetic backgrounds, line- specific disease associated SNPs or gene variants or just different state-of-maturity of the CMs used in the EHTs. In addition, efforts towards more head-to-head comparisons including batch-to-batch and clone-to-clone variability are needed.

Self-organized microtissues and organoids miss the full complement of micro-environmental cues that direct physiological maturation of CMs. EHTs can introduce natural or synthetic microenvironments that together with mechanical cues go some way to increasing physiological realism. Likewise, HoCs with microchannels have been developed which can integrate perfusion and fluidic flow, the critical feature of native tissues. In addition, most platforms are fabricated by academic labs which produce devices in small series and only few are at present commercially available. In addition, physical and chemical properties of materials may be variable with respect to absorption or retention of small molecules in the culture medium which could lead to misinterpretation of results. It is important to characterize these properties prior to use.

MHTs nevertheless offer remarkable opportunities in many applications including disease modelling and drug screening in the cardiac field particularly if populated with human cells. Data produced using current validation assays suggests that these systems can recapitulate many complex physiologies of heart tissue in healthy and diseased states with respect to structure, functionality and metabolism. However, most of these assays have not yet been used in HoCs, therefore lack options to mimic (blood and lymph) vascular flow. Most HoC designs are closed so tissues are not easily accessible for readouts. For this reason, terminal (or end-point) readouts are often preferred. Moving towards non-invasive assays and adapting these to be compatible with HoCs will be one way of addressing and providing alternatives for this issue. Integration of biosensors in chip design is an option. However, most commercial systems, for example, do not allow in-house integration of these sensors, perhaps explaining why many labs prefer their own in-house designs.

For structural characterization, high resolution imaging of 3D tissues along the Z-axis is still challenging in HoCs since most are still too thick to be imaged using conventional confocal microscopy. This means that the tissue must be removed from the platform, making high resolution imaging an end-point readout. Even though not often reported for HoCs, light-sheet microscopy and 2-photon microscopy can offer alternatives for direct on-chip imaging of live tissues and combination with transgenic cell lines expressing fluorescent marker proteins provide non-invasive structural readouts.

Metabolic studies are mainly focused on O2 consumption and glycolysis. However, most techniques are not suitable for real-time measurement in HoCs as they need either tissue lysis or effluent collection over several hours of perfusion. For example, although the Seahorse-XF is widely used on cell monolayers, microtissues and EHTs (table 1 and 2), most of the microfluidic devices are made of PDMS which is highly permeable for oxygen. Hence oxygen consumed by the tissues is replenished almost instantly downstream. In addition, they are mostly closed systems where the cell or tissue proximity is not easily accessible by instrumentation and the culture medium is delivered through continuous flow. The design flexibility however, allows, in principle for the integration of the sensors directly into the chip platform. Alternatively, non-invasive fluorescent-lifetime imaging microscopy (FLIM) allows characterization of mitochondrial metabolic oxidative changes by means of endogenous fluorescence in live samples [151].

Quantification techniques for metabolites and secretome (ELISA, MS, NMR and others reviewed in [133]) are used for microtissues and EHTs, they have not yet been adapted for HoC systems. However, some of these techniques have been applied in other OoCs, for example RAMAN spectroscopy in pancreas-on-chip [152].

Integrated or modular sensors offer in situ real-time automated tools for metabolic readouts. Integrated sensors include electrochemical sensors to measure oxygen and pH analytes as a difference of electrical current or potential [153]. However, they can also be adapted to measure non-electrically active species such as glucose and lactate. These sensors often require a transducer to detect signals. On the other hand, optical sensors can replace transducers and detect signals from a simple transparent window on top of the sensor. Integrated sensors can be positioned close to the tissue allowing real-time measurement [154]. However, they are in the system for entire culture periods which in some cases last multiple weeks while the measurement is only relevant when the system is challenged, for example with drugs. This means for enzyme-based sensors (but also others) that they might already be degraded before they are used. Integrated sensors are single use which significantly increases the cost per chip.

Modular multisensors, on the other hand, can be re-usable and thus cost efficient. They may contain several physical sensors for monitoring pH, oxygen and temperature or electrochemical sensors [155]. Modular multisensor systems in combination with modular OoC platforms can be useful to detect differential secretion of enzymes in different organs, for example in response to different compounds [82]. However, they are dependent on the

flow rate and some measurements, such as oxygen consumption in PDMS chips can be impaired if not positioned properly [155]. Electrochemical and optical sensor alternatives and their integration in OoC systems have recently been extensively reviewed [156].

Emerging technologies like FLIM, RAMAN spectroscopy and integrated sensors may greatly contribute to non-invasive metabolic analysis of living tissues inside HoC platforms.

6. Conclusions

In sum, we reviewed here different 3D cardiac tissue generation platforms in combination with hiPSC-derived cardiac cell types together with their applications and readouts. These models are emerging tools to investigate cardiac development and pathophysiology. Further refinement in the generation and readout methods might eliminate hurdles that have been discussed here and allow closer mimicry of the adult heart with a possibility to standardize, reduce costs and adopt less labor- intensive methodology.

Acknowledgements

The authors' work is supported by the European Union's Horizon 2020 research and innovation programme under grant agreement No. 812954.

References

1. K. Takahashi, K. Tanabe, M. Ohnuki, M. Narita, T. Ichisaka, K. Tomoda, S. Yamanaka, *Induction of Pluripotent Stem Cells from Adult Human Fibroblasts by Defined Factors, Cell.* (2007). https://doi.org/10.1016/j.cell.2007.11.019.
2. J.A. Thomson, *Embryonic stem cell lines derived from human blastocysts,* Science (80-.). (1998). https://doi.org/10.1126/science.282.5391.1145.
3. C. Mummery, D.W. Oostwaard, P. Doevendans, R. Spijker, S. van den Brink, R. Hassink, M. van der Heyden, T. Opthof, M. Pera, A.B. de la Riviere, R. Passier, L. Tertoolen, *Differentiation of human embryonic stem cells to cardiomyocytes: role of coculture with visceral endoderm-like cells.,* Circulation. 107 (2003) 2733–2740. https://doi.org/10.1161/01.cir.0000068356.38592.68.
4. I. Kehat, D. Kenyagin-Karsenti, M. Snir, H. Segev, M. Amit, A. Gepstein, E. Livne, O. Binah, J. Itskovitz-Eldor, L. Gepstein, *Human embryonic stem cells can differentiate into myocytes with structural and functional properties of cardiomyocytes.,* J. Clin. Invest. 108 (2002) 407–414. https://doi.org/10.1172/jci12131.
5. C.L. Mummery, J. Zhang, E.S. Ng, D.A. Elliott, A.G. Elefanty, T.J. Kamp, *Differentiation of human embryonic stem cells and induced pluripotent stem cells to cardiomyocytes: a methods overview.,* Circ. Res. 111 (2012) 344–358. https://doi.org/10.1161/circresaha.110.227512.

6. M.J. Birket, M.C. Ribeiro, G. Kosmidis, D. Ward, A.R. Leitoguinho, V. van de Pol, C. Dambrot, H.D. Devalla, R.P. Davis, P.G. Mastroberardino, D.E. Atsma, R. Passier, C.L. Mummery, *Contractile Defect Caused by Mutation in MYBPC3 Revealed under Conditions Optimized for Human PSC-Cardiomyocyte Function,* Cell Rep. 13 (2015) 733–745. https://doi.org/10.1016/j.celrep.2015.09.025.
7. M.J. Birket, C.L. Mummery, P*luripotent stem cell derived cardiovascular progenitors - A developmental perspective,* Dev. Biol. (2015). https://doi.org/10.1016/j.ydbio.2015.01.012.
8. M.C. Ribeiro, L.G. Tertoolen, J.A. Guadix, M. Bellin, G. Kosmidis, C. D'Aniello, J. Monshouwer- Kloots, M.J. Goumans, Y. li Wang, A.W. Feinberg, C.L. Mummery, R. Passier, *Functional maturation of human pluripotent stem cell derived cardiomyocytes invitro - Correlation between contraction force andelectrophysiology,* Biomaterials. (2015). https://doi.org/10.1016/j.biomaterials.2015.01.067.
9. R.P. Davis, S. Casini, ; Cathelijne, W. Van Den Berg, M. Hoekstra, ; Carol, A. Remme, C. Dambrot, D. Salvatori, ; Dorien, W.-V. Oostwaard, A.A.M. Wilde, C.R. Bezzina, A.O. Verkerk, C. Freund, C.L. Mummery, *Arrhythmia/Electrophysiology Cardiomyocytes Derived From Pluripotent Stem Cells Recapitulate Electrophysiological Characteristics of an Overlap Syndrome of Cardiac Sodium Channel Disease,* (2012). https://doi.org/10.1161/CIRCULATIONAHA.111.
10. S.R. Braam, L. Tertoolen, A. van de Stolpe, T. Meyer, R. Passier, C.L. Mummery, *Prediction of drug-induced cardiotoxicity using human embryonic stem cell-derived cardiomyocytes,* Stem Cell Res. 4 (2010). https://doi.org/10.1016/j.scr.2009.11.004.
11. C. Denning, V. Borgdorff, J. Crutchley, K.S.A. Firth, V. George, S. Kalra, A. Kondrashov, M.D. Hoang, D. Mosqueira, A. Patel, L. Prodanov, D. Rajamohan, W.C. Skarnes, J.G.W. Smith, L.E. Young, *Cardiomyocytes from human pluripotent stem cells: From laboratory curiosity to industrial biomedical platform*, BBA - Mol. Cell Res. 1863 (2016) 1728–1748. https://doi.org/10.1016/j.bbamcr.2015.10.014.
12. P. Liang, F. Lan, A.S. Lee, T. Gong, V. Sanchez-Freire, Y. Wang, S. Diecke, K. Sallam, J.W. Knowles, P.J. Wang, P.K. Nguyen, D.M. Bers, R.C. Robbins, J.C. Wu, *Drug screening using a library of human induced pluripotent stem cell-derived cardiomyocytes reveals disease-specific patterns of cardiotoxicity,* Circulation. 127 (2013). https://doi.org/10.1161/CIRCULATIONAHA.113.001883.
13. A. Moretti, M. Bellin, A. Welling, C.B. Jung, J.T. Lam, L. Bott-Flügel, T. Dorn, A. Goedel, C. Höhnke, F. Hofmann, M. Seyfarth, D. Sinnecker, A. Schömig, K.-L. Laugwitz, *Patient-specific induced pluripotent stem-cell models for long-QT syndrome.,* N. Engl. J. Med. 363 (2010) 1397–1409. https://doi.org/10.1056/nejmoa0908679.
14. P. Beauchamp, W. Moritz, J.M. Kelm, N.D. Ullrich, I. Agarkova, B.D. Anson, T.M. Suter, C. Zuppinger, *Development and Characterization of a Scaffold-Free 3D Spheroid Model of Induced Pluripotent Stem Cell-Derived Human Cardiomyocytes,* Tissue Eng. - Part C Methods. (2015). https://doi.org/10.1089/ten.tec.2014.0376.
15. B.R. Desroches, P. Zhang, B.R. Choi, M.E. King, A.E. Maldonado, W. Li, A. Rago, G. Liu, N. Nath, K.M. Hartmann, B. Yang, G. Koren, J.R. Morgan, U. Mende, *Functional scaffold-free 3-D cardiac microtissues: A novel model for the investigation of heart cells,* Am. J. Physiol. - Hear. Circ. Physiol. (2012). https://doi.org/10.1152/ajpheart.00743.2011.

16. C.P. Soares, V. Midlej, M.E.W. de Oliveira, M. Benchimol, M.L. Costa, C. Mermelstein, *2D and 3D-organized cardiac cells shows differences in cellular morphology, adhesion junctions, presence of myofibrils and protein expression,* PLoS One. 7 (2012) e38147. https://doi.org/10.1371/journal.pone.0038147.
17. P. Beauchamp, C.B. Jackson, L.C. Ozhathil, I. Agarkova, C.L. Galindo, D.B. Sawyer, T.M. Suter, C. Zuppinger, *3D Co-culture of hiPSC-Derived Cardiomyocytes With Cardiac Fibroblasts Improves Tissue-Like Features of Cardiac Spheroids,* Front. Mol. Biosci. (2020). https://doi.org/10.3389/fmolb.2020.00014.
18. E. Giacomelli, V. Meraviglia, G. Campostrini, A. Cochrane, X. Cao, R.W.J. van Helden, A. Krotenberg Garcia, M. Mircea, S. Kostidis, R.P. Davis, B.J. van Meer, C.R. Jost, A.J. Koster, H. Mei, D.G. Míguez, A.A. Mulder, M. Ledesma-Terrón, G. Pompilio, L. Sala, D.C.F. Salvatori, R.C. Slieker, E. Sommariva, A.A.F. de Vries, M. Giera, S. Semrau, L.G.J. Tertoolen, V. V Orlova, M. Bellin, C.L. Mummery, *Human-iPSC-Derived Cardiac Stromal Cells Enhance Maturation in 3D Cardiac Microtissues and Reveal Non-cardiomyocyte Contributions to Heart Disease,* Cell Stem Cell. 26 (2020) 862-879.e11. https://doi.org/10.1016/j.stem.2020.05.004.
19. R.J. Mills, B.L. Parker, G.A. Quaife-Ryan, H.K. Voges, E.J. Needham, A. Bornot, M. Ding, H. Andersson, M. Polla, D.A. Elliott, L. Drowley, M. Clausen, A.T. Plowright, I.P. Barrett, Q.-D. Wang, D.E. James, E.R. Porrello, J.E. Hudson, *Drug Screening in Human PSC-Cardiac Organoids Identifies Pro-proliferative Compounds Acting via the Mevalonate Pathway,* Cell Stem Cell. 24 (2019) 895-907.e6. https://doi.org/10.1016/j.stem.2019.03.009.
20. D.J. Richards, Y. Li, C.M. Kerr, J. Yao, G.C. Beeson, R.C. Coyle, X. Chen, J. Jia, B. Damon, R. Wilson, E. Starr Hazard, G. Hardiman, D.R. Menick, C.C. Beeson, H. Yao, T. Ye, Y. Mei, *Human cardiac organoids for the modelling of myocardial infarction and drug cardiotoxicity,* Nat. Biomed. Eng. 4 (2020) 446–462. https://doi.org/10.1038/s41551-020-0539-4.
21. A. Pointon, J. Pilling, T. Dorval, Y. Wang, C. Archer, C. Pollard, *From the Cover: High- Throughput Imaging of Cardiac Microtissues for the Assessment of Cardiac Contraction during Drug Discovery,* Toxicol. Sci. 155 (2017) 444–457. https://doi.org/10.1093/toxsci/kfw227.
22. E. Giacomelli, M. Bellin, V. V Orlova, C.L. Mummery, *Co-Differentiation of Human Pluripotent Stem Cells-Derived Cardiomyocytes and Endothelial Cells from Cardiac Mesoderm Provides a Three-Dimensional Model of Cardiac Microtissue.,* Curr. Protoc. Hum. Genet. 95 (2017) 21.9.1- 21.9.22. https://doi.org/10.1002/cphg.46.
23. M.A. Lancaster, J.A. Knoblich, *Organogenesis in a dish: Modeling development and disease using organoid technologies,* Science (80-.). 345 (2014) 1247125–1247125. https://doi.org/10.1126/science.1247125.
24. H. Clevers, *Modeling Development and Disease with Organoids,* Cell. 165 (2016) 1586–1597. https://doi.org/10.1016/j.cell.2016.05.082.
25. M.N. Giraud, C. Armbruster, T. Carrel, H.T. Tevaearai, *Current state of the art in myocardial tissue engineering,* Tissue Eng. 13 (2007) 1825–1836. https://doi.org/10.1089/ten.2006.0110.

26. J. Günter, P. Wolint, A. Bopp, J. Steiger, E. Cambria, S.P. Hoerstrup, M.Y. Emmert, *Microtissues in Cardiovascular Medicine: Regenerative Potential Based on a 3D Microenvironment,* Stem Cells Int. 2016 (2016) 1–20. https://doi.org/10.1155/2016/9098523.
27. M.N. Hirt, A. Hansen, T. Eschenhagen, *Cardiac tissue engineering : State of the art,* Circ. Res. 114 (2014) 354–367. https://doi.org/10.1161/CIRCRESAHA.114.300522.
28. L. Drakhlis, S. Biswanath, C.M. Farr, V. Lupanow, J. Teske, K. Ritzenhoff, A. Franke, F. Manstein, E. Bolesani, H. Kempf, S. Liebscher, K. Schenke-Layland, J. Hegermann, L. Nolte, H. Meyer, J. de la Roche, S. Thiemann, C. Wahl-Schott, U. Martin, R. Zweigerdt, *Human heart-forming organoids recapitulate early heart and foregut development,* Nat. Biotechnol. 39 (2021). https://doi.org/10.1038/s41587-021-00815-9.
29. P. Hofbauer, S.M. Jahnel, N. Papai, M. Giesshammer, A. Deyett, C. Schmidt, M. Penc, K. Tavernini, N. Grdseloff, C. Meledeth, L.C. Ginistrelli, C. Ctortecka, Š. Šalic, M. Novatchkova, S. Mendjan, *Cardioids reveal self-organizing principles of human cardiogenesis,* Cell. 184 (2021) 3299-3317.e22. https://doi.org/10.1016/j.cell.2021.04.034.
30. A.C. Silva, O.B. Matthys, D.A. Joy, M.A. Kauss, V. Natarajan, M.H. Lai, D. Turaga, M. Alexanian, B.G. Bruneau, T.C. McDevitt, Developmental co-emergence of cardiac and gut tissues modeled by human iPSC-derived organoids, BioRxiv. (2020). https://doi.org/10.1101/2020.04.30.071472.
31. K. Kretzschmar, Y. Post, M. Bannier-Hélaouët, A. Mattiotti, J. Drost, O. Basak, V.S.W. Li, M. van den Born, Q.D. Gunst, D. Versteeg, L. Kooijman, S. van der Elst, J.H. van Es, E. van Rooij, M.J.B. van den Hoff, H. Clevers, *Profiling proliferative cells and their progeny in damaged murine hearts,* Proc. Natl. Acad. Sci. U. S. A. (2018). https://doi.org/10.1073/pnas.1805829115.
32. C.V.C. Bouten, P.Y.W. Dankers, A. Driessen-Mol, S. Pedron, A.M.A. Brizard, F.P.T. Baaijens, *Substrates for cardiovascular tissue engineering,* Adv. Drug Deliv. Rev. 63 (2011). https://doi.org/10.1016/j.addr.2011.01.007.
33. Z. Ma, S. Koo, M.A. Finnegan, P. Loskill, N. Huebsch, N.C. Marks, B.R. Conklin, C.P. Grigoropoulos, K.E. Healy, *Three-dimensional filamentous human diseased cardiac tissue model,* Biomaterials. 35 (2014). https://doi.org/10.1016/j.biomaterials.2013.10.052.
34. Z. Ma, J. Wang, P. Loskill, N. Huebsch, S. Koo, F.L. Svedlund, N.C. Marks, E.W. Hua, C.P. Grigoropoulos, B.R. Conklin, K.E. Healy, *Self-organizing human cardiac microchambers mediated by geometric confinement,* Nat. Commun. 6 (2015). https://doi.org/10.1038/ncomms8413.
35. Y. Zhao, N.T. Feric, N. Thavandiran, S.S. Nunes, M. Radisic, *The Role of Tissue Engineering and Biomaterials in Cardiac Regenerative Medicine,* Can. J. Cardiol. 30 (2014). https://doi.org/10.1016/j.cjca.2014.08.027.
36. T. Eschenhagen, C. Fink, U. Remmers, H. Scholz, J. Wattchow, J. Weil, W. Zimmermann, H.H. Dohmen, H. Schäfer, N. Bishopric, T. Wakatsuki, E.L. Elson, *Three-dimensional reconstitution of embryonic cardiomyocytes in a collagen matrix: a new heart muscle model system,* FASEB J. 11 (1997) 683–694. https://doi.org/10.1096/fasebj.11.8.9240969.
37. R.J. Mills, J.E. Hudson, *Bioengineering adult human heart tissue: How close are we?*, APL Bioeng. 3 (2019) 010901. https://doi.org/10.1063/1.5070106.

38. N. Huebsch, P. Loskill, N. Deveshwar, C.I. Spencer, L.M. Judge, M.A. Mandegar, C.B. Fox, T.M.A. Mohamed, Z. Ma, A. Mathur, A.M. Sheehan, A. Truong, M. Saxton, J. Yoo, D. Srivastava, T.A. Desai, P.L. So, K.E. Healy, B.R. Conklin, *Miniaturized iPS-Cell-Derived Cardiac Muscles for Physiologically Relevant Drug Response Analyses*, Sci. Rep. 6 (2016) 1–12. https://doi.org/10.1038/srep24726.
39. G. Garoffolo, M. Pesce, *Mechanotransduction in the Cardiovascular System: From Developmental Origins to Homeostasis and Pathology,* Cells. 8 (2019) 1607. https://doi.org/10.3390/cells8121607.
40. A. Leonard, A. Bertero, J.D. Powers, K.M. Beussman, S. Bhandari, M. Regnier, C.E. Murry, N.J. Sniadecki, *Afterload promotes maturation of human induced pluripotent stem cell derived cardiomyocytes in engineered heart tissues,* J. Mol. Cell. Cardiol. 118 (2018) 147–158. https://doi.org/10.1016/j.yjmcc.2018.03.016.
41. K. Ronaldson-Bouchard, S.P. Ma, K. Yeager, T. Chen, L.J. Song, D. Sirabella, K. Morikawa, D. Teles, M. Yazawa, G. Vunjak-Novakovic, *Advanced maturation of human cardiac tissue grown from pluripotent stem cells,* Nature. 556 (2018) 239–243. https://doi.org/10.1038/s41586- 018-0016-3.
42. S. Ahadian, R. Civitarese, D. Bannerman, M.H. Mohammadi, R. Lu, E. Wang, L. Davenport-Huyer, B. Lai, B. Zhang, Y. Zhao, S. Mandla, A. Korolj, M. Radisic, *Organ-On-A-Chip Platforms: A Convergence of Advanced Materials, Cells, and Microscale Technologies,* Adv. Healthc. Mater. 7 (2018) 1–53. https://doi.org/10.1002/adhm.201700506.
43. S. Browne, E.L. Gill, P. Schultheiss, I. Goswami, K.E. Healy, *Stem cell-based vascularization of microphysiological systems,* Stem Cell Reports. 16 (2021). https://doi.org/10.1016/j.stemcr.2021.03.015.
44. S. Zhang, Z. Wan, R.D. Kamm, *Lab on a Chip CRITICAL REVIEW Vascularized organoids on a chip: strategies for engineering organoids with functional vasculature,* 21 (2021) 473. https://doi.org/10.1039/d0lc01186j.
45. A. Marsano, C. Conficconi, M. Lemme, P. Occhetta, E. Gaudiello, E. Votta, G. Cerino, A. Redaelli, M. Rasponi, *Beating heart on a chip: A novel microfluidic platform to generate functional 3D cardiac microtissues,* Lab Chip. 16 (2016) 599–610. https://doi.org/10.1039/c5lc01356a.
46. A. Mathur, P. Loskill, K. Shao, N. Huebsch, S.G. Hong, S.G. Marcus, N. Marks, M. Mandegar, B.R. Conklin, L.P. Lee, K.E. Healy, *Human iPSC-based cardiac microphysiological system for drug screening applications,* Sci. Rep. 5 (2015) 1–7. https://doi.org/10.1038/srep08883.
47. O. Schneider, L. Zeifang, S. Fuchs, C. Sailer, P. Loskill, *User-Friendly and Parallelized Generation of Human Induced Pluripotent Stem Cell-Derived Microtissues in a Centrifugal Heart-on-a- Chip,* Tissue Eng. - Part A. 25 (2019) 786–798. https://doi.org/10.1089/ten.tea.2019.0002.
48. Y. Xiao, B. Zhang, H. Liu, J.W. Miklas, M. Gagliardi, A. Pahnke, N. Thavandiran, Y. Sun, C. Simmons, G. Keller, M. Radisic, *Microfabricated perfusable cardiac biowire: A platform that mimics native cardiac bundle,* Lab Chip. 14 (2014). https://doi.org/10.1039/c3lc51123e.
49. A. Agarwal, J.A. Goss, A. Cho, M.L. McCain, K.K. Parker, *Microfluidic heart on a chip for higher throughput pharmacological studies,* Lab Chip. 13 (2013) 3599–3608. https://doi.org/10.1039/c3lc50350j.

50. S.S. Nunes, J.W. Miklas, J. Liu, R. Aschar-Sobbi, Y. Xiao, B. Zhang, J. Jiang, S. Massé, M. Gagliardi, A. Hsieh, N. Thavandiran, M.A. Laflamme, K. Nanthakumar, G.J. Gross, P.H. Backx, G. Keller, M. Radisic, *Biowire: A platform for maturation of human pluripotent stem cell-derived cardiomyocytes,* Nat. Methods. 10 (2013) 781–787. https://doi.org/10.1038/nmeth.2524.
51. E. Giacomelli, C.L. Mummery, M. Bellin, *Human heart disease: lessons from human pluripotent stem cell-derived cardiomyocytes,* Cell. Mol. Life Sci. 74 (2017) 3711–3739. https://doi.org/10.1007/s00018-017-2546-5.
52. D.L. Brutsaert, *Cardiac Endothelial-Myocardial Signaling: Its Role in Cardiac Growth, Contractile Performance, and Rhythmicity,* Physiol. Rev. 83 (2003) 59–115. https://doi.org/10.1152/physrev.00017.2002.
53. R.J. Mills, D.M. Titmarsh, X. Koenig, B.L. Parker, J.G. Ryall, G.A. Quaife-Ryan, H.K. Voges, M.P. Hodson, C. Ferguson, L. Drowley, A.T. Plowright, E.J. Needham, Q.-D. Wang, P. Gregorevic, M. Xin, W.G. Thomas, R.G. Parton, L.K. Nielsen, B.S. Launikonis, D.E. James, D.A. Elliott, E.R. Porrello, J.E. Hudson, *Functional screening in human cardiac organoids reveals a metabolic mechanism for cardiomyocyte cell cycle arrest,* Proc. Natl. Acad. Sci. 114 (2017) E8372–E8381. https://doi.org/10.1073/pnas.1707316114.
54. A.J.S. Ribeiro, Y.S. Ang, J.D. Fu, R.N. Rivas, T.M.A. Mohamed, G.C. Higgs, D. Srivastava, B.L. Pruitt, *Contractility of Single cardiomyocytes differentiated from pluripotent stem cells depends on physiological shape and substrate stiffness,* Proc. Natl. Acad. Sci. U. S. A. 112 (2015) 12705–12710. https://doi.org/10.1073/pnas.1508073112.
55. M. Tiburcy, J.E. Hudson, P. Balfanz, S. Schlick, T. Meyer, M.-L. Chang Liao, E. Levent, F. Raad, S. Zeidler, E. Wingender, J. Riegler, M. Wang, J.D. Gold, I. Kehat, E. Wettwer, U. Ravens, P. Dierickx, L.W. van Laake, M.J. Goumans, S. Khadjeh, K. Toischer, G. Hasenfuss, L.A. Couture, A. Unger, W.A. Linke, T. Araki, B. Neel, G. Keller, L. Gepstein, J.C. Wu, W.-H. Zimmermann, *Defined Engineered Human Myocardium With Advanced Maturation for Applications in Heart Failure Modeling and Repair,* Circulation. 135 (2017) 1832–1847. https://doi.org/10.1161/CIRCULATIONAHA.116.024145.
56. L. Ren, W. Liu, Y. Wang, J.C. Wang, Q. Tu, J. Xu, R. Liu, S.F. Shen, J. Wang, *Investigation of hypoxia-induced myocardial injury dynamics in a tissue interface mimicking microfluidic device,* Anal. Chem. 85 (2013) 235–244. https://doi.org/10.1021/ac3025812.
57. M. Lee, K.B. Jung, S. Jo, S. Hyun, K. Moon, J. Seo, S. Kim, M. Son, *Modelling cardiac fibrosis using three- dimensional cardiac microtissues derived from human embryonic stem cells,* J. Biol. Eng. 13 (2019) 15.
58. T.M. Spencer, R.F. Blumenstein, K.M. Pryse, S.L. Lee, D.A. Glaubke, B.E. Carlson, E.L. Elson, G.M. Genin, *Fibroblasts Slow Conduction Velocity in a Reconstituted Tissue Model of Fibrotic Cardiomyopathy,* ACS Biomater. Sci. Eng. 3 (2017) 3022–3028. https://doi.org/10.1021/acsbiomaterials.6b00576.
59. M. Nishiga, D.W. Wang, Y. Han, D.B. Lewis, J.C. Wu, *COVID-19 and cardiovascular disease: from basic mechanisms to clinical perspectives,* Nat. Rev. Cardiol. 17 (2020) 543–558. https://doi.org/10.1038/s41569-020-0413-9.
60. Y.Y. Zheng, Y.T. Ma, J.Y. Zhang, X. Xie, *COVID-19 and the cardiovascular system,* Nat. Rev. Cardiol. (2020). https://doi.org/10.1038/s41569-020-0360-5.

61. T. Guo, Y. Fan, M. Chen, X. Wu, L. Zhang, T. He, H. Wang, J. Wan, X. Wang, Z. Lu, *Cardiovascular Implications of Fatal Outcomes of Patients with Coronavirus Disease 2019 (COVID-19),* JAMA Cardiol. (2020). https://doi.org/10.1001/jamacardio.2020.1017.
62. C. Huang, Y. Wang, X. Li, L. Ren, J. Zhao, Y. Hu, L. Zhang, G. Fan, J. Xu, X. Gu, Z. Cheng, T. Yu, J. Xia, Y. Wei, W. Wu, X. Xie, W. Yin, H. Li, M. Liu, Y. Xiao, H. Gao, L. Guo, J. Xie, G. Wang, R. Jiang, Z. Gao, Q. Jin, J. Wang, B. *Cao, Clinical features of patients infected with 2019 novel coronavirus in Wuhan, China,* Lancet. 395 (2020) 497–506. https://doi.org/10.1016/S0140- 6736(20)30183-5.
63. A.L. Bailey, O. Dmytrenko, L. Greenberg, A.L. Bredemeyer, P. Ma, J. Liu, V. Penna, E.S. Winkler, S. Sviben, E. Brooks, A.P. Nair, K.A. Heck, A.S. Rali, L. Simpson, M. Saririan, D. Hobohm, W.T. Stump, J.A. Fitzpatrick, X. Xie, X. Zhang, P.Y. Shi, J.T. Hinson, W.T. Gi, C. Schmidt, F. Leuschner, C.Y. Lin, M.S. Diamond, M.J. Greenberg, K.J. Lavine, *SARS-CoV-2 Infects Human Engineered Heart Tissues and Models COVID-19 Myocarditis,* JACC Basic to Transl. Sci. 6 (2021). https://doi.org/10.1016/j.jacbts.2021.01.002.
64. Y. Wang, P. Wang, J. Qin, *Microfluidic Organs-on-a-Chip for Modeling Human Infectious Diseases,* Acc. Chem. Res. 54 (2021). https://doi.org/10.1021/acs.accounts.1c00411.
65. L. Yiangou, R.P. Davis, C.L. Mummery, *Using Cardiovascular Cells from Human Pluripotent Stem Cells for COVID-19 Research: Why the Heart Fails,* Stem Cell Reports. 16 (2020) 1–13. https://doi.org/10.1016/j.stemcr.2020.11.003.
66. M. Prondzynski, M.D. Lemoine, A.T. Zech, A. Horváth, V. Di Mauro, J.T. Koivumäki, N. Kresin, J. Busch, T. Krause, E. Krämer, S. Schlossarek, M. Spohn, F.W. Friedrich, J. Münch, S.D. Laufer, C. Redwood, A.E. Volk, A. Hansen, G. Mearini, D. Catalucci, C. Meyer, T. Christ, M. Patten, T. Eschenhagen, L. *Carrier, Disease modeling of a mutation in α-actinin 2 guides clinical therapy in hypertrophic cardiomyopathy,* EMBO Mol. Med. 11 (2019) 1–18. https://doi.org/10.15252/emmm.201911115.
67. E.Y. Wang, N. Rafatian, Y. Zhao, A. Lee, B.F.L. Lai, R.X. Lu, D. Jekic, L. Davenport Huyer, E.J. Knee-Walden, S. Bhattacharya, P.H. Backx, M. Radisic, *Biowire Model of Interstitial and Focal Cardiac Fibrosis,* ACS Cent. Sci. 5 (2019) 1146–1158. https://doi.org/10.1021/acscentsci.9b00052.
68. Y. Zhao, N. Rafatian, N.T. Feric, B.J. Cox, R. Aschar-Sobbi, E.Y. Wang, P. Aggarwal, B. Zhang, G. Conant, K. Ronaldson-Bouchard, A. Pahnke, S. Protze, J.H. Lee, L. Davenport Huyer, D. Jekic, A. Wickeler, H.E. Naguib, G.M. Keller, G. Vunjak-Novakovic, U. Broeckel, P.H. Backx, M. Radisic, *A Platform for Generation of Chamber-Specific Cardiac Tissues and Disease Modeling,* Cell. 176 (2019) 913-927.e18. https://doi.org/10.1016/j.cell.2018.11.042.
69. G. Wang, M.L. McCain, L. Yang, A. He, F.S. Pasqualini, A. Agarwal, H. Yuan, D. Jiang, D. Zhang, L. Zangi, J. Geva, A.E. Roberts, Q. Ma, J. Ding, J. Chen, D.Z. Wang, K. Li, J. Wang, R.J.A. Wanders, W. Kulik, F.M. Vaz, M.A. Laflamme, C.E. Murry, K.R. Chien, R.I. Kelley, G.M. Church, K.K. Parker, W.T. Pu, *Modeling the mitochondrial cardiomyopathy of Barth syndrome with induced pluripotent stem cell and heart-on-chip technologies,* Nat. Med. 20 (2014) 616–623. https://doi.org/10.1038/nm.3545.
70. L.A. Macqueen, S.P. Sheehy, C.O. Chantre, J.F. Zimmerman, F.S. Pasqualini, X. Liu, J.A. Goss, P.H. Campbell, G.M. Gonzalez, S.J. Park, A.K. Capulli, J.P. Ferrier, T. Fettah Kosar, L. Mahadevan, W.T. Pu, K.K. Parker, *A tissue-engineered scale model of the heart ventricle,* Nat. Biomed. Eng. 2 (2018) 930–941. https://doi.org/10.1038/s41551-018-0271-5.

71. E. Forte, M.B. Furtado, N. Rosenthal, *The interstitium in cardiac repair: role of the immune– stromal cell interplay,* Nat. Rev. Cardiol. 15 (2018) 601–616. https://doi.org/10.1038/s41569- 018-0077-x.
72. E. Tampakakis, H. Gangrade, S. Glavaris, M. Htet, S. Murphy, B.L. Lin, T. Liu, A. Saberi, M. Miyamoto, W. Kowalski, Y.-S. Mukouyama, G. Lee, L. Minichiello, C. Kwon, *Heart neurons use clock genes to control myocyte proliferation,* Sci. Adv. 7 (2021). https://doi.org/10.1126/sciadv.abh4181.
73. N. Milani-Nejad, P.M.L. Janssen, *Small and large animal models in cardiac contraction research: Advantages and disadvantages,* Pharmacol. Ther. 141 (2014) 235–249. https://doi.org/10.1016/j.pharmthera.2013.10.007.
74. T. Colatsky, B. Fermini, G. Gintant, J.B. Pierson, P. Sager, Y. Sekino, D.G. Strauss, N. Stockbridge, *The Comprehensive in Vitro Proarrhythmia Assay (CiPA) initiative — Update on progress,* J. Pharmacol. Toxicol. Methods. 81 (2016) 15–20. https://doi.org/10.1016/j.vascn.2016.06.002.
75. U. Saleem, B.J.V. Meer, P.A. Katili, N.A.N.M. Yusof, I. Mannhardt, A.K. Garcia, L. Tertoolen, T. De Korte, M.L.H. Vlaming, K. McGlynn, J. Nebel, A. Bahinski, K. Harris, E. Rossman, X. Xu, F.L. Burton, G.L. Smith, P. Clements, C.L. Mummery, T. Eschenhagen, A. Hansen, C. Denning, *Blinded, Multicenter Evaluation of Drug-induced Changes in Contractility Using Human- induced Pluripotent Stem Cell-derived Cardiomyocytes,* Toxicol. Sci. 176 (2020). https://doi.org/10.1093/toxsci/kfaa058.
76. B.J. van Meer, A. Krotenberg, L. Sala, R.P. Davis, T. Eschenhagen, C. Denning, L.G.J. Tertoolen, C.L. Mummery, *Simultaneous measurement of excitation-contraction coupling parameters identifies mechanisms underlying contractile responses of hiPSC-derived cardiomyocytes,* Nat. Commun. 10 (2019) 1–9. https://doi.org/10.1038/s41467-019-12354-8.
77. S.M. Ravenscroft, A. Pointon, A.W. Williams, M.J. Cross, J.E. Sidaway, *Cardiac non-myocyte cells show enhanced pharmacological function suggestive of contractile maturity in stem cell derived cardiomyocyte microtissues,* Toxicol. Sci. 152 (2016) 99–112. https://doi.org/10.1093/toxsci/kfw069.
78. M. Takeda, S. Miyagawa, S. Fukushima, A. Saito, E. Ito, A. Harada, R. Matsuura, H. Iseoka, N. Sougawa, N. Mochizuki-Oda, M. Matsusaki, M. Akashi, Y. Sawa, *Development of In Vitro Drug- Induced Cardiotoxicity Assay by Using Three-Dimensional Cardiac Tissues Derived from Human Induced Pluripotent Stem Cells.,* Tissue Eng. Part C. Methods. 24 (2018) 56–67. https://doi.org/10.1089/ten.TEC.2017.0247.
79. A. Pointon, A.R. Harmer, I.L. Dale, N. Abi-Gerges, J. Bowes, C. Pollard, H. Garside, *Assessment of cardiomyocyte contraction in human-induced pluripotent stem cell-derived cardiomyocytes,* Toxicol. Sci. 144 (2015) 227–237. https://doi.org/10.1093/toxsci/kfu312.
80. C.R. Archer, R. Sargeant, J. Basak, J. Pilling, J.R. Barnes, A. Pointon, *Characterization and validation of a human 3D cardiac microtissue for the assessment of changes in cardiac pathology,* Sci. Rep. (2018). https://doi.org/10.1038/s41598-018-28393-y.
81. P. Vulto, J. Joore, *Adoption of organ-on-chip platforms by the pharmaceutical industry,* Nat. Rev. Drug Discov. (2021). https://doi.org/10.1038/s41573-021-00323-0.

82. A. Skardal, S. V. Murphy, M. Devarasetty, I. Mead, H.W. Kang, Y.J. Seol, Y.S. Zhang, S.R. Shin, L. Zhao, J. Aleman, A.R. Hall, T.D. Shupe, A. Kleensang, M.R. Dokmeci, S. Jin Lee, J.D. Jackson, J.J. Yoo, T. Hartung, A. Khademhosseini, S. Soker, C.E. Bishop, A. Atala, *Multi-tissue interactions in an integrated three-tissue organ-on-a-chip platform,* Sci. Rep. 7 (2017) 1–16. https://doi.org/10.1038/s41598-017-08879-x.
83. J. Lee, S. Mehrotra, E. Zare-Eelanjegh, R.O. Rodrigues, A. Akbarinejad, D. Ge, L. Amato, K. Kiaee, Y. Fang, A. Rosenkranz, W. Keung, B.B. Mandal, R.A. Li, T. Zhang, H. Lee, M.R. Dokmeci, Y.S. Zhang, A. Khademhosseini, S.R. Shin, *A Heart-Breast Cancer-on-a-Chip Platform for Disease Modeling and Monitoring of Cardiotoxicity Induced by Cancer Chemotherapy,* Small. 17 (2021) 2004258. https://doi.org/10.1002/smll.202004258.
84. T. de Korte, P.A. Katili, N.A.N. Mohd Yusof, B.J. van Meer, U. Saleem, F.L. Burton, G.L. Smith, P. Clements, C.L. Mummery, T. Eschenhagen, A. Hansen, C. Denning, *Unlocking Personalized Biomedicine and Drug Discovery with Human Induced Pluripotent Stem Cell–Derived Cardiomyocytes: Fit for Purpose or Forever Elusive?*, Annu. Rev. Pharmacol. Toxicol. 60 (2020) 529–551. https://doi.org/10.1146/annurev-pharmtox-010919-023309.
85. I. Mannhardt, K. Breckwoldt, D. Letuffe-Brenière, S. Schaaf, H. Schulz, C. Neuber, A. Benzin, T. Werner, A. Eder, T. Schulze, B. Klampe, T. Christ, M.N. Hirt, N. Huebner, A. Moretti, T. Eschenhagen, A. Hansen, *Human Engineered Heart Tissue: Analysis of Contractile Force,* Stem Cell Reports. 7 (2016) 29–42. https://doi.org/10.1016/j.stemcr.2016.04.011.
86. I. Mannhardt, U. Saleem, D. Mosqueira, M.F. Loos, B.M. Ulmer, M.D. Lemoine, C. Larsson, C. Améen, T. de Korte, M.L.H. Vlaming, K. Harris, P. Clements, C. Denning, A. Hansen, T. Eschenhagen, *Comparison of 10 Control hPSC Lines for Drug Screening in an Engineered Heart Tissue Format,* Stem Cell Reports. 15 (2020) 983–998. https://doi.org/10.1016/j.stemcr.2020.09.002.
87. H.F. Lu, M.F. Leong, T.C. Lim, Y.P. Chua, J.K. Lim, C. Du, A.C.A. Wan, *Engineering a functional three-dimensional human cardiac tissue model for drug toxicity screening,* Biofabrication. 9 (2017) 025011. https://doi.org/10.1088/1758-5090/aa6c3a.
88. N.T. Feric, I. Pallotta, R. Singh, D.R. Bogdanowicz, M.M. Gustilo, K.W. Chaudhary, R.N. Willette, T.P. Chendrimada, X. Xu, M.P. Graziano, R. Aschar-Sobbi, *Engineered Cardiac Tissues Generated in the Biowire II: A Platform for Human-Based Drug Discovery,* Toxicol. Sci. 172 (2019) 89–97. https://doi.org/10.1093/toxsci/kfz168.
89. J.U. Lind, M. Yadid, I. Perkins, B.B. O'Connor, F. Eweje, C.O. Chantre, M.A. Hemphill, H. Yuan, P.H. Campbell, J.J. Vlassak, K.K. Parker, *Cardiac microphysiological devices with flexible thin- film sensors for higher-throughput drug screening,* Lab Chip. 17 (2017) 3692–3703. https://doi.org/10.1039/C7LC00740J.
90. M.C. Ribeiro, R.H. Slaats, V. Schwach, J.M. Rivera-Arbelaez, L.G.J. Tertoolen, B.J. van Meer, R. Molenaar, C.L. Mummery, M.M.A.E. Claessens, R. Passier, *A cardiomyocyte show of force: A fluorescent alpha-actinin reporter line sheds light on human cardiomyocyte contractility versus substrate stiffness,* J. Mol. Cell. Cardiol. 141 (2020) 54–64. https://doi.org/10.1016/j.yjmcc.2020.03.008.
91. H. Kolesová, V. Olejníčková, A. Kvasilová, M. Gregorovičová, D. Sedmera, *Tissue clearing and imaging methods for cardiovascular development,* IScience. 24 (2021). https://doi.org/10.1016/j.isci.2021.102387.

92. D.S. Richardson, J.W. Lichtman, *Clarifying Tissue Clearing,* Cell. 162 (2015). https://doi.org/10.1016/j.cell.2015.06.067.
93. A.D. Elliott, *Confocal Microscopy: Principles and Modern Practices,* Curr. Protoc. Cytom. 92 (2020). https://doi.org/10.1002/cpcy.68.
94. J. LoBiondo, M. Abramowitz, M.M. Friedman, *Microscope Objectives,* Curr. Protoc. Cytom. 58 (2011) 1–15. https://doi.org/10.1002/0471142956.cy0202s58.
95. O. Mastikhina, B.U. Moon, K. Williams, R. Hatkar, D. Gustafson, O. Mourad, X. Sun, M. Koo, A.Y.L. Lam, Y. Sun, J.E. Fish, E.W.K. Young, S.S. Nunes, *Human cardiac fibrosis-on-a-chip model recapitulates disease hallmarks and can serve as a platform for drug testing,* Biomaterials. 233 (2020) 119741. https://doi.org/10.1016/j.biomaterials.2019.119741.
96. I. Albert-smet, A. Marcos-vidal, J.J. Vaquero, M. Desco, A. Muñoz-barrutia, J. Ripoll, *Applications of Light-Sheet Microscopy in Microdevices,* 13 (2019) 1–15. https://doi.org/10.3389/fnana.2019.00001.
97. K. Ronaldson-Bouchard, G. Vunjak-Novakovic, *Organs-on-a-Chip: A Fast Track for Engineered Human Tissues in Drug Development,* Cell Stem Cell. 22 (2018) 310–324. https://doi.org/10.1016/j.stem.2018.02.011.
98. N. Cloonan, A.R.R. Forrest, G. Kolle, B.B.A. Gardiner, G.J. Faulkner, M.K. Brown, D.F. Taylor, A.L. Steptoe, S. Wani, G. Bethel, A.J. Robertson, A.C. Perkins, S.J. Bruce, C.C. Lee, S.S. Ranade, H.E. Peckham, J.M. Manning, K.J. McKernan, S.M. Grimmond, *Stem cell transcriptome profiling via massive-scale mRNA sequencing,* Nat. Methods. (2008). https://doi.org/10.1038/nmeth.1223.
99. J.C. Marioni, C.E. Mason, S.M. Mane, M. Stephens, Y. Gilad, *RNA-seq: An assessment of technical reproducibility and comparison with gene expression arrays,* Genome Res. 18 (2008) 1509–1517. https://doi.org/10.1101/gr.079558.108.
100. A. Mortazavi, B.A. Williams, K. McCue, L. Schaeffer, B. *Wold, Mapping and quantifying mammalian transcriptomes by RNA-Seq,* Nat. Methods. (2008). https://doi.org/10.1038/nmeth.1226.
101. Y. Deng, A. Finck, R. Fan, *Single-Cell Omics Analyses Enabled by Microchip Technologies,* Annu. Rev. Biomed. Eng. 21 (2019). https://doi.org/10.1146/annurev-bioeng-060418-052538.
102. B. Hwang, J.H. Lee, D. Bang, *Single-cell RNA sequencing technologies and bioinformatics pipelines,* Exp. Mol. Med. 50 (2018) 96. https://doi.org/10.1038/s12276-018-0071-8.
103. A.A. Kolodziejczyk, J.K. Kim, V. Svensson, J.C. Marioni, S.A. Teichmann, *The Technology and Biology of Single-Cell RNA Sequencing,* Mol. Cell. (2015). https://doi.org/10.1016/j.molcel.2015.04.005.
104. T.K. Olsen, N. Baryawno, *Introduction to Single-Cell RNA Sequencing,* Curr. Protoc. Mol. Biol. 122 (2018). https://doi.org/10.1002/cpmb.57.
C. Ziegenhain, B. Vieth, S. Parekh, B. Reinius, A. Guillaumet-Adkins, M. Smets, H.
105. Leonhardt, H. Heyn, I. Hellmann, W. Enard, *Comparative Analysis of Single-Cell RNA Sequencing Methods,* Mol. Cell. 65 (2017) 631-643.e4. https://doi.org/10.1016/j.molcel.2017.01.023.
106. S.C. van den Brink, F. Sage, Á. Vértesy, B. Spanjaard, J. Peterson-Maduro, C.S. Baron, C. Robin, A. van Oudenaarden, *Single-cell sequencing reveals dissociation-induced gene expression in tissue subpopulations,* Nat. Methods. 14 (2017) 935–936. https://doi.org/10.1038/nmeth.4437.

107. S. Black, D. Phillips, J.W. Hickey, J. Kennedy-Darling, V.G. Venkataraaman, N. Samusik, Y. Goltsev, C.M. Schürch, G.P. Nolan, *CODEX multiplexed tissue imaging with DNA-conjugated antibodies,* Nat. Protoc. 16 (2021). https://doi.org/10.1038/s41596-021-00556-8.
108. Q. Chang, O. Ornatsky, D. Hedley, *Staining of Frozen and Formalin-Fixed, Paraffin-Embedded Tissues with Metal-Labeled Antibodies for Imaging Mass Cytometry Analysis,* Curr. Protoc. Cytom. 82 (2017). https://doi.org/10.1002/cpcy.29.
109. A. Kinkhabwala, C. Herbel, J. Pankratz, D.A. Yushchenko, S. Rüberg, P. Praveen, S. Reiß, F.C. Rodriguez, D. Schäfer, J. Kollet, V. Dittmer, M. Martinez-Osuna, L. Minnerup, C. Reinhard, A. Dzionek, T.D. Rockel, S. Borbe, M. Büscher, J. Krieg, M. Nederlof, M. Jungblut, D. Eckardt, O. Hardt, C. Dose, E. Schumann, R.-P. Peters, S. Miltenyi, J. Schmitz, W. Müller, A. Bosio, *MACSima imaging cyclic staining (MICS) technology reveals combinatorial target pairs for CAR T cell treatment of solid tumors,* Sci. Rep. 12 (2022) 1911. https://doi.org/10.1038/s41598-022- 05841-4.
110. L. Miao, Y. Lu, A. Nusrat, H.Y. Abdelnasser, S. Datta, B. Zhou, R.J. Schwartz, M. Wu, *The spatiotemporal expression of notch1 and numb and their functional interaction during cardiac morphogenesis,* Cells. 10 (2021). https://doi.org/10.3390/cells10092192.
111. S. Vickovic, G. Eraslan, F. Salmén, J. Klughammer, L. Stenbeck, D. Schapiro, T. Äijö, R. Bonneau, L. Bergenstråhle, J.F. Navarro, J. Gould, G.K. Griffin, Å. Borg, M. Ronaghi, J. Frisén, J. Lundeberg, A. Regev, P.L. Ståhl, *High-definition spatial transcriptomics for in situ tissue profiling,* Nat. Methods. 16 (2019). https://doi.org/10.1038/s41592-019-0548-y.
112. S.R. Shin, T. Kilic, Y.S. Zhang, H. Avci, N. Hu, D. Kim, C. Branco, J. Aleman, S. Massa, A. Silvestri, J. Kang, A. Desalvo, M.A. Hussaini, S.K. Chae, A. Polini, N. Bhise, M.A. Hussain, H.Y. Lee, M.R. Dokmeci, A. Khademhosseini, *Label-Free and Regenerative Electrochemical Microfluidic Biosensors for Continual Monitoring of Cell Secretomes,* Adv. Sci. 4 (2017). https://doi.org/10.1002/advs.201600522.
113. C.M. Abreu, V. Thomas, P. Knaggs, A. Bunkheila, A. Cruz, S.R. Teixeira, P. Alpuim, L.W. Francis, A. Gebril, A. Ibrahim, L. Margarit, D. Gonzalez, P.P. Freitas, R.S. Conlan, I. Mendes Pinto, *Non- invasive molecular assessment of human embryo development and implantation potential,* Biosens. Bioelectron. (2020). https://doi.org/10.1016/j.bios.2020.112144.
114. S.S. Cortezzi, E.C. Cabral, M.G. Trevisan, C.R. Ferreira, A.S. Setti, D.P. de A.F. Braga, R. de C.S. Figueira, A. Iaconelli, M.N. Eberlin, E. Borges, *Prediction of embryo implantation potential by mass spectrometry fingerprinting of the culture medium,* REPRODUCTION. 145 (2013) 453– 462. https://doi.org/10.1530/REP-12-0168.
115. R.K. Iles, F.I. Sharara, R. Zmuidinaite, G. Abdo, S. Keshavarz, S.A. Butler, *Secretome profile selection of optimal IVF embryos by matrix-assisted laser desorption ionization time-of-flight mass spectrometry,* J. Assist. Reprod. Genet. 36 (2019) 1153–1160. https://doi.org/10.1007/s10815-019-01444-7.
116. H.M. Picton, K. Elder, F.D. Houghton, J.A. Hawkhead, A.J. Rutherford, J.E. Hogg, H.J. Leese, S.E. Harris, *Association between amino acid turnover and chromosome aneuploidy during human preimplantation embryo development in vitro,* Mol. Hum. Reprod. 16 (2010) 557–569. https://doi.org/10.1093/molehr/gaq040.

117. R. Jacob, M. Khan, Cardiac Biomarkers: *What Is and What Can Be,* Indian J. Cardiovasc. Dis. Women WINCARS. 03 (2018) 240–244. https://doi.org/10.1055/s-0039-1679104.
118. B. McDonaugh, M. Whyte, *The Evolution and Future Direction of The Cardiac Biomarker,* EMJ Cardiol. (2020). https://doi.org/10.33590/emjcardiol/20-00045.
119. E.W. Miller, *Small molecule fluorescent voltage indicators for studying membrane potential,* Curr. Opin. Chem. Biol. 33 (2016) 74–80. https://doi.org/10.1016/j.cbpa.2016.06.003.
120. C.O. Shea, A.P. Holmes, T.Y. Yu, J. Winter, S.P. Wells, J. Correia, B.J. Boukens, J.R. De Groot, G.S. Chu, X. Li, G.A. Ng, ElectroMap : *High-throughput open-source software for analysis and mapping of cardiac electrophysiology,* (2019) 1–13. https://doi.org/10.1038/s41598-018- 38263-2.
121. B.M. Maoz, A. Herland, O.Y.F. Henry, W.D. Leineweber, M. Yadid, J. Doyle, R. Mannix, V.J. Kujala, E.A. Fitzgerald, K.K. Parker, D.E. Ingber, *Organs-on-Chips with combined multi- electrode array and transepithelial electrical resistance measurement capabilities,* Lab Chip. 17 (2017) 2294–2302. https://doi.org/10.1039/c7lc00412e.
122. T. Shinozawa, K. Nakamura, M. Shoji, M. Morita, M. Kimura, H. Furukawa, H. Ueda, M. Shiramoto, K. Matsuguma, Y. Kaji, I. Ikushima, M. Yono, S.-Y. Liou, H. Nagai, A. Nakanishi, K. Yamamoto, S. Izumo, *Recapitulation of Clinical Individual Susceptibility to Drug-Induced QT Prolongation in Healthy Subjects Using iPSC-Derived Cardiomyocytes,* Stem Cell Reports. 8 (2017) 226–234. https://doi.org/10.1016/j.stemcr.2016.12.014.
123. I. Kehat, A. Gepstein, A. Spira, J. Itskovitz-Eldor, L. Gepstein, *High-Resolution Electrophysiological Assessment of Human Embryonic Stem Cell-Derived Cardiomyocytes,* Circ. Res. 91 (2002) 659–661. https://doi.org/10.1161/01.RES.0000039084.30342.9B.
124. A. Kalmykov, C. Huang, J. Bliley, D. Shiwarski, J. Tashman, A. Abdullah, S.K. Rastogi, S. Shukla, E. Mataev, A.W. Feinberg, K.J. Hsia, T. Cohen-karni, *Organ-on-e-chip : Three-dimensional self- rolled biosensor array for electrical interrogations of human electrogenic spheroids,* (2019).
125. Y.S. Zhang, J. Aleman, A. Arneri, *Micro-electrode channel guide (μECG) technology: an online method for continuous electrical recording in a human beating heart-on-chip You may also like From cardiac tissue engineering to heart-on-a-chip: beating challenges,* (2021). https://doi.org/10.1088/1758-5090/abe4c4.
126. N. Huebsch, P. Loskill, M.A. Mandegar, N.C. Marks, A.S. Sheehan, Z. Ma, A. Mathur, T.N. Nguyen, J.C. Yoo, L.M. Judge, C.I. Spencer, A.C. Chukka, C.R. Russell, P.L. So, B.R. Conklin, K.E. Healy, *Automated video-based analysis of contractility and calcium flux in human-induced pluripotent stem cell-derived cardiomyocytes cultured over different spatial scales,* Tissue Eng. - Part C Methods. (2015). https://doi.org/10.1089/ten.tec.2014.0283.
127. F.S. Pasqualini, A. Agarwal, B.B. O'Connor, Q. Liu, S.P. Sheehy, K.K. Parker, *Traction force microscopy of engineered cardiac tissues,* PLoS One. 13 (2018). https://doi.org/10.1371/journal.pone.0194706.
128. M. Dostanić, L.M. Windt, J.M. Stein, B.J. Van Meer, M. Bellin, V. Orlova, M. Mastrangeli, C.L. Mummery, P.M. Sarro, *A Miniaturized EHT Platform for Accurate Measurements of Tissue Contractile Properties,* J. Microelectromechanical Syst. 29 (2020). https://doi.org/10.1109/JMEMS.2020.3011196.

129. A.J.S. Ribeiro, O. Schwab, M.A. Mandegar, Y.-S. Ang, B.R. Conklin, D. Srivastava, B.L. Pruitt, *Multi-Imaging Method to Assay the Contractile Mechanical Output of Micropatterned Human iPSC-Derived Cardiac Myocytes,* Circ. Res. 120 (2017) 1572–1583. https://doi.org/10.1161/CIRCRESAHA.116.310363.
130. L. Sala, B.J. van Meer, L.G.J. Tertoolen, J. Bakkers, M. Bellin, R.P. Davis, C. Denning, M.A.E. Dieben, T. Eschenhagen, E. Giacomelli, C. Grandela, A. Hansen, E.R. Holman, M.R.M. Jongbloed, S.M. Kamel, C.D. Koopman, Q. Lachaud, I. Mannhardt, M.P.H. Mol, D. Mosqueira, V. V. Orlova, R. Passier, M.C. Ribeiro, U. Saleem, G.L. Smith, F.L. Burton, C.L. Mummery, *Musclemotion: A versatile open software tool to quantify cardiomyocyte and cardiac muscle contraction in vitro and in vivo,* Circ. Res. 122 (2018). https://doi.org/10.1161/CIRCRESAHA.117.312067.
131. B.J. van Meer, L. Sala, L.G.J. Tertoolen, G.L. Smith, F.L. Burton, C.L. Mummery, *Quantification of Muscle Contraction In Vitro and In Vivo Using MUSCLEMOTION Software: From Stem Cell- Derived Cardiomyocytes to Zebrafish and Human Hearts,* Curr. Protoc. Hum. Genet. 99 (2018) e67. https://doi.org/10.1002/cphg.67.
132. R.D. Evans, L.C. *Heather, Metabolic pathways and abnormalities,* Surg. 34 (2016) 266–272.https://doi.org/10.1016/j.mpsur.2016.03.010.
133. H. Taegtmeyer, M.E. Young, G.D. Lopaschuk, E.D. Abel, H. Brunengraber, V. Darley-Usmar, C. Des Rosiers, R. Gerszten, J.F. Glatz, J.L. Griffin, R.J. Gropler, H.-G. Holzhuetter, J.R. Kizer, E.D. Lewandowski, C.R. Malloy, S. Neubauer, L.R. Peterson, M.A. Portman, F.A. Recchia, J.E. Van Eyk, T.J. Wang, *Assessing Cardiac Metabolism,* Circ.
134. Res. 118 (2016) 1659–1701. https://doi.org/10.1161/RES.0000000000000097. R.A. Breckenridge, I. Piotrowska, K.-E. Ng, T.J. Ragan, J.A. West, S. Kotecha, N. Towers, M. Bennett, P.C. Kienesberger, R.T. Smolenski, H.K. Siddall, J.L. Offer, M.M. Mocanu, D.M. Yelon, J.R.B. Dyck, J.L. Griffin, A.Y. Abramov, A.P. Gould, T.J. Mohun, Hypoxic *Regulation of Hand1 Controls the Fetal-Neonatal Switch in Cardiac Metabolism,* PLoS Biol. 11 (2013) e1001666. https://doi.org/10.1371/journal.pbio.1001666.
135. G.D. Lopaschuk, J.S. Jaswal, *Energy Metabolic Phenotype of the Cardiomyocyte During Development, Differentiation, and Postnatal Maturation,* J. Cardiovasc. Pharmacol. 56 (2010) 130–140. https://doi.org/10.1097/FJC.0b013e3181e74a14.
136. K.S. Mdaki, T.D. Larsen, L.J. Weaver, M.L. Baack, *Age related bioenergetics profiles in isolated rat cardiomyocytes using extracellular flux analyses,* PLoS One. 11 (2016). https://doi.org/10.1371/journal.pone.0149002.
137. T.C. Kuhn, J. Knobel, S. Burkert-Rettenmaier, X. Li, I.S. Meyer, A. Jungmann, F. Sicklinger, J. Backs, F. Lasitschka, O.J. Müller, H.A. Katus, J. Krijgsveld, F. Leuschner, *Secretome Analysis of Cardiomyocytes Identifies PCSK6 (Proprotein Convertase Subtilisin/Kexin Type 6) as a Novel Player in Cardiac Remodeling After Myocardial Infarction,* Circulation. 141 (2020) 1628–1644. https://doi.org/10.1161/CIRCULATIONAHA.119.044914.
138. A.W. Robert, I.T. Pereira, B. Dallagiovanna, M.A. Stimamiglio, *Secretome Analysis Performed During in vitro Cardiac Differentiation: Discovering the Cardiac Microenvironment,* Front. Cell Dev. Biol. 8 (2020) 49. https://doi.org/10.3389/fcell.2020.00049.

139. E. Brauchle, K. Schenke-Layland, *Raman microspectroscopy for the development and screening of recombinant cell lines,* Biotechnol. J. 12 (2017) 1600412. https://doi.org/10.1002/biot.201600412.
140. N. Shen, A. Knopf, C. Westendorf, U. Kraushaar, J. Riedl, H. Bauer, S. Pöschel, S.L. Layland, M. Holeiter, S. Knolle, E. Brauchle, A. Nsair, S. Hinderer, K. Schenke-Layland, *Steps toward Maturation of Embryonic Stem Cell-Derived Cardiomyocytes by Defined Physical Signals,* Stem Cell Reports. 9 (2017) 122–135. https://doi.org/10.1016/j.stemcr.2017.04.021.
141. M. Votteler, D.A. Carvajal Berrio, M. Pudlas, H. Walles, U.A. Stock, K. Schenke-Layland, *Raman spectroscopy for the non-contact and non-destructive monitoring of collagen damage within tissues,* J. Biophotonics. 5 (2012) 47–56. https://doi.org/10.1002/jbio.201100068.
142. E. Brauchle, K. Schenke-Layland, *Raman spectroscopy in biomedicine – non-invasive in vitro analysis of cells and extracellular matrix components in tissues,* Biotechnol. J. 8 (2013) 288– 297. https://doi.org/10.1002/biot.201200163.
143. E. Harari, L. Guo, S.L. Smith, R.E. Braumann, R. Virmani, A. V. Finn, *Heart-resident macrophages: are they involved in the rhythm of every beat?*, J. Thorac. Dis. 9 (2017) 2264–2267. https://doi.org/10.21037/jtd.2017.07.43.
144. M. Hulsmans, S. Clauss, L. Xiao, A.D. Aguirre, K.R. King, A. Hanley, W.J. Hucker, E.M. Wülfers, G. Seemann, G. Courties, Y. Iwamoto, Y. Sun, A.J. Savol, H.B. Sager, K.J. Lavine, G.A. Fishbein, D.E. Capen, N. Da Silva, L. Miquerol, H. Wakimoto, C.E. Seidman, J.G. Seidman, R.I. Sadreyev, K. Naxerova, R.N. Mitchell, D. Brown, P. Libby, R. Weissleder, F.K. Swirski, P. Kohl, C. Vinegoni, D.J. Milan, P.T. Ellinor, M. Nahrendorf, *Macrophages Facilitate Electrical Conduction in the Heart,* Cell. (2017). https://doi.org/10.1016/j.cell.2017.03.050.
145. J.A. Nicolás-Ávila, A. V. Lechuga-Vieco, L. Esteban-Martínez, M. Sánchez-Díaz, E. Díaz-García, D.J. Santiago, A. Rubio-Ponce, J.L.Y. Li, A. Balachander, J.A. Quintana, R. Martínez-de-Mena, B. Castejón-Vega, A. Pun-García, P.G. Través, E. Bonzón-Kulichenko, F. García-Marqués, L. Cussó, N. A-González, A. González-Guerra, M. Roche-Molina, S. Martin-Salamanca, G. Crainiciuc, G. Guzmán, J. Larrazabal, E. Herrero-Galán, J. Alegre-Cebollada, G. Lemke, C. V. Rothlin, L.J. Jimenez-Borreguero, G. Reyes, A. Castrillo, M. Desco, P. Muñoz-Cánoves, B. Ibáñez, M. Torres, L.G. Ng, S.G. Priori, H. Bueno, J. Vázquez, M.D. Cordero, J.A. Bernal, J.A. Enríquez, A. Hidalgo, *A Network of Macrophages Supports Mitochondrial Homeostasis in the Heart,* Cell. 183 (2020). https://doi.org/10.1016/j.cell.2020.08.031.
146. J.L. Ardell, J.A. Armour, *Neurocardiology: Structure-Based Function,* in: Compr. Physiol., John Wiley & Sons, Inc., Hoboken, NJ, USA, 2016: pp. 1635–1653. https://doi.org/10.1002/cphy.c150046.
147. D.P. Zipes, J. Jalife, W.G. Stevenson, Cardiac Electrophysiology: From Cell to Bedside: Seventh Edition, 2017. https://doi.org/10.1161/01.cir.0000146800.76451.65.
148. L. Farache Trajano, N. Smart, *Immunomodulation for optimal cardiac regeneration: insights from comparative analyses,* Npj Regen. Med. 6 (2021) 1–11. https://doi.org/10.1038/s41536- 021-00118-2.

149. M. Nahrendorf, F.K. Swirski, E. Aikawa, L. Stangenberg, T. Wurdinger, J.L. Figueiredo, P. Libby, R. Weissleder, M.J. Pittet, *The healing myocardium sequentially mobilizes two monocyte subsets with divergent and complementary functions*, J. Exp. Med. (2007). https://doi.org/10.1084/jem.20070885.
150. E. Wake, K. Brack, *Characterization of the intrinsic cardiac nervous system.*, Auton. Neurosci. 199 (2016) 3–16. https://doi.org/10.1016/j.autneu.2016.08.006.
151. A. Marcek Chorvatova, M. Cagalinec, D. Chorvat, *Time-Resolved Imaging of and Its Applications for Evaluating the in Living Cardiac Cells,* in: 2021: pp. 403–414. https://doi.org/10.1007/978-1-0716-1262-0_26.
152. A. Zbinden, J. Marzi, K. Schlünder, C. Probst, M. Urbanczyk, S. Black, E.M. Brauchle, S.L. Layland, U. Kraushaar, G. Duffy, K. Schenke-Layland, P. Loskill, *Non-invasive marker- independent high content analysis of a microphysiological human pancreas-on-a-chip model,* Matrix Biol. 85–86 (2020) 205–220. https://doi.org/10.1016/j.matbio.2019.06.008.
153. E. Tanumihardja, R.H. Slaats, A.D. van der Meer, R. Passier, W. Olthuis, A. van den Berg, *Measuring Both pH and O 2 with a Single On-Chip Sensor in Cultures of Human Pluripotent Stem Cell-Derived Cardiomyocytes to Track Induced Changes in Cellular Metabolism,* ACS Sensors. 6 (2021) 267–274. https://doi.org/10.1021/acssensors.0c02282.
154. O. Schneider, A. Moruzzi, S. Fuchs, A. Grobel, H.S. Schulze, T. Mayr, P. Loskill, *Fusing spheroids to aligned µ-tissues in a Heart-on-Chip featuring oxygen sensing and electrical pacing capabilities,* BioRxiv. (2022) 2022.02.26.482011. https://doi.org/10.1101/2022.02.26.482011.
155. Y.S. Zhang, J. Aleman, S.R. Shin, T. Kilic, D. Kim, S.A.M. Shaegh, S. Massa, R. Riahi, S. Chae, N. Hu, H. Avci, W. Zhang, A. Silvestri, A.S. Nezhad, A. Manbohi, F. De Ferrari, A. Polini, G. Calzone, N. Shaikh, P. Alerasool, E. Budina, J. Kang, N. Bhise, J. Ribas, A. Pourmand, A. Skardal, T. Shupe, C.E. Bishop, M.R. Dokmeci, A. Atala, A. Khademhosseini, *Multisensor-integrated organs-on- chips platform for automated and continual in situ monitoring of organoid behaviors,* Proc. Natl. Acad. Sci. U. S. A. 114 (2017) E2293–E2302. https://doi.org/10.1073/pnas.1612906114.
156. S. Fuchs, S. Johansson, A.Ø. Tjell, G. Werr, T. Mayr, M. Tenje, *In-Line Analysis of Organ-on-Chip Systems with Sensors: Integration, Fabrication, Challenges, and Potential, ACS Biomater.* Sci. Eng. (2021). https://doi.org/10.1021/acsbiomaterials.0c01110.

Integration of hiPSC-derived macrophages into 3D cardiac microtissues

Authors and Affiliations

Ulgu Arslan[1], Nikola Popovic[1], Kendy E. Urdaneta[1], Milica Dostanic[1], Francijna E. van den Hil[1], Richard Davis[1], Christine L. Mummery[1], Valeria Orlova[1*]

[1] Department of Anatomy and Embryology, Leiden University Medical Centre, Leiden, The Netherlands

* Corresponding author

In preparation

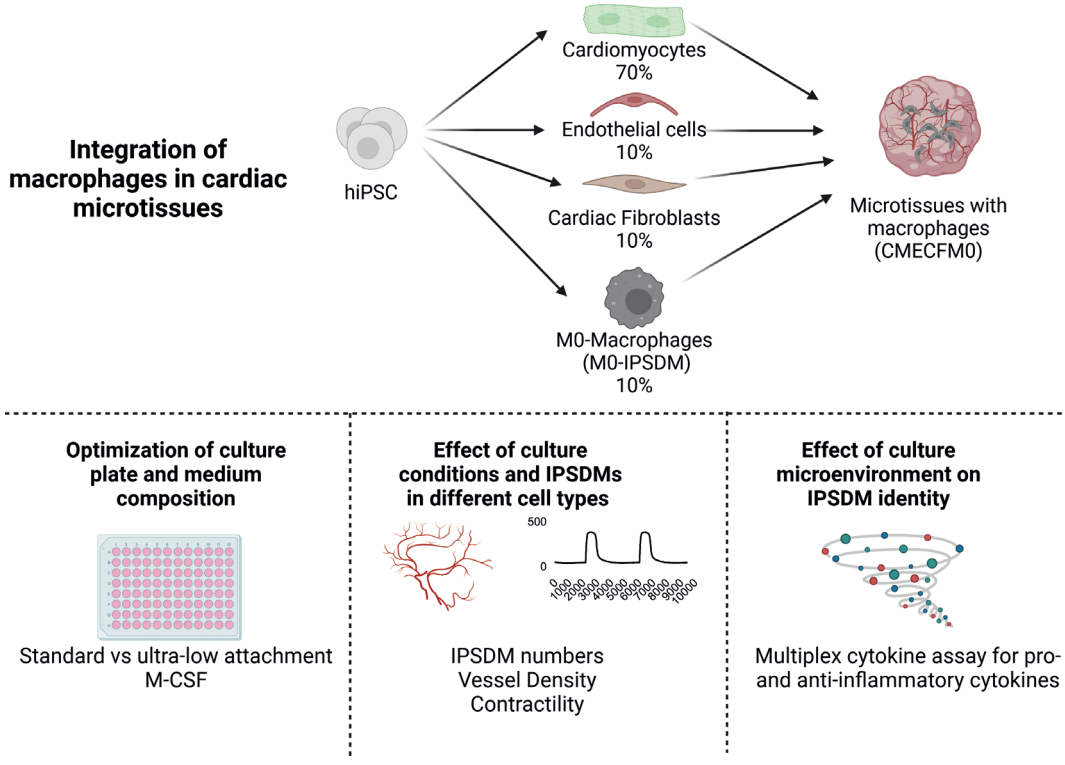

Graphical abstract

Summary

Cardiac resident macrophages (CRM) play an important role in maintaining homeostasis in health and disease in the human heart. Their involvement in tissue regeneration makes them particularly interesting as a therapeutic target in the treatment of several heart disease such as myocardial infarction and consequent fibrosis. CRMs are heterogenous in their phenotype and function. Precise targeting of CRMs in *in vivo* models presents technical challenges due to the lack of specific markers and techniques to distinguish CRMs.

In this study, we developed a 3D cardiac microtissue model using human induced pluripotent stem cell (hiPSC)-derived macrophages (IPSDMs) (CMECFM0) in addition to hiPSC-derived cardiomyocytes, endothelial cells and cardiac fibroblasts. We tested various conditions such as 96-well plate types and cell culture growth medium composition to optimize the formation and maintenance of CMECFM0.

We found that adding macrophage colony-stimulating factor (M-CSF) increased the number of IPSDMs present in CMECFM0s on days 7 and 14 of the culture period, although this diminished by day 21. M-CSF supplementation did not affect vessel density or the duration of microtissue contraction. However, we did observe significant differences in the amounts of pro- and anti- inflammatory cytokines in CMECFM0s when M-CSF was added. Our study demonstrated that IPSDMs can be integrated into the cardiac microtissues under appropriate conditions without migrating out. However, we noted that an initial increase in macrophage numbers in the microtissues was not sustained and their number decreased over time. Future studies will address why the IPSDMs disappeared but, more importantly, whether they are plastic and respond to the cardiac microtissue environment by acquiring CRM-like function and identity, adding to their value as a model of inflammation in the heart.

Keywords:

human induced pluripotent stem cells; cardiac microtissue; macrophages.

Introduction

The heart is one of the most important organs in the body and the interaction between the local tissue microenvironment and the different cellular components play an important role in health and disease. Among the cellular components, cardiac resident macrophages (CRMs) have emerged as one key element as they contribute to the structural integrity, function and immune response to stimuli in the heart (Zaman and Epelman, 2022; Ginhoux and Jung, 2014; Hulsmans et al., 2017; Nicolás-Ávila et al., 2020). Unlike their circulatory counterparts, CRMs are located in the heart throughout their lifetime. CRMs originate from the yolk-sac during early embryonic hematopoiesis, and are important for the maintenance of the healthy heart (Hoeffel and Ginhoux, 2015). Importantly, these yolk-sac derived CRMs

are mostly involved in the tissue regeneration and angiogenesis and upon injury, CRMs can self-renew through local proliferation (Epelman et al., 2014; Dick et al., 2019). Intriguingly, adult hematopoiesis coincides with the loss of the regenerative ability of the heart and with bone marrow-derived macrophages infiltrating the heart upon injury in animal models (Molawi et al., 2014). However, at present, knowledge on CRMs in the human heart is limited.

Several *in vitro* 3D tissue models have been established to study macrophages in various culture platforms and have shown their effect on tissue regeneration, for example in engineered skeletal muscle (Juhas et al., 2018). Other studies highlighted how the microenvironmental cues affect the phenotype and function of macrophages (Lavin et al., 2014; Saleh and Bryant, 2018; Dollinger et al., 2018). However, macrophage populations in tissues are heterogenous and are difficult to isolate and culture *in vitro* (Gordon and Plüddemann, 2017). Peripheral blood-derived macrophages are often used to study macrophage biology, but their developmental origin differs from that of tissue-resident macrophages and therefore they are not a true model of tissue-resident cells (Ginhoux and Jung, 2014). Human induced pluripotent stem cell (hiPSC)-derived macrophages appear on the basis of their developmental origin in differentiation could be an alternative cell source of tissue-resident macrophages (Lee et al., 2018). Recent studies demonstrated that hiPSC-derived macrophages promote intestine, skin and brain organoid maturation and functionality (Múnera et al., 2023; Hudaa Gopee et al., 2023; Song et al., 2024; Aktories et al., 2022). Furthermore, incorporating macrophages in the organoid system promoted the acquisition of tissue-specific macrophage characteristics. We hypothesized that a similar principle could apply to other organ models, including the heart.

Here we attempted to integrate hiPSC-derived macrophages (IPSDMs) (Cao et al., 2019) into 3D cardiac microtissues (MTs) (Giacomelli et al., 2020). We demonstrated that IPSDMs survived in 3D cardiac MTs for at least three weeks, although their numbers decreased over time. We did not observe effects of IPSDMs on the microvascular network density or contractile parameters under the conditions analyzed. We also showed that secreted cytokines can be detected in the medium collected from 3D cardiac MTs, but this requires large number of MTs as well as additional concentration step of the samples in order to reach the detection limit. We found both anti- and pro- inflammatory cytokines in the medium, indicating that IPSDMs resemble a mixed population of M2 and M1 sub-types. Additional studies addressing medium composition, macrophage number and timing will be required to advance the model such that it is suitable for studies on the role of macrophages in the healthy heart, as well as in cardiac disease modeling.

Methods

hiPSC lines and maintenance

Maintenance of hiPSCs were done on vitronectin-coated 6x-well plates and the medium used was TeSR-E8, all from STEMCELL Technologies, following the manufacturer's instructions. The following hiPSC lines were used in this study: LUMC0020iCTRL06 (derived from skin fibroblasts, https://hpscreg.eu/cell-line/LUMCi028-A) (Zhang et al., 2014); NIH Center for Regenerative Medicine: NCRM-1 (derived from CD34+ cord blood cells, https://hpscreg.eu/cell-line/CRMi003- A), obtained from RUDCR Infinite Biologics at Rutgers University, was modified in-house with a GFP expression cassette under the human cytomegalovirus (hCMV) early enhancer/chicken β actin (CAG) promoter using a previously established protocol (Rostovskaya et al., 2012); The Allen Cell Collection: AICS- 0061 cl.36 (derived from skin fibroblasts, https://hpscreg.eu/cell-line/UCSFi001-A-28) with mEGFP insertion site at H2B was obtained from Coriell Institute for Medical Research.

Differentiation of cardiomyocytes

hiPSC differentiation into CM was induced in 2D monolayer as described previously (Giacomelli et al., 2017; Berg et al., 2016). Shortly, Matrigel coated plates (75 µg/ml growth factor-reduced Matrigel (Corning)) was seeded with 25 × 103 cells/cm2 on day -1. On day 0, cardiac mesoderm differentiation was induced by changing E8 to B(P)EL medium (Bovine Serum Albumin [BSA] and Essential Lipids), supplemented with a cytokine mixture (20 ng/ml BMP4, R&D Systems; 20 ng/ml ACTIVIN A, Miltenyi Biotec; 1.5 µM GSK3 inhibitor CHIR99021, Axon Medchem). After 3 days, medium was refreshed with B(P)EL supplemented with XAV939 which is a WNT inhibitor (5 µM, Tocris) and incubated for 3 days. After this, B(P)EL medium was refreshed every 3-4 days.

Differentiation of cardiac fibroblasts

HiPSC differentiation to CFs was induced using an epicardial (EPI) monolayer differentiation protocol (Guadix et al., 2017) as a starting point (Giacomelli et al., 2020). Briefly, Matrigel coated 6x well plates was seeded with 25 × 103 cells per cm2 on day -1. On day 0, cardiac mesoderm was induced as described above. After 3 days, medium was refreshed with B(P) EL supplemented with XAV939 (5 µM), BMP4 (30 ng/ml) and Retinoic Acid (RA; 1 µM; Sigma Aldrich) and incubated for 3 days. On day 6, the medium was refreshed with B(P) EL medium supplemented with BMP4 (30 ng/ml) and RA (1 µM). On day 9, 15 × 103 per cm2 were seeded on fibronectin coated 6x-well plates (5 µg/ml of fibronectin from bovine plasma (fibronectin; Sigma Aldrich)) in B(P)EL medium supplemented with the TGFβ inhibitor SB431542 (10 µM; Tocris Bioscience). By day 12, EPIs were confluent and ready for passaging. EPI cells (30 cm2 per vial) were cryopreserved using CryoStor CS10 medium (0.5 ml/vial; Stem Cell Technologies).

EPI cryovials were used for further differentiation to CF in monolayer. Briefly, 25 × 103 EPIs were seeded per cm2 on tissue culture vitronection coated 6x well plates in B(P)EL medium supplemented with FGF2 (10 ng/ml; R&D Systems) on day 12. On day 13 and every 2 days thereafter, medium was refreshed with B(P)EL supplemented with FGF2 (10 ng/ml). On day 19, medium was changed from B(P)EL to Fibroblast Growth Medium 3 (FGM3; PromoCell) to expand CFs. FGM3 was refreshed every 2-3 days for approximately 10 days in total. Around day 29, CFs were confluent and ready to be passaged at 1:2 ratio. FGM3 was refreshed 24h after passaging and every 2-3 days thereafter. CFs (10cm2 per vial) were cryopreserved using CryoStor CS10 medium (0.5 ml/vial; Stem Cell Technologies).

Differentiation of endothelial cells

hiPSC differentiation to ECs was induced as described previously (Orlova et al., 2014). Briefly, hiPSCs were maintained in mTeSR-E8 medium. Mesoderm was induced between day 0-3. mTeSR-E8 medium was replaced with B(P)EL medium supplemented with 8 µM CHIR99021 (Tocris Bioscience, 4423). Cells were refreshed with vascular specification medium B(P)EL supplemented with VEGF (50 ng/ml) and 10 µM SB431542 (Tocris Bioscience, 1614) at day 3, day 6, and day 9. hiPSC-ECs were isolated on day 10 and CD31-DynabeadsTM (Thermo Fisher Scientific) was used, as previously described (Orlova et al., 2014). hiPSC-ECs were expanded in complete EC growth medium (EC-CGM) comprised of Human Endothelial-serum free medium (EC-SFM) with 1% Human platelet poor serum (P2918, Sigma) and supplemented with VEGF (30 ng/ml) and bFGF (20 ng/ml), as described previously with minor modifications (Orlova et al., 2014). hiPSC-ECs were expanded for additional 3-4 days post- isolation until confluent and cryopreserved using cryopreservation medium consists of 50% fetal bovine serum, 40% EGM2 and 10% dimethyl sulfoxide at passage number 1 (P1) (StemCell Technologies, 07930).

Differentiation to M0-IPSDMs

HiPSC differentiation to monocytes was induced following a previously established protocol (Cao et al., 2020). Shortly, hiPSCs were passaged in low ratio (10.000 cells/cm2) and maintained in mTeSR-E8 medium. On day 0, mesoderm was induced with IF9S medium supplemented with 50 ng/mL BMP4, 15 ng/mL ACTIVIN A, and 1.5 µM CHIR99021 until day 2. On day 2, medium was refreshed with IF9S supplemented with 50 ng/mL VEGF, 50 ng/mL bFGF, 50 ng/mL SCF (Miltenyi Biotec), and 10 µM SB431542. On day 5 and day 7, refreshment was done with IF9S supplemented with 50 ng/mL VEGF, 50 ng/mL bFGF, 50 ng/mL SCF, 50 ng/mL IL-6, 50 ng/mL TPO and 10 ng/mL IL-3 (all from Miltenyi Biotec). On day 9, all non-adhered cells were collected. Adherent cells were detached using TrypLE (Life Technologies) for 10 min at 37°C and combined with non-adherent cells in IF9S supplemented with 50 ng/mL IL-6, 10 ng/mL IL-3, and 80 ng/mL M-CSF (Miltenyi Biotec). 24-well ultra-low attachment plate (Corning Life Sciences) was used to seed the cells. Medium was refreshed with IF9S medium containing 50 ng/mL IL-6, 10 ng/mL IL-3, and 80 ng/mL M-CSF every 2 days after.

On day 15 non-adherent cells were collected in a tube and washed with FACS buffer (PBS, 0.5% BSA, 2 mM EDTA). Then, CD14 MicroBeads (Miltenyi Biotec) was used for CD14+ cell isolation following the manufacturer's instructions; 60 µL of MicroBeads were mixed with 1 × 107 cells. Isolated CD14+ cells were cryopreserved in CryoStor CS10 medium (STEMCELL Technologies).

To further differentiate to M0-IPSDMs , hiPSC-monocytes were thawed and plated in fetal bovine serum coated coated 2 wells of a 12-well plate in IF9S medium supplemented with 80 ng/mL M-CSF. Medium was refreshed every 2-3 days until day 7.

3D cardiac microtissue formation

MTs with three cell types were formed as described previously (Giacomelli et al., 2020). Prior to MT formation, hiPSC-ECs and hiPSC-CFs were prepared as follows: 3-4 days before MT formation, a vial of cryopreserved hiPSC-ECs and a vial of cryopreserved hiPSC-CFs were thawed and cultured either in EC-CGM on plates coated with gelatin (hiPSC-ECs), or in FGM3 on uncoated plates (hiPSC-CFs). HiPSC- CMs were thawed on Matrigel coated 12x well plate 5 days prior to MT formation day. M0-IPSDMs were thawed on overnight FBS coated 12x well plate in IF9S medium as previously described (Cao et al., 2020). On the day of MT formation (day 0), hiPSC-ECs and hiPSC-CFs were detached using TrypLE 1X for 2-3 mins at RT (EC) and 5 mins at 37 °C, 5 % CO2 (CF), centrifuged for 3 min at 1100 rpm, resuspended in B(P)EL medium and counted. hiPSC-CMs were dissociated using the TryplE 5X for 10 mins at 37°C, 5 % CO2, resuspended in B(P)EL medium and counted. M0-IPSDMs were dissociated using tryplE 1X for 5 mins at 37 °C, 5 % CO2, centrifuged for 3 min at 1100 rpm, resuspended in B(P)EL medium and counted. Cell suspensions for CMECF were combined to a total of 5000 cells (70% CM, 15 % EC and 15 % CF (CMECF) or 70 % CM, 10 % EC, 10 % CF and 10 % M0-IPSDMs (CMECFM0)) per 50 µl B(P)EL medium supplemented with VEGF (50 ng/ml) and FGF2 (5 ng/ml). Cell suspensions for CMECFM0 were combined to a total of 5000 cells (70 % CM, 10 % EC, 10 % CF and 10 % M0-IPSDMs) per 70 µl B(P)EL medium supplemented with VEGF (50 ng/ml), FGF2 (5 ng/ml) and M- CSF (80 ng/ml). For all MTs, cell suspensions were seeded either on standard V-bottom 96-well microplates (Greiner bio-one, 651161) and standard U-bottom (Greiner bio-one, 650161) or ultra- low attachment U- bottom 96-well microplates (ThermoFisher NunClon Sphera Treated, 174925) and centrifuged for 10 min at 1100 rpm. MTs were incubated at 37 °C, 5 % CO2 for 21 days with media refreshed every 3-4 days.

Immunofluorescence imaging

On day 7, 14 and 21, CMECFM0s were fixed using 4 % paraformaldehyde (PFA) for 1 h at 4 °C. Permeabilization was done using PBS(-) supplemented with 0.2 % TritonX-100 for 30 mins at RT. Then, PBS(-) supplemented with 10% fetal bovine serum (FBS) was used for blocking for at least 2 h at RT. Primary antibodies of CD68 (ThermoFisher Scientific), ACTN2 (Sigma Aldrich cat no: A7811) and CD31 (R&D Systems, cat no: AF806) was added in

blocking solution described previously and added on CMECM0 overnight at 4 °C. Secondary antibodies of donkey anti rabbit IgG, highly crossed absorbed antibody with Alexa Fluor 594 (ThermoFisher, cat no: A21206), donkey anti-mouse IgG, highly crossed absorbed antibody with Alexa Fluor 594 (ThermoFisher, cat no: A21203), donkey anti sheep IgG, highly crossed absorbed antibody with Alexa Fluor 647 (ThermoFisher, cat no: A21448) were added in blocking solution on CMECFM0 overnight at 4 °C. After each step, 3x PBS(-) wash for 20 mins was followed. After the DAPI staining (in PBS(-)), MTs were resuspended in ProLong Gold (ThermoFisher) and transferred on microscopy slides (VWR, 631-1553). Coverslips were used to mount MTs in slides. Confocal images were captured to create 3D stack using Andor Dragonfly spinning disk confocal microscope using a 40x or 63x objective. Image processing was done using Imaris 9.5 software (Bitplane, Oxford Instruments).

Characterization of vessel density and macrophage number in 3D

Whole MT images of CMECFM0 were captured using ImageXpress Micro confocal high-content imaging microscopy (Molecular Devices) using 10x objective and were then quantified for vessel density and macrophage counting using pipelines developed on the free open source CellProfiler software (https://cellprofiler.org/) (Vila Cuenca et al., 2021; Carpenter et al., 2006). Briefly, pre- processing steps enhanced image features in all images. A Gaussian filter to reduce non-specific object identification was done. Two filter steps of images of vascular density were applied to reduce non-specific segmentation from cell junctions and a minimum cross-entropy thresholding method was used to produce a binary image.

Contraction analysis

For pacing experiments, custom-made electrodes were used. MTs were stimulated at 1.2Hz with 10V/cm strength and 10 ms long stimulation pulse. Movies of spontaneous beating or paced MTs from CMECF and CMECFM0 conditions were acquired until 2-3 beats were captured at 37 °C. ThorLabs DCC3240M camera (Leica Inverted microscope IBDE), using the ThorLabs uc480 software (v 4.20), at 37 °C and 5 % CO2 at 100 frames/s and a 10x objective phase contrast objective was used for recordings. MUSCLEMOTION ImageJ macro (ImageJ v. 2.0.0-rc-49) was used to analyze recordings as described previously (Sala et al., 2018).

Multiplexed Cytokine Assay

MTs were refreshed 4 days prior to medium collection. For this, the medium in the wells was completely aspirated and 40 µl of fresh medium was added into each well. MTs were not disturbed the next 4 days until medium collection. After 4 days, the medium from 40 MTs from CMECF, CMECFM0 -M-CSF and CMECFM0 +M-CSF were collected and stored at -80 oC. On the day of the multiplex cytokine bead assay, collected medium was thawed two hours prior to the experiment. Samples were concentrated using PierceTM Protein Concentrators PES (ThermoFisher) following manufacturer's instructions.
Concentration of cytokines (IL-12p70, TNF-α, IL-6, IL-4, IL-10, IL-1β, Arginase, TARC, IL-1RA,

IL-12p40, IL-23, IFN-γ and IP-10) was measured using a LEGENDplex human macrophage/microglia Panel kit (13-plex) (BioLegend, cat no: 740511) according to the manufacturer's instructions. Samples were run on Cytek 3-Laser Aurora spectral flow cytometer (Cytek Biosciences, USA).

Statistical Analysis

GraphPad Prism 9 was used to perform statistical tests. Two-way ANOVA was applied as appropriate to test for differences in means between groups/conditions. Data are expressed and plotted as the Mean ± SD, except figure 4D-G which was plotted as the Mean ± SEM as indicated in figure legend. Detailed statistics and exact P-values are indicated in each figure legend. Statistical significance was defined as $P < 0.05$.

Results

Integration of M0-IPSDMs in 3D cardiac MTs

In order to integrate M0-IPSDMs in cardiac MTs, we first adapted a previously published protocol (Giacomelli et al. al., 2020) with keeping the percentage of CMs at 70%. Cardiac MTs with M0-IPSDMs (CMECFM0) were formed using the following predefined cell percentages: 70% CMs, 10 % ECs, 10 % CFs and 10 % M0-IPSDMs in B(P)EL medium that was additionally supplemented with VEGF (50 ng/ml), FGF2 (5 ng/ml) and M-CSF (80 ng/ml) (Figure 1A). On day 3 of MT formation, CMECFM0 (Figure 1C) were compared to MTs without IPSDMs (CMECF, Figure 1B). Both conditions formed compact MTs. However, we observed that in CMECFM0, IPSDMs appeared to be attracted by dead cells that surrounded MTs and they migrated outside of MTs, clearing-up the dead cells. We also noted that some IPSDMs attached to the bottom of the well. CMECFM0s were maintained for 21 or 31 days in culture with medium refreshment every 3-4 days. At the end of day 21 and 31, we performed immunofluorescent staining of CMECFM0s to visualize cellular subsets (Figure 1D and E, respectively). hiPSC-CMs were homogenously distributed and hiPSC-ECs self-organized into microvascular networks in day 21 and day 31 CMECFM0s. IPSDMs were evident in MTs on day 21 and 31; however, their number seemed to be higher in day 31 CMECFM0s (Figure 1E). Interestingly, IPSDMs appeared to localize close to microvascular networks.

Ultra-low attachment plates support retaining macrophages inside 3D cardiac MTs

In order to track the IPSDMs inside of MTs, we generated CMECFM0 with M0-IPSDMs from a fluorescent reporter line (NCRM1-GFP). We next compared the standard and ultra-low attachment U- bottom plates (Figure 2A). We observed that in standard U-bottom plates, IPSDMs migrated outside of MTs, as evidenced by a green fluorescent signal (Figure 2B). On the other hand, ultra-low attachment U-bottom plates prevented IPSDM migration outside of the CMECFM0. CMECFM0s were maintained until day 21 either in regular MT medium without M-CSF (-M-CSF) or with M-CSF (+M- CSF).

Figure 1

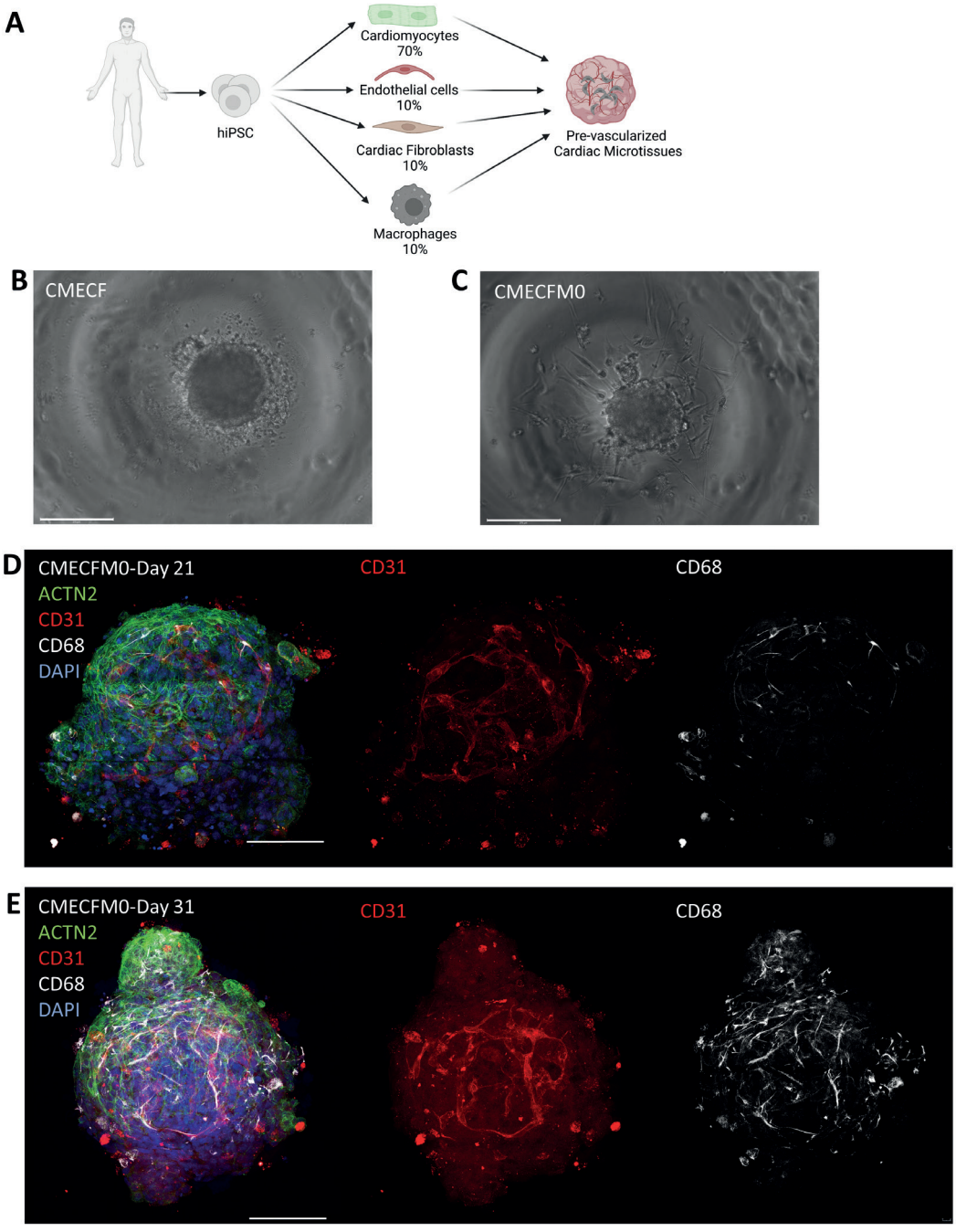

Figure 1: Integration of M0-IPSDMs in cardiac MTs. *(A) Schematic showing cellular composition of cardiac MTs with M0-IPSDMs with respective cell percentages indicated. (B, C) Representative bright-field images of cardiac MTs without IPSDMs (CMECF) (B) and with IPSDMs (CMECFM0) (C). (D, E) Immunofluorescence staining of CMECFM0 on day 21 (D) and day 31 (E) showing ACTN2 in green, CD31 in red and CD68 in white. Scale bars: 275 um (B-C), 100 um (D-E).*

Figure 2

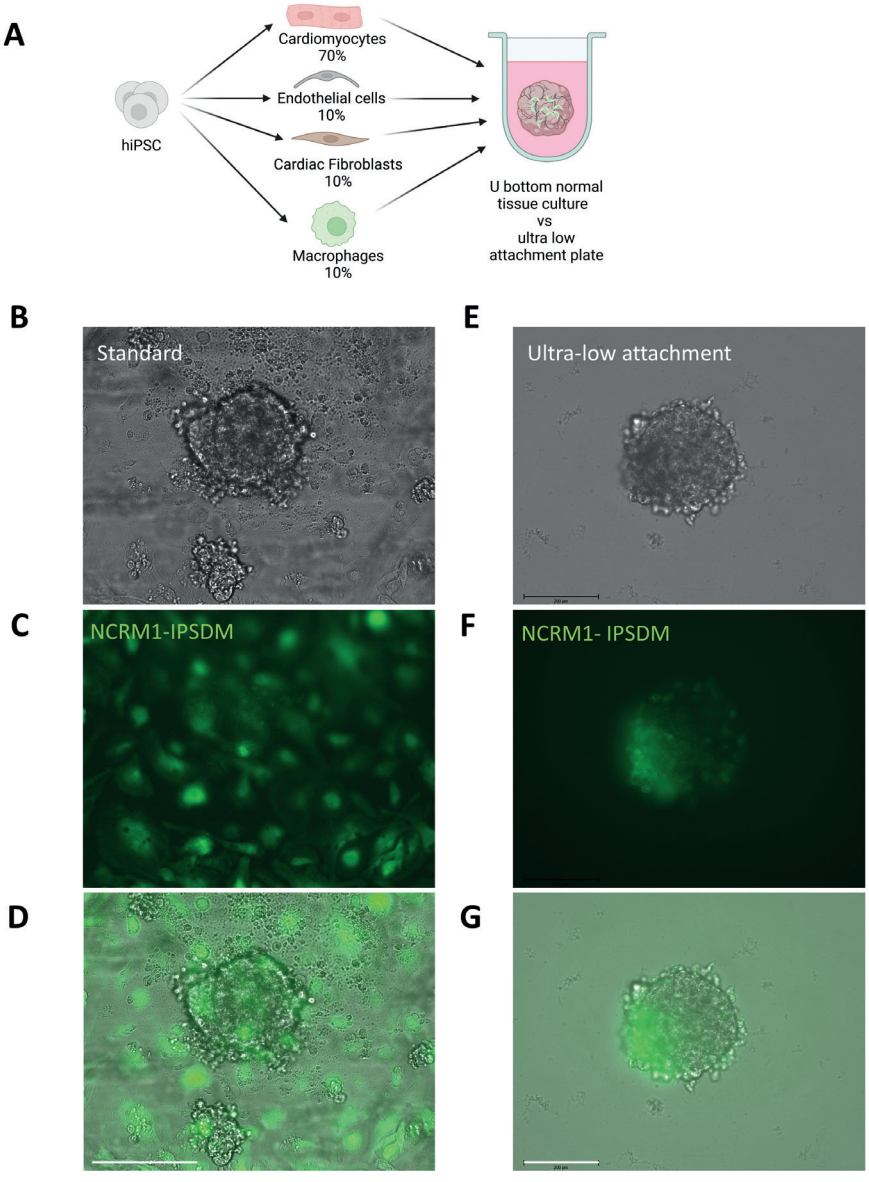

Figure 2: Optimization of the formation of CMECFM0s. *(A) Schematic showing formation of CMECFM0s in U-bottom plates. (B-G) Representative images of CMECFM0 after 21 days of formation in standard U-bottom plates (B-D) or ultra-low attachment U- bottom plates (E-G). Bright-field images of CMECFM0 are shown in B, E; M0-IPSDMs differentiated from generically encoded fluorescent hiPSC line (NCRM1-GFP) are shown after integration in cardiac MTs (in green) (C, F); Merged imaged are shown in D, G. Scale bars: 200 µm.*

Characterization of 3D cardiac MTs with M0-IPSDMs

To quantify the total number of IPSDMs at different timepoints, and also study the effect of M-CSF supplementation, we differentiated macrophages from H2B-GFP nuclear fluorescent reporter hiPSC line (Allen Institute, AICS-0061-036) (Roberts et al., 2017). Confocal imaging of CMECFM0s on day 7 (Figure 3A), 14 (Figure 3B) and 21 (Figure 3C) showed homogenous distribution of M0-IPSDMs, identified by H2B-GFP positive nuclei and CD68 immunostaining, ACTN2 positive hiPSC-CMs, and self- organized microvasculature formed by CD31 positive hiPSC-ECs.

We next quantified the total number of H2B-GFP positive IPSDM in CMECFM0s with and without M- CSF supplementation at day 7, 14 and 21. M-CSF supplementation resulted in more IPSDMs at day 7 and 14, but not 21 after MT formation (Figure 4A). The total number of IPSDM decreased overtime in both conditions, indicating that M-CSF supported macrophage proliferation at early stages of MT formation, but had no effect upon a prolonged culture. Quantification of microvascular networks and contractile parameters showed comparable vessel density between different conditions (Figure 4B) and no difference in contraction duration upon pacing at 1.2 Hz (Figure 4C), respectively.

Finally, we examined cytokine secretion using a multiplex assay (macrophage/microglia cytokine panel) that includes both pro- and anti-inflammatory cytokines. We were only able to detect some of the cytokines that could potentially be measured in the assay in CMECFM0s, and not in control MTs (CMECF). Specifically, IL-10, IL-6, IP-10 and IL-1RA were measured but IL-10, IL-6 levels were negligibly low (14.04±3.947 pg/ml and 191.4±92.93 pg/ml, respectively, mean±SEM) (Figure 4D, F). IP-10 and IL-1RA showed the highest expression in CMECFM0 with M-CSF supplementation, although IL-1RA was 10-fold higher than IP-10, suggesting that majority of IPSDMs acquired M2-like identity and only a minor subset of IPSDMs acquired M1-like identity (Figure 4E, G).

Discussion

In the present study, we optimized and characterized several culture conditions to integrate M0- IPSDMs into 3D cardiac MTs. hiPSC-derived cells; CMs, ECs, CFs and macrophages were combined in a pre-defined ratio (70% CM and 10% each non-CM cell types) in a regular V-bottom 96-well plates. CMECFM0s were compact and formed reproducibly. However, some cells migrated outside the MTs. These migratory cells were not present in CMECF which suggested that they were M0-IPSDMs. Importantly, there were dead cells surrounding MTs in CMECF condition. However, these dead cells were not present in CMECFM0 which might suggest efferocytosis by M0-IPSDMs as previously shown (Cao et al., 2019). Although we observed that some IPSDMs migrated outside, confocal images of CMECFM0 on day 21 and 31 showed that some remained in the MTs. At both time points, IPSDMs were close to the microvascular structures which is in line with the previous literature suggesting one of the niches of CRMs are vessels (Moore et al., 2017; Zaman and Epelman, 2022).

Figure 3

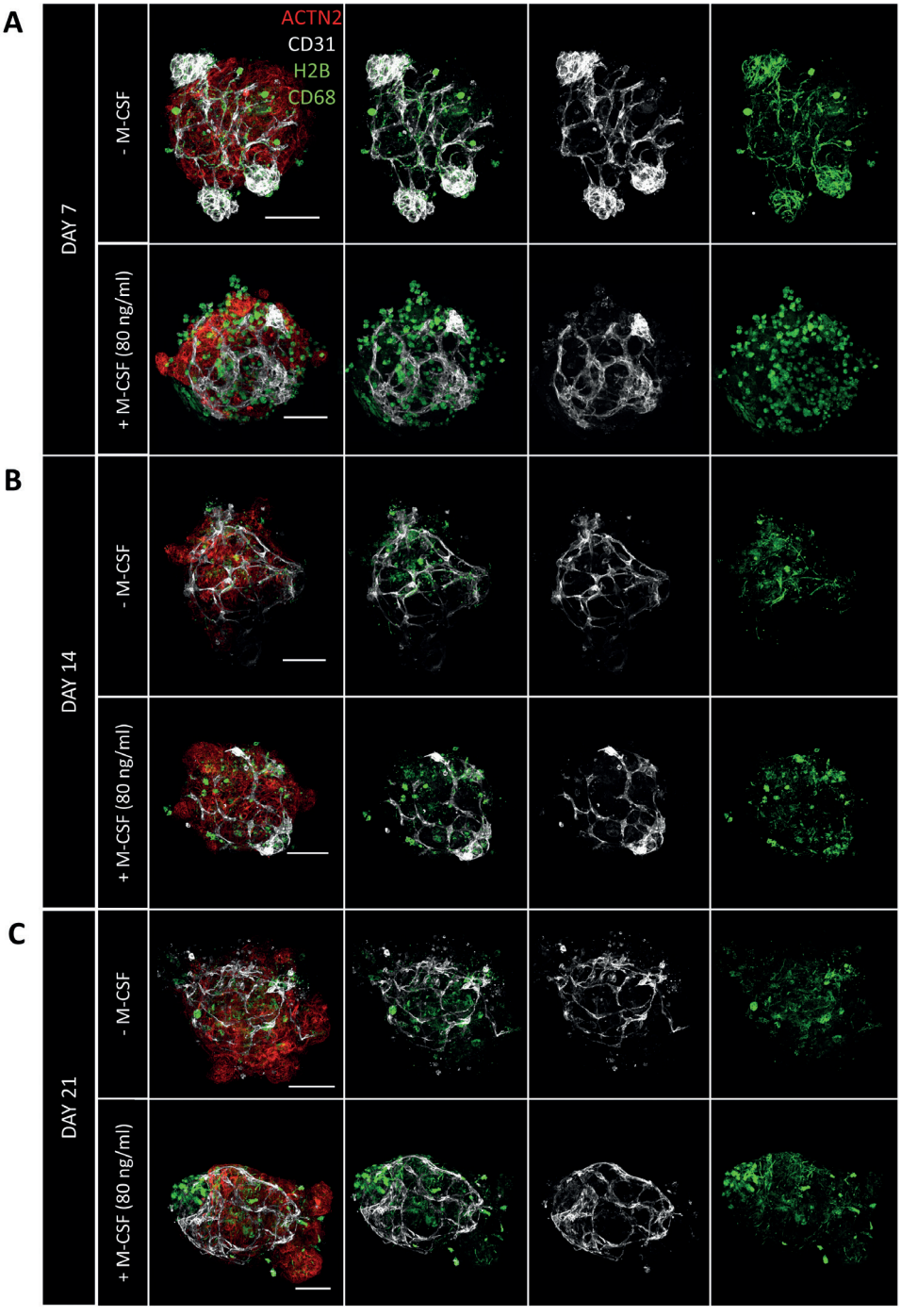

Figure 3: Cellular composition of CMECFM0s. *(A-C) Representative immunofluorescent images of CMECFM0s at different days after formation with and without M-CSF (80 ng/ml) supplementation: day 7 (A), day 14 (B) and day 21 (C). Cardiomyocytes are stained with anti-ACTN2 (red), ECs are stained with anti-CD31 (gray), M0-IPSDMs are differentiated from H2B-GFP reporter hiPSC-line and additionally stained with anti-CD68 (green). Scale bars: 100 µm.*

Figure 4

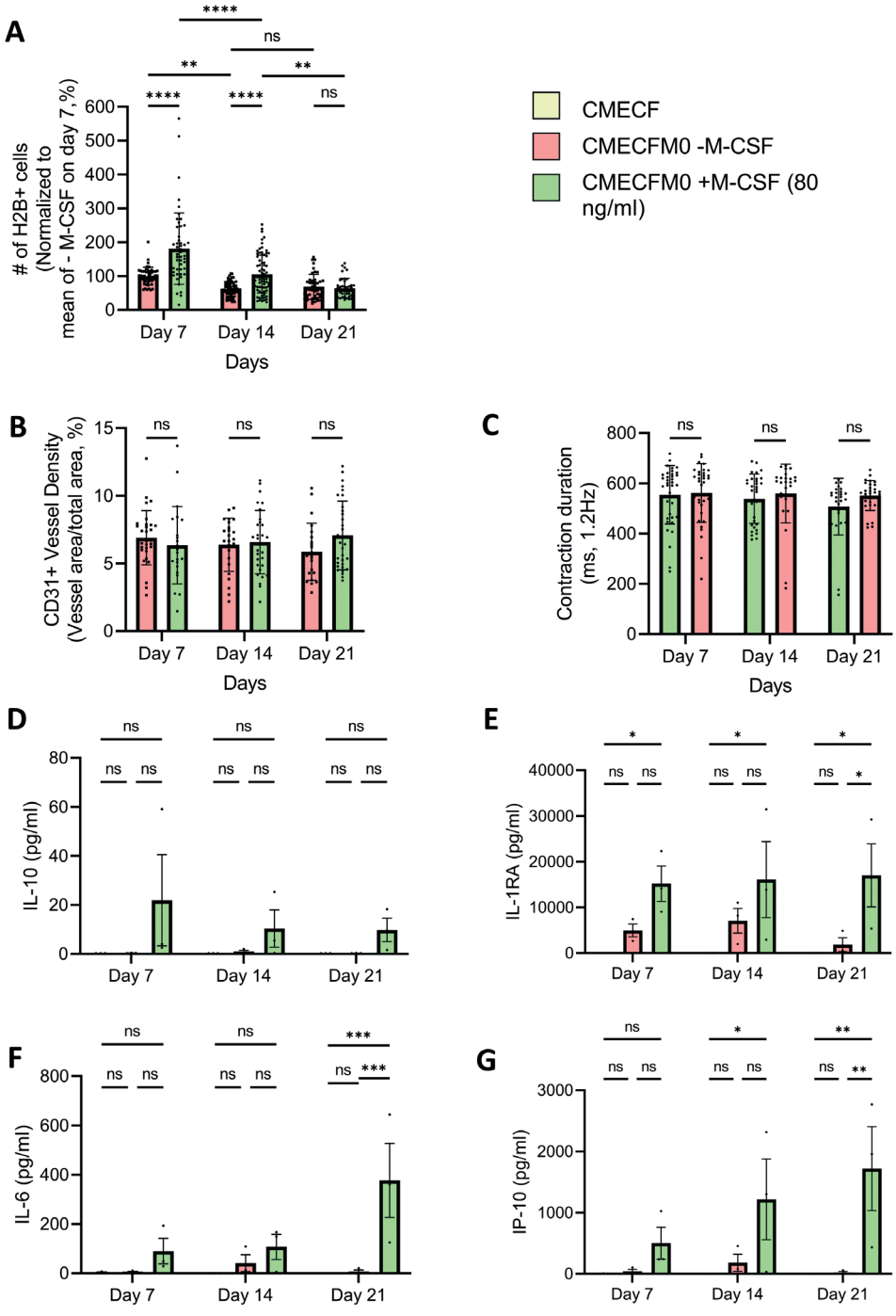

Figure 4: Characterization of CMECFM0s. *(A)Quantification of the total number of M0-IPSDMs differentiated from H2B-GFP reporter hiPSC line in CMECFM0s at day 7, 14 and 21 after formation with and without M-CSF (80 ng/ml) supplementation. n>44 from 3 independent experiment. Error bars are shown in mean±SD (B) Quantification of vessel density in CMECFM0s at day 7, 14 and 21 after formation with and without M-CSF (80 ng/ml) supplementation. n>22 from 3 independent experiment. Error bars are shown in mean±SD (C) Quantification*

*of the contraction duration of CMECFM0s at day 7, 14 and 21 after formation with and without M-CSF (80 ng/ml) supplementation. CMECFM0s were paced at 1.2 Hz. n>26 from 3 independent experiment. Error bars are shown in mean±SD (D-G) Quantification of secreted cytokines by a Multiplex assay in concentrated supernatants collected on day 7, 14 and 21 after 4 days upon medium refresh. Medium is collected from n= 40 MTs for each condition from 3 independent experiments. Yellow bars: CMECF, pink bars: CMECFM0 -M-CSF, green bars: CMECFM0 +M-CSF. Error bars (D-G) are shown as mean±SEM. *p < 0.5,**p < 0.01,***p < 0.001; ns, not significant.*

To prevent cell migration in the CMECFM0 condition, we tested other types of cell culture plates. In the regular CMECF condition, we usually use V bottom plates to seed the cells and these plates are centrifuged to sediment cells in the bottom as a compact cluster (Campostrini et al., 2021). This could perhaps increase cell death as the MTs become attached to the bottom of the wells. In an attempt to decrease cell death, we first changed the plates from V- to U-bottom using the same brand of standard 96-microwell plates. However, migratory cells were still present in these plates. Using a fluorescent hiPSC reporter line with nuclear tagging to generate M0-IPSDMs and integrate them in CMECFM0 confirmed the IPSDM identity of migratory cells. However, when we used ultra- low attachment plates, migration of cells was completely prevented and M0-IPSDMs remained in the MTs.

Previously, CMECF was generated and maintained in the MT medium (Giacomelli et al., 2020). In CMECFM0, M-CSF was supplemented in the MT medium in an attempt to enhance M0-IPSDM survival and proliferation as reported in previous studies (Otero et al., 2009). Confocal imaging of these MTs at different time points (day7, 14 and 21) showed that IPSDMs were more homogenously distributed in the MTs at the earlier time points. However, they remained in close proximity to the microvasculature which was formed by self-organization of hiPSC-ECs throughout the culture period. The number of H2B+ IPSDM increased on day 7 and 14 in CMECFM0 +M-CSF compared to -M-CSF. However, surprisingly, they were comparable on day 21 in terms of IPSDM number. In addition, there was a significant decrease in IPSDM numbers later in the culture period. This could be partly due to the MT medium as it had not been optimized for M0-IPSDMs.

To examine the effect of IPSDM on other cellular subsets, we quantified microvascular network density and contractile parameters of cardiac MTs with and without M-CSF supplementation. Despite increased IPSDM numbers upon M-CSF supplementation, we observed had no effect on the total vascular network density. This was surprising as earlier studies demonstrated that macrophages support formation of vascular networks *in vitro* and *in vivo* (Krishnasamy et al., 2017; Gamrekelashvili et al., 2016; Moore et al., 2017). In addition, contraction duration was comparable between CMECFM0 -M-CSF and +M-CSF on day 7, 14 and 21, and did not change over time. It would be interesting to investigate whether IPSDMs have an effect on electrophysiological properties or force of contraction of cardiomyocytes in the future.

To characterize the IPSDM phenotype in the CMECFM0 microenvironment, we collected medium samples to determine the cytokine release in each condition. We showed that secretion of anti- inflammatory cytokine IL-1RA was higher in CMECFM0s supplemented with M-CSF. We also detected some levels of pro-inflammatory cytokine IP-10 in

CMECFM0s supplemented with M-CSF, although it was 10-fold lower compared to IL-1RA. Surprisingly, an increase in cytokine secretion upon M-CSF supplementation did not correlate with the overall decrease in the total IPSDM number, indicating that M-CSF could promote macrophage polarization in 3D cardiac MTs. It would be interesting to characterize macrophage polarization at the single cell resolution in the future either by immunofluorescent staining or by flow cytometry using specific M1 and M2 markers or single-cell RNA sequencing.

In summary, here we optimized culture conditions to integrate M0-IPSDMs into 3D cardiac MTs. We showed that M-CSF supplementation in the medium increased IPSDM numbers at the early time points. In addition, M-CSF or IPSDMs did not have any effect on vessel density or contraction duration parameters. Integration of IPSDMs resulted in upregulation of IL-1RA and IP-10 that are anti- and pro-inflammatory cytokines respectively. Although these results suggest that the MT microenvironment affects IPSDM identity, more specific assays will be necessary to characterize them further. This platform offers potential to study M0-IPSDMs in specific tissue microenvironment to better understand their involvement in health and disease.

Acknowledgements

We thank LUMC confocal imaging facility during imaging and the Allen Cell Collection (from Coriell Institute for Medical Research), for hiPSC lines. Images were made using Biorender.com.

This work was supported by the LymphChip project with project number NWA-ORC 2019 1292.19.019 of the NWA research program 'Research on Routes by Consortia (ORC)', which is funded by the Netherlands Organization for Scientific Research (NWO); The Novo Nordisk Foundation Center for Stem Cell Medicine is supported by Novo Nordisk Foundation grants (NNF21CC0073729).

References

Aktories, P., Petry, P., Glatz, P., Andrieux, G., Oschwald, A., Botterer, H., Gorka, O., Erny, D., Boerries, M., Henneke, P., et al. 2022. *An improved organotypic cell culture system to study tissue- resident macrophages ex vivo.* Cell Reports Methods 26;2(8):100260.

Berg, C. W. van den, Elliott, D. A., Braam, S. R., Mummery, C. L., and Davis, R. P. 2016. *Differentiation of Human Pluripotent Stem Cells to Cardiomyocytes Under Defined Conditions.* Methods in molecular biology (Clifton, N.J.) 1353:163–180.

Campostrini, G., Meraviglia, V., Giacomelli, E., van Helden, R. W. J., Yiangou, L., Davis, R. P., Bellin, M., Orlova, V. V., and Mummery, C. L. 2021. *Generation, functional analysis and applications of isogenic three-dimensional self-aggregating cardiac microtissues from human pluripotent stem cells.* Nature Protocols 16(4):2213-2256.

Cao, X., van den Hil, F. E., Mummery, C. L., and Orlova, V. V. 2020. *Generation and Functional Characterization of Monocytes and Macrophages Derived from Human Induced Pluripotent Stem Cells.* Current Protocols in Stem Cell Biology 52(1):e108.

Cao, X., Yakala, G. K., van den Hil, F. E., Cochrane, A., Mummery, C. L., and Orlova, V. V. 2019. *Differentiation and Functional Comparison of Monocytes and Macrophages from hiPSCs with Peripheral Blood Derivatives.* Stem Cell Reports 12(6):1282-1297.

Carpenter, A. E., Jones, T. R., Lamprecht, M. R., Clarke, C., Kang, I. H., Friman, O., Guertin, D. A., Chang, J. H., Lindquist, R. A., Moffat, J., et al. 2006. *CellProfiler: image analysis software for identifying and quantifying cell phenotypes.* Genome Biology 7(10):R100.

Dick, S. A., Macklin, J. A., Nejat, S., Momen, A., Clemente-Casares, X., Althagafi, M. G., Chen, J., Kantores, C., Hosseinzadeh, S., Aronoff, L., et al. 2019. *Self-renewing resident cardiac macrophages limit adverse remodeling following myocardial infarction.* Nature Immunology 20(1):29-39.

Dollinger, C., Ciftci, S., Knopf-Marques, H., Guner, R., Ghaemmaghami, A. M., Debry, C., Barthes, J., and Vrana, N. E. 2018. *Incorporation of resident macrophages in engineered tissues: Multiple cell type response to microenvironment controlled macrophage-laden gelatine hydrogels.* Journal of Tissue Engineering and Regenerative Medicine 12(2):330-340.

Epelman, S., Lavine, K. J., Beaudin, A. E., Sojka, D. K., Carrero, J. A., Calderon, B., Brija, T., Gautier, E. L., Ivanov, S., Satpathy, A. T., et al. 2014. *Embryonic and adult-derived resident cardiac macrophages are maintained through distinct mechanisms at steady state and during inflammation.* Immunity 40(1):91-104.

Gamrekelashvili, J., Giagnorio, R., Jussofie, J., Soehnlein, O., Duchene, J., Briseño, C. G., Ramasamy, S. K., Krishnasamy, K., Limbourg, A., Kapanadze, T., et al. 2016. *Regulation of monocyte cell fate by blood vessels mediated by Notch signalling.* Nature Communications 7:12597.

Giacomelli, E., Bellin, M., Orlova, V. V, and Mummery, C. L. 2017. *Co-Differentiation of Human Pluripotent Stem Cells-Derived Cardiomyocytes and Endothelial Cells from Cardiac Mesoderm Provides a Three-Dimensional Model of Cardiac Microtissue.* Current protocols in human genetics 95:21.9.1-21.9.22.

Giacomelli, E., Meraviglia, V., Campostrini, G., Cochrane, A., Cao, X., van Helden, R. W. J., Krotenberg Garcia, A., Mircea, M., Kostidis, S., Davis, R. P., et al. 2020. *Human-iPSC-Derived Cardiac Stromal Cells Enhance Maturation in 3D Cardiac Microtissues and Reveal Non-cardiomyocyte Contributions to Heart Disease.* Cell Stem Cell 26:862-879.e11.

Ginhoux, F., and Jung, S. 2014. *Monocytes and macrophages: developmental pathways and tissue homeostasis.* Nature Reviews Immunology 14:392–404.

Gordon, S., and Plüddemann, A. 2017. *Tissue macrophages: Heterogeneity and functions.* BMC Biology 15(1):53.

Guadix, J. A., Orlova, V. V, Giacomelli, E., Bellin, M., Ribeiro, M. C., Mummery, C. L., Pérez-Pomares, J. M., and Passier, R. 2017. *Human Pluripotent Stem Cell Differentiation into Functional Epicardial Progenitor Cells.* STEMCR 9:1754–1764.

Hoeffel, G., and Ginhoux, F. 2015. *Ontogeny of tissue-resident macrophages.* Frontiers in Immunology 6:486.

Hudaa Gopee, N., Huang, N., Olabi, B., Admane, C., Rose Foster, A., Torabi, F., Winheim, E., Sumanaweera, D., Miah, M., Stephenson, E., et al. 2023. *A human prenatal skin cell atlas reveals immune cell regulation of skin morphogenesis 1.* Biorxiv.

Hulsmans, M., Clauss, S., Xiao, L., Aguirre, A. D., King, K. R., Hanley, A., Hucker, W. J., Wülfers, E. M., Seemann, G., Courties, G., et al. 2017. *Macrophages Facilitate Electrical Conduction in the Heart.* Cell 169(3):510-522.e20.

Juhas, M., Abutaleb, N., Wang, J. T., Ye, J., Shaikh, Z., Sriworarat, C., Qian, Y., and Bursac, N. 2018. *Incorporation of macrophages into engineered skeletal muscle enables enhanced muscle regeneration.* Nature Biomedical Engineering 2(12):942-954.

Krishnasamy, K., Limbourg, A., Kapanadze, T., Gamrekelashvili, J., Beger, C., Häger, C., Lozanovski, V. J., Falk, C. S., Napp, L. C., Bauersachs, J., et al. 2017. *Blood vessel control of macrophage maturation promotes arteriogenesis in ischemia.* Nature Communications 8(1):952.

Lavin, Y., Winter, D., Blecher-Gonen, R., David, E., Keren-Shaul, H., Merad, M., Jung, S., and Amit, I. 2014. *Tissue-resident macrophage enhancer landscapes are shaped by the local microenvironment.* Cell 159(6):1312-26.

Lee, C. Z. W., Kozaki, T., and Ginhoux, F. 2018. *Studying tissue macrophages in vitro: are iPSC-derived cells the answer?* Nature Reviews Immunology 8(11):716-725.

Molawi, K., Wolf, Y., Kandalla, P. K., Favret, J., Hagemeyer, N., Frenzel, K., Pinto, A. R., Klapproth, K., Henri, S., Malissen, B., et al. 2014. *Progressive replacement of embryo-derived cardiac macrophages with age.* Journal of Experimental Medicine 211(11):2151-8.

Moore, E. M., Ying, G., and West, J. L. 2017. *Macrophages Influence Vessel Formation in 3D Bioactive Hydrogels.* Advanced Biosystems 1, 1600021.

Múnera, J. O., Kechele, D. O., Bouffi, C., Qu, N., Jing, R., Maity, P., Enriquez, J. R., Han, L., Campbell, I., Mahe, M. M., et al. 2023. *Development of functional resident macrophages in human pluripotent stem cell-derived colonic organoids and human fetal colon.* Cell Stem Cell 30:1434- 1451.e9.

Nicolás-Ávila, J. A., Lechuga-Vieco, A. V., Esteban-Martínez, L., Sánchez-Díaz, M., Díaz-García, E., Santiago, D. J., Rubio-Ponce, A., Li, J. L. Y., Balachander, A., Quintana, J. A., et al. 2020. *A Network of Macrophages Supports Mitochondrial Homeostasis in the Heart.* Cell 183(1):94- 109.e23 .

Orlova, V. V., Van Den Hil, F. E., Petrus-Reurer, S., Drabsch, Y., Ten Dijke, P., and Mummery, C. L. 2014. *Generation, expansion and functional analysis of endothelial cells and pericytes derived from human pluripotent stem cells.* Nature Protocols 9(6):1514-31.

Otero, K., Turnbull, I. R., Poliani, P. L., Vermi, W., Cerutti, E., Aoshi, T., Tassi, I., Takai, T., Stanley, S. L., Miller, M., et al. 2009. *Macrophage colony-stimulating factor induces the proliferation and survival of macrophages via a pathway involving DAP12 and β-catenin.* Nature Immunology 10(7):734-43 .

Roberts, B., Haupt, A., Tucker, A., Grancharova, T., Arakaki, J., Fuqua, M. A., Nelson, A., Hookway, C., Ludmann, S. A., Mueller, I. A., et al. 2017. *Systematic gene tagging using CRISPR/Cas9 in human stem cells to illuminate cell organization.* Molecular Biology of the Cell 28(21):2854-2874.

Rostovskaya, M., Fu, J., Obst, M., Baer, I., Weidlich, S., Wang, H., Smith, A. J. H., Anastassiadis, K., and Francis Stewart, A. 2012. *Nucleic Acids Research* 40(19):e150.

Sala, L., van Meer, B. J., Tertoolen, L. G. J., Bakkers, J., Bellin, M., Davis, R. P., Denning, C., Dieben, M. A. E., Eschenhagen, T., Giacomelli, E., et al. 2018. *Musclemotion: A versatile open software tool to quantify cardiomyocyte and cardiac muscle contraction in vitro and in vivo.* Circulation Research 122(3):e5-e16 .

Saleh, L. S., and Bryant, S. J. 2018. *The host response in tissue engineering: Crosstalk between immune cells and cell-laden scaffolds.* Current Opinion in Biomedical Engineering 6:58-65.

Song, A. T., Sindeaux, R. H. M., Li, Y., Affia, H., Agnihotri, T., Leclerc, S., van Vliet, P. P., Colas, M., Guimond, J.-V., Patey, N., et al. 2024. *Developmental role of macrophages modeled in human pluripotent stem cell-derived intestinal tissue.* Cell Reports 43:113616.

Vila Cuenca, M., Cochrane, A., van den Hil, F. E., de Vries, A. A. F., Lesnik Oberstein, S. A. J., Mummery, C. L., and Orlova, V. V. 2021. *Engineered 3D vessel-on-chip using hiPSC-derived endothelial- and vascular smooth muscle cells.* Stem Cell Reports 16(9):2159-2168.

Zaman, R., and Epelman, S. 2022. *Resident cardiac macrophages: Heterogeneity and function in health and disease.* Immunity 55(9):1549-1563 .

Zhang, M., D'Aniello, C., Verkerk, A. O., Wrobel, E., Frank, S., Ward-Van Oostwaard, D., Piccini, I., Freund, C., Rao, J., Seebohm, G., et al. 2014. *Recessive cardiac phenotypes in induced pluripotent stem cell models of Jervell and Lange-Nielsen syndrome: Disease mechanisms and pharmacological rescue.* Proceedings of the National Academy of Sciences of the United States of America 111(50):E5383-92.

Development of Vascularized hiPSC-derived 3D cardiac microtissue on chip

Authors and Affiliations

Ulgu Arslan[1], Marcella Brescia[1], Viviana Meraviglia[1], Dennis M. Nahon[1], Ruben W.J. van Helden[1], Jeroen M. Stein[1], Francijna E. van den Hil[1], Berend J. van Meer[1], Marc Vila Cuenca1[1,2], Christine L. Mummery[1], Valeria V. Orlova[1]*

[1]Department of Anatomy and Embryology, Leiden University Medical Centre, 2333ZC Leiden, The Netherlands

[2]Department of Clinical Genetics, Leiden University Medical Center, 2333ZA Leiden, the Netherlands

* Corresponding author

This work was combined with the study in chapter 6 and published in Stem Cell Reports, 2023 Jul 11, 18:1394–1404.
DOI: 10.1016/j.stemcr.2023.06.001.

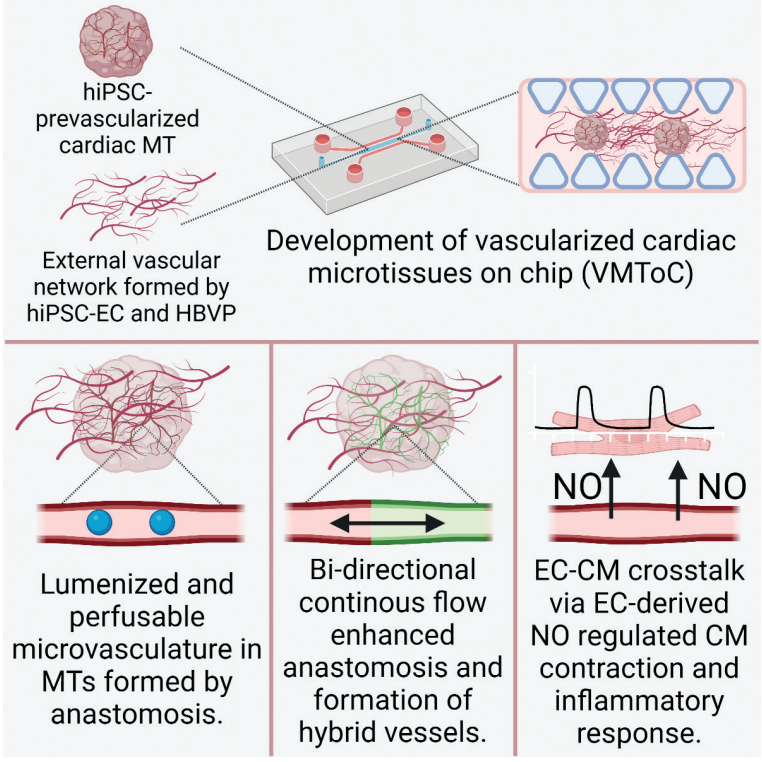

Graphical abstract

Summary

Functional vasculature is essential for delivering nutrients, oxygen and cells to the heart and removing waste products. Here, we developed an *in vitro* vascularized human cardiac microtissue (MT) model based on human induced pluripotent stem cells (hiPSCs) in a microfluidic organ-on-chip by co-culturing hiPSC-derived, pre-vascularized, cardiac MTs with vascular cells within a fibrin hydrogel. We showed that vascular networks spontaneously formed in- and around these MTs and were lumenized and interconnected through anastomosis. Anastomosis was fluid flow-dependent: continuous perfusion increased vessel density and thus enhanced the formation of the hybrid vessels. The model establishes the groundwork to integrate perfusable vasculature in microtissue/organoids, enabling the study of cellular crosstalk and its effect on functionality.

Keywords:

human induced pluripotent stem cells; cardiac microtissue; heart-on-chip.

Introduction

Cardiovascular disorders are a major cause of death around the world. The heart is a highly metabolic organ and has high energy demands for proper function. Endothelium is crucial in this process as it forms a semi-permeable barrier between cardiomyocytes (CM) and the blood, providing selective nutrient, oxygen and drug delivery to heart cells. It also mediates immune cell trafficking, for example, in the case of inflammation (Amersfoort et al., 2022). Interruption of the blood supply can lead to CM death, as in myocardial infarction (Berry and Duncker, 2020), and successful heart transplantation requires rapid restoration of blood supply to the donor heart.

Some of the current 3D microphysiological models (reviewed in Arslan et al., 2022) incorporated vascular networks inside engineered tissues but in general they were not perfusable by fluid or blood (equivalents) (Zhang et al., 2021). This has in part been addressed by either integrating organoids into a microfluidic chip or implanting them into living animals, as perfusion is also necessary for the stability and integrity of the microvascular networks (Mansour et al., 2018; Ryan et al., 2021; Takebe et al., 2013).

In the study here, we developed a fully vascularized and perfusable cardiac microtissue (MT) on-chip by integrating pre-vascularized cardiac MTs with an external vascular network formed by self- organization of human induced pluripotent stem cell derived endothelial cells (hiPSC-ECs) and human brain vascular pericytes (HBVPs) in fibrin hydrogel in a microfluidic organ-on-chip. The integration of MTs in the chips did not adversely affect formation of the external, self-organized vascular network and these networks developed robustly, inside- and around the MTs. Using this model, we demonstrated that cardiac MTs can be efficiently vascularized within days and the lumenized vascular networks in-

Figure 1

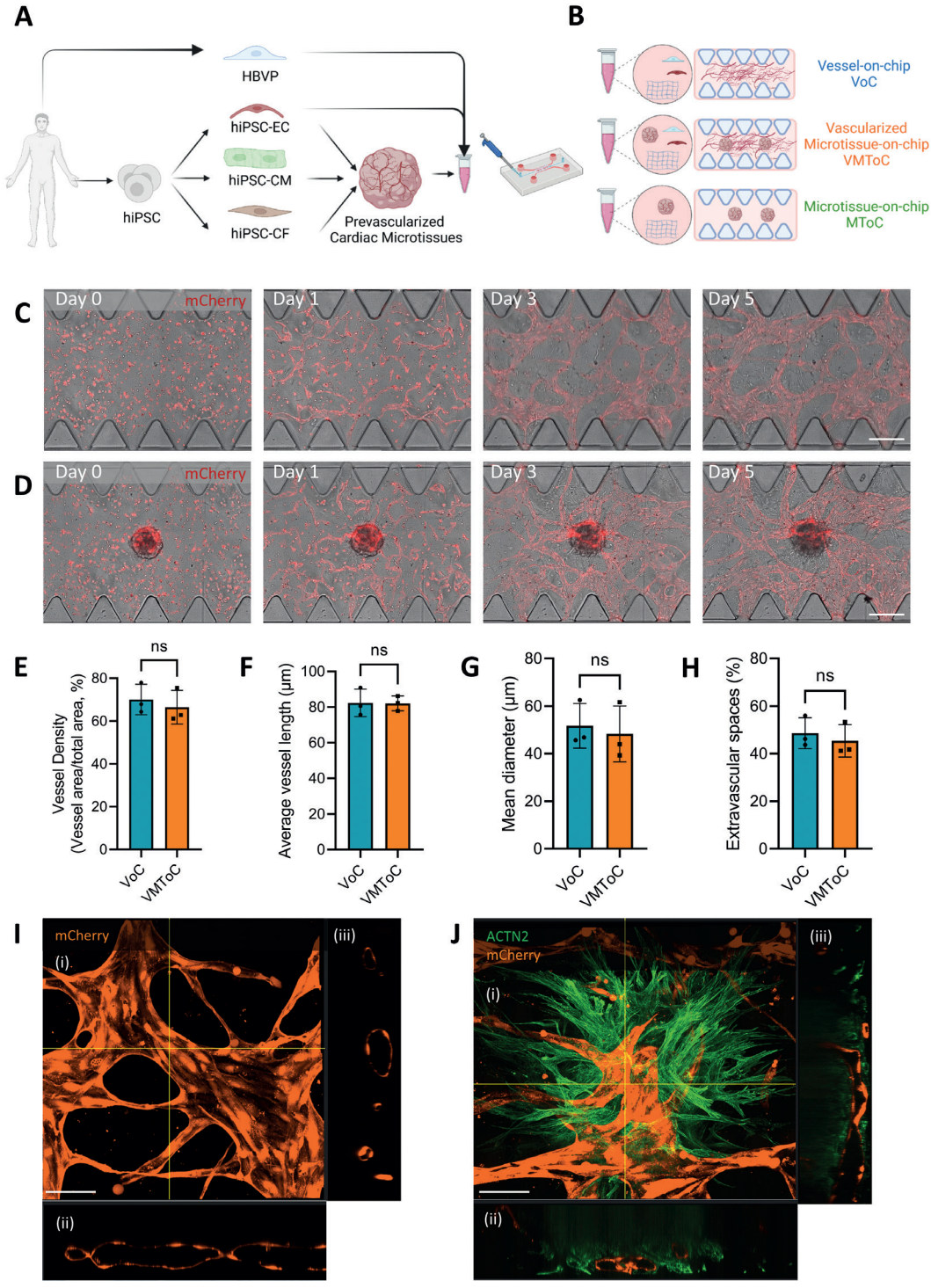

Figure 1: Characterization of the vascular network in the presence of cardiac MTs. *(A, B) Schematic overview of the vascularized cardiac MTs experimental setup (A) and conditions used in the study (B). hiPSC-EC and HBVPs*

were cocultured to form VoC; hiPSC-MTs were cocultured with hiPSC-EC and HBVPs to form VMToC; hiPSC-MTs were integrated into chips without any additional vascular cells to form MToC. (C, D) Representative images from chips on day 0, 1, 3 and 5 after seeding in the chips, which shows the development of external vascular networks in VoC (C), and VMToC (D). Images showing brightfield and hiPSC-EC (red, mCherry) (10×). Scale bars, 300 µm. (E-H) Quantification of vessel density (%) (E), average vessel length (µm) (F), mean diameter (µm) (G), extravascular spaces (%) (H). Error bars are shown as mean±SD from N = 3; three independent experiments with at least six microfluidic channels per experiment. Student's t-test; ns, not significant. (I, J) Representative confocal images of microvascular network in VoC (I) and VMToC (J) showing hiPSC-ECs (orange, mCherry) and hiPSC-CM (green, ACTN2). Images displaying maximum projection in xyz (i), xy (ii), and yz cross-sectional perspectives (iii) (40×). Scale bar, 100 µm. See also Video S1-3.

and around the MTs can be perfused. This may ultimately allow selective nutrient or drug delivery to the cells via the endothelial barrier inside the MTs, mimicking heart tissue *in vivo* even more closely.

Results

Characterization of the vascular network in the presence of cardiac MTs

The VMToC model was generated by combining prevascularized cardiac MTs (Giacomelli et al, 2020; Campostrini et al, 2021) with hiPSC-ECs and HBVPs, in a fibrin hydrogel. This MT/cell/hydrogel mix was then embedded in the gel channel of commercially available AIM Biotech 3D cell culture chips (Figure 1A). To investigate the effect of cardiac MTs on vascular network formation, we compared the VMToC model with a standard vessel-on-chip (VoC) that included hiPSC-EC and HBVP cocultures but without cardiac MTs (Figure 1B). Vascular organization in VoCs and VMToCs was already evident on day 1 (Figure 1C and D). On day 3, a complex vascular network had formed in the chips and these networks were stabilized by day 5. Quantification of the vascular network parameters such as vessel density (Figure 1E), average vessel length (Figure 1F), mean vessel diameter (Figure 1G) and extravascular space (Figure 1H) showed no significant differences between VoC and VMToC conditions. Vascular networks in VoC (Figure 1I) and the microvasculature in MTs in VMToC (Figure 1J, Video S1) were both lumenized.

To investigate whether the lumenized vasculature in cardiac MTs was actually perfusable, fluorescent beads (2 µm) were introduced into the medium in one of the media inlets of the chips. Beads entered the vascular networks from the intersection of medium-gel channel and moved spontaneously to the microvasculature in MTs (Figure 2A). Beads stayed within the microvasculature contours in the MTs indicating the interconnected vessels in the MTs were indeed perfusable (Figure 2B-E, Video S2 and S3).

Mechanism of the intra-microvascular network formation

In order to investigate the mechanism of the intra-microvascular network formation, we used hiPSC- ECs derived from two different fluorescent reporter lines (expressing mCherry or GFP). GFP- expressing hiPSC-ECs were used to prevascularize the cardiac

Figure 2

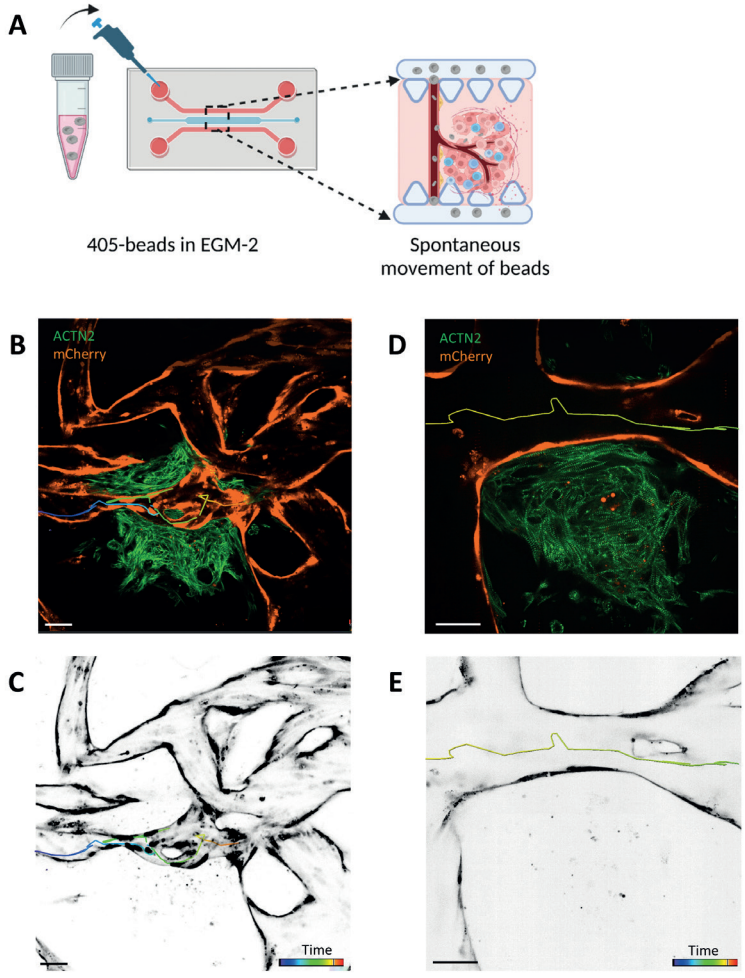

Figure 2: Cardiac MTs induce pulsative intra-microvascular flow. *(A) Schematic of the fluorescent beads (2 μm) perfusion experiment. Please see Supplemental Experimental Setup for experimental details. (B, D) Representative confocal images showing hiPSC- ECs (orange, mCherry) hiPSC-CM (green, ACTN2) and perfusion of 2 μm fluorescent beads (traces) in VMToC. (B is 20x and D is 40x with Scale bar, 50 μm. (C, E) Representative confocal images in black and white showing only vascular networks (black) and traces of beads inside (colored traces). Color coded bars represent time. Images are duplications of B and D. Scale bar, 50 μm.*

MTs and these MTs were cocultured with mCherry-expressing hiPSC-ECs and HBVPs in the chips (Figure 3A). Internal microvasculature in the MTs and external vascular network around MTs underwent anastomosis as early as day 2. Anastomosis was bidirectional in the system: (i) outside-in anastomosis where the external network invaded the MTs and anastomosed with the internal microvasculature in the MTs (Figure 3B and D); (ii) inside-out anastomosis where part of the internal microvascular network migrated outside the MT and anastomosed with the external vascular network (Figure 3C and E). As a result, hybrid vessels composed of hiPSC-ECs partly from MTs and partly from external vascular networks

Figure 3

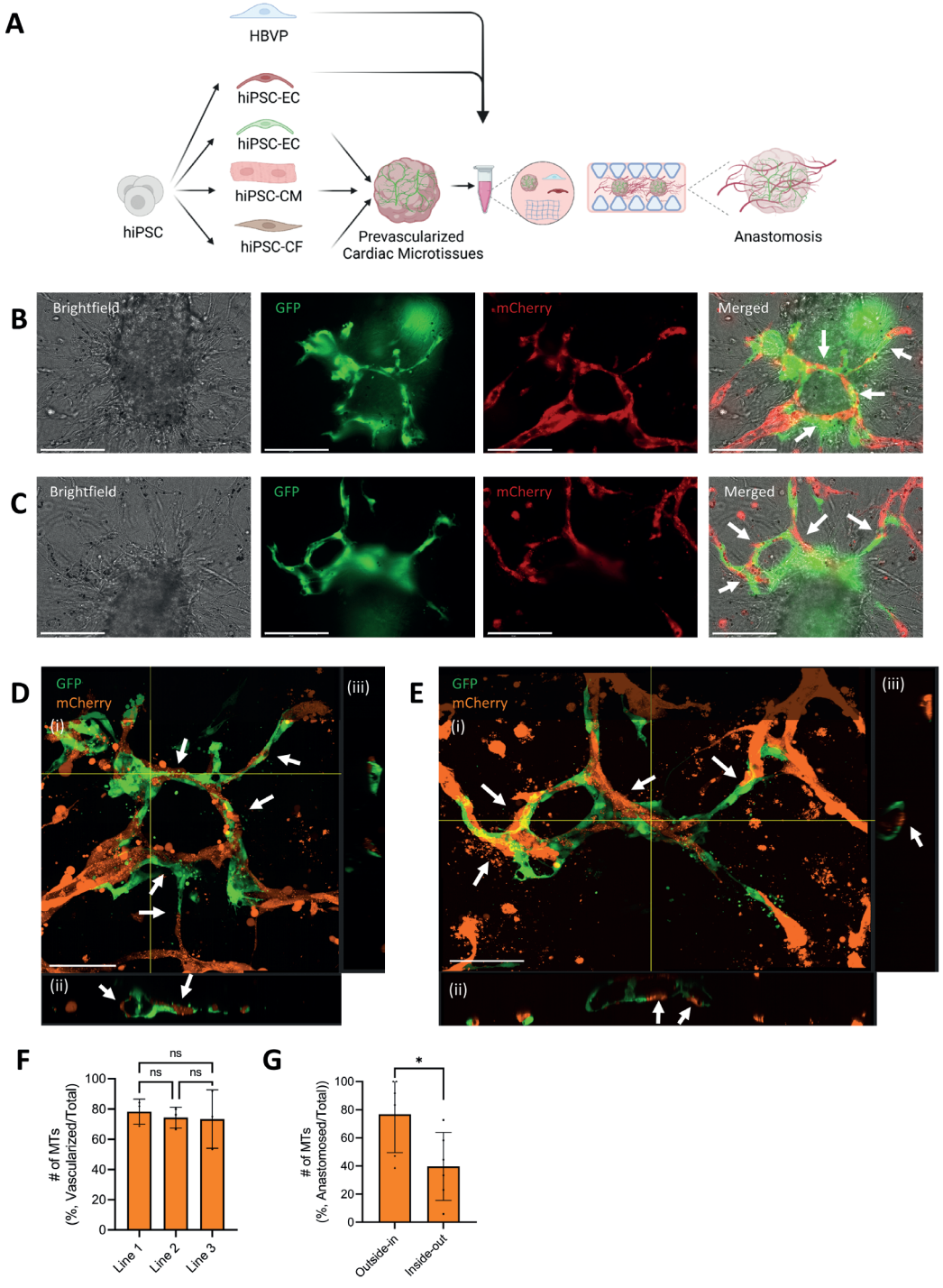

Figure 3: Mechanism of the intra-microvascular network formation. *(A) Schematic of the experimental setup. MTs were generated combining hiPSC-CMs, hiPSC-ECs (green, GFP) and hiPSC-CFs. These MTs were cocultured*

*with hiPSC-ECs (red, mCherry) and HBVPs in chips. (B, C) Representative images of outside-in (B) and inside-out (C) anastomosis and formation of hybrid vessels by interconnection of internal microvascular network (green, GFP) and external vascular network (red, mCherry) (20x). Scale bar, 150 μm. (D, E) Representative confocal images of hybrid vessels visible in B and C, respectively. Internal hiPSC-EC (green, GFP), external hiPSC-ECs (orange, mCherry). Images displaying maximum projection in xyz (i), xy (ii), and yz cross-sectional perspectives (iii) (40×). Scale bar, 100 μm. Arrows indicating the anastomosed points and hybrid lumens. (F) Quantification of number of vascularized MTs (%, number vascularized MTs/Total number of MTs). MTs contained CMs from three different hiPSC lines. Error bars are shown as mean±SD from N=3; three independent experiments with at least 10 MTs in each experiment. One- way ANOVA, ns, not significant. (G) Quantification of number of anastomosed MTs (%, #Anastomosed MTs/Total # of MTs) in independent experiments. Error bars are shown as mean±SD from N=6; six independent experiments with at least 9 MTs in each experiment. Student's t-test, *p < 0.05.*

were formed. Confocal images showed that these hybrid vessels were lumenized (Figure 3D and E). The number of vascularized tissues was comparable in all independent experiments (Figure 3F), with higher numbers of MTs showing evidence of outside-in anastomosis than those showing inside-out anastomosis (Figure 3G).

Since fluid flow is known to promote EC migration, proliferation and survival (Abe et al., 2019; Galie et al., 2014; Zhang et al., 2022) , we tested whether we could enhance the vascularization of cardiac MTs by introducing perfusion using a rocker (Figure 4A). Both intermittent and continuous perfusion resulted in anastomosis between the internal microvasculature and external vascular networks (Figure 4B and C, respectively).

However, continuous perfusion resulted in higher mCherry+ and GFP+ vessel density (Figure 4D-E) in the chips. Intermittent perfusion resulted in the formation of hybrid vessels where only a minority of cells originated in the cardiac MTs (Figure 4F). This improved substantially under continuous perfusion (Figure 4G).

Discussion

In the present study, we established vascularized and perfusable cardiac MT on a microfluidic organ- on-chip platform (VMToC) with vascular cells self-organised in fibrin hydrogel. The external vascular cells reproducibly formed a continuous vascular network in- and around the MTs and this was not affected by contraction of the MTs. Continuous perfusion generated by placing the chips on a rocker resulted in greater vascularization, improved anastomosis and enhanced formation of hybrid vessels. Since mechanistic studies on molecular pathways mediating anastomosis are challenging *in vivo*, this platform could provide an alternative way to understand this process *in vitro*. Furthermore, these networks developed robust lumens that contracted rhythmically in synchrony with surrounding CMs. This rhythmic contraction of CMs resulted in the generation of bidirectional flow as indicated by oscillatory movement of fluorescent beads into- and through the organized vascular network inside of the MT. Currently, no animal models are available that model ischemic heart disease caused by coronary microvascular obstruction (Niccoli et al., 2016; Sorop et al., 2020). Therefore, vascularized and perfusable cardiac MTs could be useful in

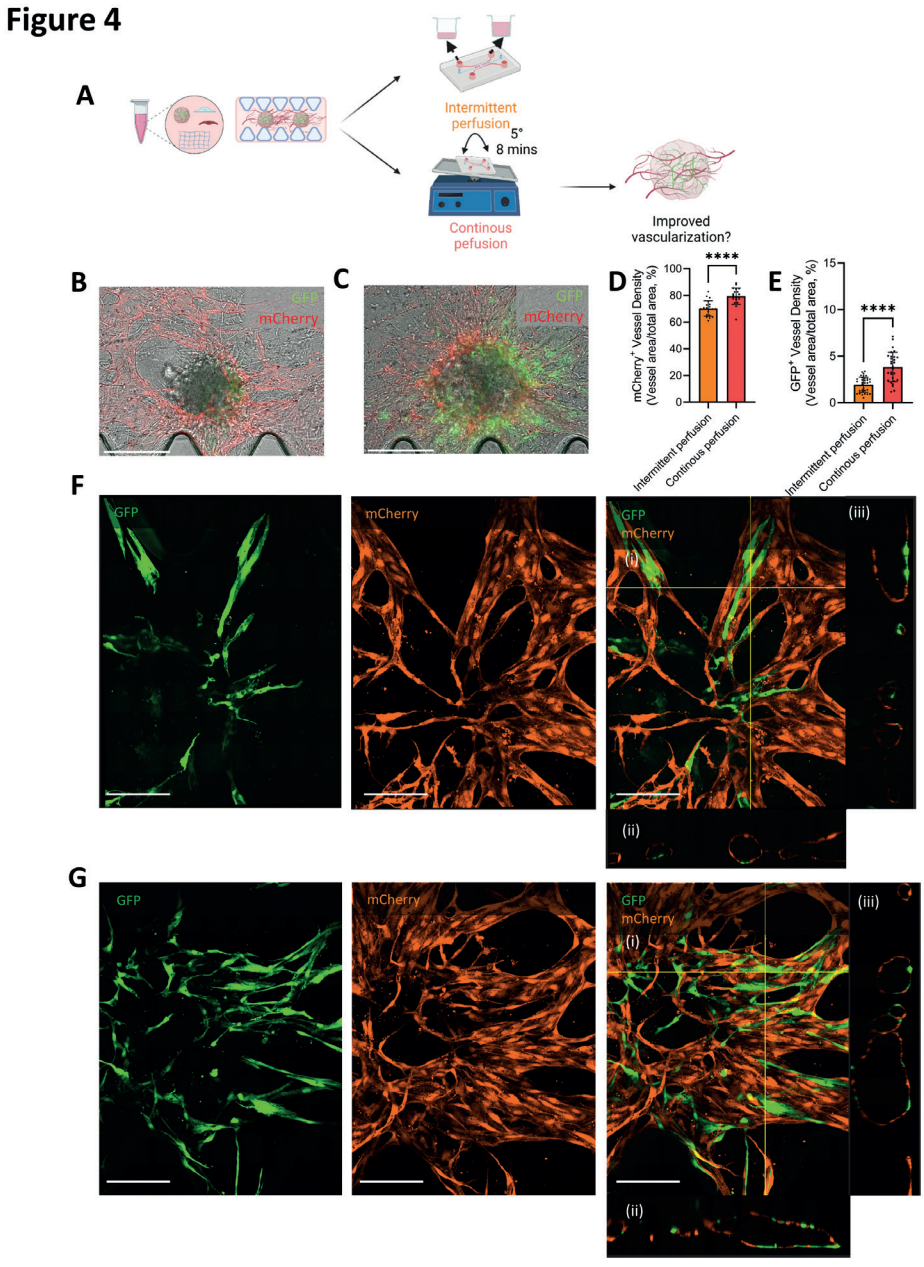

Figure 4: Continuous perfusion enhances vascularization of cardiac MTs. *(A) Schematic of the experimental setup for intermittent and continuous perfusion conditions. Chips were kept under intermittent gravity-driven flow with the medium exchange every 24 h or placed on the rocker (at a 5 degrees inclination angle and 8 min interval) to induce continuous perfusion through passive leveling between the reservoirs. (B, C) Representative images of VMToC under intermittent perfusion (B) and continuous perfusion (C) where anastomosis is visible by the formation of hybrid vessels (10x). Scale bar, 300 μm. (D) Quantification of mCherry+ vessel density (%) in intermittent and continuous perfusion conditions. Error bars are shown as ±SD from N = 3, n = 19 (intermittent perfusion) and n = 20 (continuous perfusion); three independent experiments with at least six microfluidic channels*

*per experiment. (E) Quantification of GFP+ vessel density (%) in intermittent and continuous perfusion conditions. Error bars are shown as ±SD from N = 3, n = 35 (intermittent perfusion) and n = 29 (continuous perfusion); three independent experiments with at least six microfluidic channels per experiment. (F, G) Representative confocal images of hybrid vessels formed in intermittent perfusion (F) or continues perfusion (G) conditions. Internal hiPSC-EC (green, GFP), external hiPSC-EC (orange, mCherry). Images displaying xyz (i), xy (ii), and yz cross-sectional perspectives (iii) (40×). Scale bar, 150 μm. Wilcoxon-Mann-Whitney test (D, E), ****p < 0.0001.*

studying mechanisms underlying microvascular obstruction using cardiac and vascular cells derived from patients.

Finally, although the formation of the vascular networks was robust in VMToC, we observed some batch-to-batch and plate-to-plate variability in the degree of vascularization. Vascularization of MTs was mostly through the anastomosis, so the extent of pre-vascularization in MTs might contribute to variability. In some cases where MTs were not well-vascularized, vascularization was improved by introducing continuous perfusion during later stages of culture (data not shown).

In summary, we demonstrated that 3D cardiac MTs can be integrated into microfluidic chips with the external vascular network formed by hiPSC-ECs and HBVPs. Using this model, we demonstrated that cardiac MTs can be efficiently vascularized within days and the lumenized vascular networks in- and around the MTs can be perfused. This may ultimately allow selective nutrient or drug delivery to the cells via the endothelial barrier inside the MTs, mimicking heart tissue *in vivo* even more closely. Our vascularized cardiac MT model thus provides a foundation for studies on organ-specific cellular communication, specifically for the endothelial barrier, drug screening and disease modelling.

Experimental Procedures

hiPSC lines and maintenance

hiPSCs were maintained on recombinant vitronectin-coated plates in TeSR-E8, all from STEMCELL Technologies, according to the manufacturer's instructions. The following hiPSC lines were used in this study: LUMC0059iCTRL03 (generated from skin fibroblasts, https://hpscreg.eu/cell-line/LUMCi026-A), LUMC0020iCTRL06 (generated from skin fibroblasts, https://hpscreg.eu/cell- line/LUMCi028-A) (Zhang et al., 2014); NIH Center for Regenerative Medicine: NCRM-1 (generated from CD34+ cord blood cells, https://hpscreg.eu/cell-line/CRMi003- A), obtained from RUDCR Infinite Biologics at Rutgers University, was modified in-house with a mCherry or GFP expression cassette under the human cytomegalovirus (hCMV) early enhancer/chicken β actin (CAG) promoter using a previously established protocol (Rostovskaya et al., 2012); The Allen Cell Collection: AICS-0075 (generated from skin fibroblasts, https://hpscreg.eu/cell-line/UCSFi001-A-4) with mEGFP insertion site at ACTN2 was obtained from Coriell Institute for Medical Research. hiPSC lines and cell batches of hiPSC-CMs, hiPSC-ECs and hiPSC-CFs are listed in Table 1.

Differentiation of cardiomyocytes

CM differentiation of hiPSC was induced in monolayer as described previously (Berg et al., 2016; Giacomelli et al., 2017). Briefly, 25 × 103 cells per cm2 were seeded on plates coated with 75 µg/ml growth factor-reduced Matrigel (Corning) the day before the start of differentiation (day -1). On day 0, cardiac mesoderm was induced by changing E8 to B(P)EL medium (Bovine Serum Albumin [BSA] and Essential Lipids), supplemented with a cytokine mixture (20 ng/ml BMP4, R&D Systems; 20 ng/ml ACTIVIN A, Miltenyi Biotec; 1.5 µM GSK3 inhibitor CHIR99021, Axon Medchem). After 3 days, cytokines were removed and XAV939 which is WNT inhibitor (5 µM, Tocris) was added for 3 days. After this, B(P)EL medium was refreshed every 3 days.

Differentiation of cardiac fibroblasts

CFs were differentiated from hiPSC using an epicardial (EPI) monolayer differentiation protocol (Guadix et al., 2017) as a starting point (Giacomelli et al., 2020). Briefly, 25 × 103 cells per cm2 were seeded on Matrigel at day -1. On day 0, cardiac mesoderm was induced as described above. After 3 days, cytokines were removed and XAV939 (5 µM) was added for 3 days with BMP4 (30 ng/ml) and Retinoic Acid (RA; 1 µM; Sigma Aldrich). On day 6, B(P)EL medium supplemented with BMP4 (30 ng/ml) and RA (1 µM) was refreshed. On day 9, 15 × 103 per cm2 were seeded on plates coated with 5 µg/ml of fibronectin from bovine plasma (fibronectin; Sigma Aldrich) in B(P)EL medium supplemented with the TGFβ inhibitor SB431542 (10 µM; Tocris). By day 12, EPIs were confluent and ready for passaging or analysis. EPI cells (30 cm2 per vial) were cryopreserved in CryoStor CS10 medium (0.5 ml/vial; Stem Cell Technologies).

CF differentiation was induced in monolayer. Briefly, 25 × 103 EPIs were seeded per cm2 on tissue culture plates coated with vitronectin in B(P)EL medium supplemented with FGF2 (10 ng/ml; R&D Systems) on day 12. On day 13 and every 2 days thereafter, medium was refreshed with B(P)EL supplemented with FGF2 (10 ng/ml). After 6 days (on day 19), CFs were expanded by changing B(P)EL to Fibroblast Growth Medium 3 (FGM3; PromoCell). FGM3 was refreshed every 2 days for approximately 10 days in total. After 10 days (on day 29), CFs were confluent and ready to be passaged at 1:2 ratio. FGM3 was refreshed the day after passaging and every 2 days thereafter. CFs (10cm2 per vial) were cryopreserved in CryoStor CS10 medium (0.5 ml/vial; Stem Cell Technologies).

Differentiation of endothelial cells

hiPSC differentiation to ECs was performed as described previously (Orlova et al., 2014). Briefly, hiPSCs were maintained in mTeSR-E8 medium. For mesoderm induction (day 0-3), mTeSR-E8 medium was replaced with B(P)EL medium supplemented with 8 µM CHIR99021 (Tocris Bioscience, 4423). Cells were refreshed with vascular specification medium comprised of VEGF (50 ng/ml) and 10 µM SB431542 (Tocris Bioscience, 1614) in B(P)EL at day

3, day 6, and day 9. hiPSC-ECs were isolated on day 10 using CD31-DynabeadsTM (Thermo Fisher Scientific), as previously described (Orlova et al., 2014). hiPSC-ECs were expanded in complete EC growth medium (EC-CGM) comprised of Human Endothelial-serum free medium (EC-SFM) with 1% Human platelet poor serum (P2918, Sigma), VEGF (30 ng/ml) and bFGF (20 ng/ml), as described previously with minor modifications (Orlova et al., 2014). hiPSC-ECs were expanded for additional 3-4 days post-isolation and cryopreserved using cryopreservation medium consists of 50% fetal bovine serum,40% EGM2 and 10% dimethyl sulfoxide at passage number 1 (P1) (StemCell Technologies, 07930).

3D cardiac microtissue formation

MTs were formed as described previously (Giacomelli et al., 2020). Prior to MT formation, hiPSC-ECs and hiPSC-CFs were prepared as follows: 3-4 days before MT formation, a vial of cryopreserved hiPSC-ECs and a vial of cryopreserved hiPSC-CFs were thawed and cultured either in EC-CGM on plates coated with gelatin (hiPSC-ECs), or in FGM3 on uncoated plates (hiPSC-CFs). On the day of MT formation (day 0), hiPSC-ECs and hiPSC-CFs were detached using TrypLE 1X for 2-3 mins at RT (EC) and 5 mins at 37 °C, 5 % CO2 (CF), centrifuged for 3 min at 1100 rpm, resuspended in B(P)EL medium and counted. hiPSC-CMs at day 14-21 that showed > 80 % purity, measured as the percentage of troponin positive cells by FACS, were dissociated using the TryplE 5X for 10 mins at 37 °C, 5 % CO2, resuspended in B(P)EL medium and counted. Cell suspensions were combined to a total of 5000 cells (70 % CM, 15 % EC and 15 % CF) per 50 µl B(P)EL medium supplemented with VEGF (50 ng/ml) and FGF2 (5 ng/ml). For all MTs, cell suspensions were seeded on V-bottomed 96-well microplates (Greiner bio-one) and centrifuged for 10 min at 1100 rpm. MTs were incubated at 37 °C, 5 % CO2 for 12 days with media refreshed every 3-4 days.

Cell Preparation before on chip culture

Human brain vascular pericytes (HBVPs) were purchased from ScienceCell. HBVPs were cultured in Pericyte Medium (ScienceCell, 1201) supplemented with Pericyte Growth Supplement (ScienceCell, 1252) and 2 % FBS. Cells were cryopreserved at passage number 3 (P3) using serum-free cryopreservation medium (CryoStorTMCS10) (StemCell Technologies, 07930). hiPSC-ECs (P1) were thawed and cultured on gelatin-coated plates in EC-CGM, 4 days prior to VoC seeding. HBVPs (P3) were thawed and cultured in Pericyte Medium (ScienceCell, 1201) supplemented with Pericyte Growth Supplement (ScienceCell, 1252) and 2 % FBS.

Microfluidic chip culture

Cell preparation prior to chip seeding was described in supplemental information. Commercially available microfluidic chips (AIM Biotech) were used. Cell and MT mixtures were prepared as follows: 1) 4 MT/channel in combination with 25 × 106 hiPSC-ECs/mL and 5 × 106 HBVP cells/mL (5:1 ratio) (VMToC); or 2) 25 × 106 hiPSC-ECs/mL and 5

× 106 HBVP cells/mL (VoC) were resuspended in endothelial growth medium-2 (EGM-2, Lonza) supplemented with Thrombin (4 U/mL) and then gently mixed with fibrinogen (final concentration 3 mg/mL, Sigma) at 1:1 vol ratio. Cell/hydrogel mixture was quickly loaded into the middle gel-loading channel of the microfluidic chip. Chips were incubated at room temperature for 15 min. To support vascular network formation in the presence of cardiac MTs we used a mixture of CM and EC growth medium (bovine serum albumin (BSA) and essential lipids (B(P)EL) medium and endothelial growth medium-2 (EGM-2); 50:50), supplemented with vascular endothelial growth factor (VEGF) (50 ng/mL). The γ-secretase inhibitor DAPT (10 µM) was also added to the medium on day 1 for 24 h. Intermittent gravity-driven flow in the whole chamber was induced by creating hydrostatic pressure through the addition of 100 µL medium to the right media ports and 50 µL media to left media ports in the medium channel. Medium was refreshed daily. For the continuous perfusion experiments microfluidic chips were placed on the interval rocker platform (Perfusion rocker, MIMETAS) set at a 5 degrees inclination angle and an 8 min interval from day 0 onwards. Chips were maintained until day 7 and characterized between day 5-7.

Imaging of vascularized 3D cardiac microtissues on chip

Whole channel images were captured daily with EVOSM7000 using 10x objectives. For automated imaging of whole channels and stitching, a customized plate layout was used. VMToCs and MToCs were fixed for 30 mins at 4 °C with 4% paraformaldehyde, washed 3 times in PBS (Calcium, Magnesium) and stored at 4 °C until processing. Confocal images were captured to create 3D stack using Andor Dragonfly spinning disk confocal microscope using a 20x or 40x objective. Image processing was done using Imaris 9.5 software (Bitplane, Oxford Instruments).

Characterization of vascular networks

Fields of views (FOV) from the full channels (acquired using EVOS) were arranged in size of 480X1200 pixels around the MTs. For VoC 75 FOVs and for VMToC 87 FOVs were captured from three independent experiments with at least six microfluidic channels each. These FOVs (Figure 1E-H), whole microfluidic channels (Figure S2D), and 10x images of MTs from channels (Figure S2E) were then quantified using pipelines developed on the free open source CellProfiler software (https://cellprofiler.org/) (Carpenter et al., 2006; Vila Cuenca et al., 2021). Briefly, for vessel density, pre-processing steps were applied to all images to enhance image features and a gaussian filter to reduce unspecific object identification. Two filter steps were applied to images of vascular network to reduce non-specific segmentation from cell junctions and a minimum cross-entropy thresholding method was used to produce a binarized image. The binarized images from the CellProfiler output were then analyzed using the freely available ImageJ software with a plugin

(https://imagej.nih.gov/ij/ ,https://imagej.net/DiameterJ) (Hotaling et al., 2015).

Fluorescent beads perfusion assay

Perfusion assessment of VMToC was done as described previously (Vila Cuenca et al., 2021). In brief, 405-beads (1 drop in 10 or 20 ml EGM-2, Fluoro-Max Dyed Blue Aqueous Fluorescent Particles, B0200, ThermoFisher Scientific) were added to the right medium port (100 µl) and to all other media ports (50 µl). Then, confocal image stacks and videos of the spontaneous move of the beads following the endothelial networks were acquired using DragonFly spinning disk (Andor) microscope with 20x and 40x magnification objective. Tracking of the beads was done using 3D rendering and cell tracking function in Imaris 9.5 software (Bitplane, Oxford Instruments).

Statistical analysis

Statistical analysis was performed using GraphPad Prism 9. Student's t-test, one-way ANOVA for paired or unpaired measurements were applied as appropriate to test for differences in means between groups/conditions. Kruskal–Wallis test and Wilcoxon-Mann-Whitney test were used when the normality assumption did not hold. Data are expressed and plotted as the Mean ± SD. as indicated in figure legend. Detailed statistics and exact P-values are indicated in each figure legend. Statistical significance was defined as $P < 0.05$.

Acknowledgements

We acknowledge LUMC confocal imaging facility for help with imaging and the Allen Cell Collection, available from Coriell Institute for Medical Research, for providing materials. We thank Mervyn Mol for help with CM differentiation. Images were generated using Biorender.com.

This work was supported by the European Union's Horizon 2020 research and innovation programme under grant agreement No. 812954; the Netherlands Organ-on-Chip Initiative which is an NWO Gravitation project (024.003.001) funded by the Ministry of Education, Culture and Science of the government of the Netherlands; the LymphChip project with project number NWA- ORC 2019 1292.19.019 of the NWA research program 'Research on Routes by Consortia (ORC)', which is funded by the Netherlands Organization for Scientific Research (NWO); The Novo Nordisk Foundation Center for Stem Cell Medicine is supported by Novo Nordisk Foundation grants (NNF21CC0073729).

Author Contirubutions

Conceptualization, V.V.O.; methodology, U.A., and V.V.O.; software, U.A., D.N., J.S., and B.v.M.; validation, U.A., M.B., V.M; formal analysis, U.A.; investigation, U.A., M.B., V.M, D.M.N., R.W.J.v.H, J.M.S., F.E.v.d.H.,B.v.M, M.V.C; visualisation, U.A.; resources, C.L.M. and V.V.O.; writing – original draft, U.A., M.B., C.L.M., and V.V.O.; writing – review & editing, U.A., C.L.M., and V.V.O.; supervision, C.L.M., and V.V.O.; project administration, V.V.O.; funding acquisition, C.L.M., and V.V.O.

Declaration Of Interest

C.L.M. is a cofounder of Pluriomics B.V. (now Ncardia B.V.).

References

Abe, Y., Watanabe, M., Chung, S., Kamm, R.D., Tanishita, K., and Sudo, R. (2019). *Balance of interstitial flow magnitude and vascular endothelial growth factor concentration modulates three-dimensional microvascular network formation.* APL Bioeng. 3, 36102. https://doi.org/10.1063/1.5094735.

Amersfoort, J., Eelen, G., and Carmeliet, P. (2022). *Immunomodulation by endothelial cells — partnering up with the immune system?* Nat. Rev. Immunol. 22, 576–588. https:// doi.org/10.1038/s41577-022-00694-4.

Arslan, U., Moruzzi, A., Nowacka, J., Mummery, C.L., Eckardt, D., Loskill, P., and Orlova, V. V. (2022). *Microphysiological stem cell models of the human heart.* Mater. Today Bio 14. https://doi.org/10.1016/j.mtbio.2022.100259.

Berg, C.W. van den, Elliott, D.A., Braam, S.R., Mummery, C.L., and Davis, R.P. (2016). *Differentiation of Human Pluripotent Stem Cells to Cardiomyocytes Under Defined Conditions.* Methods Mol. Biol. 1353, 163–180. https://doi.org/10.1007/7651_2014_178.

Berry, C., and Duncker, D.J. (2020). *Coronary microvascular disease: The next frontier for Cardiovascular Research.* Cardiovasc. Res. 116. https://doi.org/10.1093/cvr/cvaa035.

Carpenter, A.E., Jones, T.R., Lamprecht, M.R., Clarke, C., Kang, I.H., Friman, O., Guertin, D.A., Chang, J.H., Lindquist, R.A., Moffat, J., et al. (2006). *CellProfiler: image analysis software for identifying and quantifying cell phenotypes.* Genome Biol. 7, R100. https://doi.org/10.1186/gb-2006-7-10-r100.

Galie, P.A., Nguyen, D.H.T., Choi, C.K., Cohen, D.M., Janmey, P.A., and Chen, C.S. (2014). *Fluid shear stress threshold regulates angiogenic sprouting.* Proc. Natl. Acad. Sci. U. S. A. 111, 7968–7973. https://doi.org/10.1073/pnas.1310842111.

Giacomelli, E., Bellin, M., Orlova, V. V, and Mummery, C.L. (2017). *Co-Differentiation of Human Pluripotent Stem Cells-Derived Cardiomyocytes and Endothelial Cells from Cardiac Mesoderm Provides a Three-Dimensional Model of Cardiac Microtissue.* Curr. Protoc. Hum. Genet. 95, 21.9.1-21.9.22. https://doi.org/10.1002/cphg.46.

Giacomelli, E., Meraviglia, V., Campostrini, G., Cochrane, A., Cao, X., van Helden, R.W.J., Krotenberg Garcia, A., Mircea, M., Kostidis, S., Davis, R.P., et al. (2020). *Human-iPSC-Derived Cardiac Stromal Cells Enhance Maturation in 3D Cardiac Microtissues and Reveal Non-cardiomyocyte Contributions to Heart Disease.* Cell Stem Cell 26, 862-879.e11. https://doi.org/10.1016/j.stem.2020.05.004.

Guadix, J.A., Orlova, V. V, Giacomelli, E., Bellin, M., Ribeiro, M.C., Mummery, C.L., Pérez-Pomares, J.M., and Passier, R. (2017). *Human Pluripotent Stem Cell Differentiation into Functional Epicardial Progenitor Cells.* STEMCR 9, 1754–1764. https://doi.org/10.1016/j.stemcr.2017.10.023.

Hotaling, N.A., Bharti, K., Kriel, H., and Simon, C.G. (2015). *DiameterJ: A validated open source nanofiber diameter measurement tool.* Biomaterials 61. https://doi.org/10.1016/j.biomaterials.2015.05.015.

Mansour, A.A., Gonçalves, J.T., Bloyd, C.W., Li, H., Fernandes, S., Quang, D., Johnston, S., Parylak, S.L., Jin, X., and Gage, F.H. (2018). *An in vivo model of functional and vascularized human brain organoids.* Nat. Biotechnol. 36. https://doi.org/10.1038/nbt.4127.

Niccoli, G., Scalone, G., Lerman, A., and Crea, F. (2016). *Coronary microvascular obstruction in acute myocardial infarction.* Eur. Heart J. 37. https://doi.org/10.1093/eurheartj/ehv484.

Orlova, V. V., Van Den Hil, F.E., Petrus-Reurer, S., Drabsch, Y., Ten Dijke, P., and Mummery, C.L. (2014). *Generation, expansion and functional analysis of endothelial cells and pericytes derived from human pluripotent stem cells.* Nat. Protoc. https://doi.org/10.1038/nprot.2014.102.

Rostovskaya, M., Fu, J., Obst, M., Baer, I., Weidlich, S., Wang, H., Smith, A.J.H., Anastassiadis, K., and Francis Stewart, A. (2012). *Transposon-mediated BAC transgenesis in human ES cells. Nucleic Acids* Res. 40. https://doi.org/10.1093/nar/gks643.

Ryan, A.R., England, A.R., Chaney, C.P., Cowdin, M.A., Hiltabidle, M., Daniel, E., Gupta, A.K., Oxburgh, L., Carroll, T.J., and Cleaver, O. (2021). *Vascular deficiencies in renal organoids and ex vivo kidney organogenesis.* Dev. Biol. 477. https://doi.org/10.1016/j.ydbio.2021.04.009.

Takebe, T., Sekine, K., Enomura, M., Koike, H., Kimura, M., Ogaeri, T., Zhang, R.R., Ueno, Y., Zheng, Y.W., Koike, N., et al. (2013). *Vascularized and functional human liver from an iPSC-derived organ bud transplant.* Nature 499. https://doi.org/10.1038/nature12271.

Vila Cuenca, M., Cochrane, A., van den Hil, F.E., de Vries, A.A.F., Lesnik Oberstein, S.A.J., Mummery, C.L., and Orlova, V. V. (2021). *Engineered 3D vessel-on-chip using hiPSC-derived endothelial- and vascular smooth muscle cells.* Stem Cell Reports 16. https://doi.org/10.1016/j.stemcr.2021.08.003.

Zhang, M., D'Aniello, C., Verkerk, A.O., Wrobel, E., Frank, S., Ward-Van Oostwaard, D., Piccini, I., Freund, C., Rao, J., Seebohm, G., et al. (2014). *Recessive cardiac phenotypes in induced pluripotent stem cell models of Jervell and Lange-Nielsen syndrome: Disease mechanisms and pharmacological rescue.* Proc. Natl. Acad. Sci. U. S. A. 111. https://doi.org/10.1073/pnas.1419553111.

Zhang, S., Wan, Z., and Kamm, R.D. (2021). *Vascularized organoids on a chip: strategies for engineering organoids with functional vasculature.* Lab Chip 21, 473–488. https://doi.org/10.1039/d0lc01186j.

Zhang, S., Wan, Z., Pavlou, G., Zhong, A.X., Xu, L., Kamm, R.D., Zhang, S., Wan, Z., Pavlou, G., Zhong, A.X., et al. (2022). *Interstitial Flow Promotes the Formation of Functional Microvascular Networks In Vitro through Upregulation of Matrix Metalloproteinase-2.* Adv. Fun https://doi.org/10.1002/adfm.202206767.

Enhanced endothelial cell-cardiomyocyte crosstalk in hiPSC-derived vascularized 3D cardiac microtissues on chip through paracrine signalling

Authors and Affiliations

Ulgu Arslan[1], Marcella Brescia[1], Viviana Meraviglia[1], Dennis M. Nahon[1], Ruben W.J. van Helden[1], Jeroen M. Stein[1], Francijna E. van den Hil[1], Berend J. van Meer[1], Marc Vila Cuenca1[1,2], Christine L. Mummery[1], Valeria V. Orlova[1]*

[1]Department of Anatomy and Embryology, Leiden University Medical Centre, 2333ZC Leiden, The Netherlands

[2]Department of Clinical Genetics, Leiden University Medical Center, 2333ZA Leiden, the Netherlands

* Corresponding author

This work was combined with the study in chapter 5 and published in Stem Cell Reports, 2023 Jul 11, 18:1394–1404.
DOI: 10.1016/j.stemcr.2023.06.001.

Summary

The heart is one of the most metabolically active organs in the body. Vasculature is essential to provide selective nutrient delivery to meet its energy demand. In chapter 5, we developed an *in vitro* model of hiPSC-derived vascularized and perfusable cardiac microtissue on chip (VMToC). Here, we further characterized VMToCs function in more detail and investigated sarcomere organization and contractility. Vascularization improved endothelial cell (EC)-cardiomyocyte (CM) communication via EC-derived paracrine factors, such as nitric oxide (NO) and resulted in an enhanced inflammatory response. The platform sets the stage for studies on how organ-specific EC barriers respond to drugs or inflammatory stimuli.

Keywords:

human induced pluripotent stem cells; cardiac microtissue; heart-on-chip.

Introduction

The heart is highly vascularized. The crosstalk between vasculature and the myocardium ensures proper structure and function of the heart through the delivery of oxygen, nutrients and (blood) cells and removal of waste. Interruptions in this crosstalk have been implicated in cardiovascular disorders which are the major cause of death globally (Berry and Duncker, 2020). Several 3D microphysiological models of the human heart have been described in which cardiac stromal cell crosstalk improved human pluripotent stem cell derived CM (hPSC-CM) maturation. These systems have proven useful for modeling some types of cardiac disease and for drug screening (reviewed in Arslan et al., 2022). However, most of these models lacked functional vasculature as they were maintained in static cultures. In chapter 5, we developed a vascularized 3D cardiac microtissue on a chip (VMToC). We combined prevascularized hiPSC-derived 3D cardiac microtissues (MTs) and vascular cells (human induced pluripotent stem cell derived endothelial cells (hiPSC-EC) and human brain vascular pericytes (HBVP)) in a fibrin hydrogel in a commercial organ-on-chip culture platform. Vascular cells self-organized into an external vascular network which interconnected/anastomosed with the preexisting microvascular networks in the MTs. We showed that fluid flow was essential for the anastomosis which was enhanced by continuous perfusion. Here, we characterized VMToCs functionally. We first investigated whether vascularization affects parameters such as sarcomere organization and spontaneous or paced contraction. We showed that the sarcomere organization was not affected by the presence of vascular structures. However, contraction duration was significantly longer in VMToCs. Notably, we demonstrated that EC-CM crosstalk can be modeled in vascularized cardiac MT on chip (VMToC) cultures: by using either L-N-Nitro arginine methyl ester (L-NAME), an inhibitor of nitric oxide synthetases (NOS), or pro-inflammatory stimuli, such as interleukin-1β (IL-1β), we revealed some of the paracrine signals playing roles in the regulation of cardiac function in MTs.

Figure 1

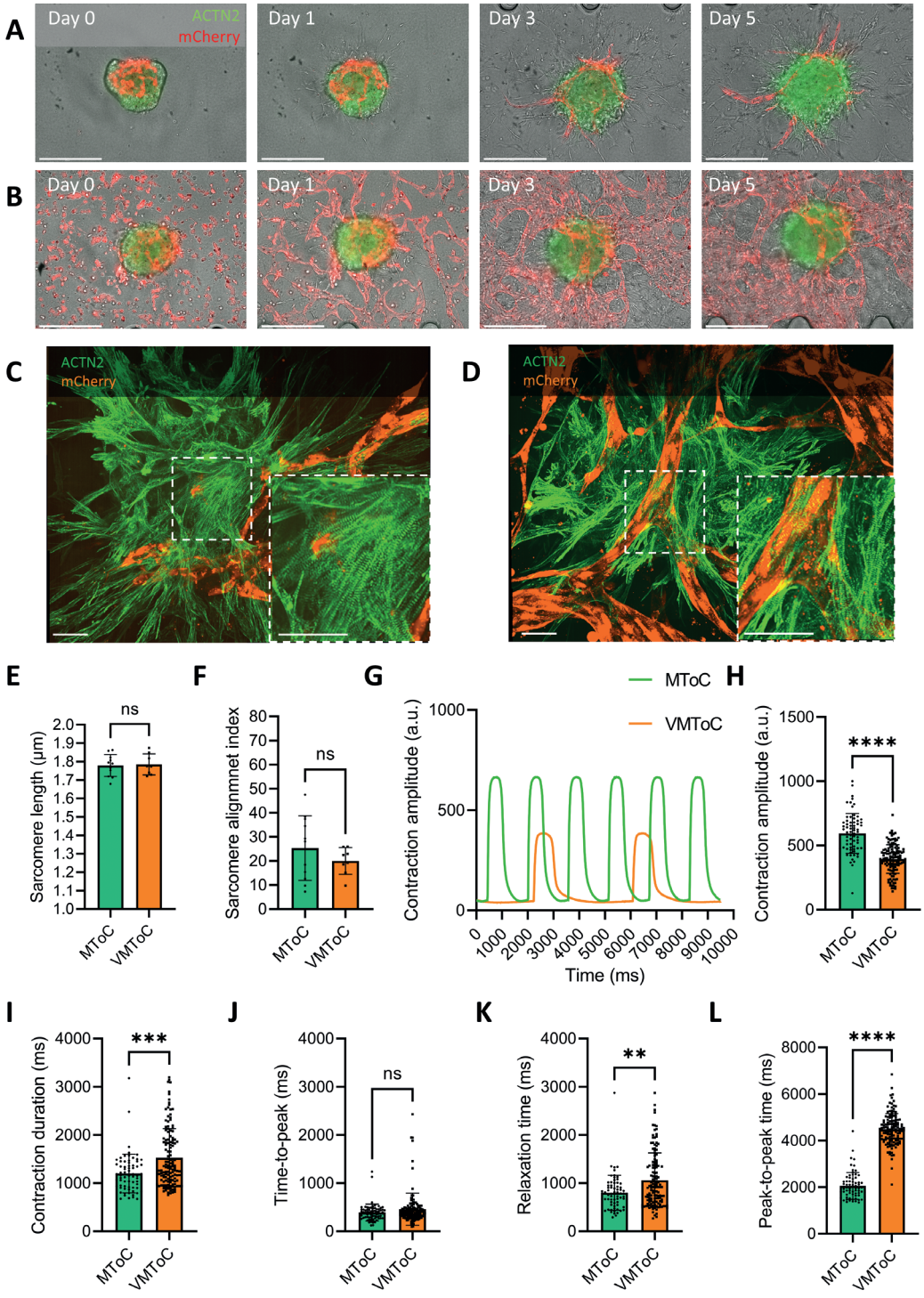

Figure 1: Characterization of contractile dynamics of cardiac MTs in MToC and VMToC. *(A, B) Representative images of MTs in chips on day 0, 1, 3 and 5 in MToC (A), and VMToC (B) (10×). Scale bar, 300 μm. (C, D)*

*Representative confocal images of sarcomeres showing hiPSC-ECs (orange, mCherry) and hiPSC-CM (green, ACTN2) in MToC (C) and VMToC (D) (40x). White dash box is the area that is zoomed 100x. Scale bar, 50 μm. (E, F) Quantification of the sarcomere parameters: sarcomere length (E); sarcomere alignment index (F); Error bars are shown as mean±SD from MToC N = 3, n = 11; VMToC N =4, n =8; three or four independent experiments with at least 8 MTs. (G) Representative beating traces of MTs from MToC (green trace) and VMToC (orange trace). (H-L) Quantification of the contraction parameters: contraction amplitude (H); contraction duration (I); time-to-peak (J); relaxation time (K); peak-to-peak time (L) in MTs with AICS-0075 hiPSC-CMs. Error bars are shown as mean±SD from MToC N = 3, n = 69; VMToC N =3, n=132; three independent experiments with 16 or 24 MTs from at least six different microfluidic channels each experiment. Student's t-test (E), Wilcoxon-Mann-Whitney test (F, and H-L). ***p < 0.001,****p < 0.0001; ns, not significant.*

Results

Characterization of cardiac MTs in the absence or presence of external vascular network

hiPSC-derived 3D cardiac microtissues (MTs) were formed using CMs, ECs, and CFs, as previously established (Campostrini et al., 2021). These MTs were maintained 12 days in static culture conditions and then integrated in AIM Biotech 3D cell culture chips. We examined cardiac MTs in the chips for any changes in their sarcomere organization and contractile properties. MTs were compared in the absence (MToC, 1A) or presence (VMToC, Figure 1B) of an external vascular network. Sarcomere morphologies appeared similar in the MToC (Figure 1C) and VMToC (Figure 1D) which was confirmed by similar sarcomere lengths (Figure 1E) and alignment indices (Figure 1F) assessed using the SOTATool (Stein et al., 2022). This indicated that there was no additional effect on sarcomere organization in the presence of an external vascular network. Contractility of cardiac MTs was analyzed using the video-based software tool MUSCLEMOTION (Sala et al., 2018). Representative beating traces showed that MTs under both conditions maintained their contractility in hydrogel (Figure 1G). However, contraction amplitude (Figure 1H) was significantly lower in VMToC, and contraction duration (Figure 1I), relaxation time (Figure 1K) and peak-to-peak time (Figure 1L) were significantly longer in VMToC. Time-to-peak (Figure 1J) was similar in both conditions.

The changes in these parameters were consistent in VMToC and MToC that were generated using a second, independent hiPSC line as a source of CMs (Figure 2A-E). In order to test whether the increase in contraction duration and relaxation time in the VMToC is not beat rate dependent, we electrically paced MTs in the chips using custom-made electrodes that fit the gel channel inlet and outlet. When the MTs were paced at 0.8 Hz and 1 Hz (Figure 2F-G), contraction duration at 90% and 50% transient was significantly higher in VMToC compared to MToC, consistent with the results under conditions of spontaneous beating (Figure 2H-I). We further investigated if the duration differences could be explained by time-to-peak or relaxation time changes. However, these parameters were highly variable and were not significantly different between VMToC and MToC even when paced (Figure 2J-K).

Figure 2

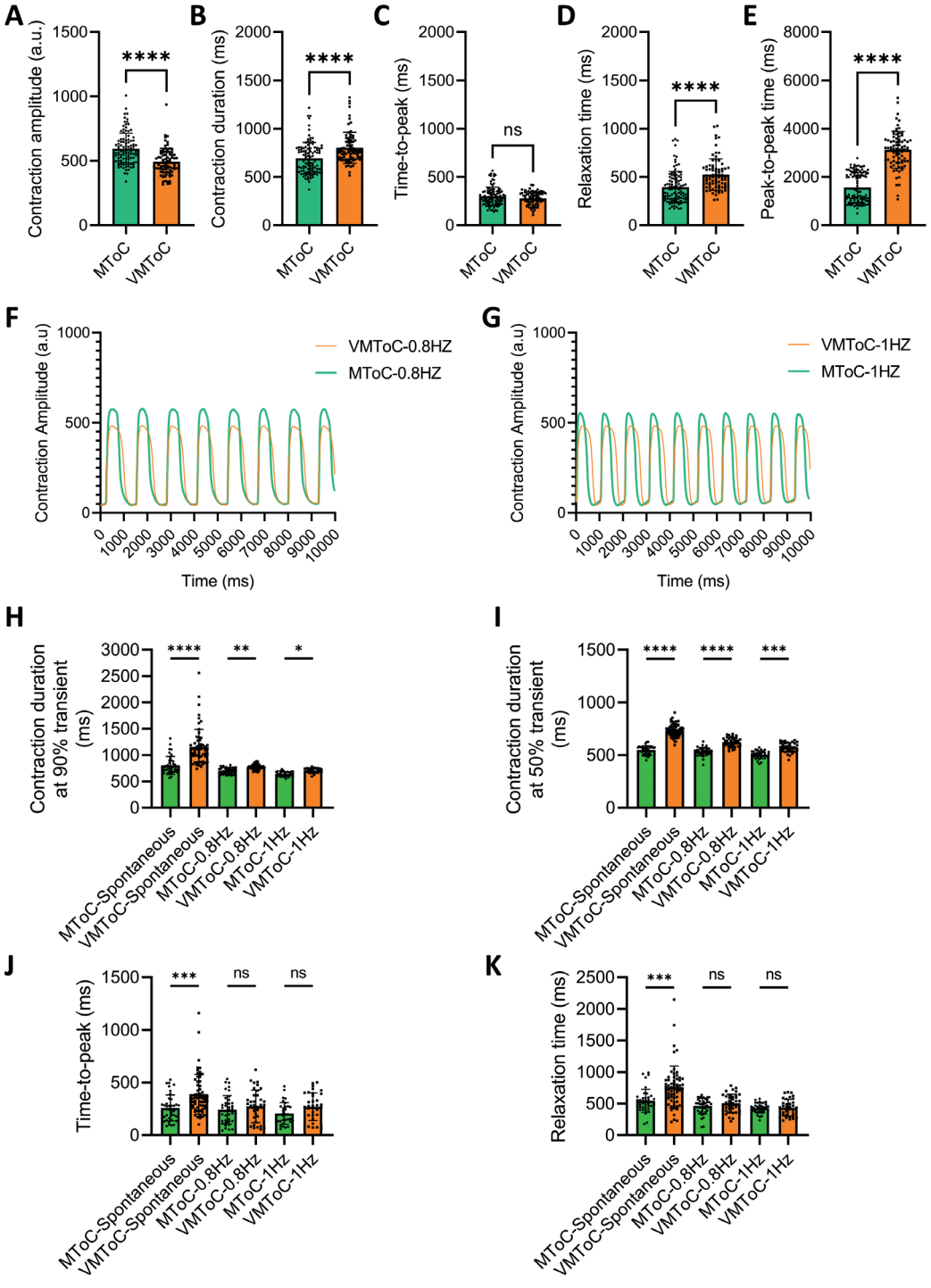

Figure 2: Characterization of contraction parameters upon pacing. *(A-E) Quantification of the contraction parameters of MToC and VMToC: contraction amplitude (A); contraction duration (B); time-to-peak (C);*

*relaxation time (D); peak-to-peak time (E) in MTs with LUMC0059iCTRL03 hiPSC-CMs. Error bars are shown as ±SD from MToC N = 3, n>30; VMToC N =3, n>26; three independent experiments with 26 MTs from at least six different microfluidic channels in each experiment. (F-G) Representative beating traces at 0.8 Hz (A) and 1 Hz (B). (H-K) Quantification of the contraction parameters during spontaneous beating, at 0.8 Hz and 1 Hz paced MTs: contraction duration at 90% transient (H); contraction duration at 50% transient (I); time-to-peak (J); relaxation time (K) in MTs with AICS-0075 hiPSC-CMs. Error bars are shown as ±SD from MToC N = 3, n >10; VMToC N =3, n>10; three independent experiments with 10 MTs from at least three different microfluidic channels were carried out for each experiment. Wilcoxon-Mann-Whitney test (A-E), Kruskal-Wallis test with Dunn's multiple comparisons test (H-K); *p < 0.05, **p < 0.01; ***p < 0.001, ****p < 0.0001; ns, not significant.*

Modeling EC-CM crosstalk in cardiac MTs

To explore whether VMToC have added value over MToC in studying inflammation, we investigated using two independent hiPSC lines for CMs whether EC-CM crosstalk can be modulated by either (1) L-NAME, a nonselective inhibitor of NOS or (2) pro-inflammatory stimuli, such as IL-1β. MToC and VMToC were incubated with L-NAME or vehicle for one hour (Figure 3A-D and 4A-D) or six hours (Figure 3E-H and 4E-H). L-NAME had no effect on the contraction time parameters: duration, time-to- peak and relaxation time in MToC after one- or six-hour incubation compared to the vehicle alone. By contrast, six-hour L-NAME exposure of VMToC cultures decreased contraction duration (Figure 3E, 4E) and relaxation time (Figure 3G, 4G) but had no effect on the time-to-peak (Figure 3F, 4F). One- hour of L-NAME incubation was more variable between the lines tested, and decreased contraction duration and relaxation time in one but not the other control line (Figure 3A, C and 4A, C). Peak-to- peak times appeared to decrease in one of the control lines tested after one and six hours, but not the other (Figure 3D, H and 4D, H).

Finally, MToC and VMToC were stimulated for twelve hours with IL-1β (10 ng/ml) to investigate the effect of pro-inflammatory cytokines. Pro-inflammatory cytokine release and contractile parameters were assessed. Stimulation with IL-1β resulted in significant upregulation of IL-6 (Figure 3I), IL-8 (Figure 3J) and cytokine chemoattractant protein 1 (MCP-1/CCL2, Figure 4K) in VMToC but not in MToC. In addition, IL-1β stimulation decreased contraction duration, relaxation time and peak-to- peak time in VMToC but had no effect on MToC (Figure 3L-O).

Figure 3

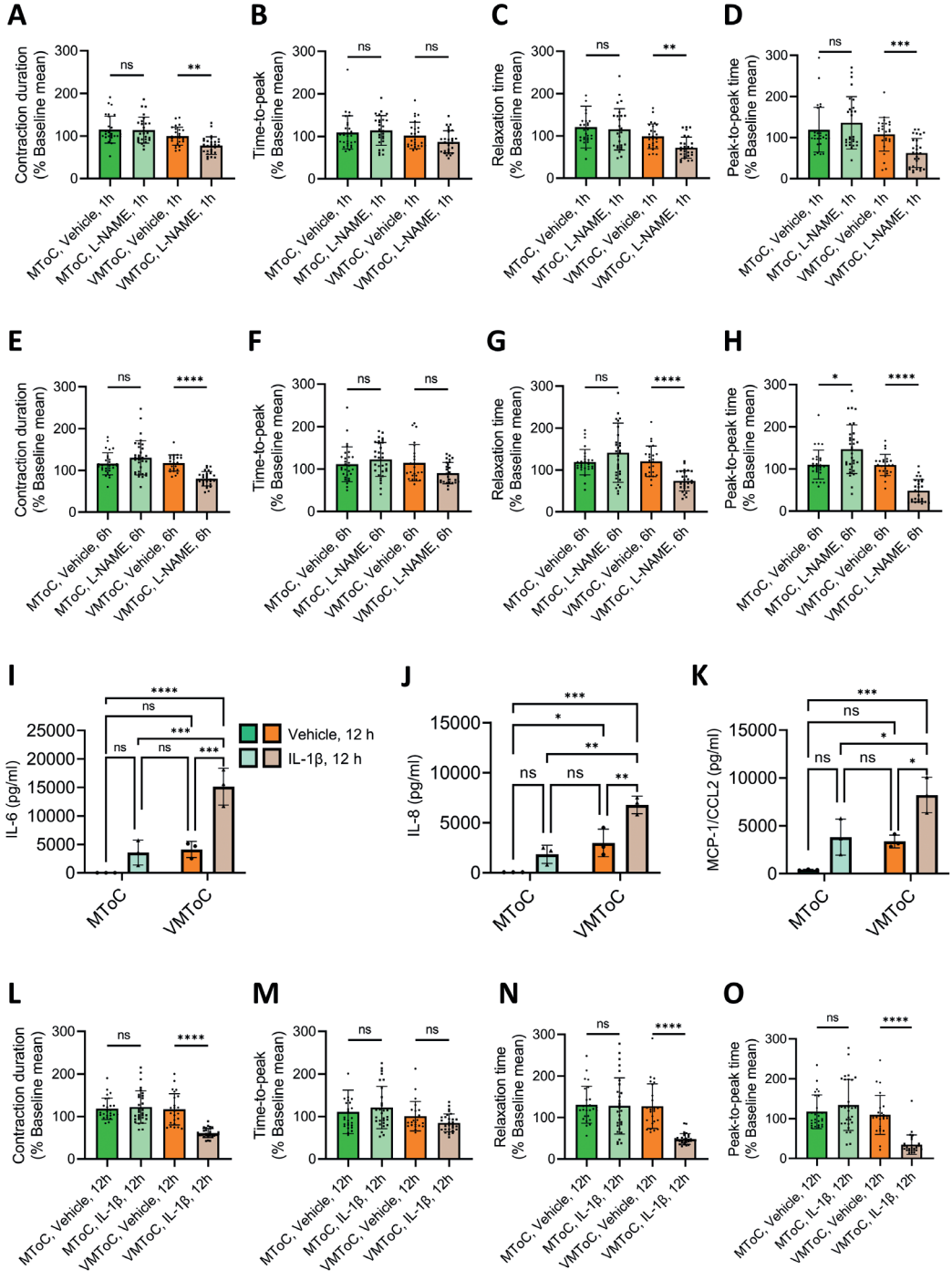

Figure 3: Altered contractile dynamics and inflammatory response of cardiac MTs regulated by EC- CM communication in VMToC but not in MToC. *(A-H) Quantification of the contraction parameters presented*

*as percentage change from the baseline mean of spontaneous beating condition, after 1 h (A-D) and 6 h (E-H) incubation with Vehicle or L-NAME (1 mM): contraction duration (A, E); time-to-peak (B, F); relaxation time (C, G); peak-to-peak time (D, H) in MTs with LUMC0059iCTRL03 hiPSC-CMs. Error bars are shown as mean±SD from MToC N = 3, n > 28 (Vehicle) and n > 27 (L-NAME); VMToC N =3, n > 24 (Vehicle) and n > 27 (L-NAME); three independent experiments with at least 7 MTs in each experiment. (I-K) Quantification of proinflammatory cytokines from the medium after 12 h incubation of IL-1β (10 ng/ml): IL-6 (I); IL-8 (J); MCP1/CCL2 (K) in MTs with LUMC0059iCTRL03 hiPSC-CMs. Y-axis shows concentration (pg/ml). Error bars are shown as mean±SD. MToC N = 3, n>3; VMToC N =3, n > 3; three independent experiments, medium was collected from at least with 3 different microfluidic channels in each experiment. (L-O) Quantification of the contraction parameters presented as percentage change from the baseline mean of spontaneous beating condition after 12 h incubation with Vehicle or IL-1β (10 ng/ml): contraction duration (L); time-to-peak (M); relaxation time (N); peak-to-peak time (O) in MTs with LUMC0059iCTRL03 hiPSC-CMs. Error bars are shown as mean±SD from MToC N = 3, n = 26 (Vehicle) and n = 30 (IL-1β); VMToC N =3, n = 25 (Vehicle) and n = 31 (IL-1β); three independent experiments with at least 7 MTs in each experiment. Kruskal-Wallis test with Dunn's multiple comparisons test (A-H, L-O), 2-way ANOVA with Šidák's multiple comparisons test (I- K), *p < 0.05, **p < 0.01, ***p < 0.001; ****p < 0.0001; ns, not significant.*

Discussion

In chapter 5, we developed a perfusable hiPSC-derived VMToC model. Here, we further characterized VMToCs in their function and EC-CM crosstalk. Previously we demonstrated that including ECs and cardiac fibroblasts (CFs) in MTs enhances CM maturation (Giacomelli et al, 2020). However, no differences in sarcomere organization were found between VMToC and MToC, indicating that further enhancement was not induced by the external vascular network. VMToCs showed characteristic low beat rates but nevertheless they continued to contract rhythmically throughout the experiments. Analysis of VMToC contractile parameters showed increased contraction duration and relaxation times. Notably, the increase in contraction duration in VMToC was not rate dependent and was maintained upon pacing at 0.8 and 1 Hz.

We further demonstrated that EC-CM crosstalk could be captured in VMToC upon delivery of stimuli via the external vascular network. Inhibition of NOS using L-NAME in VMToCs reversed the slow beating and decreased contraction duration, relaxation and peak-to-peak time. At the same time, L- NAME had no significant effect in MToC after one- or six hours incubation, except for an increase in peak-to-peak time. The effect of L-NAME in VMToC could be explained by a possible increase in endothelium-derived endothelin (ET-1) production upon NOS inhibition (Kourembanas et al., 1993; Czóbel et al., 2009). Since VMToCs contain more ECs than MToCs, this could result in a pronounced response to NOS inhibition that was not observed in MToCs. Similarly, stimulation with IL-1β for twelve hours resulted in upregulation of several pro-inflammatory cytokines, such as IL-6, IL-8 and MCP-1 in VMToC, but not in MToC, suggesting that only the vascular units were effectively responding to pro-inflammatory cytokine stimulation that are known contributors to EC dysfunction and heart failure. Stimulation with IL-1β decreased contraction duration, relaxation time and peak- to-peak time. This was somewhat unexpected since IL-1β and IL-6 are known as negative inotropes that increase NO levels via upregulating the expression of inducible NOS (iNOS) in isolated CMs (Segers et al., 2018). On the other hand, IL-1β and

Figure 4

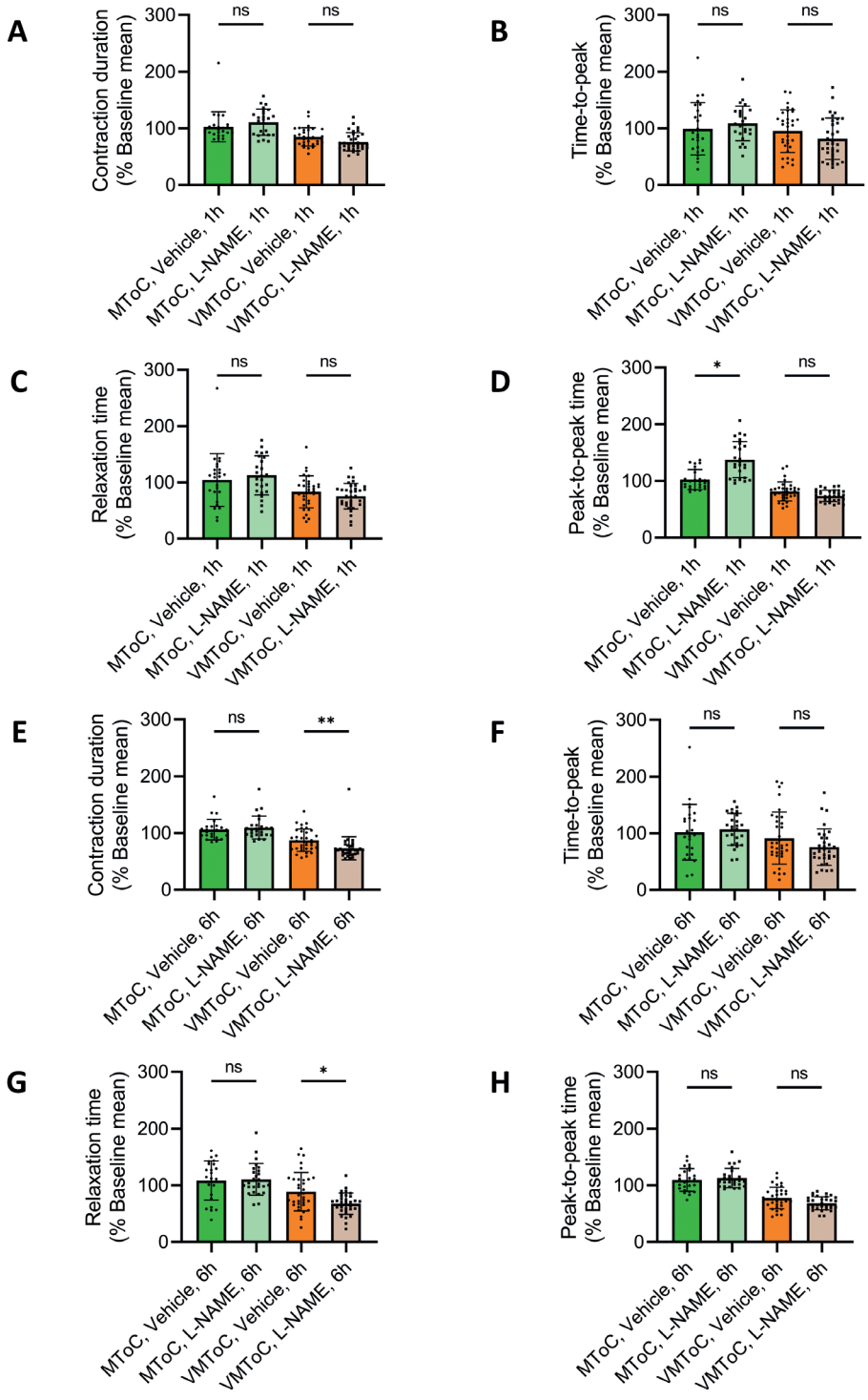

Figure 4: Altered contractile dynamics of cardiac MTs upon inhibition of EC-CM communication in VMToC but not in MToC, using a second control line. *(A-H) Quantification of the contraction parameters presented*

*as percentage change from the baseline mean of spontaneous beating condition, after 1 h (A-D) and 6 h (E-H) incubation of L-NAME (1 mM): contraction duration (A, E); time-to-peak (B, F); relaxation time (C, G); peak-to-peak time (D, H) in MTs with AICS-0075 hiPSC-CMs. Error bars are shown as ±SD from MToC N = 3, n >6; VMToC N =3, n > 7; three independent experiments with at least 6 MTs from at least four different microfluidic channels in each experiment. Data is normalized to baseline mean of each set for vehicle and L- NAME group of MTs. Kruskal-Wallis test with Dunn's multiple comparisons test (A-H). *p < 0.05, **p < 0.01; ns, not significant.*

IL-6 decrease endothelial NOS (eNOS) expression and activity in ECs (Saura et al., 2006; Kawasaki et al., 2015; Hung et al., 2010). Although we have not examined expression of iNOS and eNOS upon IL-1β treatment in VMToC vs MToC, the fact that the IL- 1β inhibitory effect was only observed in VMToC indicates the importance of the vascular component in mediating the response in CMs.

Finally, inter-batch and inter-line variability might be the result of differences in basal contractile parameters and/or drug responses in VMToCs. We showed consistency between two different hiPSC lines but further validation using more hiPSC lines may be of value as NOS levels may differ between CMs and ECs from different lines and thus affect contractile dynamics and drug responses to different extents.

In summary, we showed here that the presence of vasculature significantly affected the contraction time parameters of VMToC, However, the sarcomere organization was not affected by vascularization. We challenged EC-CM crosstalk in two ways: NOS inhibition and stimulation with a pro-inflammatory cytokine. As a result, pro-inflammatory cytokine concentration, contraction duration and peak-to-peak time significantly changed only in VMToC, but not in MToC. These results suggest that EC-CM crosstalk is enhanced in VMToC and regulated CM contraction and response to stimuli, highlighting the utility of VMToC.

Experimental Procedures

Detailed experimental procedures on hiPSC line maintenance, cardiac microtissue and cell preparation before on chip cultures can be found on chapter 5.

Microfluidic chip culture

Cells and MTs mixtures were seeded in commercially available microfluidic chips (AIM Biotech) as follows: 1) 4 MT/channel in combination with 25 × 106 hiPSC-ECs/mL and 5 × 106 HBVP cells/mL (5:1 ratio) (VMToC); or 2) 4 MT/channel (MToC) were resuspended in endothelial growth medium-2 (EGM-2, Lonza) supplemented with Thrombin (4 U/mL). This mixture was then added to fibrinogen (final concentration 3 mg/mL, Sigma) at 1:1 vol ratio and gently mixed. Final mixture was loaded into the middle gel-loading channel of the microfluidic chip. Chips were incubated at room temperature for 15 min. The chips were maintained in a medium mixture consists of (bovine serum albumin (BSA) and essential

lipids (B(P)EL) medium and endothelial growth medium-2 (EGM-2); 50:50), supplemented with vascular endothelial growth factor (VEGF) (50 ng/mL). On day 1, the γ-secretase inhibitor DAPT (10 µM) was added to the medium for 24 h. Intermittent gravity-driven flow in the whole chamber was induced by the addition of 100 µL medium to the right media ports and 50 µL media to left media ports in the medium channel which creates hydrostatic pressure. Medium was refreshed daily until day 7 and characterized between day 5-7.

L-NAME and IL-1β stimulation

On the day of L-NAME stimulation chips were refreshed with the medium supplemented with either VEGF (50 ng/mL) and distilled water (Vehicle) or VEGF (50 ng/mL) and L-NAME (1 mM, N5751, Sigma) for one or six hours. Chips were incubated at 37 °C, 5% CO2 and contraction analyses were performed after one hour or six hours.

On the day of IL-1β stimulation chips were refreshed with the medium supplemented with either VEGF (50 ng/mL) and PBS (Vehicle) or VEGF (50 ng/mL) and IL-1β (10 ng/ml, N5751, Sigma) for twelve hours. Chips were incubated at 37 °C, 5% CO2 and contraction analyses were performed after twelve hours.

Multiplex Cytokine Analysis

The medium from multiple chips were collected after twelve hours stimulation with IL-1β (10 ng/ml) or vehicle, and kept at -80 oC. On the day of the multiplex cytokine bead assay, collected medium was thawed two hours prior to the experiment. Concentration of cytokines (CXCL10, IL-1β, TNFα, CCL2, IL-6, IL-10, IFNϒ, TGFβ1 free active and IL-8) was measured using a LEGENDplex Human Essential Immune Response Panel kit (13-plex) (BioLegend, cat no: 740930) according to the manufacturer's instructions. Undiluted or eight times diluted samples were run on Cytek 3-Laser Aurora spectral flow cytometer (Cytek Biosciences, USA).

Imaging of vascularized 3D cardiac microtissues on chip

Whole channel images were captured daily using EVOSM7000 with 10x objectives. Confocal images were captured to create 3D stack using Andor Dragonfly spinning disk confocal microscope using a 40x objective. Images were processed using Imaris 9.5 software (Bitplane, Oxford Instruments).

Contraction analysis

For pacing experiments, electrodes were made in-house to fit to the gel channels of chips and used to pace MTs. MTs were stimulated at 0.8 and 1 Hz, with 15V/cm strength and 3 ms long stimulation pulse. Movies of spontaneous beating or paced MTs from VMToC and MToC

conditions were acquired for at least 10 s at 37 °C either with a ThorLabs DCC3240M camera at 100 frames/s and a 10x objective phase contrast objective (Leica Inverted microscope IBDE), using the ThorLabs uc480 software (v 4.20), or with a Leica Microsystems LAS AF6000 microscope at 37 °C and 5 % CO2. On the day of L-NAME or IL-1β stimulation, VMToC and MToC conditions were recorded for their baseline spontaneous beating prior to drug administration. Chips were recorded after both one hour incubation and six hours incubation period with vehicle and L-NAME or twelve hours incubation period with IL-1β. Contraction data were obtained by analyzing movies with the MUSCLEMOTION ImageJ macro (ImageJ v. 2.0.0-rc-49) as described previously (Sala et al., 2018).

Sarcomere analysis

Confocal images of VMToC and MToC conditions were acquired using a DragonFly spinning disk (Andor) microscope with 40x objective. In each MT, one plane from each FOVs were chosen to quantify and converted to 8-bit images. For MToC, 88 FOVs were selected in 11 MTs and for VMToC 52 FOVs were selected in 8 MTs. Sarcomere quantification data was obtained by analyzing these 8-bit images with SotaTool, as described previously (Stein et al., 2022).

Statistical analysis

Statistical analysis was performed using GraphPad Prism 9. Student's t-test, one-way or two-way ANOVA for paired or unpaired measurements were applied as appropriate to test for differences in means between groups/conditions. Kruskal–Wallis test and Wilcoxon-Mann-Whitney test were used when the normality assumption did not hold. Data are expressed and plotted as the Mean ± SD. as indicated in figure legend. Detailed statistics and exact P-values are indicated in each figure legend. Statistical significance was defined as $P < 0.05$.

References

Arslan, U., Moruzzi, A., Nowacka, J., Mummery, C. L., Eckardt, D., Loskill, P., and Orlova, V. V. 2022. *Microphysiological stem cell models of the human heart.* Materials Today Bio 14:100259.

Berry, C., and Duncker, D. J. 2020. *Coronary microvascular disease: The next frontier for Cardiovascular Research.* Cardiovascular Research 116(4):737-740.

Campostrini, G., Meraviglia, V., Giacomelli, E., van Helden, R. W. J., Yiangou, L., Davis, R. P., Bellin, M., Orlova, V. V., and Mummery, C. L. 2021. *Generation, functional analysis and applications of isogenic three-dimensional self-aggregating cardiac microtissues from human pluripotent stem cells.* Nature Protocols 16(4):2213-2256.

Czóbel, M., Kaszaki, J., Molnár, G., Nagy, S., and Boros, M. 2009. *Nonspecific inhibition of nitric oxide synthesis evokes endothelin-dependent increases in myocardial contractility.* Nitric Oxide - Biology and Chemistry 21(3-4):201-9.

Hung, M. J., Cherng, W. J., Hung, M. Y., Wu, H. T., and Pang, J. H. S. 2010. *Interleukin-6 inhibits endothelial nitric oxide synthase activation and increases endothelial nitric oxide synthase binding to stabilized caveolin-1 in human vascular endothelial cells.* Journal of Hypertension 28(5):940-51.

Kawasaki, Y., Yokobayashi, E., Sakamoto, K., Tenma, E., Takaki, H., Chiba, Y., Otashiro, T., Ishihara, M., Yonezawa, S., Sugiyama, A., et al. 2015. *Angiostatin prevents IL-1β-induced down-regulation of eNOS expression by inhibiting the NF-κB cascade.* Journal of Pharmacological Sciences 129(3):200-4.

Kourembanas, S., McQuillan, L. P., Leung, G. K., and Faller, D. V. 1993. *Nitric oxide regulates the expression of vasoconstrictors and growth factors by vascular endothelium under both normoxia and hypoxia.* Journal of Clinical Investigation 92(1):99-104.

Sala, L., van Meer, B. J., Tertoolen, L. G. J., Bakkers, J., Bellin, M., Davis, R. P., Denning, C., Dieben, M. A. E., Eschenhagen, T., Giacomelli, E., et al. 2018. *Musclemotion: A versatile open software tool to quantify cardiomyocyte and cardiac muscle contraction in vitro and in vivo.* Circulation Research 122(3):e5-e16.

Saura, M., Zaragoza, C., Bao, C., Herranz, B., Rodriguez-Puyol, M., and Lowenstein, C. J. 2006. *Stat3 mediates interelukin-6 inhibition of human endothelial nitric-oxide synthase expression.* Journal of Biological Chemistry 281(40):30057-62.

Segers, V. F. M., Brutsaert, D. L., and De Keulenaer, G. W. 2018. *Cardiac remodeling: Endothelial cells have more to say than just NO.* Frontiers in Physiology 9:382.

Stein, J. M., Arslan, U., Franken, M., De Greef, J. C., Harding, S. E., Mohammadi, N., Orlova, V. V, Bellin, M., Mummery, C. L., and Van Meer, B. J. 2022. *Software Tool for Automatic Quantification of Sarcomere Length and Organization in Fixed and Live 2D and 3D Muscle Cell Cultures In Vitro.* Current Protocols in Human Genetics 2(7):e462.

Generation and characterization of hiPSC-derived vascularized-, perfusable cardiac microtissues-on-chip

Author(s) and contact information

Ulgu Arslan[1], Francijna E. van den Hil[1], Christine L. Mummery[1], Valeria V. Orlova[1]*

[1]Department of Anatomy and Embryology, Leiden University Medical Centre, 2333ZC Leiden, The Netherlands

* Correspondence to v.orlova@lumc.nl

Accepted for a publication in Current Protocols Stem Cell Biology
2024
DOI: 10.1002/cpz1.1097

Abstract

In the heart *in vivo*, vasculature forms a semi-permeable endothelial barrier for selective nutrient- and (immune) cell delivery to the myocardium and removal of waste products. Crosstalk between the vasculature and the heart cells regulates homeostasis in health and disease. To model heart development and disease *in vitro* it is important that essential features of this crosstalk are captured. Cardiac organoid- and microtissue models often integrate endothelial cells (ECs) to form microvascular networks inside the 3D structure. However, in static culture without perfusion, these networks may fail to show essential functionality. Here, we describe a protocol to generate an *in vitro* model of human induced pluripotent stem cell (hiPSC)-derived vascularized cardiac microtissues on a microfluidic organ-on-chip platform (VMToC) in which the blood vessels are perfusable. First, prevascularized cardiac microtissues (MT) are formed by combining hiPSC-derived cardiomyocytes, ECs and cardiac fibroblasts in a pre-defined ratio. Next, these prevascularized MTs are integrated in the chips in a fibrin hydrogel containing additional vascular cells, which self-organise into tubular structures. The MTs become vascularized through anastomosis between the pre-existing microvasculature in the MT and the external vascular network. The VMToCs are then ready for downstream structural and functional assays and basic characterization. Using this protocol, cardiac MTs can be efficiently and robustly vascularized and perfused within 7 days. *In vitro* vascularized organoid and MT models have the potential to transition current 3D cardiac models to more physiologically relevant organ models that allow the role of the endothelial barrier in drug and inflammatory response to be investigated.

Basic Protocol: Generation of VMToC

Support protocol 1: Functional Characterization of VMToC

Support protocol 2: Structural Characterization of VMToC

Keywords:

human induced pluripotent stem cells; vessels-on-a-chip; cardiac microtissues; vascularization

Introduction

The healthy heart has one of the highest energy demands of all organs in the body. Vasculature is essential for regulating its function, providing (selective) nutrient-, cell- and drug delivery and removing waste products (Brutsaert, 2003). Interrupting vascular function can lead to cardiovascular disorders, a major cause of mortality worldwide (Berry and Duncker, 2020). Monitoring crosstalk between the vasculature and cells of the heart is therefore essential to address questions related to the heart development and disease and creating human models can be particularly beneficial for understating underlying

mechanisms. Human pluripotent stem cells are increasingly used as a basis for these models since they can differentiate to all cell types of the heart.

Endothelial cells (ECs) are often incorporated in organoids or microtissues (MTs) from stem cells so that they are pre-vascularized when used in *in vitro* studies (Cakir et al., 2019; Homan et al., 2019; Vargas-Valderrama et al., 2020; Giacomelli et al., 2020).Vascular networks in these tissues are often well-organized but usually not perfusable. Passive diffusion is then the only way small molecules, drugs and nutrients can penetrate organoids and MTs. Perfusion is also necessary for the stability and integrity of the microvascular networks and without it, these networks regress over time (Ryan et al., 2021). This has in part been rectified by transplanting these tissue constructs into living animals. This promotes the formation of functional vasculature through anastomosis where host vasculature and the microvascular network inside the transplanted tissues interconnect (Mansour et al., 2018; Takebe et al., 2013; Ryan et al., 2021). However, inter-species differences might alter vascularization and survival of the cells in MTs and organoids (Brady et al., 2023). We discovered that an alternative to transplantation is to place MTs in a microfluidic chip under flow: the presence of ECs in the chip outside the MT also supports anastomosis such that vasculature inside the MTs becomes lumenized (Arslan et al., 2023). Here we describe the protocol to generate these hiPSC-derived vascularized and perfusable cardiac MT on chip (VMToC) in detail.

In basic protocol 1, hiPSC-derived cardiomyocytes (CMs), ECs and cardiac fibroblasts (CFs) are thawed and combined to form pre-vascularized 3D cardiac MTs. The MTs are then combined with a fibrin hydrogel containing additional vascular cells and integrated within a channel of a commercially available microfluidic organ-on-chip platform. Vascular cells present in hydrogel start self-organizing into an external vascular network around the MTs and interconnect with the pre-existing internal vasculature in the MTs through anastomosis. Over the subsequent 5-7 days of culture in the microfluidic chips, continuous vascular networks become evident in- and around the MTs. The integrity and functionality of the vasculature formed in the VMToCs can be demonstrated by perfusing with fluorescent beads. This shows that vascular networks are lumenized and perfusable and is described in support protocol 1. Further functional characterization can be carried out by assessing either spontaneous- or (electronically) paced contractile kinetics of the beating MTs, as described in support protocol 1. Structural characterization of VMToCs can be performed by fixing and immunofluorescent staining, as described in support protocol 2.

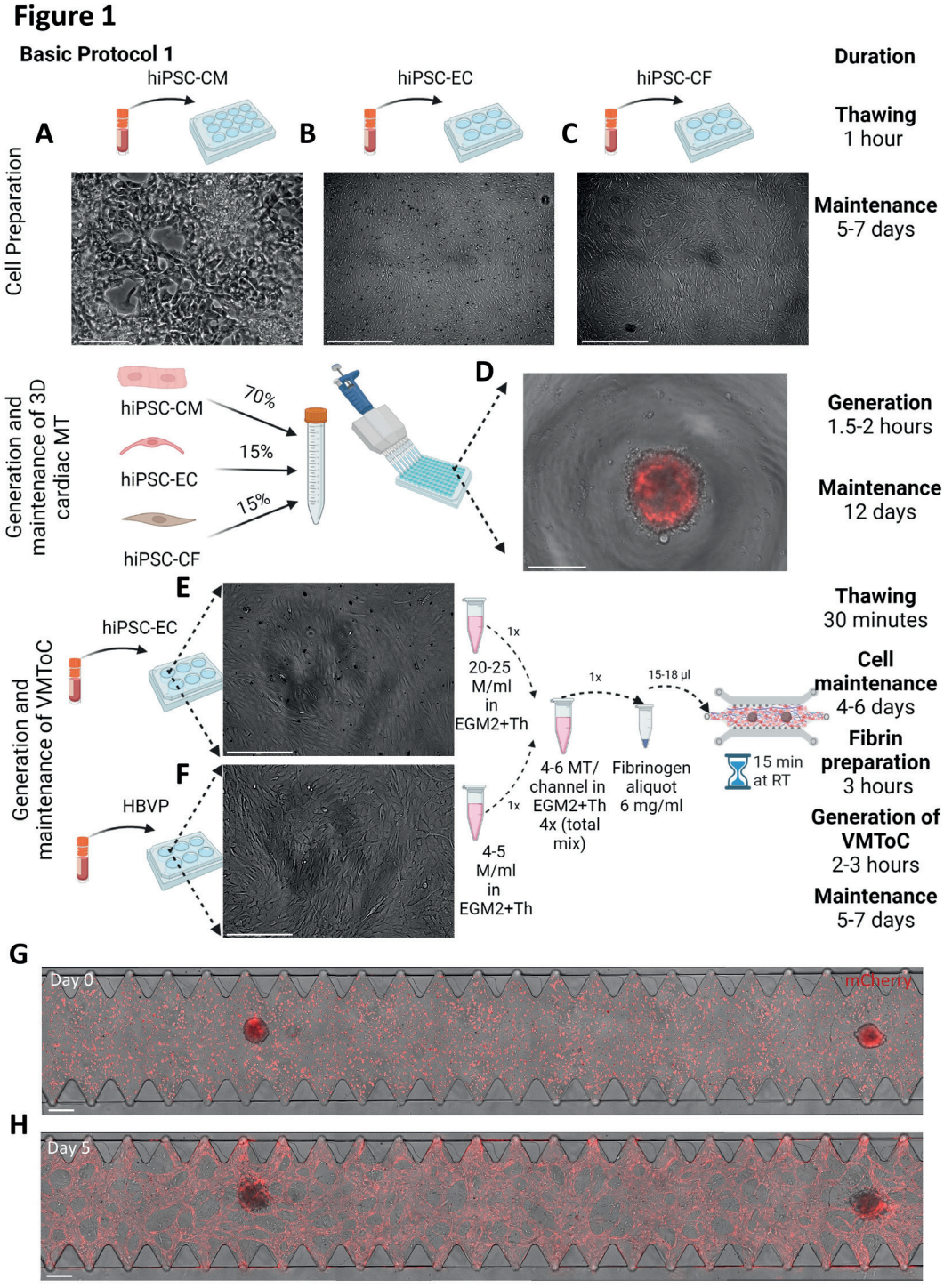

Figure 1: Schematic overview of the basic protocol 1 with representative images for each step. *(A) 10x Brightfield image of hiPSC-CMs on day 7 of thawing. (B-C) 4x Brightfield image of (B) hiPSC-ECs and (C) hiPSC-CFs on day 6 of thawing. (D) 10x Brightfield image of hiPSC-derived cardiac MTs on day 12 that shows prevascularization*

of MTs (mCherry, red). (E-F) 10x Brightfield image of (E) hiPSC-ECs and (F) HBVPs on day 6 of thawing. (G) Brightfield image of VMToCs on day 0 showing homogenous distribution of hiPSC-ECs (mCherry, red) and MTs. (H) Brightfield image of VMToCs on day 5 showing continuous vascular network developed in and around the MTs (mCherry, red). Scale bar – (A): 200 µm; (B, C): 675 µm; (D-F): 275 µm; (G, H): 250 µm. hiPSC, human induced pluripotent stem cells; CM: cardiomyocytes; EC, endothelial cells; CF, cardiac fibroblasts; HBVP, human brain vascular pericytes, MT, microtissues; VMToC, vascularized cardiac microtissue on a chip; EGM2, endothelial cell growth medium-2; Th, thrombin.

Basic Protocol
Generation of VMToC

Introductory paragraph

This protocol provides step-by-step methodology to generate hiPSC-derived 3D vascularized cardiac microtissues using a commercially available AIM Biotech IdenTx-9-Plate organ-on-chip platform. The protocol is divided into three sections. The first section describes the preparation of three different hiPSC-derived cardiac cell types to generate MTs (Fig. 1A-C). Cardiac MTs are then formed by combining the hiPSC-derived cardiac cells in a pre-defined ratio in V-shaped wells of a 96-well plate, as described previously, with minor modifications (Campostrini et al., 2021). The cells form single aggregates in each well and within 1 day, are compact and contractile cardiac MTs. hiPSC-ECs inside the MTs self-organize to form microvascular networks but without functional lumen (Fig. 1D). A mixture of hiPSC-derived endothelial cells (hiPSC-ECs, Fig. 1E), human brain primary pericytes (HBVPs, Figure 1F), the MTs and fibrinogen is pipetted into the middle channel of the AIM Biotech chips (Fig. 1G). Chips are maintained for 7 days under gravity-driven flow.

Starting from day 1 of seeding into the chip, hiPSC-ECs and HBVPs self-organize and form an external vascular network around the MTs. This external network begins interconnecting with the internal microvascular network inside the MTs in the chips (anastomosis). On day 3, vascular development continues and the anastomosis becomes more prominent. On day 5, vascular networks stabilize and a continuous vascular network in- and around the MTs is visible (Fig. 1H). Chips can be maintained until day 7. To improve vascular development further, chips can be placed at a later stage of culture (on day 3 (Fig. 2) or on day 5 (Fig. 3)) on a rocker platform to induce continuous perfusion. This promotes faster vascular development and shortens the total culture period. After the external network is developed, chips can be used for downstream applications such as modulating EC-CM crosstalk with external stimuli (Arslan et al., 2023) and testing cardiotoxicity of drugs (Di Cio et al., 2024). Characterization of these chips using structural and functional assays can be done as described in support protocol 1 and 2.

Figure 2

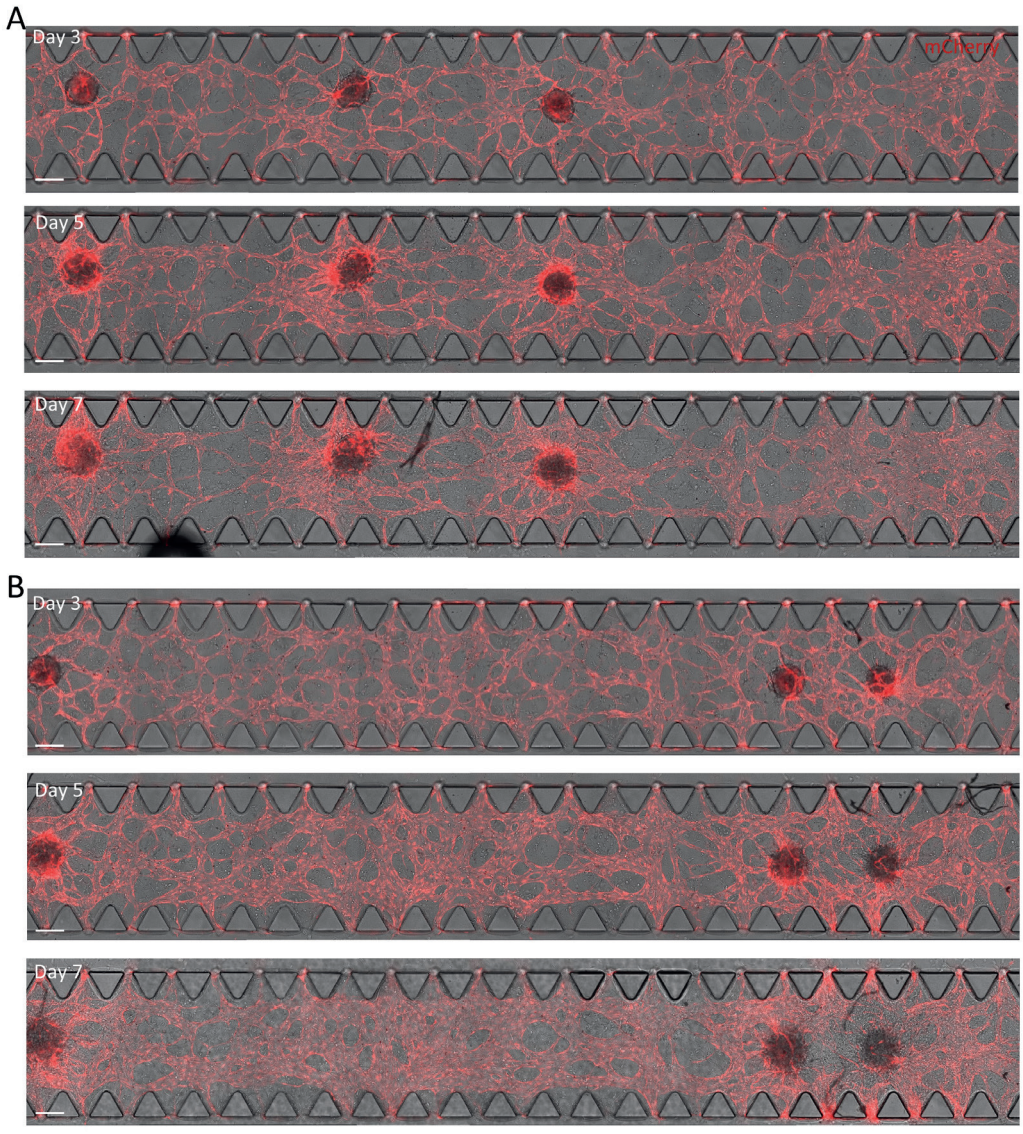

Figure 2: *(A-B) Brightfield images of 2 example VMToCs on day 3, 5 and 7 with continuous perfusion started on day 3 (mCherry, red). Scale bars: 250 µm*

Figure 3

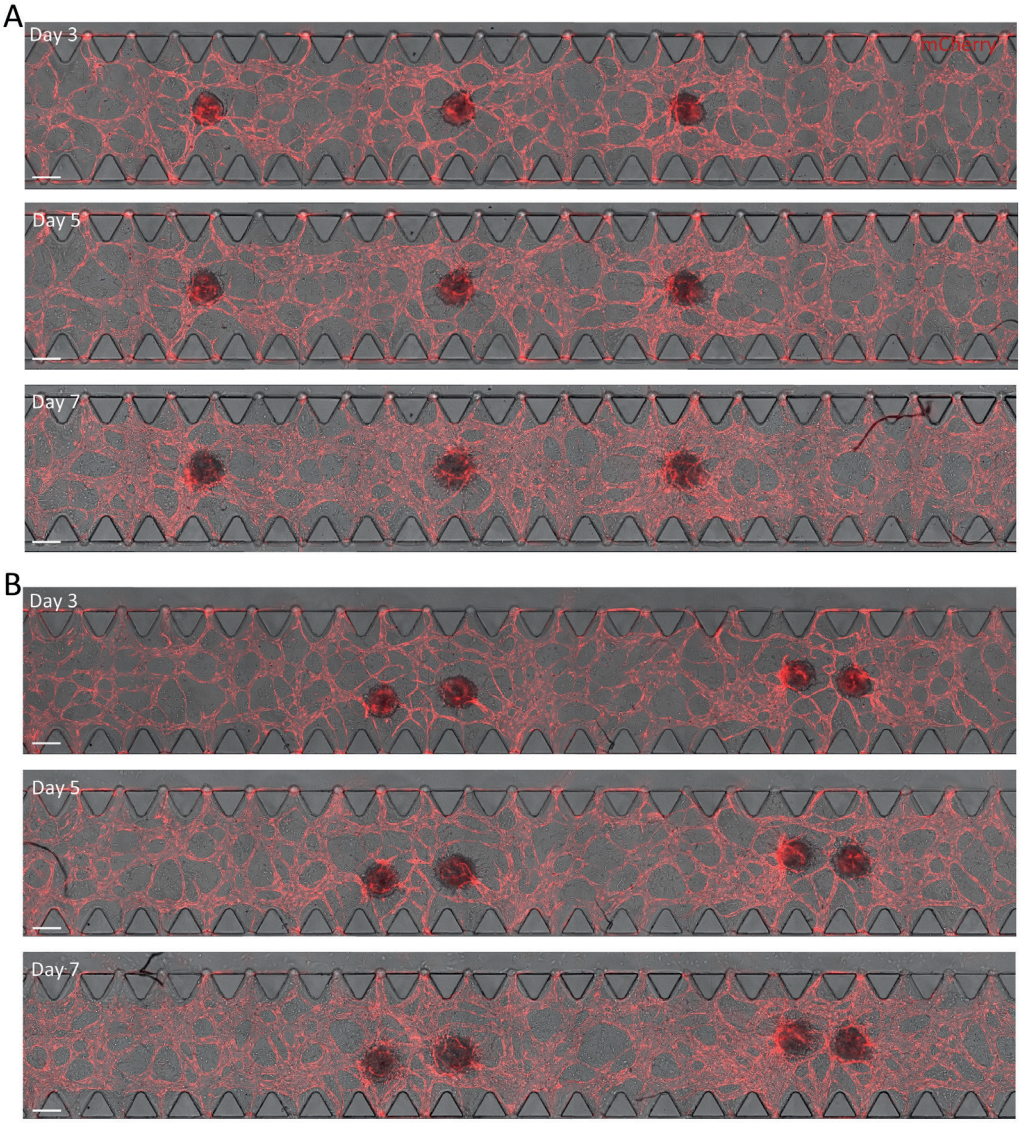

Figure 3: *(A-B) Brightfield images of 2 example VMToCs on day 3, 5 and 7 with continuous perfusion started on day 5 (mCherry, red). Scale bars: 250 µm*

Materials

- Cryopreserved hiPSC-derived CMs (Campostrini et al., 2021), ECs (Orlova et al., 2014) and CFs (Campostrini et al., 2021)
- Sterile biosafety cabinet (CleanAir)
- B(P)EL (see recipe) or MBEL (see recipe) medium, depending on the protocol used to differentiate hiPSC-CMs (Campostrini et al., 2021)
- L-Ascorbic acid 2-phosphate (AA2P), 5 mg ml–1 (see recipe)
- α-Monothioglycerol (αMTG) solution, 1.3% (v/v) (see recipe)
- Endothelial cell growth medium (EC-CGM) (see recipe)
- Fibroblast Growth Medium 3 (FGM3) (PromoCell, cat. no. C-23025)
- Matrigel coated 12 well plate (see recipe)
- Water bathe (Julabo TW20; MCO-18AIC Serial no. 08010017)
- Pipetman starter kit p20, p200, p1000 (Gilson international; cat. no. F167500S)
- 10-, 200-, and 1000-µl filter tips (Corning, cat. no. 4807, 4810, and 4809, respectively)
- Integra Pipetboy acu 2 (Boom B.V., cat. No. T155016)
- 5-, 10-, and 25-ml sterile plastic serological pipettes (Greiner Bio-One, cat. no. 606180, 607180, and 760180, respectively)
- 15- and 50-ml polystyrene conical tubes (Corning Falcon, cat. no. 352097 and 352098, respectively)
- Filtertips 1000 µl Biosphere® plus 96/Box (Sarstedt, cat. no. 70.3050.255)
- Centrifuge (Eppendorf, cat. no. 5810R)
- RevitaCell™ Supplement (100X (Thermo Fisher Scientific, cat.no. A2644501)
- CO2 cell culture incubator (Sanyo)
- Gelatin coated plate (see recipe)
- V-bottom 96 well microplates (Greiner Bio-one; cat. no. 651161)
- Dulbecco's phospohate-buffered saline without Ca+2 and Mg+2 (DPBS, Gibco, cat. no. 14190-094)
- TrypLE™ (5X) (see recipe)
- TrypLE™ Select Enzyme (1X), no phenol red (Gibco, cat. no. 12563029)
- Fuchs-Rosenthal Manual cell counter (VWR, cat. no. 631-0929)
- Trypan blue (Sigma-Aldrich, cat no, T8154-20ML)
- Human VEGF (165) IS, premium grade (Miltenyi Biotec, cat. no. 130-109-386)
- Human bFGF, premium grade (Miltenyi Biotec, cat. no. 130-093-842).

- 25-ml single use reservoirs (Avantor, cat. no. 613-1175)
- Finnpipette Multichannel Pipette p200 (ThermoFisher)
- Pericyte Medium (ScienCell, cat. no. 1201)
- Human Brain Vascular Pericytes (HBVPs; ScienCell, cat. no. SCC1200)
- Fibrinogen (Sigma-Aldrich, cat. no. F8630)
- Puradisc FP 30 Cellulose Acetate Syringe Filter, 0.2 µm, sterile (Cytiva, 10462200)
- BD Luer-Lok Syringe 50 ml (BD, cat. no. 300865)
- 1.5-ml microcentrifuge tubes (Eppendorf, cat. no. 0030 120.086)
- Eppendorf tubes 0.5ml (25-022-CI)
- EGM2 medium (see recipe)
- Thrombin (Sigma-Aldrich, cat. no. T4648-1KU)
- idenTx 9 Plate Box of 8 (Aim Biotech, cat. no. IDTX9)
- Chip medium (see recipe)
- DAPT (Sigma-Aldrich, cat. no. D5942)
- OrganoFlow® Rocker (Mimetas, cat. no. MI-OFPR-L)
- NIKON Eclipse Ti microscope

Protocol steps with step annotations

Cell preparation for MTs

This protocol is followed under aseptic conditions.

1. Follow the protocol of Campostrini et al (2021) for hiPSC differentiation, maintenance and cryopreservation of CM and CF.
2. Follow the protocol of Orlova et al (2014) for hiPSC differentiation, maintenance and cryopreservation of ECs.

If hiPSC derived cells are cryopreserved for later use, follow step 3 for thawing. Recovery period of hiPSC-CMs is 5-7 days, for hiPSC-ECs and hiPSC-CFs it is 4-6 days. Alternatively, freshly differentiated cells can be used to generate MTs. In this case, skip to step 32.

3. Pre-warm B(P)EL or MBEL, EC-CGM and FGM3 medium to room temperature (RT).
4. Prepare Matrigel coated plates (see recipe) to thaw hiPSC-CMs.
5. Thaw a vial of cryopreserved hiPSC-CMs in a hot water bath at 37 °C by moving it in a circular motion in the water until only a small piece of ice with a diameter of 1-2 mm is left inside the tube.
6. Transfer hiPSC-CMs into a 50-ml tube using 1000 µl Biosphere® filtertips.
7. Wash the vial with 1 ml B(P)EL or MBEL medium and add this on the cells drop by drop with a 1000 µl Biosphere® filtertips. Swirl the 50-ml tube with every droplet to mix and dilute the freezing medium of the cells.

Add the droplets every 6-8 seconds until the medium/freezing medium ratio reaches 10x. Then, add the droplets every 3-4 seconds until the medium/freezing medium ratio reaches 15-20x.

Swirling the tube gently is essential for higher yield of thawed hiPSC-CMs.

Using 1000 µl Biosphere® filtertips to thaw CMs is recommended (see materials). This will prevent hiPSC-CMs stress and adherence to the pipette tip walls and improve recovery.

8. Gently transfer cell/medium mix from the 50-ml tube to a 15-ml tube using a 5-ml pipette.
9. Centrifuge the 15-ml tube at 300x g for 3 mins.

After centrifugation, the pellet should be clear and compact at the bottom of the tube. If this is not the case, there might be a problem with centrifugation and a second round of centrifugation might be necessary.

10. Aspirate the supernatant.

Do not aspirate in close proximity to the pellet. There can be small amount (<20 µl) of medium left on the pellet.

11. Add 1 ml of B(P)EL or MBEL supplemented with RevitaCell (0.5x) on hiPSC-CM pellet and gently mix until there are no cell clumps visible.

Being gentle is essential in this step. Mix by pipetting up and down with a 1000 µl Biosphere® filtertips slowly until no cell clumps are visible.

12. Aspirate Matrigel from the coated plate and add the hiPSC-CMs in the coated 12-well in a circular move to distribute the cells.

Due to low recovery rate (30-40%) of hiPSC-CMs, it is recommended to thaw a vial of 3 million frozen hiPSC-CMs into one well of a 12-well plate. Recovery rate might vary between lines. With higher recovery rate (>60%), a vial can be thawed using a lower seeding density.

13. Place the plate in a 37 °C, 5% CO2 incubator for 24 hours. Refresh the medium after 24 hours with B(P)EL or MBEL medium. Then refresh the medium every 2-3 days.
14. Prepare Gelatin coated plates (see recipe) to thaw hiPSC-ECs.
15. Add 6 ml of pre-warmed EC-CGM in a 15-ml tube.
16. Thaw a vial of cryopreserved hiPSC-ECs in a water bath at 37 °C by moving the vials in a circular motion in the water until only a small piece of ice is left inside the tube.
17. Transfer hiPSC-ECs into a 15-ml tube with EC-CGM inside using a 1-ml pipette tip.
18. Wash the vial with 1 ml EC-CGM to collect all the cells and add this to the 15-ml tube.
19. Add 6 ml of pre-warmed FGM3 medium in a 15-ml tube.
20. Thaw a vial of cryopreserved hiPSC-CFs in a water bath at 37 °C by moving the vials in a circular motion in the water until only a small piece of ice is left inside the tube.
21. Transfer hiPSC-CFs to a 15-ml tube with a 1-ml pipette tip.
22. Wash the vial with 1 ml FGM3 to collect all the cells and add this to the 15-ml tube.
23. Centrifuge all tubes at 300x g for 3 mins.
24. Aspirate supernatants from each tube.
25. Add 1 ml of EC-CGM to hiPSC-ECs.
26. Mix gently by pipetting up and down with 1-ml pipette tip until no cell clumps are visible.
27. Aspirate 0.1% Gelatin from the coated 6-well plate.
28. Add hiPSC-ECs to these wells in 2 ml EC-CGM medium per well in desired ratio.

Seeding density highly depends on the proliferation and recovery rate of the cells and the culturing period. hiPSC-ECs are cryopreserved as 250-300K cells per vial. Seed in 1:4 ratio if hiPSC-ECs are used on day 3 of seeding and 1:6 if they are used on day 5 of seeding. With these ratios, at the end of the culture period, there should be between 250-300K hiPSC-ECs cells from 1 confluent (>90%) well of a 6-well plate.

29. Add 1 ml of FGM3 medium to hiPSC-CFs.
30. Add hiPSC-CFs to uncoated wells of a 6-well plate in 2 ml FGM3 medium per well in desired ratio.

Proliferation rate of hiPSC-CFs might change depending on the passage number. Cell seeding ratio should be adjusted accordingly.

31. hiPSC-ECs and hiPSC-CFs are incubated in a 37 °C, 5% CO_2 incubator. After 24-48 hours cells are refreshed with EC-CGM (ECs) or FGM3 (CFs). Then cells should be refreshed every 2-3 days.

In order to skip weekend refreshment, the medium can be topped up with 1 ml of extra medium on Friday.

MT formation

32. Pre-warm B(P)EL medium to room temperature.
33. Prepare V-bottom 96-well plates for MT seeding by labelling and adding 150 µl DPBS (-) in the outer wells of plates to prevent medium evaporation.
34. Aspirate the medium from the hiPSC-CMs and wash the well with 1 ml DPBS (-) before dissociation to remove dead cells.
35. Dissociate hiPSC-CMs with 0.5 ml TrypLE 5x per well for 10-12 mins at 37 °C, 5% CO_2.
36. Add 1.5 ml B(P)EL per well to a 15-ml tube.
37. After incubation with TrypLE 5x, dissociate hiPSC-CMs further by pipetting up and down with a 1000 µl Biosphere® filtertips until no clumps are visible.

After 10-12 mins incubation with TrypLE 5x, cells should be dissociated from the wells by pipetting up and down several times in TrypLE 5x until the mixture is completely uniform and no cell clumps are visible.

38. Add the hiPSC-CMs to the 15-ml tube with B(P)EL inside.
39. Wash the well with 1 ml of B(P)EL to collect all the cells.
40. Aspirate the medium from hiPSC-ECs and wash the well with 1 ml DPBS (-) before dissociation to remove dead cells.
41. Dissociate hiPSC-ECs with TrypLE 1x for 2-3 mins at RT.
42. Add 1 ml of B(P)EL to hiPSC-ECs to dilute the dissociation buffer.
43. Mix gently by pipetting up and down with a 1-ml pipette tip 3-4 times.
44. Add the cells to a 15-ml tube.
45. Aspirate the medium from hiPSC-CFs and wash the well with 1 ml DPBS (-) before dissociation to remove dead cells.
46. Dissociate hiPSC-CFs with TrypLE 1x for 3-5 mins (until the cells detach from the well and round up as single cells) at 37 °C, 5% CO_2.
47. Add 1 ml of B(P)EL to hiPSC-CFs to dilute the dissociation buffer.
48. Mix gently by pipetting up and down with a 1-ml pipette tip 3-4 times.
49. Add the cells to a 15-ml tube.
50. Take a 20 µl aliquot from each cell types to count using Fuchs-Rosenthal manual cell counter or any equivalent.

Aliquots can be diluted 1:2 or 1:3 either in B(P)EL or trypan blue to make counting easier.

51. Centrifuge 15-ml tubes with cells at 300x g for 3 mins.
52. Aspirate the supernatant from the tubes.
53. Add 1 ml B(P)EL in each tube and mix gently by pipetting up and down with 1000 µl Biosphere® filtertips until no clumps are visible in the tubes.
54. Prepare a mixture to form MTs containing 5000 cells in 50 µl of B(P)EL medium supplemented with 50 ng/ml VEGF and 5 ng/ml FGF for each well in a 96-well plate in the defined ratio of 70% hiPSC-CMS, 15% hiPSC-ECS and 15% hiPSC-CFS.

To ensure there is sufficient cell mixture for all wells of a 96-well plate, calculate medium and cell mixture for slightly higher number of wells. For example, there are 60 inner wells in a 96-well plate: make sufficient cell mixture for 66 wells i.e. 66x50 µl = 3300 µl of B(P)EL in total with cells for 1x 96-well plate. The outer wells are left empty.

55. Transfer the MT mixture in a 25-ml single use reservoir.
56. Seed 50 µl of MT mixture in the inner wells of a 96-well plate using a multichannel pipette.

During seeding of MTs, it is recommended to rock the reservoir with cells as this will ensure good mixing and cells will not sediment at the bottom of the reservoirs.

57. Centrifuge the plates at 300x g for 10 mins at RT.
58. Incubate MT plates at 37 °C, 5% CO_2 for 3 days without disturbing.
59. Refresh MT medium every 3-4 days with B(P)EL supplemented with 50 ng/ml VEGF and 5 ng/ml FGF until the chip experiments (step 82).

Microfluidic chips

Cell preparation for external network

60. Thaw hiPSC-ECs as described in step 14-18.
61. Add 6 ml of pre-warmed Pericyte medium in a 15-ml tube.
62. Thaw a vial of cryopreserved HBVPs in a water bath at 37 °C by moving the vials in a circular motion in the water until only a small piece of ice is left inside the tubes.
63. Transfer HBVPs to the 15-ml tube using a 1-ml pipette tip.
64. Wash the vial with 1 ml Pericyte medium to collect residual cells and add this to the 15-ml tube.
65. Centrifuge the 15-ml tube at 300x g for 3 mins.
66. Seed the cells in 1:4 ratio to use on day 3 and 1:6 to use on day 5.

In this protocol HBVPs were expanded until passage 3 and cryostored 1 M cells per vial.

67. Incubate the cells in a 37 °C, 5% CO_2 cell culture incubator for 48 h. Refresh with pericyte medium after 48 h and after that every 3-4 days.

Fibrinogen preparation

68. Prepare a 6 mg/ml fibrinogen/PBS solution in a 50-ml tube.
69. Incubate this solution for 3 h in a 37 °C water bath with a shaker.
70. After 3 h of incubation, filter the solution and collect it in a 15-ml tube. Place this tube on ice until use.
71. Prepare 10 µl aliquots of fibrin in 0.5 ml Eppendorf tubes on ice.

Chip seeding

72. Aspirate the medium from hiPSC-EC and HBVP and wash wells with DPBS (-) to remove dead cells.
73. Dissociate hiPSC-ECs and HBVPs with 1 ml of TryplE 1x for 2-3 mins until the cells detach from the wells and round up at RT.
74. Dilute the dissociation mix with EC-CGM and Pericyte medium for hiPSC-EC and HBVPs, respectively.
75. Transfer the cells to 15 ml tubes.
76. Wash the wells with respective medium to collect all the cells and transfer to 15-ml tube.
77. Take a 20 µl from each cell type to count.
78. Centrifuge the cells at 300x g for 3 min.
79. Aspirate the supernatant as much as possible without affecting the cell pellet.

It is important to remove the supernatant as much as possible for precise cell addition to the chips.

80. Prepare a 1.5 ml Eppendorf with EGM-2 medium supplemented with Thrombin (4U/ml).
81. Dilute hiPSC-EC and HBVP with EGM-2/Thrombin mix in separate 1.5 ml Eppendorf tubes.

In this protocol the cells are counted manually. Check for operator-to-operator variability. The cells are diluted as following: 25x10⁶ hiPSC-ECs per 1 ml and 5x10⁶ HBVPs per 1 ml (5:1 cell ratio).

82. Collect 30-40 MTs (for 1X idenTx 9 Plate) from the cultured plates (from step 59) using a 1-ml pipette tip from each well of a 96-well plate in a 15-ml tube.
83. Place the tube on a rack until MTs sediment.
84. When MTs are visible at the bottom of the tube, transfer MTs to a 1.5 ml Eppendorf tube using a 1-ml pipette tip.
85. When MTs are visible at the bottom of the Eppendorf tube, aspirate as much of the supernatant as possible.

86. Mix EGM2/thrombin mix with hiPSC-ECs and HBVP.

The amount of EGM-2/Thrombin to add to MTs should be decided according to the target number of channels to be loaded simultaneously. For example; each channel requires 10 µl of cell/MT mix. For 1 full plate with 9 channels, at least 90 µl of cell/MT mix is necessary. However, for precision it is recommended to add 20-30 µl extra cell/MT mix. 120 µl of cell/MT mixture is thus necessary for 1 full plate of chips. 1:1:2 (hiPSC-EC : HBVP : EGM-2/Thrombin) ratio should be followed to prepare this mixture. Following the example of 120 µl, 30 µl of hiPSC-EC, 30 µl of HBVP and 60 µl of EGM-2/Thrombin mix should be added on top of MTs, assuming all of the supernatant is removed from the MT vial.

87. Add EGM2/Thrombin and cell mix into the Eppendorf tube with MTs.
88. Mix the cell/MT/EGM-2/Thrombin mixture by pipetting up and down with a 20 µl pipette tip and take an aliquot with MTs.
89. Mix the cell/MT/EGM-2/Thrombin mix with fibrin in 1:1 ratio.

Example: Add 10 µl cell/MT/EGM-2/Thrombin mix to 10 µl fibrin aliquots.

90. Mix gently and fast by pipetting up and down with a 20 µl pipette tip not more than 3-4 times.

In order to increase the success of MT seeding in the gel channels, the cell/MT/fibrin mix should be added to one gel channel at a time. To semi-automate this process, a multi dispenser pipette can be used although it can be challenging to control the number of MTs; using this type of pipette is therefore not recommended.

91. Take 15-18 µl of this cell/MT/fibrin mix with a 20 µl pipette and seed via the gel inlet of the idenTx 9 plate chips (Fig 1).

Seeding of all channels should be performed in one continuous movement and the dispensing speed should be constant between channels to prevent channel-to-channel variability.

92. Incubate the chips for 15 mins at RT.
93. Prepare a chip medium (see recipe) during the incubation step 92
94. Slowly add 18 µl of chip medium to the inside of the left medium inlets (Fig 1).

See the medium inlets slowly filling. Medium should be visible from the right medium inlets.

95. Fill the left medium reservoir with 50 µl of chip medium and the right one with 100 µl to induce gravity-driven flow.
96. Incubate the chips in the 37 °C, 5% CO_2 cell culture incubator for 24 hours.
97. On day 1, refresh the medium with chip medium supplemented with DAPT (10 µM) for 24 hours.
98. Starting from day 2, refresh the medium with chip medium (without DAPT) daily until day 7.

In order to induce bi-directional continuous perfusion, chips can be incubated on a rocking platform using 8 degrees of inclination and 5 min intervals. Continuous perfusion by rocking can be induced as early as on day 0. However, since continuous perfusion accelerates vessel development, it is recommended to implement downstream assays on these chips earlier than day 7. Alternatively, chips can be placed on a rocker platform at a later stage (day 3 or 5) to further improve the vascularization process (See fig. 2 and 3).

Support Protocol 1
Functional Characterization of VMToC

Introductory paragraph

After generation of VMToCs, the structure and the integrity of vasculature can be assessed via a vessel perfusion assay with fluorescent beads to determine whether functional lumens have formed (Fig. 4A-B).

Figure 4

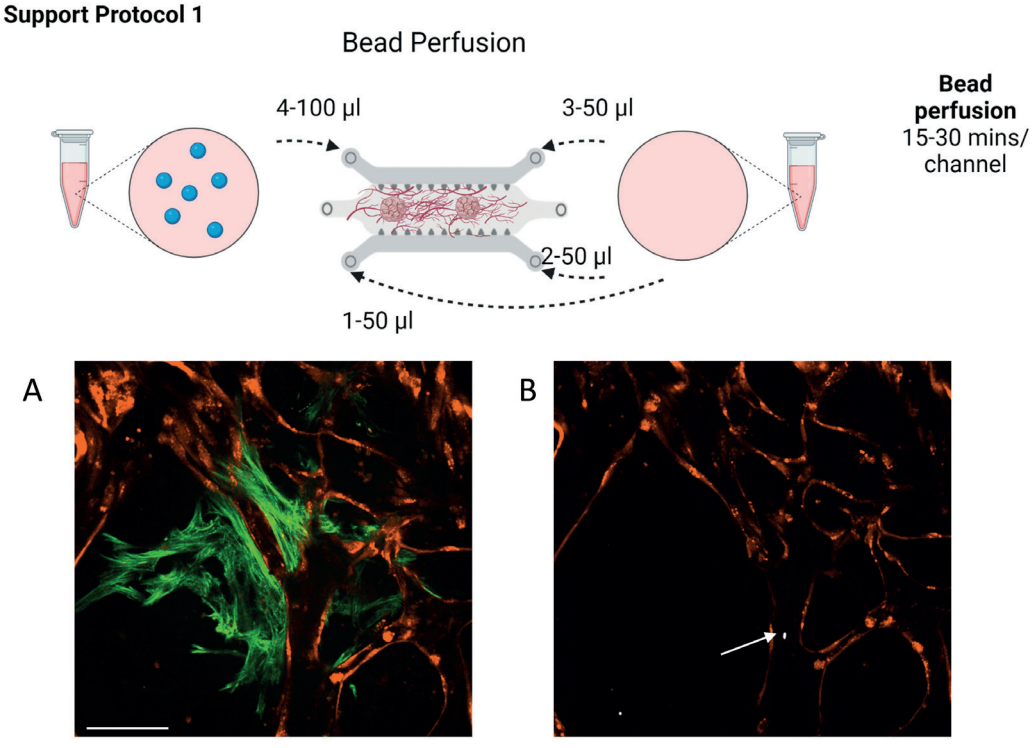

Figure 4: Schematic overview of the support protocol 1: Bead perfusion assay. *(A) Immunofluorescent imaging of VMToCs on day 5 (mCherry, orange; ACTN2, green) prior to the bead perfusion assay. (B) Immunofluorescent imaging of VMToCs with bead perfusion, arrow showing a bead moving in the microvasculature (mCherry, orange; 405 nm-beads, white). Scale bar: 100 µm*

In addition, VMToCs are contractile throughout the experiment. Therefore, it is important to follow their contractile dynamics live. In order to quantify the contractile parameters, VMToCs are recorded during spontaneous- or paced contractions. Pacing is performed using in-house electrodes that were designed to fit in the gel channels of the chips (Fig. 5). This protocol describes the pacing and recording videos for analysis with MuscleMotion software (Sala et al., 2018; van Meer et al., 2018) although other alternatives (Stebbeds et al., 2023; Huebsch et al., 2015a) can also be used.

Figure 5

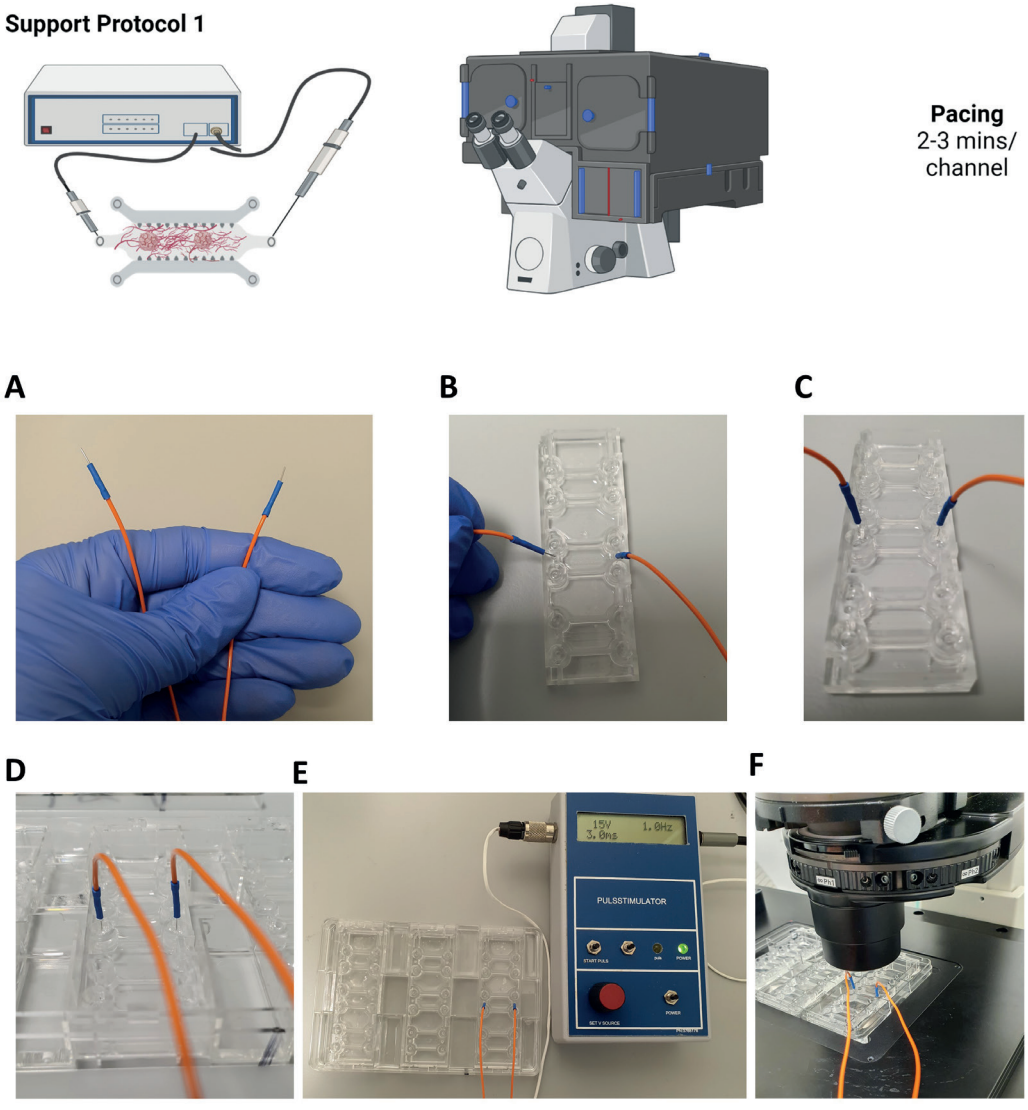

Figure 5: Schematic overview of the support protocol 1: Pacing. *(A) In-house electrodes that were used to pace VMToCs. (B) Picture of the electrodes and the chip showing integration of electrodes in the gel channel. (C) Side view of the chip with electrodes inside the gel inlet and outlet. (D) Bottom view of the plates with electrodes inside the gel inlet and outlet of a chip. (E) Pacing arrangement showing the settings for the experiment. (F) Picture of the plate with electrodes in the microscope stage.*

Materials:

- VMToC plates (Basic protocol 1)
- 405-beads (Fluoro-Max Dyed Blue Aqueous Fluorescent Particles, ThermoFisher Scientific, cat. No. B0200)
- EVOS M7000 imaging system (Thermo Fisher Scientific, cat.no. AMF7000)
- Andor Dragonfly 500 spinning disk confocal microscope
- Imaris 9.5 software (Bitplane, Oxford Instruments)
- Inverted microscope with a custom-built environmental chamber
- High-speed camera (DC3260C -High-Resolution Thorlabs)
- Custom-made pacing setup with platinum electrodes
- MUSCLEMOTION ImageJ macro (ImageJ v. 2.0.0-rc-49)

Protocol steps with step annotations

Bead perfusion assay

1. Prepare two 15-ml tubes with 10 ml chip medium (see recipe).
2. Add fluorescent bead droplets in one of the 15-ml tubes in a desired concentration (1 drop in 10 ml medium).

For bead tracking, low concentrations of beads are recommended. At low concentrations, such as 1 drop of beads mix for 10 ml chip medium, beads do not cluster together and enter the microvascular networks inside the MTs one- by-one. For higher concentrations, 1 drop of beads can be diluted in 5 ml of chip medium.

3. Prepare the appropriate microcopy station and insert the chip or the plate on imaging stage.

The use of an on-stage incubator with the microscope is recommended. MTs might slow down or stop beating when they are at room temperature for long periods. In this protocol, the Andor confocal spinning disk 500, 20x or 40x objectives are used to image dual wavelengths simultaneously. Alternatively, other confocal microscopes with similar features can be used.

4. Arrange the required field of view in which the lumen is visible with endothelial edges. This is where beads will move through.

It is recommended to take pictures of the desired field of views prior to running the bead perfusion assay (Fig. 4A).

5. A Add 50 µl of chip medium to 3 out of 4 medium reservoirs of the channel of interest.
6. Add 100 µl of chip medium with beads to the 4th medium reservoir of the channel.
7. Start recording of the video and save all the frames for analysis.

When using fluorescently tagged hiPSC-ECs in the channels, a microscope able to record 2 fluorescent channels simultaneously is recommended. If not available, it is recommended to overlay the recorded video of the fluorescent beads with the brightfield or fluorescent image taken prior to video recording in step 4.

Recording can take as long as a minute for beads to move inside the lumens. Extended recording might result in photobleaching of the fluorescently tagged cells. For video analysis, Imaris 9.5 software is used..

Pacing

8. Turn on the on-stage incubator of the inverted microscope to 37 °C, 5% CO2.
9. Place the chips inside the microscope stage when the temperature is stabilized.

With the change of temperature, contraction of MT might change. It is recommended to apply step 9 at least 30 mins before the start to allow MTs to adapt the stable temperature.

For optimal quality of the videos, they were recorded with high-speed camera capturing 100 frames per second, with 10x magnification and the field of view focused on the central MT part, avoiding the vessels or gel around. The same lighting settings were used for all the recordings to minimize the detection error in later video analysis..

10. Record movies of spontaneously beating MTs with 100 frames per second acquisition speed.

At this step there should be at least 2-3 contractions captured for optimal analysis. The duration of videos will depend on the cell line of origin.

11. Insert a pair of pacing electrodes into the inlet and outlet of the gel channel.
12. Perform the electric field stimulation of tissues with bipolar rectangular pulses of 3ms duration, 15V amplitude, using 0.8 or 1HZ frequency.

It might be necessary to optimize the voltage amplitude according to the gel channel size.

Pacing frequency should be determined according to the spontaneous contraction frequency. In order for tissues to follow the imposed rate, it is recommended to pace with at least 1-1.5x higher frequency than the spontaneous contraction frequency.

13. Record the videos.
14. Perform contraction analysis with the MUSCLEMOTION ImageJ macro as described previously (Sala et al., 2018)

Support Protocol 2
Structural Characterization of VMToC

Introductory paragraph

After the generation of VMToC, structure of the microtissues and vasculature can be characterized by various assays. This endpoint assay can be applied starting from day 4-5 depending on the vascular development in the chips. This protocol describes structural assessment of CMs and vascular networks by immunostaining (Fig. 6).

Figure 6

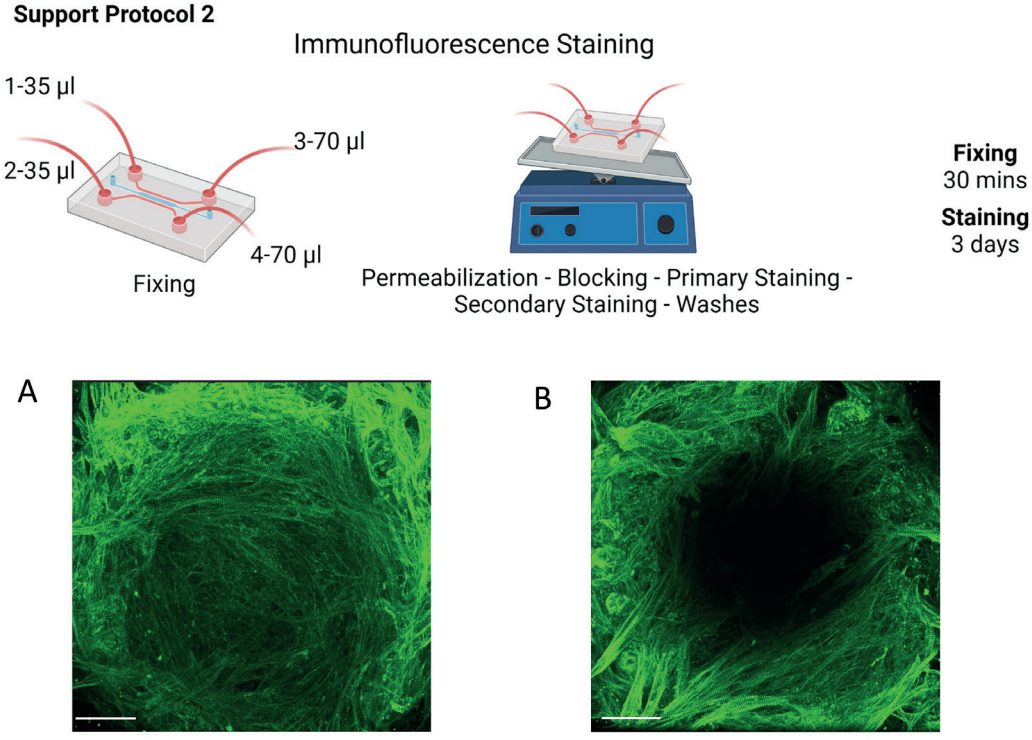

Figure 6: Schematic overview of the support protocol 2. *(A) Immunofluorescent imaging of VMToCs following the staining protocol showing proper staining of sarcomeres (ACTN2, green). (B) Immunofluorescent imaging of VMToCs following the shorter permeabilization protocol (2 h permeabilization/blocking; overnight staining with primary and secondary antibodies) showing improper staining of sarcomeres in the middle of the tissue (ACTN2, green). Scale bar: 50 µm*

Materials:

- VMToC plates (Basic protocol 1)
- Fixation solution (see recipe)
- Dulbecco's phospohate-buffered saline without Ca+2 and Mg+2 (DPBS, Gibco, cat. No. 14190-094)
- Penicillin/Streptomycin (Thermo Fisher Scientific, cat. no. 15070-063)
- Permeabilization/blocking solution (see recipe)
- Primary antibodies (see antibody table)
- Secondary antibodies (see antibody table)
- DAPI working solution (see recipe)
- EVOS M7000 imaging system (Thermo Fisher Scientific, cat. no. AMF7000)
- Andor Dragonfly 500 spinning disk confocal microscope

Protocol steps with step annotations

Fixation

1. Aspirate the medium from the inlets and outlets of the chips.
2. Fix the chips with fixation solution by adding 35 µl to the left medium inlets and 70 µl to the right medium outlets.
3. Incubate for 30 min at RT.
4. Aspirate the fixation solution.
5. Wash the chips by adding 35 µl of DPBS (-) to the left medium inlets and 70 µl to the right medium outlets.
6. Incubate for 10 min at RT.
7. Aspirate the DPBS (-).
8. Repeat steps 5-7 two more times for a total of three washes.

At this stage, the chips can be stored at 4 °C until further use. To store, add 50 µl of DPBS (-) to the left medium inlets and 100 µl in the right medium outlets.

In case the chips will be stored for a longer period, it is recommended to add penicillin streptomycin or any equivalent to the final DPBS solution to prevent contamination.

Immunostaining Protocol

9. Permeabilize and block the chips with one of the permeabilization/blocking solutions (see recipe) using the same volumes as in step 2 for 6 h at RT.
10. Dilute the primary antibodies (see antibody table) in the same permeabilization/blocking solution.
11. Add primary antibodies in the medium inlets and outlets using the same volumes as in step 2 and incubate overnight at RT.
12. Wash 3x with the same permeabilization/blocking solution following steps 5-7.

13. Prepare the secondary antibodies (see antibody table) in the same permeabilization/blocking solution.
14. Add secondary antibodies in the medium inlets and outlets using the same volumes as in step 2 and incubate overnight at RT.
15. Wash 3x with DPBS (-) following steps 5-7.
16. Prepare DAPI staining solution by diluting DAPI working solution (see recipe) in DPBS (-) (1:1000).
17. Add DAPI solution in chips following the same volume as step 2.
18. Incubate for 2 h at RT.
19. Wash 3x with PBS following steps 5-7.

It is recommended to perform the incubation steps in 9-19 on a rocker platform.

Depending on the tissue size, it might be necessary to optimize permeabilization/blocking concentration and duration with permabilization/blocking solutions for immunostaining (see recipe for alternatives). Bigger tissues might require higher concentration and/or longer incubation (see recipe for alternative 1).

20. Prepare microscopy stage with preferred filter and objective.
21. Perform imaging with EVOS M7000, Andor Dragonfly 500 spinning disk confocal microscope or other confocal microscopes.

Reagents and solutions

5X TrypLE Select solution

- Prepare a 1 mM EDTA by diluting 0.5M EDTA in DPBS (1:500). Dilute TrypLE Select 10X solution in 1:2 with 1 mM EDTA solution to prepare 5X diluted TrypLE Select solution. Store at room temperature up to 6 months.

α-Monothioglycerol (αMTG) solution, 1.3% (v/v)

- Prepare 9.87 ml Iscove's modified Dulbecco's medium (IMDM) (no phenol red) (Thermo Fisher Scientific, cat. no. 21056) and add 130 µl mono-thio glycerol (α-MTG; Sigma-Aldrich, cat. no. M6145-25 ml) in. Store up to 1 year at 4°C. Aliquots should be protected from light.

Antibodies

Antibodies	Concentration	Species	Brand	Cat no
ACTININ-2 (ACTN2)	1:800	Mouse	Sigma Aldrich	A-7732
Donkey anti mouse (488)	1:200		R&D Systems	A-21202

Basic fibroblast growth factor (FGF2) stock solution, 10 µg ml^{-1}

- Dilute FGF2 as 100 µg/ml in distilled water (dH2O; GibcoTM; Thermo Fisher Scientific, cat. no. 15230089). Dilute further as 10 µg/ml in 0.1% (w/v) Bovine Serum Albumin (BSA) in DPBS (see recipe). Prepare aliquots. Aliquots can be stored up to 1 year at –80°C. Repeated freeze-thaw cycles should be avoided.

DAPI working solution

- Reconstitute 10mg DAPI Nucleic Acid Stain, dilactate (Thermo Fisher Scientific, cat. no. D3571) in 2ml dH20. Prepare 40µl aliquots and store at -20°C. To prepare a 300µM working solution, add 1,4ml dH20 to the 40µl aliquot. Working solution can be stored at +4°C.

Permabilization/Blocking solutions for immunostaining

- Prepare permeabilization/blocking mix in 50 ml DBPS (-) following one of the recipes below. Mix the solution for a few hours by placing the tube on a roller bank at 4°C until the BSA is dissolved completely. Filter the solution using 0.22- µm-pore-size membrane filter. Store up to 4 weeks at 4°C.

Alternative 1

Composition	Volume	Concentration
Triton-X	250 µl	0.5%
Tween-20	250 µl	0.5%
BSA	0.5 g	1%
Fetal Bovine Serum (FBS)	1.5 ml	3%
Sodium deoxycholate mix	500 µl	0.01%

- Triton-x (Sigma-Aldrich, cat. No. T8787-100ml), tween-20 (Merck, cat. No. 8.22184.0500), FBS ultralow endotoxin (Biowest, cat. No. S1860-500), sodium deoxycholate (Sigma-Aldrich, cat. no. D6750-1006)

Alternative 2

Composition	Volume	Concentration
Triton-X	250 µl	0.5%
BSA	1g	2%

B(P)EL and MBEL

- Prepare B(P)EL or MBEL following the recipe below. Volumes are calculated for total 250 mL medium. Sterilize using a Stericup filter. Medium can be stored up to 3 weeks at 4°C.

Composition	B(P)EL Volume	Final concentration	MBEL Volume	Final concentration
IMDM	107.63 ml		118.125	
F12 nut. mix	113.88 ml		118.125	
PFHM-II	12.5 ml	5%		
10% (w/v) (see recipe) BSA/IMDM	6.25 ml	0.25%	6.25	0.25%
Lipids (100×)	2.5 ml	1×	2.5 ml	1×
ITS-X (100×)	250 µl	0.1×	250	0.1×
αMTG (1.3%; see recipe)	750 µl	450 µM	750	450 µM
AA2P (5 mg/ml; see recipe)	2.5 ml	0.05 m/ml	2.5 ml	0.05 m/ml
GlutaMAX (200 mM)	2.5 ml	2mM	2.5 ml	2 mM
Pen/Strep (5000 U/ml)	1.25 ml	0.5%	1.25 ml	0.5%
Trace elements B			25 µl	
Trace elements C			250 µl	

- IMDM, Iscove's modified Dulbecco's medium, no phenol red (Gibco™; Thermo Fisher Scientific, cat. no. 21056023); F12 nut. mix, Ham's F-12 nutrient mix, GlutaMAX supplement (Gibco™; Thermo Fisher Scientific, cat. no. 31765027); PFHM-II, Protein-Free Hybridoma Medium, 1× (Gibco™; Thermo Fisher Scientific, cat. no. 12040077); Lipids, chemically defined lipid concentrate(Gibco™; Thermo Fisher Scientific, cat. no. 11905031); ITS-X, insulin-transferrin-selenium-ethanolamine (100×; Gibco™, Thermo Fisher Scientific, cat. no. 51500056); GlutaMAX, GlutaMAX-1 supplement (Gibco™;

Thermo Fisher Scientific, cat. no. 35050038); Pen/Strep, Penicillin-Streptomycin (5000 U/ml; Gibco™; Thermo Fisher Scientific, cat. no. 15070063), trace Elements B 1000x solution (Thermo Fisher Scientific, cat. no. 25-022-CI), trace Elements C 1000x solution (Thermo Fisher Scientific, cat. no. 25-023-CI).

BSA, 10% (w/v) in IMDM

- Weigh 5 g of BSA (BovoStar) in a 50-ml tube and add 40 ml of IMDM on top. Mix the solution for a few hours by placing the tube on a roller bank at 4°C until the BSA is dissolved completely. Top up with 10 ml IMDM to reach final concentration of 10% (w/v) BSA. Filter using a 0.22-µm-pore-size membrane filter. Store for up to 4 weeks at 4°C.

Chip medium

- Prepare the chip medium by mixing EGM-2 with B(P)EL in 1:1 ratio. Supplement with 50 ng/mL VEGF.

EGM-2

- Add all supplements from the kit to the basal medium to prepare a 500-ml of EGM-2 following manufacturer's instructions. Add 2.5 ml Penicillin-Streptomycin (5000 U/ml; GibcoTM; Thermo Fisher Scientific, cat. no. 15070063). Store up to 6 weeks at 4°C.

Endothelial Cell Complete Growth Medium (EC-CGM)

- Prepare EC-CGM following the recipe below. Sterilize using a Stericup filter. Medium can be stored up to 2 weeks at 4°C.

Composition	Volume	Final concentration
EC-SFM	247.5 ml	
hPPS	2.5 ml	1%
VEGF, 50 µg/ml	150 µl	30 ng/ml
bFGF, 100 µg/ml	50 µl	20 ng/ml

- EC-SFM, Invitrogen, cat. no. 11111-044); hPPS, human serum from platelet-poor plasma (hPPS; Sigma-Aldrich, cat. no. P2918); VEGF, human VEGF (165) IS, premium grade (Miltenyi Biotec, cat. no. 130-109-386); bFGF, human bFGF, premium grade (Miltenyi Biotec, cat. no. 130-093-842).

Fixation solution

- Dilute 8% (wt/vol) PFA in 0.2 M phosphate buffer, pH 7.4 in order to prepare 4% (vol/vol) PFA solution. Store the solution up to 1 month at 4 °C.

Gelatin-coated 6-well plate

- Coat a or flask with 0.1% (w/v) gelatin solution 1ml/well of a 6x-well plate. Ensure that the whole surface is covered with gelatin. Incubate the plate with gelatin for 1 hr at 37°C before use. The coated plates can be stored up to 2 weeks at 4°C.

Gelatin solution, 0.1% (w/v)

- Weigh 1 g gelatin (from porcine skin, type A; Sigma-Aldrich, cat. no. G1890) and add 100 ml of dH2O on top to prepare a 1% (w/v) gelatin solution. Autoclave the solution. Aliquot in 10 mL and store this stock solution up to 1 year at –20°C.

- For 0.1% (w/v) gelatin solution, dilute stock solution in 1:10 with Dulbecco's phosphate-buffered saline (DPBS; Life Technologies, cat. no. 14190). Sterilize the solution using a 0.22-µm-pore-size membrane filter. Store up to 1 year at room temperature.

Matrigel-coated plates

- Keep Matrigel (Growth Factor Reduced; Corning, cat. no. 354230) aliquot on ice. Dilute Matrigel in cold DMEM/F12 (Gibco™; Thermo Fisher Scientific, cat. no. 31331028) in 1:120. Coat 12-well cell culture plates (Greiner Bio-one, cat. no. 665180) 1 mL/10cm². Incubate coated plates for at least 1 h at RT before use (Follow basic protocol step 12). Alternatively, coated plates can be stored at 4 °C up to 2 weeks for later use.

L-Ascorbic acid 2-phosphate (AA2P), 5 mg ml^{-1}

- Prepare AA2P by diluting 250 mg AA2P (Sigma-Aldrich, cat. no. A8960) in 50 ml dH2O. Prepare aliquots. Aliqouts can be stored up to 1 year at –20°C.

PFA, 8% (w/v)

- Weigh 40 g paraformaldehyde (PFA; Merck, cat. no. 1.04005.1000) and add 400 ml Milli-Q water on top. Heat this solution to 60°C and stir at medium speed. To dissolve the PFA, add ~10 drops of 1 N NaOH after few minutes of stirring until the solution is clear. Let the solution cool down. Add Milli-Q water until a total volume of 500 ml is reached. Store the solution up to 2 months at 4°C.

Phosphate buffer, 0.2 M (pH 7.4)

- For solution 1, weigh 8.28 g sodium dihydrogen phosphate dihydrate (NaH2PO4·2H2O; J.T. Baker, cat. no. 0326) and add 300 ml Milli-Q ultrapurified water (e.g., from a Millipore system) on top. For solution 2, weigh 10.78 g disodium hydrogen phosphate monohydrate (NaH2PO4·1H2O; Merck, cat. no. 1.06346.1000) and add 300 ml Milli-Q water on top. For 0.2 M phosphate buffer (pH 7.4), add solution 1 to solution 2 until a pH of 7.4 is reached. Store at room temperature indefinitely (no expiration date).

Sodium deoxycholate mix

- Reconstitute 0.5 g (1%) sodium deoxycholate (Sigma-Aldrich, cat. no. D6750-1006) in 50 ml DBPS. Mix well and store at RT up to 1 month.

VEGF stock solution

- Dilute VEGF as 100 µg/mL in distilled water. Dilute further as 50 µg/mL in 0.1% BSA in DPBS (Life Technologies, cat. no. 14190). Prepare 50-µL and 100- µL aliquots of VEGF. Aliquots can be stored at −80 °C.

Commentary

Background Information

Animal models such as rodents offer insights into heart development and disease. However, since there are physiological and genetic differences between rodent and human hearts, there is growing interest in using hPSC-based cardiac models (Mills and Hudson, 2019).

Many differentiation protocols described by us and others can be used to generate different types of hPSC-CMs (Zhang et al., 2012; Burridge et al., 2014; Campostrini et al., 2021; Wiesinger et al., 2022). These have proven valuable to model heart disorders like channelopathies (Giacomelli et al., 2017; Brandao et al., 2017). However, for modelling more complex disorders where more than one cell type might cause a disease state, studying hPSC-CMs alone may not be sufficient. In addition, hPSC-CMs under standard conditions are immature and whilst this is sufficient to study ion channel diseases, other conditions like cardiac myopathies, may need CMs in a more mature state. Moreover, cardiac disease may be exacerbated by inflammation or the presence of immune cells. More complex platforms with increased physiological relevance are therefore of interest.

3D cardiac MT/organoid/cardioid and engineered heart tissue models are based on the combination of self-assembly of cells, biomaterials and/or tissue engineering. Such models can (1) integrate multiple cell types and extracellular matrix components; (2) recapitulate cell-cell crosstalk between CMs and cardiac stromal (CF)- and vascular cells (EC); (3)

provide control over biomechanical and biochemical cues; and (4) consequently improve hPSC-CM maturation, at least to a postnatal state (Schmidt et al., 2023; Hofbauer et al., 2021; Mills et al., 2018; Beauchamp et al., 2020; Giacomelli et al., 2020; Richards et al., 2020; Goldfracht et al., 2020; Voges et al., 2023). However, one of the remaining hurdles has been to incorporate functional vessel-like structures which could improve oxygen, nutrient and drug transport and allow the introduction of inflammatory cells.

Organ-on-chip models are developing as one way to overcome this hurdle. MT/organoids can be cultured inside 3D microfluidic devices that enable functional vessel formation and perfusion following a similar strategy to transplantation studies where the MT/organoids are introduced into laboratory animals. In *in vitro* models, both the MTs/organoids and the vasculature can be of human origin eliminating the need for a living host (King et al., 2022; Arslan et al., 2023; Bonanini et al., 2022). In addition, human vasculature would support nutrient and drug delivery through the endothelial barrier, creating closer mimicry to the human heart.

Here, using organ-on-chip technology, we describe a protocol for an *in vitro* model of vascularized cardiac MTs all derived from hiPSCs. Cardiac MTs are first generated using a previously published protocol (Campostrini et al., 2021) with minor modifications. Specifically, to generate vascularized cardiac MTs we used hiPSC-ECs as described earlier (Orlova et al., 2014). However, depending on the application using cardiac-specific ECs might be an alternative (Campostrini et al., 2021). Cardiac-specific ECs have typical EC characteristics but express some cardiac transcription factors (Giacomelli et al 2020). We co-culture cardiac MTs here with hiPSC-ECs and HBVP in a fibrin hydrogel in the gel channel of a commercially available AIM Biotech chips as described in Basic Protocol 1. hiPSC-ECs and HBVPs self-organize into an external vascular bed around the MTs. Much as in the case of transplantation, branches of this vascular bed start anastomosis with the pre-existing internal microvasculature in the MTs. During the first 5 days of the culture, vascular development is evident. Around day 5, a continuous vascular network in- and around the MTs is formed and stabilized. Immunofluorescent imaging assays demonstrated that these vascular networks are lumenized.

In order to show whether these networks are also perfusable, beads are added in the medium channel. Beads spontaneously enter the external vascular networks from the medium-gel channel interface and end up inside the microvascular networks in the MTs. Spontaneous movement of the beads can be recorded as described in Support Protocol 1. With this, it is possible to estimate the fluid flow patterns such as speed and shear stress in the chips (Vila Cuenca et al., 2021). Alternatively, lumenized vessels can be perfused with beads as a surrogate for immune or other blood cells.

VMToCs are contractile throughout the whole experiment. Contractile parameters can be quantified either during spontaneous contraction or upon pacing. Pacing is preferred to eliminate the variability in the beat rates of different conditions and standardize it for comparison of other contraction parameters. In support protocol 1, custom-made platinum

electrodes are inserted in the gel channel inlets and outlets to stimulate VMToCs with bipolar rectangular pulses. Alternatively, commercial electrodes that fit in the gel inlet and outlet can be used. Contraction videos are recorded using a high-speed camera. These videos can be analyzed using open access software such as MuscleMotion (Sala et al., 2018) or other video based analysis tools (Huebsch et al., 2015b; Stebbeds et al., 2023) .

For further structural characterization of VMToCs, the chips are fixed and stained as described in Support Protocol 2. Staining protocol was optimized according to the tissue size, density and the specific antibody. Different permeabilization/blocking solutions were tested and the successful two alternatives were listed. However, for other tissue types, sizes and antibodies, the protocol might require further optimization. To allow easy live imaging and eliminate the staining hurdles, using fluorescently tagged hiPSC-derived cell types in tissues is highly recommended.

With this protocol, (1) we integrate 3D cardiac MTs that were well characterized structurally and functionally in terms of cell-cell crosstalk (Giacomelli et al., 2020); (2) these 3D cardiac MTs are partially mature before integration in chips; (3) the model is fully hiPSC-derived except for mural cell component in the external vascular network (HBVP) which could be replaced by hiPSC-derived smooth muscle cells (Vila Cuenca et al., 2021); (4) The number of cells required for MT formation is as low as 5000 cells, significantly reducing the number of hiPSC-derived cardiac cells required per experiment compared to other cardiac *in vitro* models. In addition, there are currently no animal- or *in vitro* models that can capture vascular defects such as endothelial dysfunction and coronary microvascular obstruction (Niccoli et al., 2016; Sorop et al., 2020). VMToCs can be useful to explore underlying mechanisms related to these defects by using patient-derived hiPSC lines.

We previously showed that vessel-on-chip without cardiac MTs can be cultured long-term (21 days) within a similar system (Vila Cuenca et al., 2021). However, VMToCs in this protocol are cultured until day 7. For longer culture, further optimization of culture conditions, such as inclusion of matrix metalloproteinase inhibitors, might be required. Another limitation is that the model is solely depend on self-organization. Therefore, it should be noted that certain levels of variability may be evident, such as the extent of vascularization. In addition, VMToCs are generated using 9x channel plates. For higher-throughput experiments, 40x channels or other high-throughput organ-on-chip platforms can be used. However, in that case, the seeding protocol should be optimized preferably for automated seeding or other more user-friendly methods.

In summary, this protocol can be used to generate vascularized and perfusable cardiac MTs efficiently in three-channel microfluidic chips and characterized within days. The model can be useful to study cell-cell crosstalk especially with the endothelial barrier, to model vascular defects and test drugs.

Critical Parameters

CMs used in this protocol reaches >85% purity. It is important to use high purity of CMs particularly when functional characterization is planned. In order to increase the purity upon thawing should it be below 80%, a short period of lactate treatment can be done (Campostrini et al., 2021). Depending on the line, the timing of thawing CMs until generation of MTs should be optimized to ensure recovery of thawed CMs.

In our protocol, MTs are integrated in the chips on day 12 after generation (Fig. 1D). This is critical as microvascular networks start self-organizing around day 8-10 in these MTs and longer culture without perfusion might lead to their regression. In order to ensure anastomosis between the external vascular network and internal microvasculature, it is important to make sure that the internal vascular structures are lumenized in the MTs at the time of integration in chips.

The number of additional vascular cells to integrate in chips with MTs is optimized according to the time necessary to form a proper vascular network around the MTs. This duration should be as short as possible to ensure the anastomosis and perfusion of MTs occur early. Higher vascular density is therefore preferred. However, the counting of cells is manual and could vary between operators. It is also noted that ECs from different hiPSC lines might have different proliferative capacities. Therefore, the number of vascular cells in chips should be optimized further for each operator and cell line.

The number of MTs inside the gel channels is critical. We observed that when multiple (more than 2) MTs are in close proximity in the gel channel, this affects the external vascular network between them and thus the vascularization of MTs (Fig. 3B). Therefore, it is recommended to have only 4-5 MTs per channel of this specific chip.

During the seeding of MT/cells/hydrogel, manual seeding is highly recommended to ensure control over the number of MTs inside the gel channels.

Seeding in chips should be performed as quickly as possible for a proper gelation of fibrin hydrogel. The plate should be kept horizontal during this process.

After seeding, to ensure proper gelation, it is critical to not move the plate for 15 mins. After this period, medium channels should be filled with medium either manually or in an automated way. In this process, we observed that bubbles can form in the medium channels. Bubbles can be removed by slow aspiration of the medium.

Notably, integration and vascularization of MTs here are robust and reproducible between lines. However, we observed that vascularization might be affected by the pre-vascularization of MTs. Even in the same multi-well plate, pre-vascularization levels of MTs might differ. This can lead to variability in vascularization levels in the chips.

In the bead perfusion assay, the beads spontaneously enter the vascular networks. If the bead concentration is too low (1 drop in 10 ml), they might not penetrate the vascular networks inside the MTs. This can be avoided by increasing the bead concentration (1 drop in 5 ml or less).

The staining protocol here is optimized according to the size and the thickness of MTs. We observed that using the same staining protocol of 3D cardiac MTs or VoC models failed to stain the middle of the MTs in VMToC (Fig. 6B). Therefore, we optimized this protocol following a staining protocol designed for denser and larger organoids like blood vessel organoids (Wimmer et al., 2019). We provided two alternative permeabilization/blocking solution and observed that alternative 1 is a stronger solution which might result in better staining with less gradient. It is recommended that this step is optimized according to the tissue size and thickness. Of note, the optimization of this protocol has been done using one antibody for CMs. Further optimization might be necessary for other antibodies. Alternatively, using fluorescently tagged hiPSC lines to derive cell types in tissues is recommended for easier imaging.

Troubleshooting

Table 1: Troubleshooting Guide for VMToC generation and characterization

Problem	Possible Cause(s)	Possible Solution(s)
MTs are not contracting in the gel channel	The seeding protocol takes too long, and the temperature changes might affect the contractility of MTs. CM yield is too low.	After providing medium in the medium channels, place the plate in the incubator for an hour. After this, MTs should start contracting. If the MTs do not start contracting after a day, discard the plate and start a new experiment. Use high purity of CMs.
Bubbles in the gel or medium channel	Rigorous mixing of the MT/cell/gel mix. Pipetting pre-existing bubbles from the Eppendorf tube.	Do not mix the MT/cell/gel mix more than 3-4 times. Do not pipette pre- existing bubbles from the tube.

Problem	Possible Cause(s)	Possible Solution(s)
MTs do not load in the gel channel	Not applying enough pressure. Too many MTs in the pipette tip. Gel channel inlet is blocked by the MTs.	Apply more pressure during the seeding of MTs. Decrease the MT number to seed per channel. Do not integrate MTs that are merged or bigger in size than the gel channel. Pipette the MT/cell/gel mix back and use the gel channel for the next round of mix.
Gel leaking to the medium channel	Applying more pressure during seeding than necessary. Improper bonding of the chips.	Keep the pressure applied during seeding stable. If this occurs in more than one channel, discard those chips.
Gel polymerization takes longer than expected	High concentration of Heparin in the cell culture growth medium	Reduce Heparin concentration in the cell culture growth medium used to prepare Thrombin and Fibrinogen solutions (Hajal et al., 2022)
Low or high vascular density in the gel channel	Difference in the final cell density caused by manual counting.	Optimize the final cell density according to the handler manual counting.
Vascular cells are not homogenously distributed	Tilting the plate during seeding. Improper mixing of the MT/cell/gel mix.	Keep the plate with chips in horizontal position during seeding. Pipette up and down gently 3-4 times before seeding in the gel channel.
Low efficiency in vascularization of MTs	The number of MTs per channel is high. The density of vascular cells is low. MTs in one channel are too close to each other.	Limit the number of MTs/channel to 4-5. Optimize the vascular cell density.

Problem	Possible Cause(s)	Possible Solution(s)
Vascular networks are not developing	The growth factors are not provided in the medium. Insuffiecient gelation of fibrin hydrogel.	Ensure 50 ng/ml VEGF is provided for the whole duration of the protocol and 10 ng/ml DAPT only on day 1. Incubate the gel for about 15 mins at room temperature after seeding. If the vascular networks are not developing 2 days after seeding, either use the rocker platform to improve vascularization or discard the plate.
Variability in contraction parameters	Recording of the moving debris around the MTs. Batch-to-batch and line- to-line variability.	Ensure that only MTs are recorded and limit recording of the surrounding areas.
Staining does not work	Too short permeabilization. Too short primary and secondary antibody incubation.	Ensure that the staining protocol here is followed. Alternative 1 as a permeabilization/blockin g solution is stronger. If MTs are larger, optimize the steps. Use fluorescently tagged lines in tissues.

Understanding Results

With regard to the seeding of MT/cell/gel mix, if the protocol is properly followed, each gel channel should have homogenously distributed vascular cells. There should be at least 1 MT in each channel. Vascular cells around the MTs will start self-organizing as early as day 1. On day 1, the internal microvascular networks will be prominent and start anastomosis with the external vascular network. Over the following days, the external vascular network will develop further and the anastomosis will become more evident. Around day 5, there will be continuous vascular network in- and around the MTs.

Chips can be used for structural and functional characterization assays as early as day 3-4 when the external vascular networks are fully developed. At this stage it is recommended to perform the bead perfusion assay if required.

In addition, MTs will be contractile throughout the whole period of the experiment. EC-CM crosstalk will modulate the contraction parameters of VMToCs, for example with increases in contraction duration and peak-to-peak times (Arslan et al., 2023). VMToCs can be used for pacing and drug testing as early as day 3-4.

Time Considerations

Basic Protocol 1

- Cell preparation takes 5-7 days in total depending on the CM recovery.
- Thawing of CMs - 30 mins.
- Thawing of ECs and CFs - 15 mins.
- MT formation - 1.5-2 hours.
- MT maintenance - 13 days in total including day 0.
- Cell preparation before chips - 6 days including the day 0.
- Fibrinogen preparation – 3-3.5 hours.
- Chip seeding in total - 2-3 hours depending on the plate numbers to seed.
- Chip maintenance - 5-7 days.

Support protocol 1

- Bead perfusion – 15 mins/MT
- Pacing – 1-1.5 hours depending on the number of MTs to be paced.

Support protocol 2

- Fixing and staining – 3 days

Conflict Of Interest Statement

The authors declare no competing interests.

Data Availability Statement

The data supporting the findings of this study are available on request from the corresponding author.

Acknowledgements

(mandatory for NIH, optional for all others)

We thank LUMC confocal imaging facility for their help during image acquiring and the Allen Cell Collection, (from Coriell Institute for Medical Research), for providing hiPSC lines. Images were generated using Biorender.com.

This work was supported by the European Union's Horizon 2020 research and innovation programme under grant agreement No. 812954; the Netherlands Organ-on-Chip Initiative which is an NWO Gravitation project (024.003.001) funded by the Ministry of Education, Culture and Science of the government of the Netherlands; the LymphChip project with project number NWA-ORC 2019 1292.19.019 of the NWA research program 'Research on Routes by Consortia (ORC)', which is funded by the Netherlands Organization for Scientific Research (NWO); The Novo Nordisk Foundation Center for Stem Cell Medicine is supported by Novo Nordisk Foundation grants (NNF21CC0073729).

Literature Cited

Arslan, U., Brescia, M., Meraviglia, V., Nahon, D. M., van Helden, R. W. J., Stein, J. M., van den Hil, F. E., van Meer, B. J., Vila Cuenca, M., Mummery, C. L., et al. 2023. *Vascularized hiPSC-derived 3D cardiac microtissue on chip.* Stem Cell Reports 18:1394–1404.

Beauchamp, P., Jackson, C. B., Ozhathil, L. C., Agarkova, I., Galindo, C. L., Sawyer, D. B., Suter, T. M., and Zuppinger, C. 2020. *3D Co-culture of hiPSC-Derived Cardiomyocytes With Cardiac Fibroblasts Improves Tissue-Like Features of Cardiac Spheroids.* Frontiers in Molecular Biosciences 7:14.

Berry, C., and Duncker, D. J. 2020. *Coronary microvascular disease: The next frontier for Cardiovascular Research.* Cardiovascular Research 116(4):737-740.

Bonanini, F., Kurek, D., Previdi, S., Nicolas, A., Hendriks, D., de Ruiter, S., Meyer, M., Clapés Cabrer, M., Dinkelberg, R., García, S. B., et al. 2022. *In vitro grafting of hepatic spheroids and organoids on a microfluidic vascular bed.* Angiogenesis 25(4):455-470.

Brady, E. L., Prado, O., Johansson, F., Mitchell, S. N., Martinson, A. M., Karbassi, E., Reinecke, H., Murry, C. E., Davis, J., and Stevens, K. R. 2023. *Engineered tissue vascularization and engraftment depends on host model.* Scientific Reports 13, 1973.

Brandao, K. O., Tabel, V. A., Atsma, D. E., Mummery, C. L., and Davis, R. P. 2017. *Human pluripotent stem cell models of cardiac disease: From mechanisms to therapies.* DMM Disease Models and Mechanisms 10(9):1039-1059.

Brutsaert, D. L. 2003. *Cardiac endothelial-myocardial signaling: Its role in cardiac growth, contractile performance, and rhythmicity*. Physiological Reviews 83(1):59-115.

Burridge, P. W., Matsa, E., Shukla, P., Lin, Z. C., Churko, J. M., Ebert, A. D., Lan, F., Diecke, S., Huber, B., Mordwinkin, N. M., et al. 2014. *Chemically defined generation of human cardiomyocytes- supplementary information.* Nature Methods 11(8):855-60.

Cakir, B., Xiang, Y., Tanaka, Y., Kural, M. H., Parent, M., Kang, Y. J., Chapeton, K., Patterson, B., Yuan, Y., He, C. S., et al. 2019. *Engineering of human brain organoids with a functional vascular-like system.* Nature Methods 16(11):1169-1175.

Campostrini, G., Meraviglia, V., Giacomelli, E., van Helden, R. W. J., Yiangou, L., Davis, R. P., Bellin, M., Orlova, V. V., and Mummery, C. L. 2021. *Generation, functional analysis and applications of isogenic three-dimensional self-aggregating cardiac microtissues from human pluripotent stem cells.* Nature Protocols 16(4):2213-2256.

Di Cio, S., Marhuenda, E., Haddrick, M., and Gautrot, J. E. 2024. *Vascularised cardiac spheroids-on-a-chip for testing the toxicity of therapeutics*. Scientific Reports 14: 3370.

Giacomelli, E., Meraviglia, V., Campostrini, G., Cochrane, A., Cao, X., van Helden, R. W. J., Krotenberg Garcia, A., Mircea, M., Kostidis, S., Davis, R. P., et al. 2020. *Human-iPSC-Derived Cardiac Stromal Cells Enhance Maturation in 3D Cardiac Microtissues and Reveal Non-cardiomyocyte Contributions to Heart Disease.* Cell Stem Cell 26:862-879.e11.

Giacomelli, E., Mummery, C. L., and Bellin, M. 2017. *Human heart disease: lessons from human pluripotent stem cell-derived cardiomyocytes.* Cellular and Molecular Life Sciences 74:3711– 3739.

Goldfracht, I., Protze, S., Shiti, A., Setter, N., Gruber, A., Shaheen, N., Nartiss, Y., Keller, G., and Gepstein, L. 2020. *Generating ring-shaped engineered heart tissues from ventricular and atrial human pluripotent stem cell-derived cardiomyocytes.* Nature Communications 11:75.

Hajal, C., Offeddu, G. S., Shin, Y., Zhang, S., Morozova, O., Hickman, D., Knutson, C. G., and Kamm, R. D. 2022. *Engineered human blood–brain barrier microfluidic model for vascular permeability analyses.* Nature Protocols 17(1):95-128.

Hofbauer, P., Jahnel, S. M., Papai, N., Giesshammer, M., Deyett, A., Schmidt, C., Penc, M., Tavernini, K., Grdseloff, N., Meledeth, C., et al. 2021. *Cardioids reveal self-organizing principles of human cardiogenesis.* Cell 184(12):3299-3317.e22.

Homan, K. A., Gupta, N., Kroll, K. T., Kolesky, D. B., Skylar-Scott, M., Miyoshi, T., Mau, D., Valerius, M. T., Ferrante, T., Bonventre, J. V., et al. 2019. *Flow-enhanced vascularization and maturation of kidney organoids in vitro.* Nature Methods 16(3):255-262.

Huebsch, N., Loskill, P., Mandegar, M. A., Marks, N. C., Sheehan, A. S., Ma, Z., Mathur, A., Nguyen, T. N., Yoo, J. C., Judge, L. M., et al. 2015a. *Automated video-based analysis of contractility and calcium flux in human-induced pluripotent stem cell-derived cardiomyocytes cultured over different spatial scales.* Tissue Engineering - Part C: Methods 21(5):467-79.

Huebsch, N., Loskill, P., Mandegar, M. A., Marks, N. C., Sheehan, A. S., Ma, Z., Mathur, A., Nguyen, T. N., Yoo, J. C., Judge, L. M., et al. 2015b. *Automated Video-Based Analysis of Contractility and Calcium Flux in Human-Induced Pluripotent Stem Cell-Derived Cardiomyocytes Cultured over Different Spatial Scales.* Tissue Engineering Part C: Methods 21:467–479.

King, O., Cruz-Moreira, D., Sayed, A., Stevens, M. M., Rasponi, M., and Terracciano, C. M. 2022. *Functional microvascularization of human myocardium in vitro.* Cell Reports Methods:100280.

Mansour, A. A., Gonçalves, J. T., Bloyd, C. W., Li, H., Fernandes, S., Quang, D., Johnston, S., Parylak, S. L., Jin, X., and Gage, F. H. 2018. *An in vivo model of functional and vascularized human brain organoids.* Nature Biotechnology 36(5):432-441.

van Meer, B. J., Sala, L., Tertoolen, L. G. J., Smith, G. L., Burton, F. L., and Mummery, C. L. 2018. *Quantification of Muscle Contraction In Vitro and In Vivo Using MUSCLEMOTION Software: From Stem Cell-Derived Cardiomyocytes to Zebrafish and Human Hearts.* Current Protocols in Human Genetics 99, e67.

Mills, R. J., and Hudson, J. E. 2019. *Bioengineering adult human heart tissue: How close are we?* APL Bioengineering 3:010901.

Mills, R. J., Voges, H. K., Porrello, E. R., and Hudson, J. E. 2018. *Disease modeling and functional screening using engineered heart tissue.* Current Opinion in Physiology 1:80–88.

Niccoli, G., Scalone, G., Lerman, A., and Crea, F. 2016. *Coronary microvascular obstruction in acute myocardial infarction.* European Heart Journal 37(13):1024-33.

Orlova, V. V., Van Den Hil, F. E., Petrus-Reurer, S., Drabsch, Y., Ten Dijke, P., and Mummery, C. L. 2014. *Generation, expansion and functional analysis of endothelial cells and pericytes derived from human pluripotent stem cells.* Nature Protocols 9(6):1514-31.

Richards, D. J., Li, Y., Kerr, C. M., Yao, J., Beeson, G. C., Coyle, R. C., Chen, X., Jia, J., Damon, B., Wilson, R., et al. 2020. *Human cardiac organoids for the modelling of myocardial infarction and drug cardiotoxicity.* Nature biomedical engineering 4:446–462.

Ryan, A. R., England, A. R., Chaney, C. P., Cowdin, M. A., Hiltabidle, M., Daniel, E., Gupta, A. K., Oxburgh, L., Carroll, T. J., and Cleaver, O. 2021. *Vascular deficiencies in renal organoids and ex vivo kidney organogenesis.* Developmental Biology 477:98-116.

Sala, L., Van Meer, B. J., Tertoolen, L. G. J., Bakkers, J., Bellin, M., Davis, R. P., Denning, C., Dieben, M. A. E., Eschenhagen, T., Giacomelli, E., et al. 2018. *Musclemotion: A versatile open software tool to quantify cardiomyocyte and cardiac muscle contraction in vitro and in vivo.* Circulation Research 122(3):e5-e16.

Schmidt, C., Deyett, A., Ilmer, T., Haendeler, S., Torres Caballero, A., Novatchkova, M., Netzer, M. A., Ceci Ginistrelli, L., Mancheno Juncosa, E., Bhattacharya, T., et al. 2023. *Multi-chamber cardioids unravel human heart development and cardiac defects.* Cell 186:5587-5605.e27.

Sorop, O., Van De Wouw, J., Chandler, S., Ohanyan, V., Tune, J. D., Chilian, W. M., Merkus, D., Bender, S. B., and Duncker, D. J. 2020. *Experimental animal models of coronary microvascular dysfunction.* Cardiovascular Research 116(4):756-770.

Stebbeds, W., Raniga, K., Standing, D., Wallace, I., Bayliss, J., Brown, A., Kasprowicz, R., Dalmas Wilk, D., Deakyne, J., Clements, P., et al. 2023. *CardioMotion: identification of functional and structural cardiotoxic liabilities in small molecules through brightfield kinetic imaging.* Toxicological Sciences 195(1):61-70.

Takebe, T., Sekine, K., Enomura, M., Koike, H., Kimura, M., Ogaeri, T., Zhang, R. R., Ueno, Y., Zheng, Y. W., Koike, N., et al. 2013. *Vascularized and functional human liver from an iPSC-derived organ bud transplant.* Nature 499(7459):481-4.

Vargas-Valderrama, A., Messina, A., Mitjavila-Garcia, M. T., and Guenou, H. 2020. *The endothelium, a key actor in organ development and hPSC-derived organoid vascularization.* Journal of Biomedical Science 27, 67.

Vila Cuenca, M., Cochrane, A., van den Hil, F. E., de Vries, A. A. F., Lesnik Oberstein, S. A. J., Mummery, C. L., and Orlova, V. V. 2021. *Engineered 3D vessel-on-chip using hiPSC-derived endothelial- and vascular smooth muscle cells.* Stem Cell Reports 16(9):2159-2168.

Voges, H. K., Foster, S. R., Reynolds, L., Parker, B. L., Devilée, L., Quaife-Ryan, G. A., Fortuna, P. R. J., Mathieson, E., Fitzsimmons, R., Lor, M., et al. 2023. *Vascular cells improve functionality of human cardiac organoids.* Cell Reports 42(5):112322.

Wiesinger, A., Li, J., Fokkert, L., Bakker, P., Verkerk, A. O., Christoffels, V. M., Boink, G. J. J., and Devalla, H. D. 2022. *A single cell transcriptional roadmap of human pacemaker cell differentiation.* eLife 11:e76781.

Wimmer, R. A., Leopoldi, A., Aichinger, M., Kerjaschki, D., and Penninger, J. M. 2019. *Generation of blood vessel organoids from human pluripotent stem cells.* Nature Protocols 14(11):3082-3100.

Zhang, J., Klos, M., Wilson, G. F., Herman, A. M., Lian, X., Raval, K. K., Barron, M. R., Hou, L., Soerens, A. G., Yu, J., et al. 2012. *Extracellular matrix promotes highly efficient cardiac differentiation of human pluripotent stem cells: The matrix sandwich method.* Circulation Research 111(9):1125- 36.

General Discussion

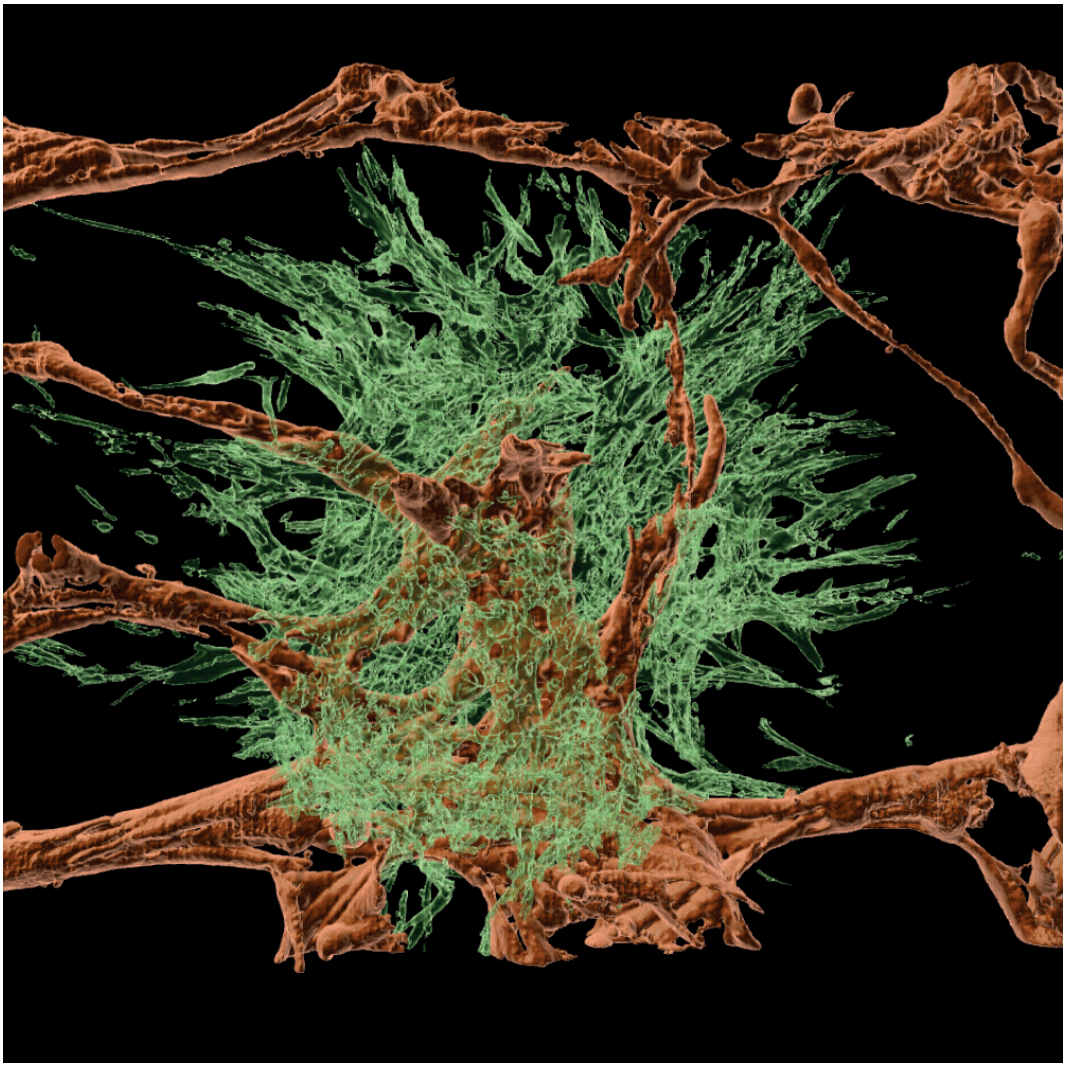

3D reconstruction of VMToC showing lumenized microvascular network formed by hiPSC-ECs (mCherry, orange) embedded in hiPSC-CMs (ACTN2, green).

General discussion

In this thesis we developed hiPSC- derived 3D cardiac tissue models integrating various cardiac cell types and other important components such as immune cells and functional vasculature. We defined optimal medium conditions for the incorporation of immune cells, specifically macrophages within the microtissues. Notably, culture plate type was important to keep macrophages inside the microtissues and prevent them migrating out; the microenvironment of microtissues also exerted an influence on the phenotype that macrophages acquired.

Besides immune cells, by introducing endothelial and mural cells in an microfluidic organ-on-chip platform, we facilitated the self-organization of lumenized external vessels around microtissues through which fluid could flow. The endothelial cells in the microtissues were able to link with external vasculature in the microfluidic chips forming a continuous vascular network and became perfusable under flow. This was evidenced by the passage of small fluorescent beads through the synthetic vasculature. These models offer opportunities to recapitulate more complex human cardiac microenvironment, study cardiac cell dialogue and pathophysiology of disease, to enable discovery of new strategies for understanding disease mechanisms and supporting drug development.

Current 3D Cardiac Models

Since the initial discovery of human embryonic and induced pluripotent stem cells (hESC or hiPSC, collectively called hPSC), they became a renewable cell source which could differentiate into all cells of the body (Thomson, 1998; Takahashi et al., 2007, 2006). hESCs were originally differentiated in aggregates called embryoid bodies, which when exposed to different stimuli or growth factors, could directed to form derivatives of different germ layers. However, this was at low efficiency. Much effort was placed in converting these protocols to high differentiation efficiency, 2D models using defined factors and culture medium without fetal calf serum as supplement. These protocols were effective in both hESC and hiPSC. hPSC-derived 2D models are valuable to give insights into the phenotypes of specific cell types. However, they essentially failed to answer questions related to organ development and (patho)-physiology. This was mostly because they missed key components of the real organ and did not show the same functional cellular maturity or crosstalk between cells. Going back once more to better defined hPSC-derived 3D models, has provided new perspectives and these are now regarded as holding significant potential for truly recapitulating their *in vivo* counterparts and modelling complex disorders more accurately. In **chapter 2**, we reviewed current state-of-the- art 3D cardiac models that can integrate multiple cell types, chemical and mechanical microenvironmental cues. In this short review, we reflected on their current use and perspectives on their future utility as cardiac models. In **chapter 3**, we discussed and compared these 3D cardiac models. We reviewed in detail their applications now that maturation methods are improving, allowing better human disease modelling, study of development and screening of drugs. We focused on the structural and functional readouts that are current practice, highlighting the more non- invasive options. Finally, we discussed future perspectives for their implementation both in industry and academia.

Establishment of 3D Cardiac Microtissue that Integrates Immune Components

Central to much of this thesis, has been the use of cardiac microtissues, developed in our lab to better model the heart. Upon starting the research described here, protocols had been established to generate hiPSC-derived cardiomyocytes (CM, Giacomelli et al., 2020), endothelial cells (EC, Giacomelli et al., 2017; Orlova et al., 2014) and cardiac fibroblasts (CF,

Giacomelli et al., 2020). By integrating CMs with vascular and stromal cells, it had been shown CM maturation could be achieved, at least to a post-natal stage (Giacomelli et al., 2020). In 2D culture, CMs only reach developmental stages equivalent to mid-gestation. Several other groups also developed 3D cardiac models that mainly focus on these three cell types as they represent the key components of the cardiac microenvironment and their interactions play crucial roles in maintaining homeostasis in health and disease further (Beauchamp et al., 2020; Mills et al., 2019; Richards et al., 2020). However, immune cells which are the underlying trigger of many diseases, including several of the heart like myocardial infarction, are important for creating more comprehensive and relevant models. Our group had previously induced hiPSC differentiation to immune cell types such as monocytes and macrophages (IPSDMs) (Cao et al., 2020). Interestingly, these IPSDMs have higher efferocytosis and endocytosis activity compared to blood-derivatives which suggests their resemblance to yolk-sac derived cardiac resident macrophages (CRMs, Cao et al., 2019). Yolk-sac derived CRMs are mainly involved in regeneration and angiogenesis and they can self-renew (Epelman et al., 2014; Dick et al., 2019; Bajpai et al., 2018). By contrast, postnatally, they lose their capacity for self-renewal and are replaced partially by blood-circulatory monocytes which are more involved in pro-inflammatory processes (Epelman et al., 2014; Bajpai et al., 2018). This switch in the immune population in the heart determines its response to inflammatory stimulus like injury.

In an effort to address questions related to IPSDM phenotype in tissue microenvironment, in **chapter 4**, we used IPSDMs differentiated according to the established protocols, and optimized conditions to integrate them into 3D cardiac microtissues together with CMs, ECs and CFs. In our first attempts, we encountered several problems: (1) macrophages migrated outside of microtissues; (2) they attached to culture surface of the wells; (3) the number of macrophages inside the microtissues were not very high at the end of 21 days culture period (Chapter 4, Figure 1).

Towards solving these problems, we first optimized the plate type. Following our previous microtissue protocol, we initially used a standard V-bottom plates to generate microtissues with IPSDMs (CMECFM0) in which IPSDMs migrated outside and attached to the wells. As a result, at the end of 21 days culture period, the number of IPSDMs inside CMECFM0s were very low. Surprisingly, the numbers seemed to increase upon longer term culturing (31 days). However, to date, we do not know the effect of longer culture periods on other cell types, especially on CMs. Therefore, we did not continue with microtissues that were cultured longer than 21 days.

Our first hypothesis for the migration problem was the increased cell death in the V bottom plates. After seeding the cells in these plates, centrifugation is necessary to form a compact microtissue. However, also because of the centrifugation, microtissues become stuck to the bottom of wells which might increase cell death. As a result, we believe the IPSDMs are actually attracted to the dead cells and this could be the reason for migration. To decrease the cell death, microtissues were instead generated using standard U-bottom plates; in this case, the microtissues formed but did not stick to the bottom of the plates. However, IPSDM

migration and attachment to the wells was still evident in this plate type, suggesting that the first hypothesis on attraction to dead cells was incorrect (Chapter 4, Figure 2B-D). We then tried ultra-low attachment U-bottom plates which eliminated both the migration and attachment problems. In these plates, IPSDMs remained inside the microtissues and microtissues showed compact formation (Chapter 4, Figure 2E-G). Furthermore, in these plates, the boundaries of microtissues were intact and "clean". This was different from the microtissues without IPSDMs where there was usually a halo of cells present around the microtissue. This possibly indicates an efferocytosis of IPSDMs in microtissues. However, to confirm this hypothesis, further tests, such as live-dead imaging of microtissues with and without IPSDMs, should be done.

Once the most appropriate protocol had been identified, we next characterized the effect of culture conditions on different cellular subsets. We showed that macrophage colony stimulating factor (M- CSF) significantly increased the IPSDM number in microtissues in earlier culture periods (Chapter 4, Figure 3). This confirms a previous report on the effect of M-CSF on survival and proliferation of IPSDMs (Otero et al., 2009). Interestingly, IPSDMs numbers on day 21 microtissues with and without M-CSF were similar and overall IPSDM numbers decreased over the 21 days culture period (Chapter 4, Figure 4A). This apparent discrepancy could be partly explained by the culture medium. Here, we used B(P)EL medium with growth factor supplements. This medium had previously been used to culture the microtissues (Campostrini et al., 2021), but not for the IPSDMs. Switching to a medium that can support IPSDM survival in the long-term could be a solution.

IPSDMs did not impact vessel density and contraction duration of the microtissues on day 7, 14 and 21 (Chapter 4, Figure 4B and C). Surprisingly though, previous reports on macrophages suggests their role in supporting vessels and cardiac electrophysiology (Hulsmans et al., 2017; Harari et al., 2017; Hulsmans et al., 2018; Moore et al., 2017; Zaman and Epelman, 2022; Gamrekelashvili et al., 2016; Krishnasamy et al., 2017). However, the parameters that were examined in this study were limited mainly due to the assays and software available. Therefore, these results might not cover all mechanisms that were involved in the cellular crosstalk as we did in the present system, which might explain the lack of confirmation of previous studies. Further investigation on vessel parameters such as diameter or integrity and contraction force and electrophysiological parameters might reveal IPSDM crosstalk with other cell types in the model.
Finally, we collected medium from microtissues (1) without IPSDMs (CMECF); (2) CMECFM0 without M-CSF supplement; (3) CMECFM0 with M-CSF supplement on day 7, 14 and 21. Initially, we determined the secreted cytokine composition in these collected media using multiplexed cytokine assay. However, the cytokine concentrations in CMECFM0 were very close to the upper detection limit of the assay. Because the values were close to the level noise within the assay, it was difficult to draw reliable conclusions. To solve this problem, we concentrated our samples using a column concentrator. Even after this additional step, however, we were only able to detect 4 cytokines, 2 of which were still very low. Cytokine profiles of the CMECFM0, however, showed a mixture of pro- (IL-6 and IP-10) and anti- (IL-10 and IL-1RA) inflammatory cytokines. Although IL-6 and IL-10 concentrations were

very low and therefore might not report accurate values (Chapter 4, Figure 4D, F), the mixed nature of the cytokine profile detected suggested the presence of heterogenous populations of IPSDMs in CMECFM0s. This is similar to the situation *in vivo* (Bajpai et al., 2018). In addition, IL-1RA concentrations was higher than IP-10 concentrations (Chapter 4, Figure 4E, G) which indicates that a majority of IPSDM population in CMECFM0s acquired M2-like anti-inflammatory phenotype while a minor population apparently acquired the M1-like pro-inflammatory phenotype. Unexpectedly, there was a significant increase in all cytokines in CMECFM0 with M-CSF supplement compared to without M-CSF on day 21. This was surprising as the IPSDM numbers on day 21 in these 2 conditions are similar. However, these results might suggest a possible role of M-CSF in triggering a phenotype in IPSDMs in the long-term. More specific assays such as flow cytometry, single cell level assays or staining might be necessary to investigate the effect of microenvironment on IPSDM phenotype.

3D Cardiac Models that Integrate Blood Vessel Cells and form functional vasculature

Many of the current 3D cardiac models lack functional vasculature. ECs are key players in the vasculature as they form the inner barrier of vessels and transfer nutrients, oxygen and cells to other tissue components (Aird, 2007, 2012).

Although most of the tissue models previously discussed incorporated primary- or hPSC-derived ECs which self-organized into microvascular-like networks, the models are generally cultured in static conditions, e.g in multiwell plates without fluidic flow. A previous study reported the importance of perfusion for the stability and integrity of vasculature (Ryan et al., 2021). Although microvascular networks inside these 3D models might be lumenized, the lack of fluid flow inside the networks mean that these lumens might collapse through the culture period. Therefore, these microvascular- like networks are not perfusable, and thus in this respect are not functional. In **chapter 5**, we developed an hiPSC-derived perfusable vascularized 3D cardiac microtissues (VMToC) using a commercially available organ-on-chip platform from AimBiotech. We combined 3D cardiac microtissues with single hiPSC-ECs and mural cells in a microfluidic chip under gravity-driven flow. For mural cell component, we used human brain vascular pericytes (HBVPs) as they were commercially available and easy to culture without the extra time and resources needed to differentiate hiPSC. However, hiPSC-derived smooth muscle cells could be used as an alternative (Vila Cuenca et al., 2021).

Initially, we tried different hydrogels such as bovine collagen 1 and Matrigel mix (results not shown in this thesis) as they provide more physiological microenvironment. However, in these mixed hydrogels, cells did not form 3D vessel-like structures, but rather stayed in monolayer. On the other hand, cultures in fibrin hydrogel showed evidence of 3D vessel formation, which was in line with a previous study (Vila Cuenca et al., 2021). Using fibrin hydrogel additionally eliminated batch-to-batch variability of collagen-based hydrogels.

In addition, other critical parameters such as (1) cell numbers to form external vascular networks; and (2) optimal day to integrate microtissues in the chips after seeding of cells to form vasculature, had to be optimized to increase the success and efficiency of the protocol. We found that the higher cell numbers are necessary to fix the formation of the external network and its interconnection/anastomosis with the preexisting internal microvasculature in the microtissues. Notably, for optimal anastomosis, prevascularized microtissues were integrated in the chips as early as day 12 of their static culture period to give enough time to hiPSC-ECs to start the self-organization. Microtissues from later time points were not successfully vascularized, most probably due to the regression of formed microvasculature in the microtissues which hindered anastomosis and perfusion in the chips. After achieving optimal conditions to integrate prevascularized microtissues with hiPSC-ECs and HBVPs in fibrin hydrogel in the chips, we characterized several structural and functional parameters in the chips.

As early as day 1 after seeding, hiPSC-ECs and HBVPs started self-organizing into a complex external vascular network which already showed evidence of anastomosis with the preexisting microvascular network in the cardiac microtissues (Chapter 5, Figure 1). Vascular density was not negatively affected by the presence of contractile cardiac microtissues. Vascular structures in- and around the microtissues were lumenized. That the vessels were lumenized, could be demonstrated by perfusion of fluorescently-tagged beads which followed the whole contour of microvascular networks inside the microtissues (Chapter5, Figure 2). The movement of the beads was oscillatory, following the rhythmic contraction of the cardiac microtissue. This offers the possibility to perfuse immune cells through these vascular networks in the future although it was not done in the present work. It would also address the challenge of incorporation of immune cells into 3D tissues described earlier. We finally showed that anastomosis is fluid flow dependent; continuous perfusion increased both the microvascular and external vascular density (Chapter 5, Figure 3 and 4).

In **chapter 6**, further characterization of contractile dynamics in spontaneous or paced contraction of VMToCs showed significant increase in contraction duration and peak-to-peak time parameters, compared to chip cultures that include only prevascularized cardiac microtissues without the external network around (MToC) (Chapter 6, Figure 1 and 2). This is in-line with a previous study (King et al., 2022), indicating possible crosstalk between EC and CMs. We challenged this crosstalk in two ways: (1) using an inhibitor of nitric oxide synthase (L-NAME) for a short- and long-term; (2) using a pro-inflammatory cytokine (IL-1β) (Chapter 6, Figure 3 and 4). Short-term effects of L-NAME were variable between different hiPSC-CM lines. However, long-term incubation of L-NAME (6h) and IL-1β (12h) showed significant decrease in contraction duration and peak-to-peak time parameters in VMToCs. There was no significant change in these parameters in MToCs. These results indicated increased crosstalk between EC-CM in VMToCs via paracrine signalling, most probably due to the higher numbers of ECs in the culture system. Similar to previous findings (Voges et al., 2023), these results suggest the importance of vascular cells in cardiac functionality and response to drugs.

In **chapter 7**, we described a detailed protocol to generate and characterize VMToCs. With this protocol, it is possible to generate vascularized organoid/microtissues in 5-7 days (Chapter 7, Figure 1-3) efficiently. The protocol described characterization of vessel structures and integrity by bead perfusion assay (Chapter 7, Figure 4). To investigate contractile function, VMToCs can be electrically paced to ensure all microtissues beat at the same rate for measurement (Chapter 7, Figure 5). Functional assays can be carried out as early as day 4, depending on the vascular development. VMToCs can be characterized structurally by fixing and immunofluorescence staining (Chapter 7, Figure 6), although using fluorescently-tagged lines would eliminate an extra staining step besides providing opportunities to live-image tissues and improve image quality.

Compared to the previous 3D cardiac models, the models optimized and developed in this thesis present many advantages, which are summarized as follows;

1. The models can all be based entirely on hiPSC-derived cells. This means that all cellular components can have the same genetic background, important for immune cell interaction but also reducing variability between experiments. In Chapter 5, 6 and 7, primary HBVP were used for convenience but hiPSC-derived smooth muscle cells can replace HBVPs in chips as they are comparable in functional support of ECs (Vila Cuenca et al., 2021).
2. The cardiac microtissues used in this thesis are based on Giacomelli et al., 2020; CMs in microtissues are structurally and functionally similar to neonatal CMs.
3. IPSDMs were successfully integrated into 3D cardiac microtissues, increasing the complexity of the model and providing a basis to study how IPSDMs impact the heart.
4. It is possible to seed chips with fewer cells than used previously in vascularized cardiac tissue models (King et al., 2022).
5. VMToCs provide an *in vitro* perfusable platform to study EC-CM crosstalk without the need for *in vivo* transplantation facilitating the study of EC dysfunction and testing drug responses.

Limitations and Future perspectives

Although the models described in this thesis could be useful in studying cellular crosstalk in- and with blood vessels, as well as modelling disease and testing drugs, they do still have a number of challenges that remain to be addressed to increase utility. Some of those related as such to the models developed here, are mentioned in the relevant sections above. More general limitations and their impact on possible future perspectives are as follows;

1. Although the models integrate multiple cell types that are important for structure and function, the inclusion of more cell types might lead to more comprehensive modelling of the human heart. For example, the nervous system is important in controlling heart function and addition of sympathetic/parasympathetic or other nerve cells could be useful. Previous studies highlighted the importance of neuronal control on cardiac function such as heart rate and blood flow (Zipes et al., 2017). Dysregulation in heart-

brain axis might cause cardiac pathophysiology (Wake and Brack, 2016). To date, innervation remains largely unexplored in *in vitro* models (Das et al., 2020; Soucy et al., 2020).

2. Incorporation of organoids representing other tissues could extend the utility of the vascularized organoids-on chip models. Other platform examples include vascularization of kidney (Homan et al., 2019), liver (Jin et al., 2018), brain (Salmon et al., 2022), lung (Park et al., 2019; Jain et al., 2018) and different tumor organoids (Sobrino et al., 2016; Straehla et al., 2022). These models are promising to study the impact of fluid flow and increase access to cells and factors in blood/culture medium.
3. Long-term culture might be beneficial in cases where a disease phenotype only emerges late after disease onset, is chronic or long-term or repeated drug exposure is of interest. Long- term culture and the effects on cells in the chips were not investigated. This could also reveal the roles of different cell types in the tissue microenvironment, as in, for example, the IPSDM phenotype described in chapter 4, and CM function described in chapter 5-6.
4. For contractile tissue, contraction force is an important measure of phenotype; it can be affected by many factors including mechanical and chemical stimuli and disease. The analysis software used in this thesis, MuscleMotion, is convenient and low tech, but it gives the contraction amplitude as arbitrary units (Sala et al., 2018). The software was designed to measure relative (pixel)changes in a movie but it is sensitive to light changes. It is therefore not suitable as such to compare contraction amplitude changes between different samples unless light intensities can be carefully controlled. Further investigation for force changes, where for example, cardiac tissue contract against a resistance is a quantitative alternative. Vector flow analysis (Hayakawa et al., 2012) can also provide quantitative readouts but analysis is slow, requiring substantial computer time.
5. Batch-to-batch and even well-to-well variability remains a challenge in 3D tissue cultures. In order to reduce variability arising from other factors besides cell source and culture platform, the on-chip culture conditions should be standardized. Currently, there are many chip designs available commercially or custom-made. However, commercial platforms cannot be easily modified to adapt to the research question. Therefore, many labs prefer custom-made platforms for the ability to modify the design relevant to the questions to be addressed. Due to high costs of commercial platforms and more time-consuming nature of custom-made platforms, currently standardization remains a big challenge, not least in the organ-on-chip field. However, initiatives such as EUROoCS, CEN and CENELEC actively promote and encourage labs to consider more on the standardization practices. Currently, efforts are underway to advance towards this step.
6. Whilst the models described in this thesis may have value in disease modeling (Orlova et al., 2022), for testing pipelines in drug development, higher-throughput platforms would be needed. This is not straightforward with the methods developed here; in addition to standardization, miniaturization and robotics to reduce costs will likely be required.

In the long-term, hiPSC-based 3D cardiac models may in some cases be able to compliment animal models, and provide better outcomes in predicting efficacy and toxicity for humans. As these models carry the genetic background of the individual that they are derived from, they are highly relevant to patients and could be used in precision medicine approaches. However, at present, the models developed in this thesis and described above could still be improved, as indicated. Nevertheless, as they are, they might be able to help bridge the gap between preclinical and clinical research.

References

Aird, W. C. 2012. *Endothelial cell heterogeneity.* Cold Spring Harbor Perspectives in Medicine 2(1):a006429.

Aird, W. C. 2007. *Phenotypic heterogeneity of the endothelium: I. Structure, function, and mechanisms.* Circulation Research 100(2):158-73.

Bajpai, G., Schneider, C., Wong, N., Bredemeyer, A., Hulsmans, M., Nahrendorf, M., Epelman, S., Kreisel, D., Liu, Y., Itoh, A., et al. 2018. The human heart contains distinct macrophage subsets with divergent origins and functions. Nature Medicine 24:1234–1245.

Beauchamp, P., Jackson, C. B., Ozhathil, L. C., Agarkova, I., Galindo, C. L., Sawyer, D. B., Suter, T. M., and Zuppinger, C. 2020. *3D Co-culture of hiPSC-Derived Cardiomyocytes With Cardiac Fibroblasts Improves Tissue-Like Features of Cardiac Spheroids.* Frontiers in Molecular Biosciences 7:14.

Campostrini, G., Meraviglia, V., Giacomelli, E., van Helden, R. W. J., Yiangou, L., Davis, R. P., Bellin, M., Orlova, V. V., and Mummery, C. L. 2021. *Generation, functional analysis and applications of isogenic three-dimensional self-aggregating cardiac microtissues from human pluripotent stem cells.* Nature Protocols 16 16(4):2213-2256.

Cao, X., van den Hil, F. E., Mummery, C. L., and Orlova, V. V. 2020. G*eneration and Functional Characterization of Monocytes and Macrophages Derived from Human Induced Pluripotent Stem Cells.* Current Protocols in Stem Cell Biology 52(1):e108.

Cao, X., Yakala, G. K., van den Hil, F. E., Cochrane, A., Mummery, C. L., and Orlova, V. V. 2019. *Differentiation and Functional Comparison of Monocytes and Macrophages from hiPSCs with Peripheral Blood Derivatives.* Stem Cell Reports 12(6):1282-1297.

Das, S., Gordián-Vélez, W. J., Ledebur, H. C., Mourkioti, F., Rompolas, P., Chen, H. I., Serruya, M. D., and Cullen, D. K. 2020. *Innervation: the missing link for biofabricated tissues and organs.* npj Regenerative Medicine 5,11.

Dick, S. A., Macklin, J. A., Nejat, S., Momen, A., Clemente-Casares, X., Althagafi, M. G., Chen, J., Kantores, C., Hosseinzadeh, S., Aronoff, L., et al. 2019. *Self-renewing resident cardiac macrophages limit adverse remodeling following myocardial infarction.* Nature Immunology 20 20(1):29-39.

Epelman, S., Lavine, K. J., Beaudin, A. E., Sojka, D. K., Carrero, J. A., Calderon, B., Brija, T., Gautier, E. L., Ivanov, S., Satpathy, A. T., et al. 2014. *Embryonic and adult-derived resident cardiac macrophages are maintained through distinct mechanisms at steady state and during inflammation.* Immunity 40(1):91-104.

Gamrekelashvili, J., Giagnorio, R., Jussofie, J., Soehnlein, O., Duchene, J., Briseño, C. G., Ramasamy, S. K., Krishnasamy, K., Limbourg, A., Kapanadze, T., et al. 2016. *Regulation of monocyte cell fate by blood vessels mediated by Notch signalling.* Nature Communications 7:12597.

Giacomelli, E., Bellin, M., Orlova, V. V, and Mummery, C. L. 2017a. *Co-Differentiation of Human Pluripotent Stem Cells-Derived Cardiomyocytes and Endothelial Cells from Cardiac Mesoderm Provides a Three-Dimensional Model of Cardiac Microtissue.* Current protocols in human genetics 95:21.9.1-21.9.22.

Giacomelli, E., Bellin, M., Sala, L., Meer, B. J. van, Tertoolen, L. G. J., Orlova, V. V, and Mummery, C. L. 2017b. *Three-dimensional cardiac microtissues composed of cardiomyocytes and endothelial cells co-differentiated from human pluripotent stem cells.* Development 144:1008–1017.

Giacomelli, E., Meraviglia, V., Campostrini, G., Cochrane, A., Cao, X., van Helden, R. W. J., Krotenberg Garcia, A., Mircea, M., Kostidis, S., Davis, R. P., et al. 2020. *Human-iPSC-Derived Cardiac Stromal Cells Enhance Maturation in 3D Cardiac Microtissues and Reveal Non-cardiomyocyte Contributions to Heart Disease.* Cell Stem Cell 26:862-879.e11.

Harari, E., Guo, L., Smith, S. L., Braumann, R. E., Virmani, R., and Finn, A. V. 2017. H*eart-resident macrophages: Are they involved in the rhythm of every beat?* Journal of Thoracic Disease 9(8):2264-2267.

Hayakawa, T., Kunihiro, T., Dowaki, S., Uno, H., Matsui, E., Uchida, M., Kobayashi, S., Yasuda, A., Shimizu, T., and Okano, T. 2012. *Noninvasive evaluation of contractile behavior of cardiomyocyte monolayers based on motion vector analysis.* Tissue Engineering - Part C: Methods 18(1):21-32.

Homan, K. A., Gupta, N., Kroll, K. T., Kolesky, D. B., Skylar-Scott, M., Miyoshi, T., Mau, D., Valerius, M. T., Ferrante, T., Bonventre, J. V., et al. 2019. *Flow-enhanced vascularization and maturation of kidney organoids in vitro.* Nature Methods 16(3):255-262.

Hulsmans, M., Clauss, S., Xiao, L., Aguirre, A. D., King, K. R., Hanley, A., Hucker, W. J., Wülfers, E. M., Seemann, G., Courties, G., et al. 2017. *Macrophages Facilitate Electrical Conduction in the Heart.* Cell 169(3):510-522.e20.

Hulsmans, M., Sager, H. B., Roh, J. D., Valero-Muñoz, M., Houstis, N. E., Iwamoto, Y., Sun, Y., Wilson, R. M., Wojtkiewicz, G., Tricot, B., et al. 2018. *Cardiac macrophages promote diastolic dysfunction.* Journal of Experimental Medicine 215 (2): 423–440.

Jain, A., Barrile, R., van der Meer, A. D., Mammoto, A., Mammoto, T., De Ceunynck, K., Aisiku, O., Otieno, M. A., Louden, C. S., Hamilton, G. A., et al. 2018. *Primary Human Lung Alveolus-on-a- chip Model of Intravascular Thrombosis for Assessment of Therapeutics.* Clinical Pharmacology and Therapeutics 103(2):332-340.

Jin, Y., Kim, J., Lee, J. S., Min, S., Kim, S., Ahn, D. H., Kim, Y. G., and Cho, S. W. 2018. *Vascularized Liver Organoids Generated Using Induced Hepatic Tissue and Dynamic Liver-Specific Microenvironment as a Drug Testing Platform.* Advanced Functional Materials 28,37.

King, O., Cruz-Moreira, D., Sayed, A., Stevens, M. M., Rasponi, M., and Terracciano, C. M. 2022. *Functional microvascularization of human myocardium in vitro.* Cell Reports Methods:100280.

Krishnasamy, K., Limbourg, A., Kapanadze, T., Gamrekelashvili, J., Beger, C., Häger, C., Lozanovski, V. J., Falk, C. S., Napp, L. C., Bauersachs, J., et al. 2017. *Blood vessel control of macrophage maturation promotes arteriogenesis in ischemia.* Nature Communications 8(1):952.

Loh, K. M. M., Chen, A., Koh, P. W. W., Deng, T. Z. Z., Sinha, R., Tsai, J. M. M., Barkal, A. A. A., Shen, K. Y. Y., Jain, R., Morganti, R. M. M., et al. 2016. *Mapping the Pairwise Choices Leading from Pluripotency to Human Bone, Heart, and Other Mesoderm Cell Types.* Cell 166(2):451-467.

Mills, R. J., Parker, B. L., Quaife-Ryan, G. A., Voges, H. K., Needham, E. J., Bornot, A., Ding, M., Andersson, H., Polla, M., Elliott, D. A., et al. 2019. *Drug Screening in Human PSC-Cardiac Organoids Identifies Pro-proliferative Compounds Acting via the Mevalonate Pathway.* Cell Stem Cell 24:895-907.e6.

Moore, E. M., Ying, G., and West, J. L. 2017. *Macrophages Influence Vessel Formation in 3D Bioactive Hydrogels.* Advanced Biosystems 1.

Orlova, V. V., Van Den Hil, F. E., Petrus-Reurer, S., Drabsch, Y., Ten Dijke, P., and Mummery, C. L. 2014. *Generation, expansion and functional analysis of endothelial cells and pericytes derived from human pluripotent stem cells.* Nature Protocols 9(6):1514-31.

Orlova, V. V., Nahon, D. M., Cochrane, A., Cao, X., Freund, C., van den Hil, F., Westermann, C. J. J., Snijder, R. J., Ploos van Amstel, J. K., ten Dijke, P., et al. 2022. *Vascular defects associated with hereditary hemorrhagic telangiectasia revealed in patient-derived isogenic iPSCs in 3D vessels on chip.* Stem Cell Reports 17(7):1536-1545.

Otero, K., Turnbull, I. R., Poliani, P. L., Vermi, W., Cerutti, E., Aoshi, T., Tassi, I., Takai, T., Stanley, S. L., Miller, M., et al. 2009. *Macrophage colony-stimulating factor induces the proliferation and survival of macrophages via a pathway involving DAP12 and β-catenin.* Nature Immunology 10(7):734-43.

Park, J. Y., Ryu, H., Lee, B., Ha, D. H., Ahn, M., Kim, S., Kim, J. Y., Jeon, N. L., and Cho, D. W. 2019. *Development of a functional airway-on-a-chip by 3D cell printing.* Biofabrication 11(1):015002.

Richards, D. J., Li, Y., Kerr, C. M., Yao, J., Beeson, G. C., Coyle, R. C., Chen, X., Jia, J., Damon, B., Wilson, R., et al. 2020. *Human cardiac organoids for the modelling of myocardial infarction and drug cardiotoxicity.* Nature biomedical engineering 4:446–462.

Ryan, A. R., England, A. R., Chaney, C. P., Cowdin, M. A., Hiltabidle, M., Daniel, E., Gupta, A. K., Oxburgh, L., Carroll, T. J., and Cleaver, O. 2021. *Vascular deficiencies in renal organoids and ex vivo kidney organogenesis.* Developmental Biology 477:98-116.

Sala, L., Van Meer, B. J., Tertoolen, L. G. J., Bakkers, J., Bellin, M., Davis, R. P., Denning, C., Dieben, M. A. E., Eschenhagen, T., Giacomelli, E., et al. 2018. *Musclemotion: A versatile open software tool to quantify cardiomyocyte and cardiac muscle contraction in vitro and in vivo.* Circulation Research 122(3):e5-e16..

Salmon, I., Grebenyuk, S., Abdel Fattah, A. R., Rustandi, G., Pilkington, T., Verfaillie, C., and Ranga, A. 2022. *Engineering neurovascular organoids with 3D printed microfluidic chips.* Lab on a Chip 22, 1615-1629.

Sobrino, A., Phan, D. T. T., Datta, R., Wang, X., Hachey, S. J., Romero-López, M., Gratton, E., Lee, A. P., George, S. C., and Hughes, C. C. W. 2016. *3D microtumors in vitro supported by perfused vascular networks.* Scientific Reports 6:31589.

Soucy, J. R., Bindas, A. J., Brady, R., Torregrosa, T., Denoncourt, C. M., Hosic, S., Dai, G., Koppes, A. N., and Koppes, R. A. 2020. *Reconfigurable Microphysiological Systems for Modeling Innervation and Multitissue Interactions.* Advanced Biosystems 4(9):e2000133.

Straehla, J. P., Hajal, C., Safford, H. C., Offeddu, G. S., Boehnke, N., Dacoba, T. G., Wyckoff, J., Kamm, R. D., and Hammond, P. T. 2022. *A predictive microfluidic model of human glioblastoma to assess trafficking of blood–brain barrier-penetrant nanoparticles.* Proceedings of the National Academy of Sciences of the United States of America 119(23):e2118697119.

Takahashi, K., Tanabe, K., Ohnuki, M., Narita, M., Ichisaka, T., Tomoda, K., and Yamanaka, S. 2007. *Induction of Pluripotent Stem Cells from Adult Human Fibroblasts by Defined Factors.* Cell 131(5):861-72.

Takahashi, K., Yamanaka, S., Zhang, Y., Li, Y., Feng, C., Li, X., Lin, L., Guo, L., Wang, H., Liu, C., et al. 2006. *Induction of Pluripotent Stem Cells from Mouse Embryonic and Adult Fibroblast Cultures by Defined Factors.* Cell 126(4):663-76.

Thomson, J. A. 1998. Embryonic stem cell lines derived from human blastocysts. Science 282(5391):1145-7.

Vila Cuenca, M., Cochrane, A., van den Hil, F. E., de Vries, A. A. F., Lesnik Oberstein, S. A. J., Mummery, C. L., and Orlova, V. V. 2021. *Engineered 3D vessel-on-chip using hiPSC-derived endothelial- and vascular smooth muscle cells.* Stem Cell Reports 16(9):2159-2168.

Voges, H. K., Foster, S. R., Reynolds, L., Parker, B. L., Devilée, L., Quaife-Ryan, G. A., Fortuna, P. R. J., Mathieson, E., Fitzsimmons, R., Lor, M., et al. 2023. *Vascular cells improve functionality of human cardiac organoids.* Cell Reports 42(5):112322.

Wake, E., and Brack, K. 2016. Characterization of the intrinsic cardiac nervous system. Autonomic neuroscience : basic & clinical 199:3–16.

Zaman, R., and Epelman, S. 2022. *Resident cardiac macrophages: Heterogeneity and function in health and disease.* Immunity 55(9):1549-1563.

Zipes, D. P., Jalife, J., and Stevenson, W. G. 2017. *Cardiac Electrophysiology: From Cell to Bedside: Seventh Edition.*

Appendix

Summary

The heart is one of the most important and complex organs with multiple layers and cell types. The dialogue between different cell types is critical for the structure and function of the heart. Moreover, the proper flow of blood through the whole organ is essential to keep all cells healthy and functional. Many 3D cardiac *in vitro* models incorporate multiple cardiac cell subsets to achieve complexity and physiological relevance. However, the lack of functional vasculature and immune components potentially limit their utility, especially in applications such as drug testing and disease modelling. Functional vasculature is important for selective nutrient, drug and cell transport to the other cell types. Immune cells play crucial roles in maintaining homeostasis in health and dysregulation of this innate and inflammatory cell type may trigger disease. Therefore, modelling these two critical components of the heart – fluidic flow and immune components- is important in using them to reveal underlying mechanisms in health and disease.

This thesis describes ways to integrate human induced pluripotent stem cells (hiPSC)-derived vascular and immune components in 3D cardiac microtissue platforms to study cellular crosstalk and its effect on cardiac response to chemical cues.

Chapter 1 provides a general introduction to the heart and its microenvironment. It delves in to importance of different components in the heart with a specific highlight on immune cells and vascular cells. It discusses different options to model the heart with a focus on *in vitro* alternatives.

In **Chapter 2** and **3**, current *in vitro* 3D cardiac models are reviewed with a focus on their applications, readouts and limitations. Implementation of future perspectives can increase the complexity, and possibly the relevance and value of these models.

Chapter 4 focuses on integration of hiPSC-derived macrophages (IPSDMs) into 3D cardiac microtissues consisting of cardiomyocytes, endothelial cells and cardiac fibroblasts. This chapter describes the optimization of culture conditions, such as culture plate type and medium components, and investigates their effect on different cellular subsets including IPSDMs, cardiomyocytes and endothelial cells. In summary, cardiac microtissues with IPSDMs can best be cultured in an ultra-low attachment plate since this ensures IPSDMs remain inside the tissues and localize near vessel structures. The number of IPSDMs in microtissues increases after addition of macrophage colony stimulating factor in medium in the early culture period. However, we found that overall IPSDM number throughout the culture period significantly decreases which might be due to the incompatibility of culture medium with IPSDMs. IPSDMs do not have a significant impact on cardiomyocyte contraction duration and vessel density parameters. Finally, cytokine profile of microtissues

with IPSDMs showed a mixture of pro- (IL-6 and IP-10) and anti- (IL-10 and IL-1RA) inflammatory cytokines, suggesting a heterogenous population of IPSDMs in the tissues. However, the higher concentration of anti- inflammatory cytokine (IL-1RA) might suggest that majority of IPSDMs acquire an M2-like macrophage phenotype while minor population is M1-like.

Chapter 5 describes a vascularized and perfusable hiPSC-derived 3D cardiac microtissue on a chip platform (VMToC). Here, prevascularized 3D cardiac microtissues were cultured together with an external vascular network which is formed by a self-organization of hiPSC-ECs and mural cells in a fibrin hydrogel. Contractile microtissues did not negatively impact the vascular formation, as evident with comparable vessel parameters in VMToCs and vessel-on-chip without microtissues. In short-term, preexisting microvascular networks in the microtissues and the external vascular network around them start interconnecting/anastomosing and forming continuous lumenized vascular networks. These vascular networks can be perfused with beads where beads show oscillatory moves synchronized with the rhythmic beating of the tissues. Continuous bidirectional perfusion promotes an increase in the vessel density in and around the microtissues.

Chapter 6, further characterizes VMToCs functionally and establishes the utility of the platform. Vascularization did not significantly alter VMToC's sarcomere organization. VMToCs showed longer contraction duration and peak-to-peak time in their spontaneous and paced contraction, suggesting an enhanced endothelial cell-cardiomyocytes crosstalk. When this crosstalk was challenged by either nitric oxide synthase inhibitor or pro-inflammatory cytokine, VMToCs showed significant changes in their contraction parameters. These results indicate that the presence of vascular cells in VMToCs regulates their contractile dynamics and response to drugs.

Chapter 7 provides a step-by-step protocol to generate VMToCs. Supporting protocols describe functional characterization by bead perfusion assay and pacing; and structural characterization of VMToCs by fixing and immunofluorescent staining.

Chapter 8 summarizes 3D cardiac microtissue models that were developed in this thesis, highlighting their advantages. Limitations and future perspectives to improve these models are also discussed at the end of this chapter.

Samenvatting

Het hart is een van de belangrijkste en meest complexe organen met meerdere lagen en celtypen. De interactie tussen verschillende celtypen is cruciaal voor de structuur en functie van het hart. Bovendien is een goede doorbloeding van het orgaan essentieel om alle cellen gezond en functioneel te houden. Veel 3D cardiale *in vitro* modellen bevatten meerdere hartcel subsets om complexiteit en fysiologische relevantie te bereiken. Het ontbreken van functionele vasculatuur en immuuncomponenten beperkt echter mogelijk hun bruikbaarheid, vooral in toepassingen zoals het testen van medicijnen en het modelleren van ziekten. Functionele vasculatuur is belangrijk voor selectief transport van voedingsstoffen, medicijnen en cellen naar de andere celtypen. Immuuncellen spelen een cruciale rol in het handhaven van homeostase in gezondheid, en ontregeling van dit aangeboren inflammatoire celtype kan ziekten veroorzaken. Daarom is het modelleren van deze twee kritieke componenten van het hart – vaculatuur met bijbehorend microfluidisch stroming en immuuncomponenten - belangrijk om onderliggende mechanismen in gezondheid en ziekte te onthullen.

Dit proefschrift beschrijft manieren om humane geïnduceerde pluripotente stamcel (hiPSC)-afgeleide vasculaire- en immuuncomponenten te integreren in 3D hartmicroweefselplatforms om cellulaire interactie en het effect daarvan op de respons van het hart op chemische signalen te bestuderen.

Hoofdstuk 1 geeft een algemene inleiding over het hart en zijn micro-omgeving. Het gaat in op het belang van verschillende componenten in het hart met een specifieke nadruk op immuuncellen en vasculaire cellen. Het bespreekt verschillende opties voor het modelleren van het hart met een focus op *in vitro* alternatieven.

In **Hoofdstuk 2** en **3** worden de toepassingen, uitlezingen en beperkingen van bestaande 3D *in vitro* hartmodellen besproken. De implementatie van toekomstige perspectieven kan de complexiteit, en mogelijk de relevantie en waarde, van deze modellen vergroten.

Hoofdstuk 4 richt zich op de integratie van hiPSC-afgeleide macrofagen (IPSDM's) in 3D hartmicroweefsels bestaande uit cardiomyocyten, endotheelcellen en hartfibroblasten. Dit hoofdstuk beschrijft de optimalisatie van kweekcondities, zoals het type kweekplaat en mediumcomponenten, en onderzoekt het effect ervan op verschillende cellulaire subsets, waaronder IPSDM's, cardiomyocyten en endotheelcellen. Samenvattend kunnen hartmicroweefsels die IPSDM's bevatten het beste gekweekt worden in een ultra-laag hechtingsplaat, omdat dit ervoor zorgt dat IPSDM's in de weefsels blijven en zich in de buurt van vasculaire structuren lokaliseren. Het aantal IPSDM's in microweefsels neemt toe na toevoeging van macrofaagkoloniestimulerende factor in het medium in de vroege kweekperiode. We vonden echter dat het totale aantal IPSDM's significant afneemt tijdens de kweekperiode, wat te wijten kan zijn aan de incompatibiliteit van het kweekmedium met IPSDM's. IPSDM's hebben geen significante invloed op de contractietijd van cardiomyocyten en vasculaire dichtheidsparameters. Tot slot toonde het cytokineprofiel

van microweefsels met IPSDM's een mix van pro- (IL-6 en IP-10) en anti- (IL-10 en IL-1RA) ontstekingscytokinen, wat duidt op een heterogene populatie van IPSDM's in de weefsels. De hogere concentratie ontstekingsremmende cytokine (IL-1RA) zou er echter op kunnen wijzen dat de meerderheid van de IPSDM's een M2-achtig macrofaagfenotype krijgt, terwijl de kleinere populatie M1-achtig is.

Hoofdstuk 5 beschrijft een gevascullariseerd en perfuseerbaar hiPSC-afgeleid 3D hartmicroweefsel op een chipplatform (VMToC). Hier werden vooraf gevascullariseerde 3D hartmicroweefsels gekweekt samen met een extern vasculair netwerk dat zich vormt door zelforganisatie van hiPSC-ECs en murale cellen in een fibrine hydrogel. Contractiele microweefsels hadden geen nadelige invloed op de vorming van het vasculaire netwerk, zoals bleek uit de vergelijkbare vasculaire parameters in VMToC's en bloedvat-op-een-chip zonder microweefsels. Op korte termijn beginnen reeds bestaande microvasculaire netwerken in de microweefsels en het externe vasculaire netwerk eromheen zich met elkaar te verbinden/anastomoseren en vormen ze continue gelumeniseerde vasculaire netwerken. Deze vasculaire netwerken kunnen worden geperfuseerd met kleine flurescerend bolletjes waarbij hun oscillerende bewegingen is te zien die gesynchroniseerd zijn met het ritmische kloppen van de weefsels. Continue bidirectionele perfusie bevordert een toename van de vasculaire dichtheid in en rond de microweefsels.

In **hoofdstuk 6** worden VMToC's verder functioneel gekarakteriseerd en wordt het nut van het platform aangetoond. Vascularisatie veranderde de sarcomeerorganisatie van VMToC's niet significant. VMToC's vertoonden een langere contractieduur en piek-tot-piektijd in hun spontane en gestimuleerde contractie, wat duidt op een verbeterde interactie tussen endotheelcellen en cardiomyocyten. Wanneer deze interactie werd verstoord door stikstofoxidesynthaseremmer of pro-inflammatoir cytokine, vertoonden VMToC's significante veranderingen in hun contractieparameters. Deze resultaten geven aan dat de aanwezigheid van vaatcellen in VMToC's hun contractiedynamiek en respons op medicijnen reguleert.

Hoofdstuk 7 biedt een stapsgewijs protocol om VMToC's te genereren. Ondersteunende protocollen beschrijven functionele karakterisatie door perfusiemetingen en pacing; en structurele karakterisatie van VMToC's door fixatie en immunofluorescente kleuring.

Hoofdstuk 8 geeft een samenvatting van 3D hartmicroweefselmodellen die in dit proefschrift zijn ontwikkeld en benadrukt hun voordelen. Beperkingen en toekomstige perspectieven om deze modellen te verbeteren worden ook besproken aan het einde van dit hoofdstuk.

Curriculum Vitae

Ulgu Arslan was born and grew up in Turkey where she completed a Bachelor degree in Molecular Biology and Genetics in Bilkent University, Ankara. After graduation, Ulgu moved to Belgium where she obtained a Master degree in Biomedical Science with a specialization in Neuroscience at University of Antwerp. The topic of her master thesis was "Characterization of electrophysiological and morphological differences between KCNQ2 related benign familial neonatal epilepsy and developmental and epileptic encephalopathy using hiPSC-derived 2D neurons and 3D brain organoids".

After completion of her Master degree, she moved to the Netherlands where she worked as a PhD fellow at Leiden University Medical Centre at the department of Anatomy and Embryology. Here, she carried out research in the group of Dr. Valeria Orlova, with Prof. Dr. Christine Mummery as her promoter. The main project in her PhD was the "Development of a hiPSC-derived vascularized 3D cardiac microtissues using organ-on-chip technologies". This project was supported by the Marie-Curie International Training Network as part of the European Organ-on-Chip consortium (EUROoC), and the Novo Nordisk Foundation. In addition, she worked on a project entitled "Integration of hiPSC-derived immune components in 3D cardiac microtissues".

The results of her research are presented in this thesis.

List of Publications

Perspectives for Future Use of Cardiac Microtissues from Human Pluripotent Stem Cells.

Arslan, U., Orlova, V. V., and Mummery, C. L. 2022b. ACS Biomaterials Science and Engineering 8(11):4605-4609. doi: 10.1021/acsbiomaterials.1c01296.

Microphysiological stem cell models of the human heart.

Arslan, U.#, Moruzzi, A.#, Nowacka, J.#, Mummery, C. L., Eckardt*, D., Loskill, P.*, and Orlova, V. V.* 2022a. Materials Today Bio 14:100259. doi: 10.1016/j.mtbio.2022.100259 #Joint first authorship

Software Tool for Automatic Quantification of Sarcomere Length and Organization in Fixed and Live 2D and 3D Muscle Cell Cultures *In Vitro*.

Stein, J. M., **Arslan, U.**, Franken, M., De Greef, J. C., Harding, S. E., Mohammadi, N., Orlova, V. V, Bellin, M., Mummery, C. L., and Van Meer, B. J. 2022. Current Protocols in Human Genetics 2(7):e462. doi: 10.1002/cpz1.462.

Vascularized hiPSC-derived 3D cardiac microtissue on chip.

Arslan, U., Brescia, M., Meraviglia, V., Nahon, D. M., van Helden, R. W. J., Stein, J. M., van den Hil, F. E., van Meer, B. J., Vila Cuenca, M., Mummery, C. L., Orlova V. V. 2023. Stem Cell Reports 18:1394–1404. doi: 10.1016/j.stemcr.2023.06.001.

Generation and characterization of hiPSC-derived vascularized-, perfusable cardiac microtissues-on-chip

Arslan, U., van den Hil, F. E., Mummery, C. L., Orlova V. V. 2024. Current Protocols:Stem Cell Biology. doi: 10.1002/cpz1.1097.

Acknowledgement

I would like to take a moment to express my heartfelt gratitude for the support and guidance I got over the years.

Dear Christine and Valeria, I am grateful for the opportunity to have worked under your supervision. I value the role you played in facilitating my professional and personal endeavors. Thank you for your time and effort to overseeing my PhD, believing in me and challenging me throughout the years.

To my dear colleagues in the Anatomy and Embryology department, thank you for your hard work, your friendship and for your support.

To each member of Stem Cell Group, and with a special thanks to Nikola, Linda, Cyriel, Maury, Ruben, Mehmet, Celine, and Ouafa I wish to express my gratitude for the enriching brainstorming sessions, shared laughter, and moments of anticipation. Despite being physically separated by floors and even buildings with some of you, I deeply felt your support in every encouraging word and gesture.

The members of hiPSC core facility, I appreciate your efforts in helping me.

To the current and past Orlova group members, to each and every one of you, thank you very much for your kindness and support. I am inspired by the collective spirit of teamwork that defines the group. I wish you all the best of luck and hope to come across in future endeavors.

To Vivi, Marcella, Giulia and Berend, I am incredibly happy to have met you and learned from you. I cannot thank you enough for your guidance and support anytime I needed. It meant a lot to me.

Dear Dorien and Mervyn, as I reflect on my journey, I am amazed at the countless times I have knocked your door, seeking your expertise. Your patience and dedication to help me navigate through all the problems I encountered has been nothing but admirable. And for that, I appreciate you.

To my dear friend Lisa, you have been my steadfast companion, patiently enduring my endless stream of questions. But not only professionally. From sharing a laughter during breaks to lending a listening ear during challenging times, your friendship has enriched my PhD experience in ways I could have never imagined. Thank you very much for the countless memories and the bonds of friendship that have grown stronger with each passing day.

To my dear friends Sara, Milica and Theano- beyond our academic journey and collaboration in the lab, you became my pillars of strength and my refuge in times of uncertainty. Together we laughed, we cried and we celebrated each milestone. And as we step forward, side

by side, may our friendship continue to flourish and our shared experiences continue to deepen. Thank you for making my final years at LUMC truly unforgettable. Though things may come to an end, the memories we've created together will last a lifetime.

To Cemre, Tarek, Joel and Ioanna I am overwhelmed with gratitude for your support and friendship. It's remarkable how even geographical boundaries couldn't hinder our shared moments of joy, heartfelt conversations, and stimulating scientific discussions. From brainstorming solutions to challenges to refining presentation skills, thank you for being there for me, for cheering me on from afar and for reminding me that true friendship knows no bound. I am looking forward to share many more golden memories, success stories and practice presentations because it is never enough.

So here's to you, my dear colleagues-turned-friends—the greatest gift of my PhD journey.

To Jaco, Irene, Thom, Petro and Justus- thank you for your unconditional love and support throughout this journey. Your presence in my life has enriched it beyond measure and I am blessed to have you by my side through every step of my journey. With deepest appreciation and endless love.

To Friso, my partner in crime, my husband. What a journey! Words seem inadequate to convey the depth of my appreciation for you. Through every twist and turn, every win and challenge, you have been there to share the moment with me and support me the best you can. I am filled with profound gratitude for the journey we have shared and the beautiful future that lies ahead. Thank you for being my greatest supporter.

Anneme, babama ve canim ablama – elele, zorluklara gogus gere gere yurudugumuz bu uzun ve mesakatli yolun da sonuna geldik. Mesafelere ragmen her daim yanimda oldugunuz icin, kosulsuz sevgi ve desteginiz icin, bitmek bilmeyen skype konusmalarimiz icin ve en onemlisi de her karanligin sonunda bir aydinlik olduguna beni inandirdiginiz icin size cok tesekkur ederim. Siz yanimda oldugunuz surece ben her seyi basaririm. Daha guzel basarilara yine hep birlikte yol almak dilegiyle.

To all my family members- In the rollercoaster of life, family is my seatbelt that holds me tight through every twist and turn, ensuring I conquer every peak and valley with resilience, strength and boundless love.